THE ROLE OF HISTONE DEACETYLASE 3 IN CHONDROGENESIS AND OSTEOARTHRITIS.

By

Dimitra Tsompani, MRes

Thesis submitted for the degree of Doctor of Philosophy

Institute of Cellular Medicine

March 2017

Abstract

Histone deacetylases (HDACs) regulate the acetylation pattern of chromatin to control gene expression. Previous studies reported class I HDACs and specifically HDAC3 as a key regulator of *MMP1/13* expression, the major collagenases in cartilage. Moreover, HDAC inhibitors were shown to have a chondroprotective role in *in vivo* models of osteoarthritis. The aim of this study was to examine the role of HDAC3 in catabolic gene expression in osteoarthritis and in chondrocyte differentiation *in vivo* and *in vitro*.

Chemical inhibitors against all HDACs (e.g. TSA) and specifically against HDAC3 (Apicidin) were used in conjunction with HDAC3 RNAi in human SW1353 chondrocytes, stimulated with IL-1 and in a mesenchymal stem cell (MSC) chondrogenic differentiation model. Gene expression was quantified using qRT- PCR and protein by western blotting, immunohistochemistry and biochemical methods. RNA microarray analysis was performed following RNAi or Apicidin treatment, across a time-course of IL-1 stimulation in chondrocytes to identify critical regulators of catabolic gene expression. Subsequently the role of E2F-1 transcription factor was studied with gain or loss of function experiments. E2F-1 activity on MMP1/13 was assessed by luciferase reporter gene activation and interaction with HDAC3 determined by immunoprecipitation. The role of HDAC3 in murine development was determined by generating a cartilage specific conditional knockout mouse model.

HDAC3 is essential for IL-1- induced *MMP1/13* and *FRA1* expression in chondrocytes. Microarray analysis suggests the E2F-1 transcription factor may mediate the effect of HDAC3 on gene expression regulation. Accordingly, modulation of E2F1 levels alters IL-1 induced *MMP1/13* expression and HDAC3 appears to interact with E2F1. Additionally, HDAC3 regulates anabolic gene expression, including *COL2A1* and *ACAN*, during MSC chondrogenesis and is required for normal endochondral ossification, since conditional deletion resulted in embryonic lethality.

We propose a novel role for HDAC3 in the regulation of catabolic and anabolic gene expression.

Acknowledgements

Firstly, I would like to thank my supervisors Professor David Young and Dr Matt Barter for training me at the bench and for remaining supportive and were always happy to help from my first day in the lab.

I would also like to thank my PhD assessors, Professor John Loughlin and Dr Kasia Pirog for making important questions during my assessments and for offering constructive comments and guidance over the past three years. Thanks also go to Andrew Skelton for analyzing my microarray (**Chapter 4**), Sharon Watson for performing the immunohistochemistry and part of the histology experiments, Kathleen Cheung for providing part of the RNA-seq data presented in (**Chapter 6**, **Figure 6.1**) and also for helping analyzing my microarray data, Dr Craig Bullock for teaching me the DMM-surgery, Beth Gibson and Robert Jackson for teaching me many of the techniques used for the results presented in **Chapter 7**, Professor Drew Rowan for his co-supervision and finally everyone in David's Young group for helping me towards successful completion of this thesis. Thanks to the fellow students and postdocs in the MRG for making the lab a great working environment to be.

Thanks to my caring partner, Dimitris, who patiently listens to my frustrations and enthusiastically celebrates my successes. Finally, I would like to thank my supportive family, especially my parents, Maria and Konstantinos, who taught me to work hard and never give up.

This work was funded by Arthritis Research UK.

Declaration

The work reported in this thesis was performed from October 2013 to September 2016. All work was carried out in the Musculoskeletal Research Group, Institute of Cellular Medicine, Newcastle University. All experiments were carried out by myself under the guidance of my supervisors Prof. David Young and Dr Matt Barter.

No part of this thesis has been submitted for the award of any other degree.

Contents

List of Figures

List of Tables

Abbreviations

AAF	Alanyl-Alanylphenylalanyl-aminoluciferin
ABC	Avidin/Biotin complex
AC	Articular Cartilage
ADAMTS	A Disintegrin And Metalloproteinase with Thrombospondin Motifs
ANOVA	Analysis of variance
AP-1	Activator Protein 1
APS	Ammonium persulphate
ATCC	American Type Culture Collection
BMP-2	Bone Morphogenetic Protein-2
BNC	Bovine Nasal Cartilage
bp	Base pairs
BSA	Bovine serum albumin
CBC	Comparative Biology Centre
cKO	conditional Knockout
co-IP	co-Immunoprecipitation
CXCL1	C-X-C motif ligand 1
DAB	Diaminobenzidine
DAPI	Diamidino-2-phenylindole
DF1	DharmaFECT transfection reagent
dH2O	Distilled H2O
DMB	Dimethyl-Methylene Blue
DMEM	Dulbecco's Modified Eagle's Medium

DMF	Dimethyleformamide
DMM	Destabilisation of the Medial Meniscus
DMSO	Dimethyl Sulfoxide
dNTP	Deoxyribonucleotide triphosphate
ECL	Electrochemiluminescence
ECM	Extracellular Matrix
EDTA	Ethylenediaminetetraacetic acid
EMSA	Electro-Mobility Shift Assays
EMT	Epithelial-to-mesenchymal transition
ERK	Extracellular Signal-Regulated Kinases
EtBr	Ethidium bromide
EUCOMM	The European Conditional Mouse Mutagenesis Program
FACIT	Fibril associated collagen with interrupted triple helix
FBS	Foetal bovine serum
FGFs	Fibroblast Growth Factors
FLP	Flippase
FLS	Fibroblast-Like Synoviocytes
FPKM	Fragments per kilobase of exon per million fragments mapped
FRET	Fluoroscent resonance energy transfer
FRT	Flippase Recognition Target sites
GAG	Glycosaminogycan
GAPDH	Glyceraldehyde 3-phosphate dehydrogenase
GATHER	A Gene Annotation Tool to Help Explain Relationships
GFP	Green Fluorescent Protein

HAT	Histone acetyltransferases
HBB	Human Haemoglobin
HDAC	Histone Deacetylase
HDACi	Histone Deacetylase inhibitor
HEK293T	Human Embryonic Kidney cells 293
HEPES	4-(2-hydroxyethyl)-1-piperazineethanesulfonic acid
HET	Hetrozygous
HMA	Hypo-Methylating Agent
HPLC	High Performance Liquid Chromatography
HPV	Human Papilloma Virus
HRP	Horse Radish Peroxidase
HS	Hydrophobic Spacer
HZ	Hypertrophic Zone
IB	Immunoblotting
ICD	Intercanthal Distance
ICSBP	Interferon Consensus Sequence Binding Protein
IEG	Immediate Early Genes
IFN	Interferon
IGF	Insulin Growth Factor
IKK	IκB kinase
IL	Interleukin
IL-1R AcP	IL-1 receptor accessory protein
IL-1R	IL-1 receptor
IMPC	International Mouse Phenotypic Consortium

IP	Immunoprecipitation
IPA	Ingenuity Pathway Analysis
IRAK	Interleukin-1 Receptor Associated Kinase
IRF3	IFN regulatory factor 3
ISRE	Interferon Stimulated Response Element
IκB	Inhibitor of κB
JAK	Janus Kinase
JNK	c-Jun NH2-terminal kinase
KEGG	Kyoto Encyclopedia of Genes and Genomes
KOMP	Knockout Mouse Project
LB	Luria-Broth
LGB	Lower gel buffer
LPS	Bacterial lipopolysaccharide
MAPK	Mitogen-activation protein kinase
MAPKK	MAPK kinase
MEKK1	MAP and ERK kinase kinase
MIA	Mono-Iodoacetate
M-MLV	Moloney Murine Leukaemia Virus
MMP	Matrix metalloproteinase
MMTL	Medial Meniscotibial Ligament
MSC	Mesenchymal Stem Cells
MT-MMPs	Membrane Type- Matrix Metalloproteinases
MW	Molecular Weights
N-CoR	Nuclear receptor co-repressor

NES	Nuclear Export Signal
NFY	Nuclear Factor Y (Y-box binding factor)
NF-κB	Nuclear Factor- kappa B
NIK	NF-kappaB inducing kinase
NLS	Nuclear Localisation Signal
NP	Nanoparticles
OA	Osteoarthritis
OSM	Oncostatin M
PBS	Phosphate Buffered Saline
PCA	Principal Component Analysis
PCR	Polymerase Chain Reaction
PCU	Polar Connecting Unit
PECAM-1	Platelet Endothelial Cell Adhesion Molecule-1
PI	Propidium Iodide
PSACH	Pseudochondrodysplasia
PVDF	Polyvinylidene Difluoride
PZ	Proliferating Zone
qRT-PCR	quantitative Reverse Transcription- Polymerase Chain Reaction
RA	Rheumatoid Arthritis
Rb	Retinoblastoma
RIN	RNA integrity number
RIPA	RadioImmunoprecipitation Assay
RL	Renilla
RLU	Relative Light Unit

RNAi	RNA interference
RNAPII	RNA Polymerase II
RSN	Robust Spline Normalisation
RT	Reverse Transcription
RT-PCR	Reverse Transcription- Polymerase Chain Reaction
RZ	Resting Zone
SAHA	Suberoylanilide Hydroxamic Acid
SD	Standard Deviation
SDS-PAGE	Sodium Dodecyl Sulfate - Polyacrylamide Gel Electrophoresis
SEM	Standard Error of the Mean
shRNA	short hairpin RNA
siRNA	small interfering RNA
SMRT	Silencing Mediator for Retinoic acid and Thyroid hormone receptor
SNP	Single Nucleic Polymorphism
SOB or SOC	Super Optimum Broth
STAT	Signal Transducer and Activator of Transciption
SWI/SNF	SWItch Sucrose/ Non fermentable
TAE	Tris-Acetate-EDTA
TEMED	Tween-20, N,N,N',N'-Tetramethylethylenediamine
TGF-β	Treansforming Growth Factor- beta
THP	Total Hip Replacement
TJR	Total Joint Replacement
TK	Thymidine Kinase
TKR	Total Knee Replacement

TLR	Toll-Like Receptor
TNF-α	Tomour Necrosis factor α
TSA	Trichostain A
TSS	Transcription Start Site
UPL	Universal Probe Library
UTR	Untranslated Region
VEGF	Vascular Endothelial Growth Factor
VST	Variance Stability Transformation

Chapter 1. Introduction

1.1 Articular Cartilage: Structure and Function.

Articular cartilage is the connective tissue of the synovial joints that provide a smooth, lubricated surface for articulation and load-bearing, minimising at the same time the stress on the subchondral bone. (Fox et al. 2009) Unlike the majority of other tissues, articular cartilage lacks blood vessels and nerves and is subject to harsh mechanical stress. The unique and complex structure of articular cartilage, together with environmental factors, and also lifestyle usually lead to the initiation and progression of major human diseases, including rheumatoid arthritis (RA) and osteoarthritis (OA). (Goldring & Marcu 2009) Most importantly, articular cartilage has a limited ability of self-repair and healing and hence once the damage has initiated, it leads to a series of catabolic events that result in the degradation of the tissue. (Simkin 2008) This degradation of articular cartilage is mediated by the expression of specific matrix metalloproteinase enzymes, also called collagenases, produced at least in part by the sole cartilage cell type, the chondrocyte. (Drissi et al. 2005)

Articular cartilage is composed of a dense extracellular matrix (ECM) that includes many sub-components and some sparse (<10%) specialised chondrocytes. Articular cartilage can be divided into four distinct zones: 1) the superficial zone, 2) the middle zone, 3) the deep zone and 4) the calcified zone. In total articular cartilage in an adult human knee is approximately 2-4mm thick with each zone being of variable depth (Fox et al. 2009) (see **Figure 1.1**). The superficial zone comprises 10-20% of articular cartilage and protects deeper layers from mechanical stresses. This zone contains mainly collagen type II and IX fibres that are packed tightly and aligned parallel to the cartilage surface. There is also a relatively high number of flattened chondrocytes and the integrity of this layer is imperative in the protection and maintenance of deeper layers. This zone is in contact with synovial fluid and is responsible for most of the tensile properties of cartilage, which enable it to resist the sheer, tensile and compressive forces imposed by articulation. Below to the superficial zone and before the deep and calcified zone, there is the middle zone that comprises 40-60% of articular cartilage and it contains proteoglycans and thicker collagen fibres. Here, there are less chondrocytes and the collagen fibrils are aligned in an angle rather than parallel to the cartilage surface. Functionally, the middle zone is the first line of resistance to compressive forces. The deep zone comprises approximately 30% of articular cartilage volume and provides the greatest resistance to mechanical stresses, since it contains the larger collagen fibres, the highest proteoglycan percentage and the lowest water concentration. The chondrocytes of this zone

are usually arranged in columns parallel to the collagen fibres. Between the deep zone and the last calcified zone there is also the tidemark that distinguishes the previous two zones. Last but not least, there is the calcified zone that plays an important role in maintaining the structural integrity of articular cartilage as it anchors the collagen fibres of the deep zone in the subchondral bone. The number of chondrocytes here is small and the chondrocytes are hypertrophic. (Fox et al. 2009)

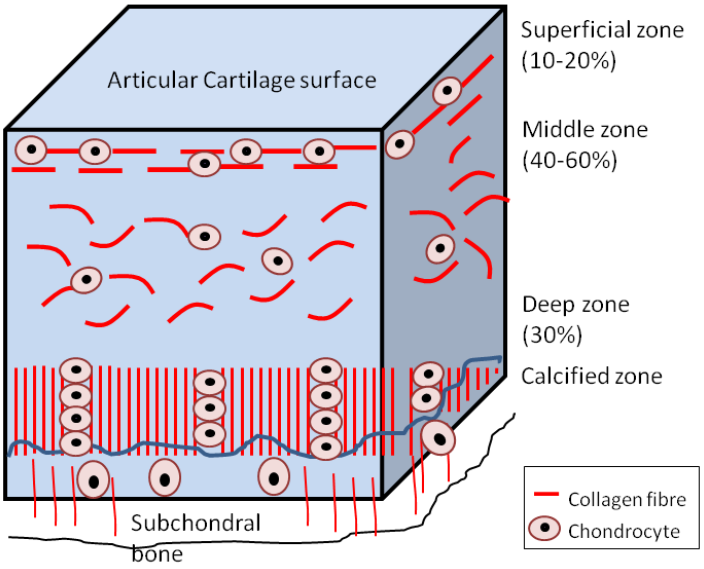

Figure 1.1. Healthy articular cartilage and articular zones. Adapted from (Fox et al. 2009).

Preservation of articular cartilage homeostasis depends on maintaining cartilage unique structural composition and organisation of the matrix throughout development (Martel-Pelletier et al. 2008). Cartilage strength and function depend on both the properties of the tissue and on their structural parameters (ECM and chondrocytes).

1.1.1 Extracellular Matrix (ECM)

The ECM is a complex of macromolecules that is principally composed of collagen and proteoglycans with other glycosylated or non-glycosylated proteins present in a smaller amount. Together with water, these components are critical for the maintenance of the mechanical properties of ECM, with the collagenous network mainly responsible for the tensile strength of articular cartilage and the proteoglycans (mainly aggrecan) for the elastic properties of ECM. It also serves as a reservoir of growth factors and cytokines that in turn are responsible for cell activation and gene expression. (Chiara & Cancedda 2009)

The most abundant component of articular cartilage is **water** constituting approximately 60-80% of the total weight. The rest is mainly accounted for by cartilage fibres and proteoglycans. The water content decreases from the superficial to deeper zones while the amount of collagen and proteoglycan is increased. Water flow also serves to distribute nutrients to chondrocytes in addition to providing lubrication. (Fox et al. 2009)

Collagen is the most abundant structural macromolecule in ECM. Type II collagen represents 90% to 95% of the collagen in ECM and forms fibres intertwined with proteoglycan aggregates. (Fox et al. 2009) In particular, it is composed of three identical α1 polypeptide chains that intertwine, like all collagens, to form a triple helix. This basic structure of any collagen is characterized by the presence of a glycine at every third amino acid of the polypeptide sequence that forms the triple helix. Other types of collagen, for example collagen type I, IV, V, VI, IX and XI represent only a smart part of the total volume in ECM and help to stabilise the collagen II fibres network that provides the shape and tensile stiffness of the tissue. Interestingly, although collagen is resistant to degradation by most proteases, it can be cleaved by the action of collagenases. In mammals there are three main collagenases, named matrix metalloproteinases (MMP-) MMP-1, MMP-8 and MMP-13, with MMP-13 favouring the cleavage of type II collagen over other fibrillar collagens. Further collagen degradation can be processed by other MMPs, for example MMP-2 and MMP-9 (Fox *et al.*, 2009; Martel-Pelletier *et al.*, 2008).

The importance of type II collagen in cartilage formation and function is demonstrated by the consequence of type II collagen (*COL2A1*) gene mutations which give both growth plate and articular cartilage abnormalities. (Byers 2001) To date, over 100 different mutations have been detected, the most common being missense substitutions in a glycine codon in an exon encoding the helical region of the pro-α-chain. In this region there is an absolute requirement of glycine in every third amino acid and replacement by any other amino acid perturbs triple helix formation. This result in a dominant negative effect due to both intracellular degradation of the newly synthesised procollagen molecule and perturbation of fibres formation, thus weakening the cartilage. (Martel-Pelletier et al. 2008) The site of the mutation determines the severity of the disease. Stickler syndrome for example is characterised by nonsense mutations and the phenotype is a consequence of haploinsufficiency. (Ahmad et al. 1991) The mildest phenotype is caused by an arginine to cysteine substitution in the triple helical region. (Pun et al. 1994)

Type XI collagen is another collagen that is less abundant than type II collagen in cartilage, and its abundance decreases from about 10% in fetal cartilage to 3% in adult articular

cartilage. (Eyre et al. 2006) Mutations in the gene also results in chondrodystrophic phenotypes, one of which is the Stickler syndrome, which can result from mutations either in type II or type XI collagen genes. Early onset of osteoarthritis is a common feature of these disorders. (Byers 2001) Type IX collagen is a member of the FACIT (Fibril associated collagen with interrupted triple helix) family and is also cartilage specific. It does not form a collagen fibril but is instead present at the surface of the type II/ XI fibril. Specific mutations have been described for type IX collagen giving rise to multiple epiphyseal dysplasia. Early onset of osteoarthritis is again a feature of this disorder. (Byers 2001)

Articular collagen also contains other types of collagen including type VI, which accounts for about 1% of its total collagen content. (Eyre et al. 2006) However, its content is increased in OA cartilage. (Söder et al. 2002) Mutations in any of the type VI collagen results in congenital muscular dystrophy, although it is not clear how this may affect cartilage function. Type X collagen is also cartilage specific, which under normal conditions is present in the hypertrophic zone of growth plate cartilage where it participates in endochondral ossification, the process of long bone growth. Although type X collagen is not a component of normal articular cartilage, it is present in OA cartilage and can be cleaved by MMP1. Mutations to the gene result in the development of metaphyseal dysplasia. (Bateman 2001; Boos et al. 1999)

Proteoglycans are the second most abundant component of ECM accounting for 5-10% of the tissue total weight. The proteoglycans in articular cartilage are complex macromolecules that consist of a central hyaluronic acid filament to which multiple monomers are noncovalently attached, with the most important one being aggrecan. Aggrecan itself is the largest in size and the most abundant by weight proteoglycan in cartilage and is made up of 3 core globular domains (G1-3). These domains are intersected by a glycosaminogycan (GAG) -rich region which is composed of a keratin sulphate region and two chondroitin sulphate regions. These regions are negatively charged which in turn creates a hydrophilic environment resulting in hydration of aggrecan. Thus, high concentrations of aggrecan are necessary in articular cartilage to resist compressive loads. A decrease in the GAG content can lead to overcompression and subsequent secretion of proteases by the chondrocytes that can lead to tissue degeneration (Martel-Pelletier *et al.,* 2008). Other proteoglycans in cartilage include biglycan, decorin and fibromodulin and are characterized by their ability to interact with collagen. (Fox et al. 2009)

1.1.2 Chondrocytes

Despite the hypoxic environment, 2% of the total volume of articular cartilage is constituted of a highly specialised and metabolically active type of cell, the chondrocyte. Chondrocytes of articular cartilage (AC) and of cartilage undergoing mineralization (Growth Plate, GF) are biochemically distinguishable although they originate from the same chondroprogenitor cell source. For example the AC chondrocytes (also termed as 'maturationally arrested') primarily act to maintain the ECM by expressing collagen types II, VI, IX, XI and aggrecan. AC chondrocytes do not proliferate significantly, yet respond to a variety of stimuli including growth factors and mechanical loads, although rarely do they create cell-to-cell contact interactions in order to promote signal transduction between the cells (Fox *et al.,* 2009; Drissi *et al.,* 2005). Comparatively, mineralizing cartilage is composed of chondrocytes (GF) that surpass this maturational stage, as evidenced by acceleration of proliferation, increased cell volume and expression of other markers such as type X collagen and alkaline phosphatase. (Böhme et al. 1995)

Mineralizing chondrocytes are also responsible for the development of bone. In terms of endochondral ossification, mesenchymal tissue differentiates into cartilage which is then replaced by bone. Endochondral ossification can be divided into five distinct phases (**Figure 1.2**). First, the mesenchymal stem cells (MSC) commit to becoming cartilage cells. This process is stimulated by sonic hedgehog (Shh) that induces expression of Pax1 transcription factor that will then induce a cascade of downstream transcription factors. During the second phase, the MSC condense and differentiate into chondrocytes. BMPs appear to be critical at this stage, because they will induce the expression of the adhesion molecules N-cadherin, N-CAM and the transcription factor Sox9. N-cadherin seems to be important for the initiation of these condensations and N-CAM for the maintenance of them. Sox9 will activate the expression of type II collagen and aggrecan, both critical for cartilage function. During the third phase, the chondrocytes proliferate rapidly. In the fourth phase, the chondrocytes stop dividing and become hypertrophic. This step appears to be mediated by Runx2 transcription factor that is crucial both for the intramembranous and endochondral ossification. Runx2 is itself regulated by histone deacetylase 4 (HDAC4), a chromatin remodelling enzyme. These hypertrophic chondrocytes alter the matrix they produce (by adding collagen X and fibronectin), to enable it to become mineralised by calcium phosphate. They also produce VEGF, which can transform MSC into blood vessels and recruits bone cell progenitors from the bloodstream. In the fifth phase, the hypertrophic chondrocytes either die by apoptosis and the cells that surround the cartilage model differentiate into osteoblasts (Gilbert S, 2010) or

differentiate into osteobalsts (Zhou et al. 2014). The osteoblasts will then start producing bone matrix. (Gilbert S, 2010)

In contrast to the chondrocytes undergoing endochondral ossification (e.g. growth plate), AC-chondrocytes (resting zone, **Figure 1.1**) do not fully mature and remain arrested before terminal hypertrophy occurs. These chondrocytes are also responsible for the maintenance and repair of ECM components via the production of a group of degradative enzymes such as matrix metalloproteinases. They can also encode and release many of the ECM components including glycoproteins, and this production can be affected by proinflammatory cytokines, such as interleukin 1 (IL-1) and tumor necrosis factor α (TNFα) and other growth factors, for instance insulin-like growth factors and transforming growth factor β (TGFβ). However, the molecular mechanisms and the pathways underlying this production of molecules by the chondrocytes are not yet completely clear. (Kevorkian et al. 2004; Davidson et al. 2006)

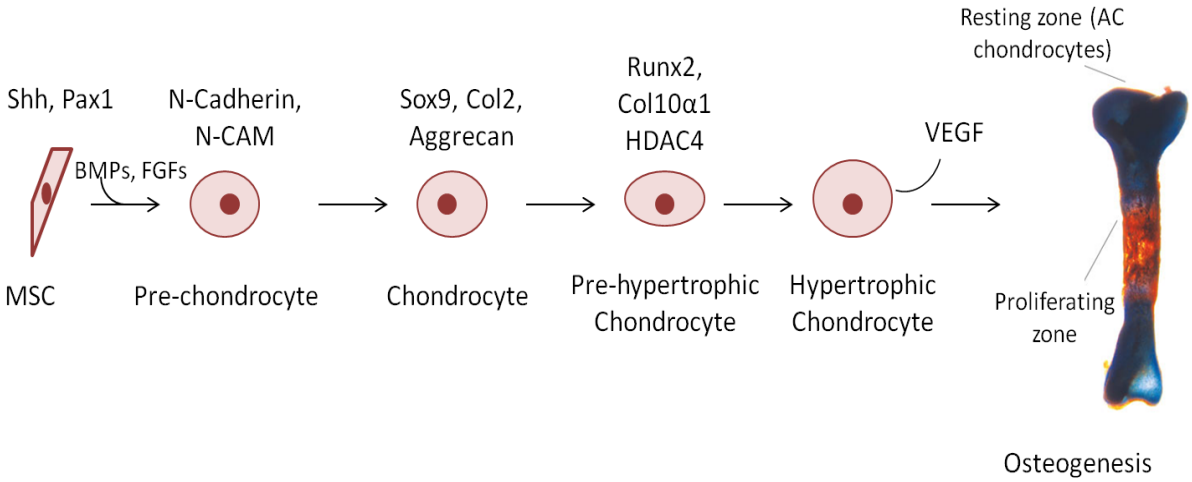

Figure 1.2. Control of endochondral ossification.

Active paracrine and transcription factors during the transition of cartilage to bone. Adapted from (Pitsillides and Beyer, 2011).

AC chondrocytes maintain normal and healthy ECM by renewing the ECM components with new products, while at the same time are protected by the potentially damaging mechanical forces by the ECM components. It has been previously shown that inactivity of the joint leads to cartilage degradation and so a normal movement of the joint is considered to be crucial for maintaining a healthy articular cartilage. Nevertheless, in case of an imbalance between the anabolic synthesis and the catabolic degradation of cartilage products, human diseases such as osteoarthritis can develop (Drissi *et al.*, 2005).

1.2 Arthritis

According to Arthritis Research UK (http://www.arthritisresearchuk.org/), arthritis is the biggest cause of pain and mobility disability in UK, with one fifth of the population seeking consultation for a musculoskeletal condition in general practise each year. As previously mentioned, the destruction of key components of cartilage, such as collagen II and aggrecan lead to the progression of cartilage degeneration that characterise the disease endpoints of both rheumatoid arthritis and osteoarthritis. This loss of cartilage can lead to the development of many symptoms including pain and narrowing in the range of movements, increasing disability and decreasing patient's morbidity and quality of life.

1.2.1 Osteoarthritis

Osteoarthritis (OA) is the most common form of arthritis affecting mainly people over the age of 45. Data collected over a seven-year period revealed that a total of 8.75 million people in UK have sought treatment for OA, with women to be more likely to develop the disease. The most common skeletal site for OA to be developed is the knee, followed by the hip and then by the wrist, the ankle and other sites. The most common symptoms of OA include joint pain, stiffness, swelling and loss of mobility (http://www.arthritisresearchuk.org/system/search-results.aspx?keywords=osteoarthritis). An increase in the numbers of those affected by OA is expected to occur together with the increasing prevalence of obesity and ageing of society. (Peach et al. 2005)

OA is characterised by degradation and eventually loss of articular cartilage, remodelling of the subchondral bone with some inflammation of the synovial membrane. There are numerous alterations in the osteoarthritic cartilage, and these involve metabolic and morphologic changes of chondrocytes as well as biochemical and structural changes in ECM components (Martel-Pelletier et al. 2008). However OA is considered to be a disease of the whole joint and not just the cartilage. In an OA knee joint, articular cartilage becomes damaged so the joint does not move as smoothly (**Figure 1.3**). In particular articular cartilage roughens and becomes thin and the subchondral bone sclerosis. All the tissues within the joint become more active as they try to repair the damage. In particular, the bone at the end of the joint grows outwards, forming bony spurs, known as osteophytes. The synovium (the inner layer of the joint capsule that produces the synovial fluid) might thicken and produce extra fluid. This causes the joint to swell. The production of inflammatory cytokines is also induced in an OA

knee and this will cause more damage. The ligaments that hold the joint together slowly stiffen making movements even more difficult. (Little and Hunter, 2013)

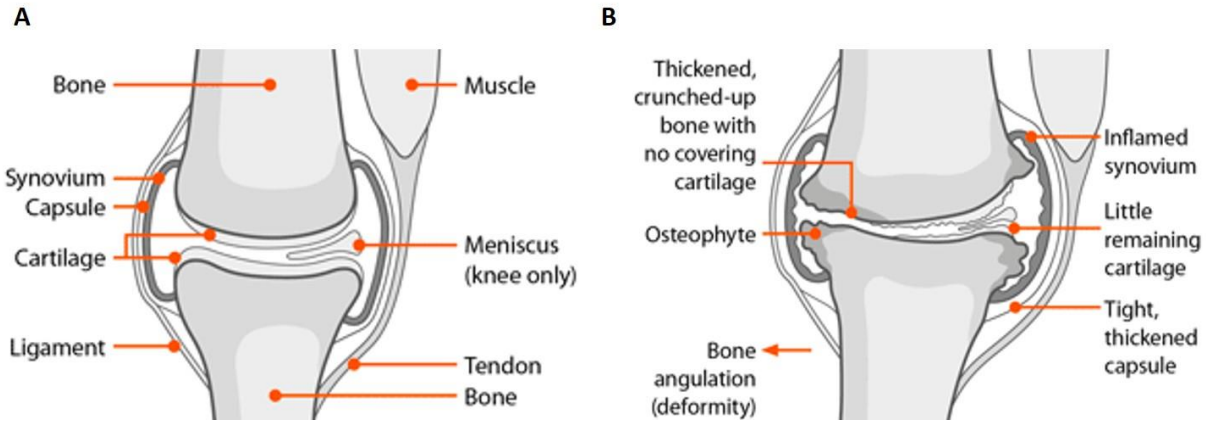

Figure 1.3. Normal and osteoarthritic knee (by http://www.arthritisresearchuk.org/)

A. A normal joint in comparison to **B.** A joint that has been deformed by severe osteoarthritis. The cartilage covering the ends of the bones gradually roughens and becomes thin, and the bone underneath thickens. All the tissue within the joint becomes more active than normal. The bone at the end of the joint grows outwards, forming bony spurs called osteophytes. The synovium may thicken and produce extra fluid, which then causes the joint to swell. The capsule and ligaments slowly thicken and contract as they would try to stabilise the joint.

With reference to the pathogenesis of the disease, increasing age, gender female, weight that can cause excess load-bearing and nutritional deficiencies, as well as a major genetic component and appear to be important for the vulnerability of the joint to develop OA. Moreover, the misalignment of the joint, muscle weakness, alterations of the structural integrity for example meniscus damage or a previous injury can facilitate the progression of the disease and define a group with high risk of developing OA (Hunter & Felson 2006) (**Figure 1.4**). OA is a complex disease in terms of genetic association of specific genetic loci in the initiation and the progression of the disease.

Evidence for genetic component in OA comes from family and twin studies, which estimate the genetic component of OA to be between 40% and 80%, which is similar to many other complex traits (Van Meurs 2017). Many genes or genetic loci are associated with the initiation and/or the progression of OA in different skeletal sites. Candidate gene studies were initially focused on ECM genes for example *COL2α1* (12q13.11), *COL11α1* (1p21.1) and *COL11α2* (6p21.32) and non-collagenous genes including *COMP* and *matrilin 3*, mutations of which have been implicated in osteochondrodysplasia pseudochondrodysplasia (PSACH) (Peach et al. 2005) with early onset OA (van Meurs, 2017). Other studies were also focused

on genes influencing bone density, since subchondral sclerosis appears early in OA or genes encoding for inflammatory cytokines (Peach et al. 2005). However, most recent heritability studies in European populations based in twins, siblings and families revealed only three loci including *GDF5*, chromosome 7q22 and *MCF2L* that were associated with high risk of developing hip or knee osteoarthritis (Day-Williams et al. 2011; Evangelou et al. 2009; Miyamoto et al. 2007; Valdes et al. 2011). An unbiased large-scale genome wide association study in 7410 unrelated patients was recently completed and the data obtained were compared with publicly available data from 11009 unrelated controls (from UK and other European countries). Most of the above cases (80%) had primary osteoarthritis requiring a hip or knee joint replacement. The most significant region to be associated with patients with primary osteoarthritis who were undergoing total joint replacement (TJR) was located on chromosome 3; a missense polymorphism within exon 3 of *GNL3* gene and a SNP situated in the 3' prime untranslated region (UTR) of the *GLT8D1* gene. The remaining significant signals were derived from patients who were undergoing total hip replacement (THP); a SNP located in intron 18 of the *ASTN2* gene, a polymorphism found 38kb upstream of *FILIP1* and 70kb upstream of *SENP6,* a SNP located 59kb downstream of *KLHDC5* and 96kb downstream of *PTHLH* and finally a polymorphism located in intron 2 of *CHST11* gene (Zeggini *et al.,* 2012, arcOGEN Consortium). In conclusion, these eight novel loci including the three previously established OA susceptibility loci in European populations on chromosome 7q22, in the *GDF5* and *MCF2L* genes make the current total of eleven OA susceptibility loci. Interestingly, a more recent study by (Lindner et al. 2015) suggested that three previously identified susceptibility loci including rs5009270 (near *IFRD1* gene), rs6976 (near GLT8D1 gene) and rs4836732 (within the *ASTN2* gene) may contribute to hip OA susceptibility by altering proximal femur shape.

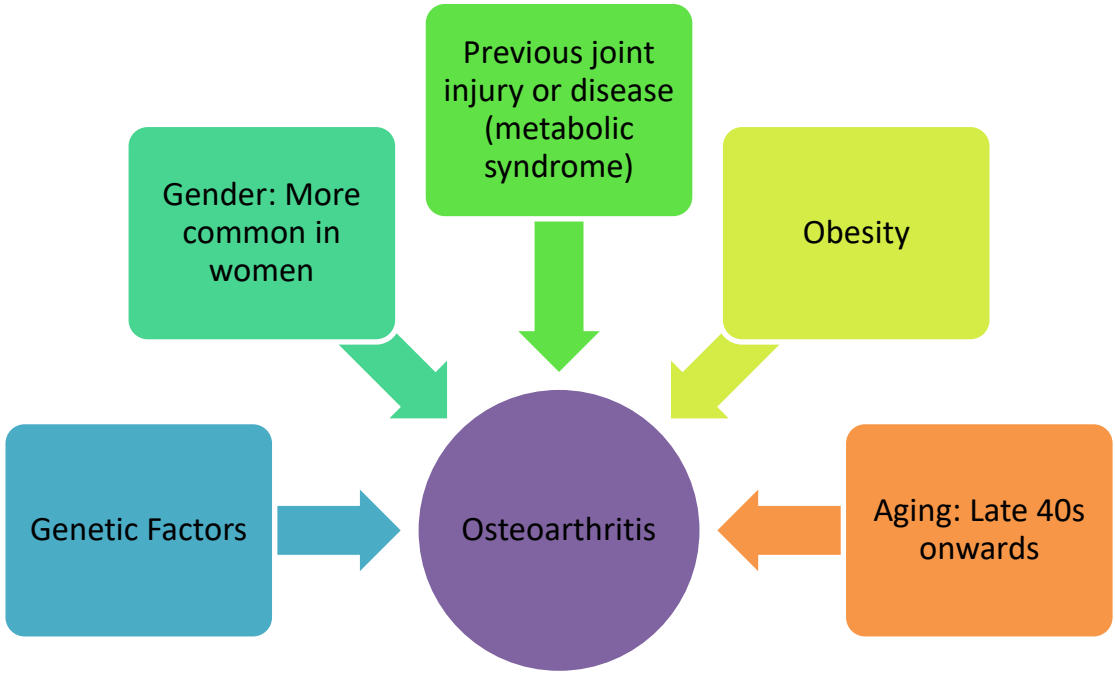

Figure 1.4. Risk factors for osteoarthritis.

Cartilage homeostasis is usually maintained by a balanced turnover between the anabolic and catabolic processes. In OA patients an imbalance between anabolic and catabolic factors produced by the chondrocytes, (in normal cartilage the maintenance of balance would be responsible for maintaining structural integrity of the tissue), occurs, in favour of the latter. Interestingly, an increase of the anabolic factors also occurs but is not sufficient to reverse tissue damage. During the progression of OA, an increase in the pro-inflammatory cytokines IL-1β, Tumour Necrosis factor α (TNF-α), IL-6 and IL-17 maintain the catabolic phenotype. (Mueller & Tuan 2011)

1.3 Matrix metalloproteinases and cartilage degradation.

Physiological and pathophysiological turnover can coexist in articular cartilage. Although there are distinct molecular mechanisms that mediate cartilage turnover leading to self-repair and regeneration of the ECM components, there are also those mechanisms that can lead to cartilage degeneration and the development of arthritis. In particular, inappropriate articular cartilage destruction in OA patients is largely the result of elevated expression and activities of proteolytic enzymes. (Goldring & Marcu 2009) Disturbance of cartilage homeostasis can lead to an increasing metabolic activity of chondrocytes and activation of the irreversible pathological processes causing cartilage erosion. The irreversibility of these processes is due to a very low regeneration rate of the basic ECM components; for example collagen has an

estimated half-life of over 100 years, and aggrecan with a more moderate regeneration rate has an estimated half-life of 3-24 years (Karsdal et al. 2008). Many proteases have been identified to play crucial roles in cartilage degradation, but serine proteinases and metalloproteinases are the only extracellular members and so are able to cleave cartilage components. In OA, these degradative enzymes are produced primarily by chondrocytes (Goldring & Marcu 2009) and also by synoviovytes (Wassilew wt al. 2010; Volk et al. 2003), due to inductive stimuli, joint injury with attendant destabilization, mechanical stress, oxidative stress, cell matrix interactions and changes in growth factor responses and matrix during aging. (Goldring & Marcu 2009)

Of the proteinases that can cleave cartilage collagens and proteoglycans, matrix metalloproteinases and aggrecanases have been given the greatest attention because they can degrade cartilage collagens and proteoglycans. (Cawston & Wilson 2006; Sandy 2006; Rengel et al. 2007) These include the collagenases MMP1, MMP8 and MMP13, the gelatinases (MMP2 and MMP9), stomelysin-1 (MMP3), and membrane type-1 (MMP14). (Murphy & Nagase 2008) Hence, a better understanding of the enzymes involved in cartilage degradation, in terms of their regulation and specific function, is a prerequisite in order to achieve successful specific pharmacological targeting.

1.3.1 Matrix metalloproteinases (MMPs).

The matrix metalloproteinase family (MMP) consists of 23 zinc and calcium dependent enzymes (endopeptidases) that are involved in the degradation of ECM components. Low expression of MMPs in healthy cartilage can contribute to cartilage remodelling and turnover. (Fox et al. 2009) However, there is now significant evidence for the overexpression of MMPs in tissues derived from patients with arthritic disease. In the development of OA, inflammatory cytokines such as IL-1 successfully bind to their receptors in chondrocytes, activating downstream pathways, for instance NF-κB and activator protein 1 (AP-1) that will up-regulate the expression of MMPs. (Kevorkian et al. 2004; Davidson et al. 2006)

MMPs can be classified into 5 distinct categories depending on their target-substrates, structure and cellular localisation (**Figure 1.5**): the matrilysins, collagenases, stromelysins, gelatinases and membrane type (MT)-MMPs. However, some MMPs for instance, MMP11, MMP12, MMP19, MMP20, MMP23 and MMP28 do not fall into any of these groups and some other, for example MMP14 belongs to more than one group. (Murphy & Nagase 2009)

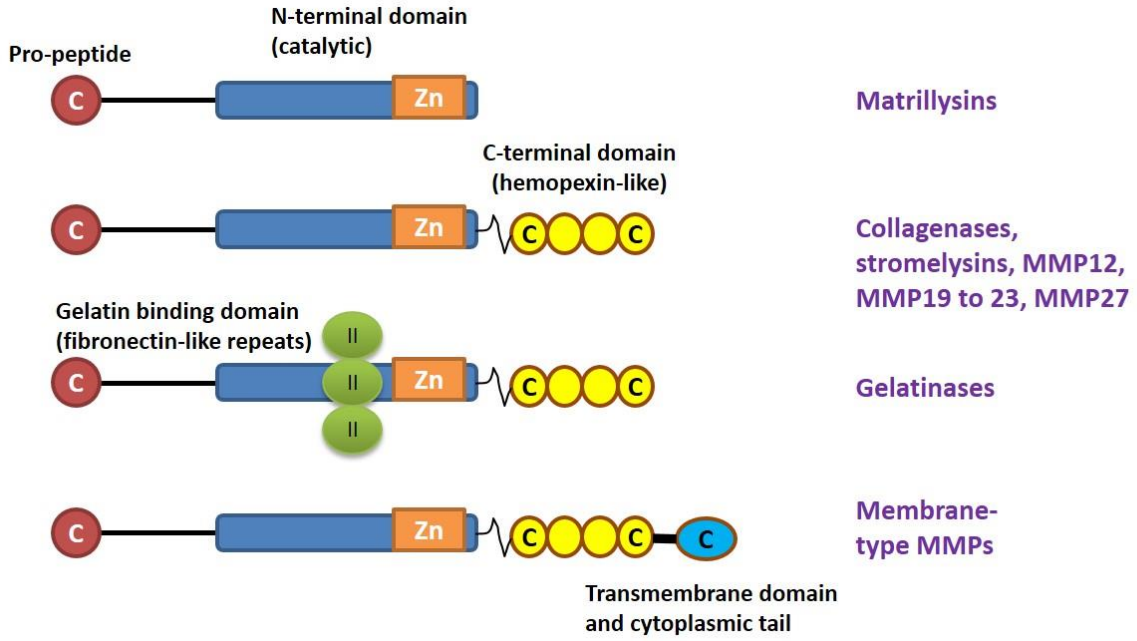

Figure 1.5. Basic structure of various matrix metalloproteinases (MMPs).

MMPs consist of a pro-peptide (red) that maintain the enzyme in a latent state, a catalytic domain (blue) with the active catalytic Zinc (Zn-orange), and with the exceptions of matrillysins a COOH-terminal domain (yellow) with homology to the serum protein hemopexin. The latter two domains are connected by a linker peptide. Gelatinases also have an insert of three fibronectin type II repeats (green) in the catalytic domain, which is involved in substrate recognition. Membrane type MMPs contain a transmembrane domain (black) and a cytoplasmic domain (blue) at the COOH- terminus, that anchors these enzymes in the cell membrane. Adapted from (Murphy et al. 2002).

There are three main collagenases; collagenase 1 (MMP1), collagenase 2, also called neutrophil collagenase (MMP8) and collagenase 3 (MMP13) (**Table 1.1**). (Murphy & Nagase 2009) They consist of a pro-petide, calatytic and hemopexin domain (**Figure 1.5**). They play an important role in cleaving collagen type I, II and III into characteristic ¼ or ¾ fragments, but they also have activity against other ECM molecules and soluble proteins. (Murphy & Nagase 2009) The catalytic domains of collagenases can cleave non-collagenous substrates, but they are unable to cleave collagen in the absence of their hemopexin domains (Chung et al. 2004).

In the context of pathological collagen degradation that characterise both rheumatoid arthritis (RA) and OA, collagenases are the most pertinent MMPs (Murphy et al. 2002). Kozaci et al. (1998) defined, in a tissue culture model system that MMP3, MMP8 and MMP13 are unlikely to be involved in proteoglycan degradation but play major roles in type II collagen degradation. MMP1 and MMP13 are both produced by the chondrocytes, but MMP1 is also produced by the synovial fibroblast which is one reason why it is thought that MMP1 is the

main collagenase in RA, whilst MMP13 is the main collagenase in OA. (Van Meurs 2017) However, other expression studies suggest that the amount of MMP1 produced by chondrocytes is 10 times more than the amount of MMP13 produced, and also these two collagenases co-localise peri-cellularly to chondrocytes, indicating that collagen proteolysis is driven by not only MMP13, but equally by MMP1 (Elliot et al. 2003). MMP13 also degrades aggrecan, giving it a dual role in cartilage degeneration. Moreover, MMP13 plays a key role in cartilage degeneration, since its expression can be induced by many pathways.

Interestingly, MMP13 knockout mice have been found to be somewhat resistant to cartilage degradation (in the presence of aggrecan deletion), when compared with wild-type littermates, using an OA surgical-induced mouse model (Little et al. 2009). Furthermore, postnatal overexpression of MMP13 in hyaline cartilages of the mouse resulted in an OA-like similar phenotype, with loss of proteoglycan and type II collagen cleavage and synovial hyperplasia. These findings suggest that MMP13 overexpression might lead to the progression of OA (Neuhold et al. 2001).

MMP8 and MMP14 can be collagenolytic and are expressed by cells within the synovial joints, but their contribution to cartilage degeneration has not yet been established. (Murphy & Nagase 2009) Other MMPs, such as MMP2, MMP3, MMP9, MMP10 and MMP19 are also elevated in arthritis and along with MMP13 these enzymes cleave non-collagen ECM components. (Cawston & Wilson 2006) Although, many MMPs have been associated with matrix turnover, other MMPs (MMP1, MMP2, MMP3, MMP9, MMP12, MMP13 and MMP19) are also linked to osteoclastic resorption and cleavage of non-collagenous proteins of the bone matrix and clearly play roles beyond ECM cleavage. (Andersen et al. 2004)

MMPs-Collagenases	**Other names**	**Substrate specificity**
MMP-1	Interstitial collagenase (Collagenases-1)	Collagen I, II, III, VII, VIII, X and aggrecan, gelatin, proteoglycan link protein
MMP-8	Neutrophil collagenases (Collagenase-2)	Collagen I, II, III, V, VII, VIII, X and aggrecan, gelatine, fibronectin
MMP-13	Collagenase-3	Collagen I, II, III, IV and gelatine, plasminogen activator inhibitor 2, aggrecan

Table 1.1. Collagenase activities and specific substrates. Adapted from (Murphy et al. 2002).

Gelatinases A (MMP2) and B (MMP9) share similar proteolytic activity and degrade ECM components such as type IV, V and XI collagens, laminin and aggrecan. MMP2 also has the ability to degrade collagens type I, II and III similar to collagenases, but MMP9 does not.

However, the collagenolytic activity of MMP2 is much weaker than MMP1 and any other collagenase in solution. (Murphy et al. 2002) Stromelysins (MMP3, MMP10 and MMP11) have the same structure as collagenases, though they are unable to cleave collagens. MMP3 and MMP10 can cleave some ECM molecules and participate in pro-MMP activation, but MMP11 has very weak proteolytic activity towards ECM components. Finally, matrilysins MMP7 and MMP26 lack the hemopexin domain and are both able to degrade several ECM components. (Murphy et al. 2002)

1.3.2. A Disintegrin and Metalloproteinase with Thrombospondin Motifs (ADAMTS).

Other proteases that have been implicated in articular cartilage damage are the ADAMTS (a disintegrin and metalloproteinase with thrombospondin motifs) proteases for example, ADAMTS4, ADAMTS5 and ADAMTS9 that are able to cleave matrix components including aggrecan, versican and brevican (Porter et al. 2006). ADAMTS5 knockout mice showed significant reduction in the severity of cartilage destruction after surgically destabilising the joint in comparison with wild-type mice. This was the first report of a single gene deletion capable of abrogating the course of cartilage destruction in an animal model of osteoarthritis and demonstrated that ADAMTS5 is the main aggrecanase in cartilage. (Glasson et al. 2005) Mice lacking both ADAMTS4 and ADAMTS5 showed resistant in cartilage degradation following surgical destabilisation and cartilage explants stimulated with IL-1 and retinoic acid showed decreased aggrecanase degradation to a level comparable with that in the ADAMTS5 knockout mice. (Majumdar et al. 2007) ADAMTS5 (-/-) joints also showed minor subchondral bone changes in contrast to wild-type mice where substantial changes were found (Botter et al. 2009) and were resistant to pain-related behaviour during the course of knee osteoarthritis (Malfait et al. 2010).

1.4 Proinflammatory cytokines.

Proinflammatory cytokines are potent regulators of numerous biological processes and are tightly regulated in the body. Chronic uncontrolled levels of such cytokines can initiate and derive many pathologies, including autoimmune diseases such as RA and cancer. (Rider et al. 2016) In particular, during the progression of OA, the catabolic phenotype is maintained by a number of pro-inflammatory cytokines, including Interleukin-1β (IL-1β) and tumor necrosis factor α (TNF-α), IL-6 and IL-17. The best studied cytokines in degenerative cartilage disease are IL-1β and TNF-α. (Mueller & Tuan 2011)

1.4.1 Interleukin 1 (IL-1).

The IL-1 family includes 7 ligands with agonist activity (IL-1α, IL-1β, IL-18, IL-33, IL36α and IL-36β), three receptor antagonists (IL-1Ra, IL-36Ra, IL-38) and an inflammatory cytokine IL-37. Members of the IL-1 receptor family include 6 receptor chains forming 4 signalling receptor complexes, two decoy receptors (IL-1R2, IL-18BP) and two negative regulators (TIR8 or SIGIRR, IL-1RAcPb). A tight regulation via receptor antagonists, decoy receptors and signaling inhibitors ensures a balance between amplification of innate immunity and uncontrolled inflammation. IL-1 affects cells of the innate and adaptive immune system and exerts a wide variety of biological functions including promoting fever, vasolidation, haematopoiesis, lymphocyte activation, leucocyte attraction and extravasation, angiogenesis and antibody synthesis (Garlanda et al. 2013)

Despite a low percentage homology (only 26%), IL-1α and IL-1β activate the same cell surface receptor and have a practically identical range of biological activities. (Afonina et al. 2015) Interestingly, IL-1β but not IL-1α deficiency was shown to result in impaired febrile and acute-phase inflammatory responses in a turpentine-induced model of local inflammation and tissue injury. On the other hand IL-1α has been uniquely implicated in initiating sterile inflammation in response to dying cells by inducing neutrophil recruitment, whereas IL-1β has been shown to recruit macrophages only in a later phase. (Afonina et al. 2015)

Both IL-1α and IL-1β are synthesized as precursor proteins that are post-translationally cleaved to the active forms (17kDa each) and can be produced by synovial cells, osteoblasts, endothelial cells and a number of other cells. Their production can be triggered by other cytokines, microorganisms, endotoxins and other antigens. In response to ligand binding of the receptor, a complex sequence of combinatorial phosphorylation and ubiquitination events results in activation of nuclear factor kappaB signaling and the JNK and p38 mitogen-activated protein kinase pathways, which, cooperatively, induce the expression of canonical IL-1 target genes (such as IL-6, IL-8, MCP-1, COX-2, I kappa B alpha, IL-1 alpha, IL-1 beta, MKP-1) by transcriptional and posttranscriptional mechanisms. Of note, most intracellular components that participate in the cellular response to IL-1 also mediate responses to other cytokines (IL-18 and IL-33), Toll-like-receptors (TLRs), and many forms of cytotoxic stresses. (Weber et al. 2010)

IL-1β is the most well studied cytokine in OA and is found in the synovial fluid of OA patients and is expressed by the synovial tissue and the chondrocytes (Mueller and Tuan, 2011). The level of IL-1β is increased in the OA joint. IL-1β has been proven to be associated with an increase in the expression of matrix-degrading enzymes and also decrease the

synthesis of ECM components by the chondrocytes (Mueller and Tuan, 2011). Interestingly, intra-articular injection of IL-1β in rabbit knee joints induces proteoglycan loss. These effects of IL-1β are mediated by receptor IL-1RI, whose density is increased in OA cartilage, which in turn increases the sensitivity of chondrocytes to IL-1β. IL-1β and TNF-α alone or synergistically, can inhibit synthesis of collagen and proteoglycans by the chondrocytes and induce the production of degrading enzymes. (Cawston et al. 2003)

1.4.2 Tumour Necrosis Factor α (TNF-α)

TNF-α acts synergistically with IL-1β to suppress ECM synthesis and stimulate the expression of matrix-degrading enzymes. Both IL-1β and TNF-α, alone or in combination, inhibit synthesis of proteoglycan and collagen in chondrocytes.(Saklatvala 1986; Goldring et al. 1988) Blocking TNF-α and/or IL-1β decrease the degeneration of collagen II and aggrecan and also decrease the expression of MMPs. (Kobayashi et al. 2005) In response to stimulation by catabolic cytokines, chondrocytes produce more prostaglandin E2, and bone morphogenetic protein-2 (BMP-2), both of which increase type II collagen expression. This can be interpreted as an attempt by the chondrocytes to compensate for the increased loss of ECM. (Fukui et al. 2003)

1.4.3 IL-1-mediated cell signalling pathways.

There are many pathways that are directly regulated by cytokines such as IL-1, IL-17 or TNF-α. These include the mitogen- activated protein kinases (MAPK), nuclear factor-κB (NF-κB), activator protein- 1 (AP-1), the Janus kinase/ signal transducers and activators of transcription (JAK/STAT) pathway and the phosphatidylinositol 3-kinase (PI3K) pathway. (Rowan & Young 2007)

NF-κB family of transcription factors includes five members: p50, p52, p65, c-Rel and RelB that homo- or hetero-dimerize to provide differential biological effects. Of these only p65, c-Rel and RelB have c-terminal transactivation domains, which contain binding sites for other co-regulators. (Panday et al. 2016) The key event in NF-κB activation is the phosphorylation and subsequent ubiquitination and degradation of IκB inhibitory protein. The classical NF-κB pathway is activated in response to cytokines including IL-1 and TNFα or bacterial products (lipopolysaccharides, LPS) which activate the inhibitory κB kinases (IKK). IKKβ phosphorylates IκBα at serine 32 and 36, resulting in poly-ubiquitination and degradation by the 26S proteasome. This release of NF-κB, classically p50:p65 heterodimers, from its

inhibitor IκBα, leads to NFκB nuclear translocation and subsequent gene target activation (Pereira and Oakley, 2007). More than 150 genes are regulated by NF-κB family of transcription factors and involved in inflammation, immunity, cell proliferation, differentaition and survival (Panday et al. 2016). Importantly, it has been proposed that NF-κB has transcriptional regulation over MMP1 and MMP13 collagenases and blocking the NF-κB pathway reduce *MMP1* and *MMP13* expression in synovial fibroblasts and human and bovine chondrocytes in response to IL-1 (Liacini et al. 2002). Interestingly, DNA-bound p50 and p52 homodimers and heterodimers repress κB- mediated transcription by preventing the binding of transcriptionally active NF- κB dimers or through recruitment of deacetylases (Zhong et al. 2002). Indeed, Elshakrawy and colleagues (Elsharkawy et al. 2010) showed that the p50:p50:HDAC1 repressory complex inhibits multiple pro-inflammatory genes including *CCL2*, *CXCL10*, *Gm-CSF* and *MMP13* and binding of both p50 and HDAC1 has been detected in their gene promoters in wild type normal cells, but not in nfkb1(-/-) cells.

IL-1 can also trigger the phosphorylation of important kinases including mitogen activated protein kinase (MAPK) pathways. Activation of MAPK will result in a series of phosphorylation cascades that culminate in the activation of effector molecules such as transcription factors that induce transcription of target genes. There are three distinct pathways that are encompassed within MAPK activation: i) extracellular-signal regulated kinase (ERK), ii) Jun N-terminal kinase (JNK) and iii) p38 kinase. These specific pathways are involved in the transduction of the pro-inflammatory cytokine IL-1 signal that causes collagenase expression and cartilage degradation. JNK and p38 kinase, in addition to NF-κB signaling pathway, have been implicated in the regulation of *MMP1* and *MMP13* expression in human articular chondrocytes (HACs). (Mengshol et al. 2002) Mengshol and colleagues (2002) further demonstrated the importance of these three MAPK pathways in the regulation of *MMP1* and *MMP13* expression in the SW1353 chondrosarcoma cell line. For example inhibition of p38 kinase by SB 203580 blocked IL-1 mediated *MMP13* expression in HACs and the SW1353 cell line, with similar effects on *MMP1* in the SW1353 cells (Mengshol et al. 2002). Furthermore, JNK inhibition led to a 60% decrease of *MMP13* expression in SW1353 cell, with no significant effect on *MMP1* expression. Also pharmaceutical inhibition of JNK pathway decreased joint destruction in a rat arthritis model in part due to decreased *MMP1* expression (Han et al. 2000). The mechanism of action on MMPs expression by these three pathways is not yet clear. The JNK MAPK pathway activates c-Jun and NF-κB pathways, both of which can activate the expression of MMPs, while the ERK and p38 MAPK pathways can activate STAT (Rowan & Young 2007)

BMPs, members of TGF-β superfamily of proteins are directly affected by IL-1 cytokines. In particular, BMP-2, BMP-7 and BMP-4 are the most well studied BMPs in terms of their expression in articular cartilage. BMP-2 is up-regulated in OA patients by IL-1, resulting in an increase in the expression of type II collagen. In healthy articular cartilage, BMP-7 would promote biosynthesis of ECM molecules, but is down-regulated in OA chondrocytes (Fukui et al. 2003; Drissi et al. 2005). Although the expression of BMPs is highly dependent on IL-1 and TNF-α cytokines, there are also some BMPs antagonists, such as gremlin and follistatin, that regulate the levels of BMPS, by binding to BMPs receptors (Mueller & Tuan 2011).

Fibroblast Growth factors (FGFs) act mainly through the NF-κB signalling pathway depending on the receptor they bind. In terms of OA, FGF-2 and FGF-18 have been extensively studied. FGF-2 binds the FGF receptor type 1 and act mainly as a catabolic factor for cartilage homeostasis by activating NF-κB downstream signalling pathways. Whereas, FGF-18 binds to FGF receptor type 3 and has clearly anabolic effects in matrix components biosynthesis (Mueller and Tuan, 2011).

1.5 Immediate Early genes and the Activator-Protein 1 family of transcription factors.

Immediate early genes (IEG) encode a plethora of transcription factors that control cell proliferation, differentiation and survival by altering specific transcriptional programs. Most of them share common characteristics; for example, they have an abundance of RNA polymerase II at their promoters, high affinity TATA boxes, small exon numbers and are rapidly induced usually after only 30min-1h of growth factor/cytokine/interferon stimulation without the requirement for protein synthesis. (Hargeaves et al. 2009) In addition, IEG are believed to have a characteristic chromatin structure. Several studies had shown that acetylation at histone H3 lysine 9 and 14 remain consistently present prior to and after gene expression stimulation, and thereby generating a constitutively permissive and open to transcription factors structure. (Healy et al. 2012)

Many of the critical targets of the signalling cascades that are activated by cytokine or growth factor stimulation are transcription factors which then regulate secondary response genes. IEG induction is mediated by one of the two mitogen-activated protein kinase (MAPK) signalling pathways: either the RAS-MAPK pathway which is activated by growth factor stimulation and mitogens and results in activation of extracellular signal related kinase 1 and 2 (ERK1/2) or the p-38 MAPK pathway, which is activated by UV or stress (McCay and Morrison, 2007).

Both of these pathways results in the phosphorylation and activation of regulatory proteins involved in IEG expression, including members of the ETS- domain family (such as ELK1 and ETS1/2, which bind to the IEG promoter and complex with lysine acetyltransferases), regulatory factors such as the SRF and mediator complex which are essential for IEG induction (Fowler et al. 2011)

Two of the most well characterised IEG are the *FOS* (*c-fos*) and *JUN* (*c-jun*) that belong to the Activated-Protein 1 (AP1) family of transcription factors. These genes form a heterodimer *c-jun/c-fos* complex that is necessary for the induction of AP1-responsive target genes (Rowan and Young, 2007). It has been proposed that AP-1 DNA binding sites within the promoters of *MMP1* and *MMP13* are important for regulating expression of these genes in chondrocytes. The MMP1 promoter is activated by Jun complexes as well as the Fos/Jun heterodimer, whereas MMP13 induction by IL-1 requires c-Fos (Benderdour et al. 2002). MMP3 and MMP9 are also positively regulated by c-Fos containing AP-1. Interestingly, co-transfection studies that were performed to reveal the transcriptional effect of *c-jun* showed that *c-jun* transcriptional activity can be amplified by *c-fos* and also that the *c-jun/c-fos* complex is more active as a transcriptional activator than *c-jun* alone. Litherland et al, (2010) also showed that silencing of *c-fos* and *c-jun* expression was sufficient to abrogate IL-1 and Oncostatin M (OSM) stimulated collagenase expression and over-expression of *c-fos* and *c-jun* was sufficient to induce transcription of the *MMP1* in the absence of stimulus. Interestingly, histone deacetylases (HDACs) which are involved in gene silencing are upregulated in FOS-transformed cells and are required for c-Fos dependent invasion. (McGarry et al. 2004)

1.6 Epigenetic modification and gene expression regulation

1.6.1 Chromatin remodelling

Chromatin is the complex of DNA and proteins (mainly histones) that condense to form a chromosome during cell division. The compaction also helps to package DNA to fit into the cell nucleus. (Nishibuchi & Déjardin 2017) The basic repeating unit of chromatin is the nucleosomes. In each nucleosome, 146 base pairs of DNA is wrapped around an octamer of core histone proteins formed by four histone partners: an H3-H4 tetramer and two H2A- H2B dimers. Structural changes in chromatin control gene expression. Histones are basic proteins consisting of a globular domain and a charged NH_2-terminus (histone tail) that protrudes from the nucleosome.(Jenuwein & Allis 2001) Epigenetics is the study of heritable changes in gene

activity that are not caused by changes in the DNA sequence. For example histone modifications, DNA methylation or phosphorylation alters chromatin structure to facilitate gene transcription (Kim & Kaang 2017). Chromatin remodelling that occurs during development will erase almost every epigenetic tag from the parents to the offspring, but a small minority of epigenetic marks will remain through to the next generation unchanged. A characteristic example is genomic imprinting during which some genes keep their epigenetic marks and will start the process of development with those epigenetic tags in place (Kouzarides 2007).

At least eight different categories of epigenetic post-translational histone modifications have been identified and more than 60 different sites where modifications can take place have been found. Enzymes that are responsible for acetylation, methylation, phosphorylation, ADP-ribosylation, deimination, ubiquitination and proline isomerisation have been determined and the modifications they mediate function either by disrupting chromatin contacts or by remodelling chromatin structure making it more or less accessible to transcription factors and other non-histone proteins (**Figure 1.6**). (Kouzarides 2007) Thus, the nature of histone amino-termini modifications revealed a 'histone code' hypothesis which predicts that the modification marks on the histone tails should provide binding sites for effector proteins which allow regulatable contacts with the underlying DNA. The enzymes mediating these histone tail modifications are highly specific for particular amino acid positions and modifications on the same or different histone tails may be independent and generate various combinations on any nucleosome. (Jenuwein & Allis 2001) However, under different conditions many modifications can determine expression or repression, adding complexity to the concept of a code. (Kouzarides 2007)

The timing of the appearance of each chromatin modification depends on the signalling conditions within the cell. For example for actively transcribed genes, it has been found that acetylation of histone H3K9/K14 is enriched in the promoter and the 5'- UTR of the coding regions. Whereas, acetylation of H2BK16, H4K8 and K16 within and 3'-UTR of coding regions were not correlated with transcription. It is generally believed that a modification occurs in a genetic region under certain conditions (for example when a gene is transcribed) and this state is reversed when the gene is silent. (Liu et al. 2005)

Histone methylation can either occur in a lysine or arginine and may be one of many different forms: mono-, di-, or tri- methyl for lysines and mono-, or di-methyl for arginines. It is mediated by enzymes called histone methyltransferases and histone demethylases. Three methylation sites are implicated with the activation of transcription: H3K4, H3K26 and

H3K79, and three are associated with transcriptional repression: H3K9, H3K27 and H4K20. (Kim & Kaang 2017)

Little is known about histone phosphorylation and gene expression. MSK1/2 and RSK2 in mammals, and SNF1 in budding yeast, have been shown to target H3S10. A role for H3S10 has been demonstrated in regulating NF-κB-regulated genes and also for immediate early genes such as *c-fos* and *c-jun* by allowing phospho-binding of 14-3-3 protein on chromatin. (Macdonald et al. 2005)

Ubiquitination has been found on H2A (K119) and H2B (K120 in humans) and linked to both transcriptional activation (H2BK120) and repression (H2AK119). It is unclear how ubiquitination functions; it might recruit additional factors to chromatin or physically keep chromatin 'open', due to its large size. (Wang et al. 2006)

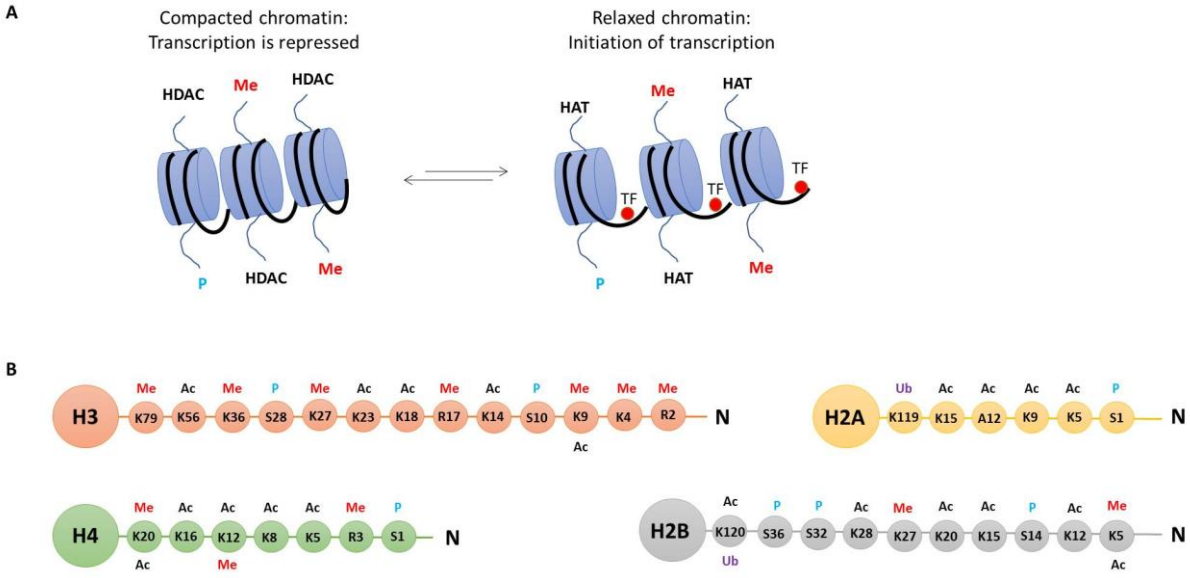

Figure 1.6. Transcription process and its regulation by histone modifications.

A. Schematic representation of a nucleosome (bue-purple). DNA (black) is wrapped around the nucleosome. Dark blue represents histone tails that can be post-translationally modified by HDAC/HAT complexes, methyltransferases/demethylases (Me) or phosphorylases (P). Red circles represent transcription factor binding. Transcriptional activation or repression in chromatin depends on a combination of histone modifications. **B.** Epigenetic modifications identified on histone N-tail domains. Adapted from (Bannister & Kouzarides 2011).

1.6.2 Acetylation of histones

Acetylation of histones is probably the most well understood modification, with hyperacetylation to be associated with an increase in gene transcription and hypoacetylation to have the opposite effect. Alfrey et al. (Allfrey et al. 1964) first reported histone acetylation in 1964. Since then, it has been shown that the acetylation of lysines is a highly dynamic process and regulated by two families of enzymes, the histone acetyltransferases (HATs) and histone deacetylases (HDACs). The HATs utilize acetyl CoA as a cofactor to catalyse the transfer of an acetyl group in the ε-amino group of lysines. (Bannister & Kouzarides 2011) Important acetylation sites are K9 and K14 on histone H3 and K5, K8, K12 and K16 on histone H4. (Nishibuchi & Déjardin 2017) Acetylation neutralizes the lysine's positive charge. This action favors an open chromatin structure and releases the histone tails from the linker DNA, make it accessible by transcription factors. Chromatin regions that are marked by acetylated lysines catalysed by HATs are generally more actively transcribed, whereas genomic regions that are bound by HDACs are inactive (**Figure 1.6 A**). (Bannister & Kouzarides 2011)

There are two major classes of HATs: type A and type B. The type B are mainly cytoplasmic acetylating free histones and not those already compacted into chromatin. This class of HATs are highly conserved and all type B HATs share homology with HAT1. The type A HATs are a more diverse group of enzymes than type B and can be further classified into three categories depending on amino-acid sequence homology and conformational structure: GNAt, MYST and CBP/p300 families. Type A HATs are structural components of multiprotein co-activatory or co-repressory complexes. These complexes may act either in a site-specific manner, when they are recruited by specific binding activators on the DNA or in a broad manner whereby they function in larger genomic areas. (Kretsovali et al. 2012) For example, purified GCN5 acetyltransferase acetylates free histones, but not those present within a nucleosome. However, when it is part of the SAGA complex, it efficiently acetylates nucleosomal histones. (Grant et al. 1997)

1.6.3 Histone Deacetylases (HDACs).

The histone deacetylase (HDAC) family involve four classes. Class I HDACs include HDAC1, 2, 3 and 8 and these members are more closely related to the yeast transcriptional factor RPD3. Class II HDACs involve HDAC4, 5, 6, 7, 9 and 10 and these are more closely related to HDA1, another deacetylase found in yeast. Class III HDACs are also refered to as

sirtuins and are homologues to yeast Sir2. This class of HDACs, in contrast to the other three classes of HDACs, requires the co-factor NAD^+ for their activity- importantly they are not inhibited by the broad-spectrum HDAC inhibitor TSA. Finally class IV HDAC contain only one member HDAC11, which has low sequence similarity with all the other HDACs. HDACs oppose the effect of HATs by removing acetyl-groups from histone tails, restoring their positive charge. This stabilizes the local chromatin architecture and is consistent with HDACs being predominantly transcriptional repressors. (Bannister & Kouzarides 2011) Contrary to their consideration as repressors, HDACs can also induce transcription as it was found for some selected interferon-stimulated early response genes (Sakamoto et al. 2004).

Class I HDACs are expressed in most cell types whereas class II HDACs have a more restricted pattern of expression indicating a possible contribution to differentiation and developmental processes. Most class I HDACs have a nuclear localisation signal (NLS), thus they can be found in the nucleus where they exert their function. However some class I HDACs, for example HDAC3 have a nuclear export signal (NES) and can be also found in the cytoplasm. Class II HDACs on the other hand can be found either in the nucleus or out in the cytoplasm depending on certain cellular signals (De Ruizter et al. 2003). Despite their name, histone deacetylases, especially those that carry a nuclear export signal have non-histone targets-substrates such as tubulin (Kretsovali et al. 2012), thus they are occasionally termed more generally as lysine deacetylases (KDACs). In general, HDACs have relatively low substrate specificity by themselves. Instead, HDAC recruitment and specificity is usually mediated by multi-protein complexes often with more than one HDAC members. For instance HDAC1 is found together with HDAC2 within the NuRD, Sin3A and co-REST complexes. (Bannister & Kouzarides 2011)

Analysis of knockout (KO) mice lacking Hdac revealed their functions during mammalian development and differentiation (see **Table 1.2** for class I Hdac KO). For example deletion of Hdac1 is embryonic lethal by embryonic day 9.5 (E9.5) due to cell proliferation and growth defects (Lagger et al. 2002). Although, cardiac- specific deletion of Hdac1 had no significant effect due to functional redundancy with Hdac2, conditional deletion of both Hdac1 and Hdac2 from the heart induced lethality due to cardiac arrhythmias, dilated cardiomyopathy and up-regulation of genes encoding encoding skeletal muscle-specific contractile proteins and calcium channels (Montgomery et al. 2007). Global Hdac3 deletion is also embryonic lethal due to deficient gastrulation that is potentially connected to failure of the DNA damage repair mechanisms (Bhaskara et al. 2011). Also conditional tissue-specific deletion of Hdac3 has pointed to an involvement in liver (Knutson et al. 2008)and heart (Montgomery et al.

2008) function, as well as in bone formation (Razidlo et al. 2010) and very recently in endochondral ossification (Carpio et al. 2016). Finally, global and conditional deletion of Hdac8 in cranial neural crest cells leads to lethality due to skull instability (Haberland, Montgomery, et al. 2009).

Class I Hdac KO	Loss of function phenotype	Time of lethality of knockouts	Reference
Hdac1	Growth retardation and proliferation defects	E10.5	Lagger et al. 2002
Hdac2	Cardiac malformation	P1	Montgomery et al. 2007
cKO Hdac1/Hdac2-Heart	Functional redundancy in the heart, brain, endothelial cells, smooth muscle and neural crest cells	Viable, due to functional redundancy postnatally and in adulthood	Montgomery et al. 2007
Hdac3	Gastrulation and DNA repair defects	E9.5	Bhaskara et al. 2010
cKO Hdac3-Bone (skeleton)	Impaired intramembranous and endochondral ossification, thinner calvarial bones, smaller size of long bones, shorter lifespan, more adipocytes than osteoblasts	Mostly before weaning	Razidlo et al. 2010
icKO Hdac3-Liver	Hepatomegaly-Lipid and cholesterol homeostasis disrupted	Viable	Knutson et al. 2008
icKO Hdac3-Heart	Diet (high fat) induced- hypertrophic cardiomyopathy and heart failure	Die within weeks (if high fat diet)	Sun et al. 2011
cKO Hdac3-Cartilage	Embryonic lethal	Between E12.5 and E16.5	Carpio et al. 2016
icKO Hdac3-Cartilage	Delayed secondary ossification centre formation, altered maturation of growth plate chondrocytes and increased osteoclast activity in the primary spongiosa	Viable	Carpio et al. 2016
Hdac8	Affects intramembranous ossification-Craniofacial defects	P1	Haberland et al. 2009

Table 1.2.Class I Hdac Knockout mouse models. cKO: conditional Knockout, icKO: inducible conditional Knockout.

HDAC4 is found to regulate skeletogenesis and knockout mice die in the first weeks postnatal due to premature endochondral ossification of cartilage which interferes with breathing (Vega et al. 2004). HDAC5 and HDAC9 control cardiac development in a redundant manner, since single knockout mice are viable, though the double knockout mutant is lethal due to defects in cardiac development (Chang et al., 2004). HDAC7 is specifically expressed in the endothelial

cells of the cardiovascular system (Chang et al. 2006) and HDAC6 and HDAC10 regulate cytoskeletal dynamics by controlling the acetylation of cytoskeletal proteins such as tubulin (Q. Zhang et al. 2008).

1.6.4 Histone Deacetylase 3 (HDAC3).

HDAC3 belongs to class I HDACs, is a 428 amino acid (aa) protein with an estimated molecular mass of 49 kDa and shares 53% of aa sequence similarity with HDAC1 and 52% homology with HDAC2. HDAC3 is ubiquitiously expressed and shares common features with HDAC1 and HDAC2, such as deacetylation of histone substrates and transcriptional repression when targetted to promoters. (Yang et al. 1997; Karagianni & Wong 2007) Apart from the role of class I HDACs on deacetylating histone tails and playing a role in transcriptional repression when binding to a promoter, HDAC3 can also associate with YY1 DNA- binding factor and increase its repression activity (Dangond *et al.,* 1998; Yang *et al.,* 1997; Emiliani *et al.,* 1998). However, HDAC3 has a unique C-terminus that shares no apparent similariy with other HDACs indicating it may not be completely redundant with other HDACs. This is also suggested by the differential localization of HDAC3, which through its nuclear export signal (NES) can be found apart from the nucleus, in the cytoplasm and plasma membrane. (Yang et al. 2002)

Through its association with the silencing mediator for retinoic acid and thyroid hormone receptor (SMRT) and/or nuclear receptor co-repressor (N-CoR), HDAC3 is recruited to specific promoters where it deacetylates histones and mediates silencing of corresponding genes. Other components of this complex include the transducing β-like 1 (TBL1), the TBL1-related protein (TBL1R1) and the G protein pathway suppressor 2 (GPS-2) (**Figure 1.7**). (Millard et al. 2017) Both TBL1 and TBLR1 interact directly with N-CoR and SMRT but not with HDAC3 and are not required for HDAC3 enzymatic activity. Histone deacetylation by HDAC3 and N-CoR/SMRT causes transcriptional repression in two ways. First, the removal of acetyl-groups increases the affinity of histone tails to the DNA backbone, which yields a closed chromatin conformation intractable to transcription and second by reducing the recruitment of bromo-domain co-activators, such as chromatin associated proteins and HATs that typically bind the acetyl lysine motifs and promote transcription. (McQuown & Wood 2011)

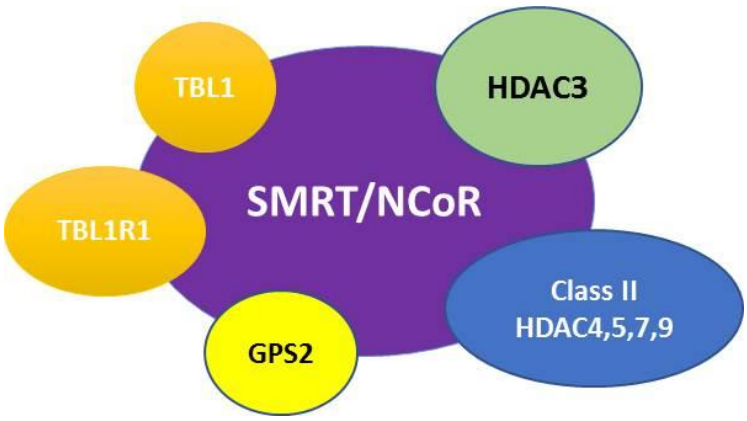

Figure 1.7. HDAC3 interacts with the SMRT and/or N-CoR co-repressors (complex of SMRT and N-CoR shown in purple) to silence gene transcription. TBL1, TBLR1 and GPS2 interact directly with SMRT/NCoR but not with HDAC3.

SMRT/ NCoR is unique among the class I HDAC complexes in terms of it also recruits the class II HDAC4/ 5/ 7 and 9. The role of the class II HDACs in this complex has yet to be established. Adapted from (Millard et al. 2017).

The existence of different HDACs and HDAC complexes has raised the question of potential specificity in their target-substrates and functions. In particular, Johnson et al. showed that HDAC3 completely deacetylates H2AK5, H4K5 and H4K12, but only partially deacetylate H3, H2B, H4K8 and H4K16.Compared with HDAC1, HDAC3 also deacetylated H4K8, H4K16 and H2B at the same rate, but it deacetylated H4K5, H4K12 and H2AK5 much more rapidly. (Johnson et al. 2002) Interestingly, the enzymatic activity of HDAC3 has also been shown to be regulated by phosphorylation at Ser424 by CK2 (Casein kinase 2) and dephosphorylated by serine/threonine phosphatase 4. (Zhang et al. 2005) In addition to protein-protein interactions and phosphorylation, subcellular localization may serve as another regulatory mechanism for HDAC3. For example, export of N-CoR to the cytoplasm in response to IL-1β stimulation has been proposed as a mechanism of de-repression of a set of NF-κB regulated genes (Baek et al. 2002). The reverse process, nuclear translocation of HDAC3 has been described as a mechanism of inhibition of PPARγ by TNFα. Cytoplasmic HDAC3 was shown to associate with IκBα and TNFα-treatment induced degradation of the latter and HDAC3 release, allowing it to enter the nucleus and repress PPARγ (Gao et al. 2006).

Apart from histone tails substrates, HDAC3 also targets non-histone proteins indicating its role extends beyond direct transcriptional regulation. One such target is the NF-κB protein RelA. HDAC3 has been shown to inhibit NF-κB signaling by deacetylating RelA which triggers its nuclear export via interaction with inhibitory IκB (Chen et al. 2001). Other non-

histone substrates include the myocyte enhancer factor 2 (MEF2) as well as the acetyltransferases PCAF and p300/CBP. (McQuown & Wood 2011)

In vivo studies showed that *HDAC3* is necessary for normal embryonic development since global knockout of Hdac3 was embryonic lethal by embryonic day E9.5 due to gastrulation defects. Also a conditional knockout mouse expressing Cre recombinase under the control of osterix promoter revealed the role of Hdac3 in bone formation. The resulted conditional knockout (cKO) mice had severe deficits in intramembranous and endochondral ossification. Moreover, calvarial bones were severely thinner and the trabecular volume of femurs was decreased by 75% in the Hdac3 cKO. Fewer osteoblasts and more bone marrow adipocytes were also detected in the cKO when compared with wild-type or heterozygous littermates. Microarray analysis also revealed that many developmental signaling pathways were affected by the Hdac3 deficiency, indicating in this way that Hdac3 is an important regulator of normal skeletal development. (Razidlo *et al.,* 2010). More recently, Carpio et al. supported that *HDAC3* is important for normal endochondral ossification and Hdac3 deficient chondrocytes exhibited reduced abundance of chondrogenic genes such as *COL2α1*, *Ihh*, *ACAN* and *COL10α1*. (Carpio et al. 2016)

1.6.5 Histone deacetylase inhibitors (HDACi).

As described above, the perceived mechanism of action of HDACs involve removing acetyl groups from histone tails resulting in the DNA wrapping tighter around the nucleosome, hence diminishing accessibility of transcription factors. HDAC inhibitors (HDACi) were discovered as various structurally diverse compounds that bind to the active site of HDACs, displacing the zinc and blocking substrate access, usually in reversible manner. (Bose et al. 2014) Different classes of HDACi based on structure include the hydroxamates (ie. Trichostatin A), fatty acids, benzamides (ie. MS-275) and cyclic peptides (ie. Apicidin) (**Figure 1.8**). (New et al. 2012)

Trichostatin A (TSA) is the most well-known reversible HDAC inhibitor (HDACi). Yoshida and his colleagues first reported (Yoshida et al. 1990) TSA as a *Streptomyces* product which could inhibit the cell cycle of rat fibroblasts in the G1 and G2 phases at very low concentrations. Like most other HDAC inhibitors, TSA has the optimal conformation to fit into the active site of HDACs and inhibit their function. All HDACs are thought to be equally sensitive to inhibition by TSA in low (nanomolar) concentration. The benzamide class of HDACi show more selectivity towards inhibiting the class I HDACs. Such an inhibitor is

Chidamide which has been recently licensed for treating T-cell lymphoma (Lu et al. 2016) Another HDACi that shows more selectivity is RGFP966, which selectively targets HDAC3 over HDAC1 and HDAC2. (Millard et al. 2017) Apicidin is another class I selective HDACi which preferentially inhibits HDAC3 in *in vitro* experiments (in the nanomolar range) over HDAC2 and HDAC1. (Khan & Davie 2013)

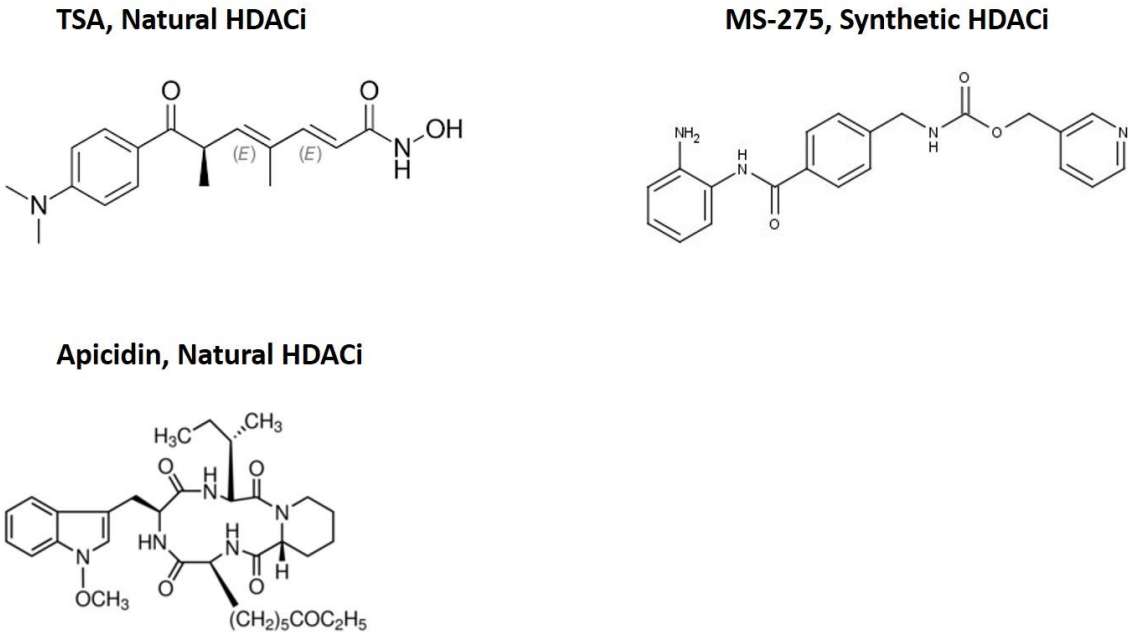

Figure 1.8. Representative structures of HDACi used in this study.

The major clinical application of HDACi has been in the treatment of cancer where they cause terminal differentiation and apoptosis of cancer cells. HDACi have been approved for clinical use (**Table 1.3**), others are currently in clinical trials or in preclinical development. SAHA (vorinostat) and FK228 (romidepsin) for example were licensed for the treatment of advanced cutaneous T-cell lymphoma. (Bose et al. 2014) Belinostat and panbinostat have also been recently approved for the treatment of peripheral T-cell lymphoma and multiple myeloma respectively. (Poole 2014; VanderMolen et al. 2011) Givinostat is currently in clinical trial for haematologic malignancies, for example Hodgkin lymphoma and multiple myeloma and has also been shown to reduce the production of pro-inflammatory cytokines in vitro and systemic inflammation in vivo. (Losson et al. 2016) HDACi have been also used in neurology for many years as mood stabilisers and anti-epileptic cards, with valproic acid being the most prominent amongst them. (New et al. 2012)

Furthermore mocetinostat and entinostat are two examples of benzamides currently in clinical studies for the treatment of Hodgkin lymphoma. Valproic acid is a short chain fatty acid which has been used in the treatment of epilepsy for more than two decades and it was shown that it has beneficial effects in solid tumours including neuroblastomas, neuoroendocrine carcinomas, glioblastomas and in cervical cancer. Another 32 HDACi are currently in clinical trials in the USA (https://clinicaltrials.gov/), and UK (https://www.ukctg.nihr.ac.uk/).

HDACi	Indication	Licencing body	Year licensed	Reference
Vorinostat (Zolinza)	Cutaneous T cell lymphoma	FDA	2007	Mann et al. 2007
Romidepsin (Isodax)	Cutaneous T cell lymphoma	FDA	2011	VanderMolen et al. 2011
Belinostat (Beleodaq)	Peripheral T cell lymphoma	FDA	2014	Poole et al. 2014
Panbinostat (Farydak)	Multiple myeloma	FDA/EMA	2016	Raedler et al. 2016
Chidamide (Epidaza)	Peripheral T cell lymphoma	Chinese FDA	2016	Lu et al. 2016

Table 1.3. HDACi licenced for clinical use. Adapted from (Millard et al. 2017).

1.7 The Retinoblastoma protein and E2Fs regulate the cell cycle.

1.7.1 The Retinoblastoma (Rb) protein

The Retinoblastoma gene, Rb1 or Rb, was the first tumour suppressor gene to be identified in humans. Studies following the inheritance patterns of a pediatric tumor of the retina, showed that deletion or mutation of chromosome 13q14.1-13q14.2 could result in retinoblastoma and patients could also be victim of a secondary non-ocular tumor, such as osteosarcoma. (Cavenee et al. 1983; Friend et al. 1986) These studies also showed that mutation in the Rb gene could be hereditary and also occur during gametogenesis. The Rb gene encodes for a nuclear phosphoprotein with weak DNA binding activity. (White et al. 1983) It was found that the Rb can form stable protein-protein complexes with viral oncoproteins of adenovirus E1A and SV-40 T-antigen, both of which form tumour in rodents, in addition to the human

papilloma virus (HPV) E7, which causes cancers in humans. (Ludlow et al. 1989; Dyson et al. 1989)

Rb is one of three proteins of the pocket protein family made up of Rb (p105), p107, and p130. The common pocket domain is used to bind to viral oncoproteins, transcription factor and other proteins. The pocket domain is comprised of two pocket domains A and B which are separated by a spacer (as shown in **Figure 1.9**). The spacer region is utilised for cyclin binding, while other proteins including HDACs, E2Fs and viral oncoproteins bind to region B. (Classon et al. 2002) Studies have shown that Rb can bind to about 100 different proteins including HDACs, HATs, kinases, histone demethylases, phosphatases and transcription factors, serving as a conduit of cell cycle regulation and gene expression initiation or repression. These interactions assist Rb in the regulation of the G1 checkpoint, blocking S-phase entry and cell growth, differentiation during embryogenesis and adult tissue development, regulation of apoptosis and chromosomal stability. (Giacinti & Giordano 2006) Aside from E2F-mediated cell cycle regulation, Rb can also regulate stability of cell cycle inhibitor p27 through an interaction with anaphase-promoting complex/ cyclosome (APC/C). (Ji et al. 2004; Binné et al. 2007)

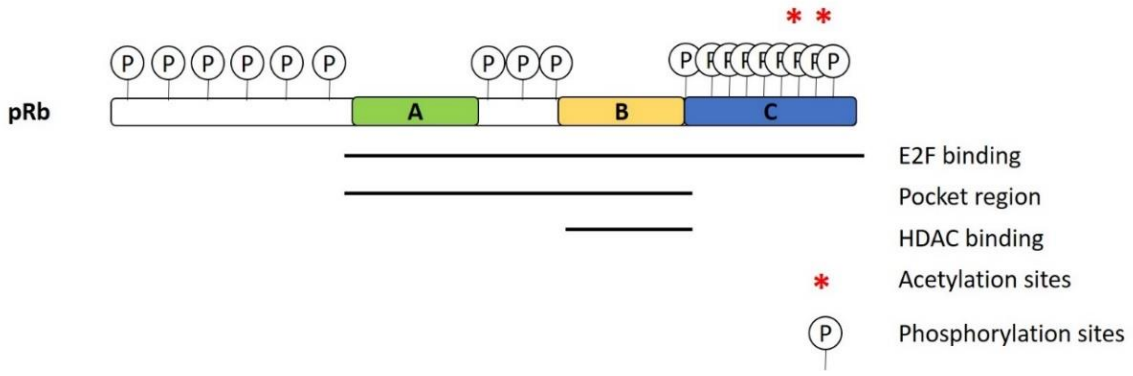

Figure 1.9. The retinoblastoma (pRb) protein.

Region A and B are required for the interaction of the protein with E2Fs and many other transcription factors. Domain C within the carboxy-terminus of pRb is important for E2F binding. Phosphorylation and acetylation sites are also indicated. Adapted from (Classon & Harlow 2002).

Rb can also regulate the transcriptional output of other transcription factors besides E2F. (Noé et al. 1998; Lee et al. 2006) For example, Rb can associate with HES1 to promote stronger binding of Runx2 to target gene promoters. Rb also associates with Sp1, HIF1α and MYOD transcription factors to modulate gene transcription. Aside from being a transcription co-

factor, Rb is also an adaptor protein that can recruit a variety of co-activators/ co-repressors to target gene promoters. (Noé et al. 1998; Lee et al. 2006)

1.7.2 Rb and cell cycle.

Two of the most important proteins involved in the cell cycle machinery are cyclin-dependent kinases (cdk) and cyclins. Cyclin/cdk complexes are formed during distinct phases of the cell cycle and are involved in the phosphorylation of target proteins. (Giacinti & Giordano 2006) In particular, Cdk4/6 in association with D-type cyclins is exclusive for the phosphorylation and inactivation of Rb family proteins, initiating transition into the S phase. (Brewer et al. 1999; Satyanarayana et al. 2009) When in its hypo-phosphorylated form, Rb associates with E2F factors and block their ability to activate expression of genes that are necessary for the S-phase progression. Rb is thought to inhibit expression of E2F-regulated genes in two ways: by directly binding and blocking the activation domain of E2F proteins or by active repression through the recruitment of HDAC, SWI/SNF factors, polycomb group proteins or methyltransferase. (Dyson et al. 2002; Dahiya et al 2001; Vandel et al. 2001) Progression of the cells through the G1 and S phases requires phosphorylation and thus inactivation of Rb protein.

The E2F family of transcription factors consists of eight E2F family members: E2F-1 to -8. Functional E2F co-exist with a DP transcription factor to act as heterodimers. Each of the E2Fs can heterodimerise with either DP1 or DP2, although the E2F-7 can bind DNA independently of DP. (Ormondroyd et al. 1995) There are functional and structural differences between the E2F family members. E2F-1, E2F-2 and E2F-3 are transcriptional activators, which interact with Rb. E2F-4 and E2F-5 are transcriptional repressors which mostly interact with p130 and p107. E2F-6 interacts with polycomb proteins and represses transcription. E2F-7 and E2F-8 are also believed to repress specific promoters. (Di Stefano et al. 2003; De Bruin et al. 2003; Christensen et al. 2005)

The Rb protein together with E2Fs are the main regulator of the mammalian cell cycle. Rb physically interacts with E2F-1, -2 and -3 via their transcription activation domain repressing their transcriptional activity. However, in response to mitogenic signalling, Rb is inactivated in the G1 phase of the cell cycle via phosphorylation by cyclin dependent kinases 2, 4 and 6, leading to its dissociation from E2F1-3. This facilitates the expression of various genes that are necessary for DNA synthesis and cell cycle progression, including cyclin E, dihydrofolate reductase and DNA polymerase α. Not surprisingly, oncogenic mutations target the Rb- E2F

pathway to promote cell proliferation. The Rb gene itself is mutated in a variety of cancers, while mutations in signaling molecules like K-Ras, $p16^{INK4}$ and PTEN that affect Rb function are prevalent in almost all cancers. (Johnson et al. 2012)

1.7.3 Regulation of MMPs by E2Fs.

Existing functional evidence provided by a high-density oligonucleotide array in HeLa cells identified E2F-1 target genes by examining the localisation of E2F-1 binding sites. This study demonstrated that the majority of E2F-1 binding sites are located in core promoters and that 50% of the sites overlap with Transcription Start Sites (TSS). (Bieda et al. 2006) cDNA microarray also revealed novel E2F-1 target genes, including MMP16 and MMP2 which are involved in promoting tumour invasion and metastasis. (Stanelle et al. 2002) More recently, E2F-1 was found to regulate *MMP9, MMP14* and *MMP15* gene expression and most importantly E2F-1 binding sites were predicted in all 23 human MMP promoters. *E2F-1* siRNA depletion reduced the expression of these genes in two different cell lines with a corresponding reduction in collagen degradation activity. (Johnson et al. 2012) These results were partly confirmed by an independent study which indicated decreased *MMP9* and *MMP16* expression following *E2F-1* depletion in a small cell lung cancer (SCLC) cell line. Further experiments demonstrated that E2F-1 trascriptionally controlled the expression of Sp1 and p65, which in turn promoted MMP9 activity in the SCLC cells. (Li et al. 2014)

1.8 Aims of this study

As mentioned previously, collagen degradation is a key step in the initiation and progression of osteoarthritis that leads to articular cartilage loss and MMP1 and MMP13 enzymes play a key role in this process. The expression of these genes is induced by pro-inflammatory cytokine signalling via the chondrocyte and is regulated by a number of signalling pathways, as well as histone modifications and DNA methylation (Roach et al. 2005). Previous work within the lab has shown that broad-spectrum HDAC inhibitors including TSA and sodium butyrate can reduce cytokine-induced metalloproteinase expression at the mRNA and protein level, in the chondrosarcoma cell line SW1353 and also in primary human articular chondrocytes (HACs). In addition to that, in a bovine nasal cartilage (BNC) explants assay, the same compounds were shown to inhibit cytokine-induced cartilage degradation via the reduction of MMP expression (Young *et al.,* 2005). Moreover, the chondroprotective role of HDAC inhibitors is also supported in *in vivo* models of osteoarthritis (Culley *et al.,* 2013; Chen *et al.,* 2010). With the use of selective HDAC inhibitors, class I HDACs were implicated in the regulation of MMP expression, and RNAi studies introduced HDAC3 as a potentially key regulator of their expression (Culley *et al.,* 2013).

This study aims to investigate:

1. The consequences of HDAC3 loss on gene expression programmes related to cartilage degeneration using a chondrosarcoma cell line (SW1353) and also determine whether HDAC3 is involved in cell signalling pathways associated with osteoarthritis (**Chapter 3.** HDAC3 regulates collagenases expression and NF-κB in chondrocytes.).
2. To define the mechanism by which HDAC3 regulates gene expression in chondrocytes by performing RNA microarray analysis of global gene expression changes following RNAi of HDAC3 or HDAC3i (**Chapter 4.** Identification of differentially regulated genes by HDAC3 using RNA microarray analysis.).
3. To investigate a possible interaction of E2F-1 and HDAC3 in chondrocytes and determine the mechanism by which E2F-1 and by interacting with HDAC3 controls *MMP1* and *MMP13* expression in chondrocytes (**Chapter 5.** Regulation of *MMP1* and *MMP13* expression by HDAC3 involves the E2F-1 transcription factor.).
4. To determine how HDAC inhibition, and particularly HDAC3 depletion or selective inhibition, affects chondrogenic differentiation *in vitro*, using human bone marrow-derived mesenchymal stem cells (**Chapter 6.** The role of HDAC3 in chondrogenesis in a human mesenchymal stem cell model system.).
5. To determine the effects of HDAC3 loss:
   - On the DMM-induced OA mouse model and through the delivery of class I specific HDACi (eg. TSA, Apicidin) via intra-articular injections.
   - In chondrocyte- specific Hdac3- null mice or wild- type littermates (by generating a cartilage specific HDAC3 conditional knockout mouse model. (**Chapter 7.** The effect of Hdac3 loss in cartilage murine development.)

Chapter 2. Materials and Methods

2.1 Materials

2.1.1 Antibodies

All antibodies used for immunoblotting, co-immunoprecipitation (co-IP) and Chromatin Immunoprecipitation (ChIP) experiments are listed in **Table 2.1**. Polyclonal secondary goat anti-mouse and anti-rabbit immunoglobulins/HRP conjugated antibodies were purchased from Dako (Cambridgeshire, UK). Mouse monoclonal anti-rabbit IgG Light chain specific HRP (ab99697, Abcam, Cambridge, UK) and Mouse TrueBlot ULTRA: Anti-Mouse Ig HRP (18-8817-30, tebu-bio, Peterborough, UK) were used as the secondary antibodies for the co-IP experiments.

Antibody	Species	Purchased from	Catalogue Number	Dilution for Immunoblotting	Monoclonal/ Polyclonal	Experiment
HDAC3	Rabbit	Abcam	ab7030	1:2500	Polyclonal	IB
E2F1 (C- 20)	Rabbit	Santa Cruz	sc-193	1:2500	Polyclonal	IB
Anti- FLAG-M2	Mouse	SIGMA-Aldrich	F1804	1:2000	Monoclonal	IP
Anti- HA tag (HA C5)	Mouse	Abcam	ab18181	1:1000	Monoclonal	IP
Acetylated histone H3	Rabbit	Cell signaling	#9715	1:2500	Polyclonal	IB
Acetylated α-tubulin	Mouse	Abcam	ab24610	1:1000	Monoclonal	IB
Acetylated Lysine	Rabbit	Abcam	ab80178	1:1000	Polyclonal	IB
Glyceraldehyde-3-Phosphate Dehydrogenase (GAPDH)	Mouse	MILLIPORE	MAB374	1:40000	Monoclonal	IB
β-catenin	Rabbit	Cell Signaling	#9562	1:1000	Polyclonal	IB
E2F-1	Mouse	MILLIPORE	#17-10061	1µg antibody/ 10^6 cells	Monoclonal	ChIP
HDAC3	Mouse	MILLIPORE	#17-10238	4µg antibody/ 3 x 10^6 cells	Monoclonal	ChIP

Table 2.1. Antibodies used for immunoblotting (IB), immunoprecipitation (IP) and chromatin IP (ChIP) experiments. All antibodies were purchased from either Cell Signaling Technology (Beverly, MA, USA), Santa Cruz Biotechnology (CA, USA), Sigma-Aldrich (Poole, UK), Millipore (Watford, UK) or Abcam (Cambridge, UK) as stated.

2.1.2 Immunoblotting Reagents

Ammonium persulphate (APS), β-mercaptoethanol, bovine serum albumin (BSA), polyoxyethylene sorbitan (Tween-20), N,N,N',N'-Tetramethylethylenediamine (TEMED), Triton X-100 and Kodak high-speed X-ray film were all purchased from Sigma-Aldrich (Poole, UK). A standard stock solution of bovine serum albumin (BSA) Fraction V was purchased from Fischer Scientific UK Ltd (Leicestershire, UK). BradfordUltra reagent was purchased from Expedeon (Cambridge, UK). A 37.5:1 mix of acrylamide/bis-acrylamide was purchased from Severn Biotech Ltd. (Worcestershire, UK). PageRuler™ pre-stained protein ladder was purchased from Thermo Scientific (Leicestershire, UK). Immobilon-P polyvinylidene difluoride (PVDF) 0.45µM membrane and Immobilon western chemiluminescent HRP substrate were purchased from Millipore (Watford, UK). Enhanced chemiluminescence (ECL) and ECL-advanced western blotting detection reagents were purchased from GE Healthcare Life Sciences (Buckinghamshire, UK). Marvel non-fat dry milk powder was purchased from Premier Foods (St. Albans, UK).

2.1.3 Cells

2.1.3.1 Cell lines

SW1353

SW1353 cells were purchased from the American Type Culture Collection (ATCC) (HTB-94) and cultured in Dulbecco's Modified Eagle's Medium: Nutrient Mixture F-12 (DMEM/F-12) culture medium as described in section **2.2.1** ***Cell culture***. This cell line initiated from a primary grade II chondrosarcoma of the right humerus of a 72 year old Caucasian female in 1977. Full details for this cell line's characteristics and culture method can be found at the ATCC website (www.atcc.org/).

HEK 293T

HEK 293T cells were purchased from the ATCC and cultured in DMEM as described in section **2.2.1** ***Cell culture***. This cell line, originally referred to as 293tsA1609neo originated from a foetus, is a highly transfectable derivative of human embryonic kidney 293 cells and contains the SV40 T- antigen. Full details can be found at the ATCC website (www.atcc.org/).

2.1.3.2 Mesenchymal stem cells

Mesenchymal stem cells (MSC) were obtained from LONZA and cultured in MSCBM™ (PT-3238 and PT-4105) growth medium. The phenotypes of all donors of MSCs were tested by Flow Cytometry on a FACSCantoII system (Becton Dickinson, Oxford, UK) using a human MSC phenotyping kit (Miltenyi, Biotec, Bisley, UK) with positive staining for CD73, CD90 and CD105 and negative staining for CD14, CD20, CD34 and CD45 (Zeybel et al. 2012; Barter et al. 2015). Cells were also demonstrated to be capable of osteogenic and adipogenic differentiation (Barter et al. 2015).

2.1.4 Cell culture reagents

DMEM/F-12 (High glucose, 21331020) and DMEM culture media were both purchased from Gibco, Life Technologies Ltd. (Paisley, UK). Foetal bovine serum (FBS), Dulbecco's phosphate buffered saline (PBS), trypsin-EDTA (derived from porcine pancreas), L-glutamine, penicillin-streptomycin, and dimethyl sulphoxide (DMSO), were purchased from Sigma-Aldrich (Poole, UK). MSCBM™ Mesenchymal Stem Cell Growth BulletKit™ medium (PT-3001) and high glucose DMEM for chondrogenic differentiation were purchased form LONZA (LONZA Sales AG, Basel, Switzerland).

2.1.5 Transfection reagents

DharmaFECT Transfection Reagent 1 was used for transfection of cells with ON-TARGETplus SMARTpool small interfering RNAs (siRNAs) or siGENOME Non-targeting Pool #2 (siControl), all purchased from Dharmacon (Leicestershire, UK). For transient transfections with plasmid DNA, FuGENE HD transfection reagent was used and purchased from Promega (Southampton, UK).

2.1.6 Plasmids

HA-E2F1 and HA-DP1 plasmids as well as a CDC6-luciferase reporter construct were a kind gift of Professor Nicholas La Thangue from the University of Oxford (Oxford, UK) and have been previously described (Milton et al., 2006). FLAG-HDAC3 (#13819) was obtained from Addgene and deposited by Eric Verdin (USCF School of Medicien, San Fransisco, USA). GFP plasmid, NF-κB firefly luciferase reporter and pRL-TK *Renilla* expression vectors were a gift from Dr Matt Barter (Newcastle University, Newcastle, UK). 3.2 kb MMP13 (enhancer + proximal promoter), 1.6 kb MMP13 (proximal promoter only) have been previously

described (Schmucker et al., 2012) and MMP1 firefly luciferase expression vectors were provided by Professor David Young (Newcastle University, Newcastle, UK).

2.1.7 Histone Deacetylase Inhibitors

The Histone Deacetylase inhibitors (HDACi) used in this study are summarised in **Table 2.2**. Following serum starvation, SW1353 cells were treated with the appropriate concentration of HDACi (explained in each experiment separately) for 30min, before IL-1α stimulation was performed. Alternatively, MSC were treated either one day before chondrogenesis or on the day of chondrogenic differentiation induction and were left to differentiate for 7 days. Following 3 days of differentiation, the media was replaced and no HDACi was added. The cells were allowed to differentiate for a further four days. The HDACi was dissolved either in sterile DMSO or sterile filtered 100% ethanol as indicated in each experiment and according to manufacturer's instructions. These diluents were used as vehicle controls and compared to the HDACi treated cells.

Compound (HDACi)	**Source**	**Code**	**Inhibits**	**IC_{50} (nM)**	**Reference**
Trichostatin (1mg) ≥98% (HPLC) from *Streptomyces hygroscopicus*	SIGMA-Aldrich	T8552	All HDACs	2 for **HDAC1** 3 for **HDAC2** 4 ± 1 for **HDAC3, HDAC6**	Khan et al., 2008
MS-275 (1mg)	Santa Cruz	SC279455	HDAC1 HDAC2 HDAC3	181 ± 62 for **HDAC1** 1155 ± 134 for **HDAC2** 2311 ± 803 for **HDAC3**	Khan et al., 2008
Apicidin (1mg) ≥98% (HPLC) from *Streptomyces sp*.	SIGMA-Aldrich	A8851	HDAC2 HDAC3	120 ± 28 for **HDAC2** 43 ± 7 for **HDAC3**	Khan et al., 2008

Table 2.2. Histone Deacetylase inhibitors (HDACi) used during this study. Trichostatin (TSA) and Apicidin were bought from Sigma Aldrich (Poole, UK), while MS-275 was purchased from Santa Cruz Biotechnology (CA, USA).

Cell death was quantified as an indicator of the cytotoxicity effects of the HDAC inhibitors used in this study, in the SW1353 and the MSC-treated cells. The GloMax® Discover System in combination with the CytoTox-Glo™ Cytotoxicity Assay (Promega, Southampton, UK) were used according to manufacturer's instructions. Briefly, cells were cultured for the desired period and in the end media was collected. 50µl of the CytoTox-Glo™ Cytotoxicity

Assay was added to each sample and incubated at room temperature for 15 minutes. Luminescence was then measured using the GloMax® Discover System. The homogeneous CytoTox-Glo™ Cytotoxicity Assay is a single-reagent-addition luminescent assay that measures the number of dead cells in cell populations. The assay uses a luminogenic peptide substrate (alanyl-alanylphenylalanyl-aminoluciferin; AAF-Glo™ Substrate) to measure "dead-cell protease activity", which is released from cells that have lost membrane integrity. The AAF-Glo™ Substrate cannot cross the intact membrane of live cells, does not generate any appreciable signal from the live-cell population and therefore selectively detects dead cells. **Figure 2.1** shows the cytotoxicity of TSA and Apicidin in the SW1353 (**Figure 2.1 A-B**) and MSC (**Figure 2.1 C**) - treated cells.

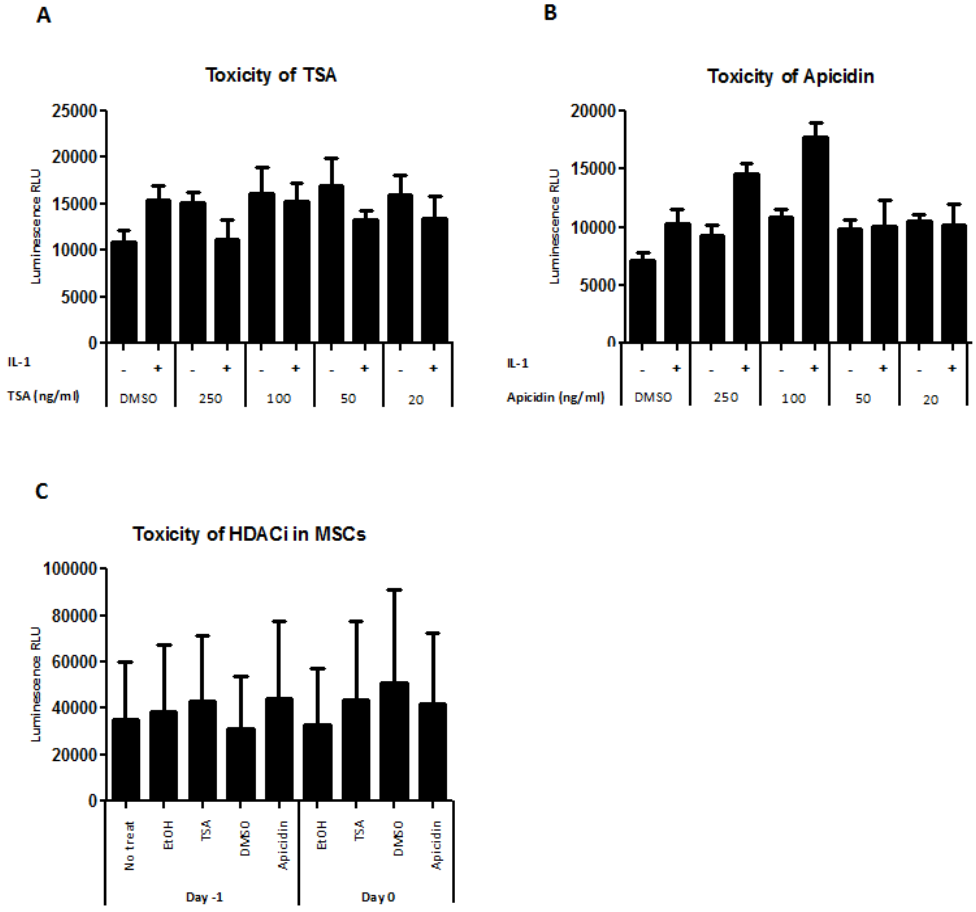

Figure 2.1. Toxicity of different concentrations of TSA and Apicidin in SW1353 and MSC cells.

A- B. SW1353 cells were incubated for 30min with increasing concentrations of TSA or Apicidin before IL-1α (0.5ng/ml) stimulation for 6h was performed. **C.** MSC were incubated with 100ng/ml of HDACi before inducing chondrogenic differentiation (Day -1) or at the day of the induction (Day 0) and cultured thereafter for 7 days The media was then collected and a toxicity assay was performed using the CytoTox-Glo™ Cytotoxicity Assay according to manufacturer's instructions. The luminescence for each sample was detected by GloMax® Discover System and the results were quantified using Microsoft Office Excel. For statistical analysis, one-way ANOVA with a Bonferroni multiple comparison test was performed.

2.1.8 General molecular biology reagents

Ampicillin and Luria-Broth EZMix™ powder (LB) were purchased from Sigma-Aldrich (Poole, UK). Bacto Agar was purchased from Scientific Laboratory Supplies (Nottingham, UK). Molecular biology grade agarose was purchased from Severn Biotech Ltd. (Worcestershire, UK). Super Optimum Broth (SOB or SOC) medium and Subcloning Efficiency™ DH5α™ Competent Cells were bought from Invitrogen, Life Technologies Ltd. (Paisley, UK). GeneRuler™ 100bp and 1kb DNA ladders, Phire Reaction Buffer and Phire Hot Start II DNA Polymerase were purchased from Thermo Scientific (Leicestershire, UK). FastDigest® restriction enzymes were purchased from Thermo Fisher Scientific (Leicestershire, UK). Cells-to-cDNA II lysis buffer was purchased from Ambion, Ambion (Europe) Ltd. (Huntingdon, UK). Random hexamers $p(dN)_6$ were synthesised by Integrated DNA Technologies (IDT) (Leuven, Belgium). Deoxyribonucleotide triphosphate (dNTP) mix was purchased from Bioline (London, UK). RNase-, DNase-free water and all real-time reverse transcriptase quantitiative polymerase chain reaction (real-time qRT-PCR) primers and probes and regular desalted oligonucleotides were purchased from Sigma-Aldrich (Poole, UK). Probe library probes were purchased from Roche, Roche Diagnostics Ltd. (West Sussex, UK). Moloney Murine Leukaemia Virus (M-MLV) reverse transcriptase, 5X First Strand Buffer and 100mM DTT were all purchased from Invitrogen, Life Technologies Ltd. (Paisley, UK) and TaqMan® gene expression master mix was purchased from Applied Biosystems, Life Technologies Ltd. (Paisley, UK). Protein G, A, or a mixture of G/A PLUS-Agarose beads for immunoprecipitation (IP) or chromatin immunoprecipitation experiments (ChIP) was purchased from Santa Cruz Biotechnology (CA, USA). Stellar Competent Cells were purchased from Takara Bio Europe/Clontech (Paris, France). Vectorshield® Mounting Medium with DAPI for Fluorescence was purchased from Vector Laboratories (Peterborough, UK).

2.1.9 Commercially available kits

PureYield™ Plasmid Miniprep, Dual-Luciferase® Reporter Assay, Dual-Glo® Luciferase Reporter Assay Systems were purchased from Promega (Southampton, UK). ChIPAb+ E2F-1 (#17-10061) and ChIPAb+ HDAC3 (#17-10238) kits were purchased from MILLIPORE (Watford, UK).

2.2 Methods

2.2.1 Cell culture

Reagents

- HEK293T cells and DMEM culture media containing 2mM L-glutamine, 100U/ml penicillin, 100µg/ml streptomycin and 10% (v/v) FBS
- SW1353 cells and DMEM-F12 culture media containing 2mM L-glutamine, 100U/ml penicillin, 100µg/ml streptomycin and 10% (v/v) FBS
- MSC cells with MSCBM™ Mesenchymal Stem Cell Growth BulletKit™ medium
- Chondrogenic differentiation media: 47.5ml DMEM (Dulbecco's Modified Eagle's Media; LONZA 12-614, 4.5 g/L Glucose) , 50µl 100µM Dexamethasone (SIGMA-Aldrich, D4902-25mg) , 50µl 10µg/ml TGF-β3 (PeproTech INC., #100-36E-100UG), 500µl 5mg/ml ascorbic-acid-2-phosphate (SIGMA-Aldrich, A8960-5G), 500µl 4mg/ml proline (SIGMA-Aldrich, P5607-25G), 500µl L-Glutamine, 100U/ml penicillin, 100µg/ml streptomycin, 500µl 100x ITS+L premix (Insulin, transferrin, selenium+ Linoleic acid) (Corning- 354352)
- Freezing medium: 90% (v/v) FBS and 10% (v/v) DMSO

Method

Cells were plated into vented T75cm^2 flasks and incubated at 37°C with 5% CO_2 (v/v) in a humidified incubator until they reached approximately 90% confluence. For passaging, cells were washed with sterile PBS and detached by incubation for 2-3min with trypsin-EDTA and then split into further T75cm^2 flasks every 72 hours, or were plated onto the appropriate culture dishes for experimentation. For long-term storage in liquid nitrogen, cells were resuspended in freezing medium, transferred to cryovials, and frozen gradually at -80°C overnight before being transferred for storage in liquid nitrogen.

SW1353/HEK293T cells were seeded overnight at a density of 10,000 cells/ cm^2 in 96-well plates for mRNA quantification or at 150,000 cells/cm^2 in 6-well plates for immunoblotting. Prior to cytokine stimulation, culture media was removed and the cells were washed with PBS and then cultured overnight with serum-free DMEM culture media at 37^{o}C in 5% (v/v) CO_2/humidified air.

MSC were seeded at a density of 18,000 /cm^2 cells in 10cm petri dishes and siRNA transfection was performed when the required confluency was achieved (as described in section **2.2.7** ***RNA interference (RNAi)***). The cells were subsequently seeded in transwells

(**Figure 6.1**) at a density of 500,000 cells per transwell with chondrogenesis differentiation media for up to 14 days at 37ºC in 5% (v/v) CO_2/humidified air, replacing the chondrogenic media every 2-3 days. (Barter et al. 2015)

2.2.2 Generation and use of expression vectors

Expression vectors used in this study can be found in section ***2.1.6 Plasmids***.

2.2.2.1 Bacterial Transformation

Reagents

- LB (EZMix (Sigma-Aldrich, Poole, UK) in dH_2O, autoclaved)
- LB-agar (LB plus 15g/L,- Bacto Agar in dH_2O autoclaved) with addition of (100µg/ml) ampicillin

Method

2µl of plasmid DNA was added to 20µl Subcloning Efficiency™ DH5α™ Competent Cells and incubated on ice for 30 minutes before a 20 second heat-shock at 42°C. SOC medium was added to the cells and incubated at 37°C with shaking for 1 hour. Next, the transformation mixture was spread onto LB-agar plates and incubated inverted at 37°C overnight. The following day individual colonies were selected and incubated in 5ml of LB supplemented with ampicillin (100µg/ml) at 37°C on an orbital shaker at 225rpm for 16 hours prior to miniprep isolation.

2.2.2.2. Minipreps

Minipreps were performed using the PureYield™ plasmid miniprep system (Promega, Southampton, UK) following the manufacturer's protocol. Plasmid DNA was eluted in 30µl nuclease-free water for minipreps. DNA concentration was determined using the NanoDrop ND-1000 spectrophotometer.

2.2.3 Cartilage digestion of MSC-derived cartilage discs

Reagents

- 0.1M Phosphate buffer pH 6.5
- Papain (SIGMA Aldrich)
- Cysteine- HCl

- EDTA
- Starstedt tubes

Method

Two different solutions of 0.1M phosphate buffer pH 6.5 were made. Solution A contained 9.36g/ 600ml dH_2O 0.1M Na_2HPO_4 and solution B contained 7.1g/ 500ml dH_2O 0.1M NaH_2PO_4. Next 137ml from solution A was mixed with 63ml from solution B and the pH was confirmed at 6.5. The phosphate buffer was stable for one week and was used to make the papain solution (0.25g/10ml phosphate buffer), the cysteine-HCl solution (0.078g/ 10ml phosphate buffer) and the EDTA (0.19g/10ml phosphate buffer). Cartilage discs produced after a 14-day differentiation period of MSC were put in Starstedt tubes and a mix of phosphate buffer, papain solution, cysteine-HCl solution and EDTA was added as shown in **Table 2.3**. The cartilage discs were then incubated at 65^oC overnight. The following day 450µl of phosphate buffer were added per tube and the samples were either kept at 4^oC and assayed at the same day, or stored at -20^oC to be assayed at a later stage.

	Per transwell = 1 disc (µl)	**Per cell pellet or ¼ of a disc (µl)**	**Per plate (10cm) (µl)**
Phosphate buffer	420	105	3500
papain	120	30	1000
Cysteine- HCl	60	15	500
EDTA	60	15	500

Table 2.3. Digestion of cartilage.

2.2.4 Glycosaminoglycan (GAG)/ Dimethyl-methylene blue (DMB) assay

GAG/DMB assay can be used to measure proteoglycan degradation by determining the amount of glycosaminoglycan in a sample. (Burkhardt et al. 2001)

Reagents

- Dimethyl-methylene blue (DMB) pH 3 (3.04g glycine, 2.37g NaCl, 95ml 0.1M HCl make up to 1L of dH_2O, add 16mg DMB, Absorbance ~0.3 at 530nm, store at RT, light sensitive)
- 1mg/ml chondroitin sulphate

Method

In a flat bottomed 96-well plate a series of chondroitin sulphate concentrations beginning from 0mg/ml up to 40mg/ml were diluted in phosphate buffer and then 40µl were added to

each well in duplicate. 40µl of each sample prepared as described above in section **2.2.3** were also added in other wells in duplicate and 250µl of DMB solution were added in each well and the plate was immediately read in a plate reader at 530nm.

2.2.5 PicoGreen DNA quantification

Reagents

- Quant-iT™ PicoGreen® dsDNA Assay Kit (P7589, Thermo Scientific Leicestershire, UK)

Method

The Picogreen Reagent was prepared in 1 X TE buffer provided by the kit. Then the DNA standard (100µg/ml) was prepared in Eppendorfs by diluting in 1 X TE buffer and the appropriate amount was added in triplicate in a clean black 96-well plate. The DNA stock was diluted 1:50 in 1 X TE to make a working solution of 2µg/ml and was then added in a series of concentrations starting from 0 up to 1000ng/ml. Each sample was also diluted 1:4 in 1 X TE Buffer and then added in duplicate. Finally PicoGreen working solution was added to each well, the wells were mixed and incubated for 2-5 minutes at room temperature, protected from light, before measuring the sample fluorescence using a Fluorostar fluorescence microplate reader and standard wavelengths (excitation ~480nm, emission ~520nm). The DNA concentration of the unknown samples was then calculated from the standard curve. The results obtained from the GAG assay above were subsequently normalised with reference to the DNA levels contained to each sample and expressed as µg GAG/ µg DNA.

2.2.6 Hydroxiproline assay

Hydroxiproline assay can be used to measure collagen content in tissue homogenates. The procedure is based on hydrolysis of the tissue homogenate and subsequent determination of the free hydroxiproline in hydrolyzates. (Reddy and Enwemeka, 1996)

Reagents

- Concentrated HCl (12M)
- Chloramin T (7% w/v in water, dilute 1:5 in acetate citrate buffer, make up before use)
- Acetate citrate buffer (57 g sodium acetate, 37.5 g trisodium citrate, 5.5 g citric acid, 358 mL propan-2-ol per litre of distilled water)

- p-Dimethylaminobenzaldehyde (DAB; Sigma Aldrich) 20 g dissolved in 30 mL of 60% per-chloric acid (VWR Int Ltd). Dilute 1:3 in propan-2-ol immediately before use.
- Hydroxyproline (OHPro; Sigma. 1 mg/mL stock dissolved in water). This may be stored in aliquots at –20◦C

Method

Cartilage discs were incubated at 37°C in a humidified atmosphere of 5% v/v CO2 for 24 hours, after which the medium was replaced with serum-free DMEM containing cytokines and/or HDAC inhibitors; each treatment was performed in quadruplicate. Supernatants were harvested on day 7, the treatments were replaced, and the explants were incubated until day 14, when the remaining cartilage and medium were harvested. The remaining cartilage explants were digested in papain overnight at 65°C. Hydroxyproline release was assayed as a measure of collagen degradation at 560nm. (see also Hui and Cawston, 2010 for detailed protocol)

2.2.7 RNA interference (RNAi)

Standard ON-TARGET plus SMARTpool siRNAs were purchased from Dharmacon (Leicestershire, UK). The ON-TARGET plus collection takes advantage of a dual-strand modification pattern to decrease off-target effects by up to 90%. SMARTpool siRNAs contain 4 siRNAs that target different regions of the target gene to maximise potency and specificity; the sequences of which can be found in **Table 2.4**.

ON-TARGETplus non-targeting Control siRNA	ON-TARGETplus Human HDAC3 (8841) siRNA	ON-TARGETplus Human E2F1 (1869) siRNA	ON-TARGETplus Mouse HDAC3 (15183) siRNA
UAAGGCUAUGAAGAGAUAC	AACAAGAUCUGUGAUAUUG	UCGGAGAACUUUCAGAUCU	GGGAAUGUGUUGAAUAUGU
AUGUAUUGGCCUGUAUUAG	GGAAUGCGUUGAAUAUGUC	GAGAAGUCACGCUAUGAGA	CGGCAGACCUCCUGACGUA
AUGAACGUGAAUUGCUCAA	GCACCCGCAUCGAGAAUCA	GAGCAGAUGGUUAUGGUGA	GCACCCGCAUCGAGAAUCA
UGGUUUACAUGUCGACUAA	AAAGCGAUGUGGAGAUUUA	GAACAGGGCCACUGACUCU	UAUAAGAAGAUGAUCGUCU

Table 2.4. The 4 sequences which make up the ON-TARGETplus SMARTpool siRNAs for HDAC3, E2F1 and the non-targeting siRNA.

Method

SW1353 were seeded in a 96-well plate at a density of 1.5 x 10^4 cells/cm^2. The following day, at around 50% cell confluency, cells were transfected with different concentrations of siRNA targeting HDAC3 (siHDAC3), E2F-1 (siE2F-1) or a non-targeting control siRNA (siCon) using DharmaFECT transfection reagent 1 (DF1). In separate tubes, the siRNA and DF1 were diluted in the appropriate volume of serum-free, antibiotic-free DMEM and incubated at room temperature for 5 minutes. Both tubes were then combined and incubated at room temperature for a further 20 minutes. Following incubation, an appropriate volume of serum-containing DMEM was added to the transfection mix; culture medium was aspirated from the cells in each well and replaced with the transfection mix. Cells were then incubated at 37°C in 5% (v/v) CO_2 for the required time as described in each experiment independently. Alternatively, MSC were seeded in 10cm dishes at a density of 18,000/cm^2 cells/ dish and siRNA transfection was performed when the cells acquired the required confluency (45-55%), as described above. The cells were then incubated for three days at 37^{o}C in 5% (v/v) CO_2 before chondrogenic differentiation was performed as described in (Barter et al. 2015).

Different concentrations of ON-TARGET siRNAs were used starting from 5-100nM and knockdown efficiency was determined using quantitative real-time PCR and immunoblotting (see also **Figure 3.7**). Following optimisation, the 50nM of siRNA concentration was determined to be optimal, and as such was the concentration of all the siRNAs used in the subsequent experiments of this thesis. The optimal minimum transfection time has generally been found to be 24h for efficient knockdown for the SW1353 cells (thesis of Dr Heather Bromby, Newcastle University, Newcastle upon Tyne, UK) and 3 days for the MSC and these times were used in this thesis.

2.2.8 Luciferase reporter assays

NF-κB, MMP1 and MMP13 reporter assays

A pNFκB-Luc Vector (provided by Dr Matt Barter, Newcastle University, UK) gene assay was conducted using the Dual-Luciferase Reporter Assay System (Promega, Southampton, UK) according to the manufacturer's protocol. The two MMP13 luciferase reporter constructs have been previously described (Schmucker et al., 2012) and both of them, and the MMP1 luciferase construct were a kind gift of Professor David Young, (Newcastle University, Newcastle upon Tyne, UK). Briefly, cells were seeded into 48-well or 96-well plates at 1.5 x 10^4/cm^2 and the next day transfected with the appropriate concentration of *Firefly* luciferase

reporter and *Renilla* (pRL-TK, PROMEGA) expression vectors. Following transient transfection of the expression vectors for 24h, cells were serum starved overnight before IL-1 stimulation was performed for 6h. After incubation with IL-1 the cells were washed in PBS and lysed in 30µl passive lysis buffer (1 X) provided by the kit. Next, cell lysate was added to a cross-talk-free, white walled 96-well plate (PerkinElmer, Wellesley, MA, USA), luciferase assay reagent was injected to initiate the firefly luciferase reaction and luminescence was measured using a Glomax-Multi+ Detection System (Promega, Southampton, UK). After the firefly initial expression reading, a second reagent was injected to stop the reaction and luminescence for *Renilla* luciferase was subsequently measured.

For experiments in which NF-κB luciferase reporter was used, 100ng of the reporter was transfected together with 6ng of *Renilla* reporter for 24 hours before serum starvation and IL-1 stimulation was performed. For experiments in which MMP13 or MMP1 luciferase reporters were used with or without over-expressing HA-E2F1 and HA-DP1 plasmids DNA, 96-well plates were used and 25ng of each MMP reporter together with 50ng of HA-E2F1, 50ng HA-DP1 and 1.5ng of *Renilla* reporter were transfected for 24 hours before serum starvation and IL-1 stimulation was performed.

2.2.9 Protein analysis

2.2.9.1 Whole Cell Lysis

Reagents

- Lysis buffer (50mM Tris-HCl, pH 7.4, 10% (v/v) glycerol, 1mM EDTA, 1mM EGTA pH 8.0), 1mM Na_3VO_4, 5mM NaF, 10mM β-glycerol phosphate, 5mM $Na_4P_2O_7$, 1% (v/v) Triton X-100, 1µM microcystin-LF and 1 Complete protease inhibitor Mini tablet (Roche Diagnostics, West Sussex, UK) for 50ml of buffer

Method

Cells were seeded in 12-well or 6-well plates at a density of 150,000 cells/cm^2. After the appropriate experimental period, the plates were transferred on ice, culture medium was removed and cells were washed with ice-cold PBS. Ice-cold lysis buffer (containing 0.01% (v/v) β-mercaptoethanol) was added at 75µl/well or 100µl/well for 12- or 6-well plates, respectively. Cells were scraped and the cell suspension transferred to a cooled Eppendorf for 20 minutes incubation on ice. Following incubation the lysates were centrifuged at 4°C for 3 minutes at 10 000 x g. Supernatants were removed and immediately either stored at -80°C or a Bradford protein assay was performed.

2.2.9.2 Bradford Assay

Method

Bradford protein assays were used for protein quantification of the cell lysates. A range of standards of 0-4 mg/ml BSA (2mg/ml stock concentration) were made using increasing increments of 0.4 mg/ml in a flat bottomed 96 well plate, making each well volume up to 10µl with dH_2O. Next, 3µl of each sample was added to the plate together with 3µl of lysis buffer as a loading control, making each volume up to 10µl with dH_2O. 150µl of Bradford Ultra Reagent were then added to each well according to the manufacturer's instructions. A 5 minutes incubation at room temperature followed and the absorbance was then measured at 595nm using a Tecan Sunrise microplate absorbance reader. A standard curve was then drawn using Microsoft Office Excel and the protein concentration of each sample was calculated, after subtracting the absorbance of the lysis buffer control. The protein content of samples was then equalised using 5X Laemmli sample buffer and dH_2O. The samples were then boiled for 5 minutes and were loaded onto a SDS-PAGE gel (described in section **2.2.9.3 Immunoblotting**) or frozen at -20^{o}C.

2.2.9.3 Immunoblotting

Reagents

- Separating gel solution: dH_2O, 4x lower gel buffer (LGB) (1.5M Tris-Base pH8.8, 0.4% SDS (w/v)), 37.5:1 acrylamide/bis-acrylamide 40%, APS and TEMED
- Stacking gel solution: 4 X upper gel buffer (UGB) (0.5M Tris- HCl pH 6.8, 0.4% (w/v) SDS), APS, TEMED
- 10 X Running buffer (250mM Tris Base, 2M Glycine and 10% (w/v) SDS)
- Transfer buffer (20mM Tris Base, 0.6M glycine and 20% (v/v) methanol) & Methanol
- Tris buffered saline (TBS)-Tween (TBS-T) (150mM NaCl, 10mM Tris Base pH7.4, 0.1% (v/v) Tween-20)
- 5X Laemmli sample buffer (0.1 M Tris-HCl, pH 6.8, 0.35 M SDS, 20% (v/v) glycerol, 0.01% bromophenol blue and 10% (v/v) β-mercaptoethanol)
- Polyvinylidene difluoride membrane (PVDF) (#88518, Thermo Scientific, Leicestershire, UK) and blotting paper
- Stripping buffer (for 1L): 15g Glycine, 1g SDS, 10ml Tween 20, pH 2.2, bring volume up to 1L with ultrapure dH_2O

Method

Cell lysate samples containing 5X Laemmli sample buffer were heated at 100°C for 5 minutes prior to loading onto a 10% SDS-polyacrylamide gels. For the separating gel, acrylamide/bis-acrylamide 40% solution was diluted with 4X LGB and water at the correct volumes to give a 10% gel. 10µl TEMED and 30µl APS 0.2% (w/v) were added to the gel solution for polymerisation and the gel poured into 1.0mm Bio-Rad separator glass plates (Bio-Rad Laboratories, Hemel Hempstead, UK). Stacking solution made up of 4X UGB, polymerised with TEMED and APS and was then added on top of the polymerised separating gel, with combs inserted. The SDS-PAGE gels were electrophoresed at 140V using the Bio-Rad mini-PROTEAN gel vertical electrophoresis system (Bio-Rad Laboratories, Hemel Hempstead, UK) in which the gel plates are inserted into a sealed casting frame and placed into a tank filled with 1 X Running buffer. PageRuler™ pre-stained protein ladder (#26616, Thermo Scientific, Leicestershire, UK) was loaded onto the gel alongside the protein samples.

After electrophoresis, proteins were transferred from the gel to a PVDF membrane by electroblotting in transfer buffer using a Scie-Plas V20-SDB 20 x 20cm semi-dry blotter at 1mA/cm2 for 1.5 hours. Membranes were blocked for 1 hour in TBS-T containing 5% (w/v) non-fat dry milk powder. After thoroughly washing in TBS-T 3 times for 5 minutes each with gentle agitation, membranes were incubated overnight at 4°C with primary antibody (see **Table 2.1**) with gentle agitation, diluted according to manufacturer's instructions in primary antibody dilution buffer (TBS-T containing 5% BSA). The membrane was then incubated overnight and the following day 3 washes with TBS-T (3 times for 5 minutes each with gentle agitation) were performed. The membrane was then incubated with horseradish peroxidase (HRP)-conjugated secondary antibody (diluted 1:5000 in TBS-T, 5% milk) for one hour at room temperature with gentle agitation. Membranes were again washed for 3 x 5 minutes with TBS-T and then visualised on high-speed X-ray film using ECL detection reagents.

To allow probing with a different antibody, membranes were incubated in stripping buffer for 5-10 minutes. The buffer was discarded and fresh stripping buffer was added to the membrane and 5-10 minutes incubation followed. After washing with PBS twice for 10 minutes each time and with TBS-T twice for 5 minutes, membranes were then incubated with the desired primary antibody overnight as described above. An anti-GAPDH or anti-β catenin antibody was used to ensure equal loading, as indicated in each experiment.

2.2.10 Immunoprecipitation (IP)

Method

HEK293T cells were seeded in 10cm dishes at a density of 4 x 10^6 cells/dish. The following day cells were transfected with the appropriate tagged protein for 24 hours as outlined in section **2.2.2** ***Generation and use of expression vectors***. The next day whole cell lysis was performed as described above (in section **2.2.9.1 Whole Cell Lysis** and cell lysate protein was quantified using Bradford assay as in section **2.2.9.2 Bradford Assay**.

For IP experiments 300µg of protein lysate was used. First the lysate was pre-cleared by adding 3µg of irrelevant antibody (IgG mouse). Samples were then placed on ice for one hour and then incubated at 4ºC with end-over-end rotation with 20µl added Protein G PLUS-agarose conjugate suspension. After a 10 minutes centrifugation at 14,000 x g at 4ºC, supernatants were removed for IP.

On ice, 3µg of the IP antibody was added to the pre-cleared lysate and incubated overnight with end-over-end rotation at 4ºC. The following day 20µl Protein G PLUS-agarose conjugate suspension was added to each sample. The samples were then incubated for 3 hours at 4ºC with end-over-end rotation. The complex lysate-antibody-beads was collected by centrifugation at 10, 000 x g for 1 minute at 4ºC and the supernatant was discarded. The bead pellet was then washed 3 times with washing buffer (10mM Tris-HCl pH 7.5, 1mM EDTA pH 8.0, 150mM NaCl, 1% (v/v) NP-40, 0.2mM Na-Orthovanadate and 1x cOmplete™ Protease inhibitor cocktail). After the last wash, the washing buffer was discarded and the bead pellet resuspended in 2 X Laemmli buffer and heated to 100ºC for 5 minutes. The samples were centrifuged at 4ºC for 1 minute at 10, 000 x g and then left to stand for 1 minute at room temperature. The supernatant was collected and electrophoresis was performed as in section **2.2.9.3 Immunoblotting**.

2.2.11 RNA analysis

2.2.11.1 Cell lysis

The Ambion® Cells-to-cDNA™ II lysis buffer was used to yield cell lysates for reverse transcription from SW1353 cells in culture and MSCs differentiated into pellets. The lysis buffer integrates RNase inactivation into an RT-PCR compatible cell lysis buffer, eliminating RNA isolation altogether.

For the transwell differentiation of MSC, RNA isolation using TriZOL and ¼ of two cartilage discs (technical replicates) from two independent MSC donors (biological repeats) per time-point were performed.

Reagents

- Ambion® Cells-to-cDNA™ II Lysis Buffer (ThermoFisher Scientific)
- Molecular grinding resin and pestles (G-Biosciences)
- TriZOL
- Chloroform
- 100% Isopropanol
- 75% (v/v) Ethanol
- RNase-free H_2O

Method

Cell lysis was performed using Cells-to-cDNA II lysis buffer following the manufacturer's protocol. For RT-PCR, 96-well culture plates were used for the SW1353 cells and 14ml falcon tubes for the MSC differentiation into pellets. After siRNA transfection/HDACi treatment and IL-1 stimulation, cell culture medium was removed and cells were washed in ice-cold PBS. Next, cells were lysed in 30µl ice-cold Cells-to-cDNA II lysis buffer per well/falcon tube, transferred to a 96-well PCR plate and heated to 75°C for 15 minutes to ensure RNase inactivation. Lysates were then stored at -80°C or reverse transcription was performed immediately as described below.

To homogenise the differentiated cartilage discs 20µl grinding resin together with 250µl of TriZOL were pipetted into the ¼ of each cartilage disc contained in an Eppendorf tube. Homogenisation followed by using pestles and grinding against the side of the tube. The pellet resin was then removed by centrifugation and the supernatant was transferred to a new Eppendorf tube. The lysate was incubated for 5 minutes at room temperature and then 50µl of chloroform per 100µl TriZOL was added and shaken vigorously for 15 seconds. Following two minutes incubation at room temperature, samples were centrifuged at 13,000 rpm for 15 minutes at 4^{o}C. After the centrifugation, the aqueous phase (~250µl) was transferred to a fresh tube and 50µl of isopropanol per 100µl of TriZOL was added and the samples were vortexed. The samples were then incubated for 10 minutes at room temperature, before 10 minutes centrifugation at 13,000 rpm at 4^{o}C. The supernatant was discarded and the pellet was washed with 75% (v/v) ethanol, vortexed and centrifuged at 10,000 rpm for 5 minutes at 4^{o}C. Following centrifugation, the ethanol was removed and the pellet was air dried for 10 minutes at room temperature and then resupended in 20µl of RNase-free H_2O. Samples were then quantified to determine RNA concentration, using NanoDrop ND-1000 spectrophotometer,

and either stored at -80^{o}C or reverse transcription was performed immediately as described below.

2.2.11.2 Reverse transcription

Method

For reverse transcription of SW1353 cells or MSC differentiated into pellets, 8µl of the lysate produced using the Cells-to-cDNA II lysis buffer was transferred to a new 96-well PCR plate to which final concentrations of 0.375µM dNTPs and 10ng/µl random hexamers $p(dN)_6$ were added to each well and heated to 70°C for 5 minutes. The samples were then placed on ice and 5 X First Strand Buffer, final concentration of 10mM DTT and 0.5µl 200U/µl M-MLV reverse transcriptase were added. The reaction was made up to 20µl total volume per well with dH_2O, incubated at 37°C for 50 minutes followed by incubation at 75°C for 15 minutes. To this cDNA, 30µl dH_2O was added for target gene quantification and diluted further 1:50 for housekeeping gene (18S) quantification. The cDNA was stored at -20°C prior to analysis or quantified immediately by real-time qRT-PCR.

If TriZOL RNA isolation was performed, 500ng of total RNA was transferred to a new 96-well PCR plate and volume was adjusted to 8µl with H_2O to which 10mM dNTPs and 1µg/µl random $p(dN)_6$ were added to each well and heated to 70°C for 5 minutes. An identical process as above (Cells-to-cDNA) was performed, however the cDNA produced was then diluted 1:50 with dH_2O for target gene quantification and diluted 1:10 further for 18S quantification.

2.2.11.3 Taqman® Probe-Based Real- time qRT-PCR

Reagents

- Taqman Fast Universal PCR Mastermix (2 X)

Method

For quantification of target genes using the cDNA prepared above, a 6µl reaction mix of 2 X TaqMan gene expression master mix, 200nM of each forward and reverse primers, 150nM probe were made up with H2O and added to each well of a FAST Optical 96-well qPCR plate. Similarly, for quantification of the housekeeping gene a 5µl reaction mix of 2 X TaqMan gene expression master mix, 300nM of each forward and reverse primers and 75nM probe was prepared. Next, 4µl or 5µl diluted cDNA was used for target or housekeeping gene

quantification respectively and added to each well to give a total 10µl reaction. Real-time qRT-PCR was performed using the ABI 7900HT Fast Real-time PCR system (Applied Biosystems, Life Technologies Ltd., Paisley, UK). Oligonucleotide primers and probes were designed using the Roche ProbeFinder Assay Design Software (Roche, Applied Science) and the sequences are shown in **Table 2.5**. Thermocycling parameters were: 95°C for 10 minutes followed by 40 cycles of 95°C for 15 seconds and 60°C for 1 minute.

Gene	Primer	Primer sequence (5'-3')	Probe
Human *ACAN*	Forward Reverse	AGACGGCTTCCACCAGTGT GGGAGTGTGGATGGGGTAT	Probe library #20
Human *CCL2*	Forward Reverse	AGTCTCTGCCGCCCTTCT GTGACTGGGGCATTGATTG	Probe library #40
Human *COL10A1*	Forward Reverse	CACCTTCTGCACTGCTCATC GGCAGCATATTCTCAGATGGA	Probe library #6
Human *COL11A1*	Forward Reverse	AGGTCCTCCTGGAAAACGAG TCACCTTGTCTTCCCTCTGC	Probe library #1
Human *COL1A1*	Forward Reverse	CCCCTGGAAAGAATGGAGATG TCCAAACCACTGAAACCTCTG	5'-TTCCGGGCAATCCTCGAGCA-3'
Human *COL2A1*	Forward Reverse	ACCTTCATGGCGTCCAAG AACCAGATTGAGAGCATCCG	5'-AGACCTGAAACTCTGCCACCCTG-3'
Human *COL9A1*	Forward Reverse	AGATAATCCTCAAGTTTCTGTTCCA GCAGCTCATGGCAAGTTTCT	Probe library #89
Human *E2F-1*	Forward Reverse	TCCAAGAACCACATCCAGTG CTGGGTCAACCCCTCAAG	Probe library #5
Human *FRA1*	Forward Reverse	AACCGGAGGAAGGAACTGAC CTGCAGCCCAGATTTCTCA	Probe library #4
Human *IL6*	Forward Reverse	CAGGAGCCCAGCTATGAACT GAAGGCAGCAGGCAACAC	Probe library #45
Human *IL8*	Forward Reverse	AGACAGCAGAGCACACAAGC AGGAAGGCTGCCAAGAGAG	Probe library #72
Human *JUNB*	Forward Reverse	ATACACAGCTACGGGATACGG GCTCGGTTTCAGGAGTTTGT	Probe library #49

Human *JUND*	Forward Reverse	CAGCGAGGAGCAGGAGTT GAGCTGGTTCTGCTTGTGTAAAT	Probe library #81
Human *MATN3*	Forward Reverse	TTCCAGGAAACCTTCTGTGC TGTATCCTTGGCTACACTCACAGT	Probe library #60
Human *MMP1*	Forward Reverse	AAGATGAAAGGTGGACCAACAATT CCAAGAGAATGGCCGAGTTC	5′FAM-CAGAGAGTACAACTTACATCGTGTTGCGGCTC-TAMRA 3′
Human *MMP13*	Forward Reverse	AAATTATGGAGGAGATGCCCATT TCCTTGGAGTGGTCAAGACCTAA	5′FAM-CTACAACTTGTTTCTTGTTGCTGCGCATGA-TAMRA 3′
Human *N-CAD*	Forward Reverse	GGTGGAGGAGAAGAAGACCAG GGCATCAGGCTCCACAGT	Probe library #66
Human *N-CAM*	Forward Reverse	GCGTTGGAGAGTCCAAATTC GGGAGAACCAGGAGATGTCTTT	Probe library #51
Human *RUNX2*	Forward Reverse	GGAGTGGACGAGGCAAGAGTTT AGCTTCTGTCTGTGCCTTCTGG	Probe library #29
Human *SERPINB2*	Forward Reverse	CATGGAGCATCTCGTCCAC ACTGCATTGGCTCCCACTT	Probe library #1
Human *SOX9*	Forward Reverse	CTGGTACTTGTAATCCGGGTG ACTTGCACAACGCCGAG	5′FAM-TCTGGAGACTTCTGAACGAGAGCGA- TAMRA 3′
Human *TNFAIP6*	Forward Reverse	GGCCATCTCGCAACTTACA GCAGCACAGACATGAAATCC	Probe library #34
Human *WNT7B*	Forward Reverse	TGGCGTCCTGTACGTGAA TCTTGTTGCAGATGATGTTGG	Probe library #49
Human *18S*	Forward Reverse	CGAATGGCTCATTAAATCAGTTATGG TATTAGCTCTAGAATTACCACAGTTATCC	5′FAM-TCCTTTGGTCGCTCGCTCCTCTCCC0-TAMRA 3′

Table 2.5. Sequences of Taqman qRT-PCR primers and corresponding Universal Probe Library (UPL) probe numbers/ probes.

2.2.11.4 SYBR Green Real- time qRT-PCR

Reagents

- Platinum® SYBR® Green qPCR SuperMix-UDG with ROX (Thermo Scientific, Leicestershire, UK).

Method

For quantification of target genes using the cDNA prepared from the cartilage discs, 4.8µl of SYBR Green mix together with 0.2µl ROX (Reference dye), 250nM of each forward and

reverse primer were added in a Fast Optical 96-well qPCR plate. To this 4µl of cDNA was added to make up a final volume of 10µl. This was then subject to a denaturation stage at 95ºC for 2 minutes followed by 40 cycles of 95ºC for 15sec and 60ºC for 1 minute. All SYBR Green reactions included a final dissociation stage of 95ºC for 15sec and 60ºC for 15sec. All reactions were performed using the ABI 7900HT Fast Real-time PCR system. Oligonucleotide SYBR Green primer sequences can be found in **Table 2.6**.

Gene	Primer	Primer sequence (5'-3')
Human *ATF2*	Forward	TCCAGCTGCAGTCCCACT
	Reverse	TTTTTGCTTCTGACTGTACTGGTT
Human *c-FOS*	Forward	AGAATCCGAAGGGCCTTGAC
	Reverse	TCCGCTTGGAGTGTATCAGTC
Human *HDAC3*	Forward	GGGTGGTGGTGGTTATACTGTC
	Reverse	ATGAAACGGGGTCTGAAGTGTGGAGTAGGT
Human *FOSB*	Forward	CAGGCGGAGACAGATCAGTTG
	Reverse	CCAGCACAAACTCCAGACGTT
Human *FRA1*	Forward	ACAGATCAGCCCGGAGGAAG
	Reverse	CTTCCAGTTTGTCAGTCTCCGC
Human *FRA2*	Forward	CAGCAGAAATTCCGGGTAGATATG
	Reverse	TATGGGTTGGACATGGAGGTG

Table 2.6. Sequences of SYBR Green qRT-PCR primers.

All primers were purchased from SIGMA Aldrich (Poole,UK).

2.2.12 Generation of a cartilage specific HDAC3 conditional knockout mouse model.

To determine the role of HDAC3 in endochondral ossification, HDAC3 was conditionally deleted in cells expressing Cre recombinase under the control of Col2α1 promoter (called *HDAC3(Fl/Fl); Col2-Cre(+)* or *HDAC3*$^{Cart\Delta Ex3}$). The steps taken for the generation of the conditional knockout mouse model are summarised in Chapter 7- Figure 7.5. Briefly, three males and three females HDAC3$^{tm1a(EUCOMM)Wtsi}$ targeted; knockout first allele (reporter-tagged insertion with conditional potential) mice, were purchased from the University of Veterinary Medicine, (Vienna, Austria) and detailed information as well as phenotypic data are available from the International Mouse Phenotypic Consortium (IMPC, at http://www.mousephenotype.org/data/search/gene?kw="hdac3").

These mice accounted for the parental line (P) and carried one Wild-type (Wt) allele and a HDAC3 target locus allele (shown in **Figure 2.2**), containing a lacZ-neomycin reporter

cassette flanked by two 48bp FRT sites and a floxed exon 3 (one loxP site either side of exon 3). Presence of the HDAC3 target locus allele was confirmed using primer pairs 1 and 2 (see **Table 2.7** and **Figure 2.2**). These mice are called *HDAC3(+/Fl)* hereafter.

The parental line *HDAC3(+/Fl)* was bred with mice expressing FLP recombinase ubiquitously (Rodriguez et al., 2000; Dymecki 1996), to promote site-specific DNA recombination in the presence of an FRT site and remove the lacZ-neomycin cassette. These breedings resulted in the F1 generation of mice, which were called *HDAC3(+/Fl); FLP(+)* and carried one Wt allele and a Post-FLP HDAC3 locus allele. For genotyping, primer pairs 3 and 4 (**Table 2.7**) were used to confirm FLP recombination and absence of the lacZ-neomycin reporter. Presence of FLP was also confirmed using a PCR reaction which will specifically amplify FLP gene and one example is shown in **Figure 2.3**.

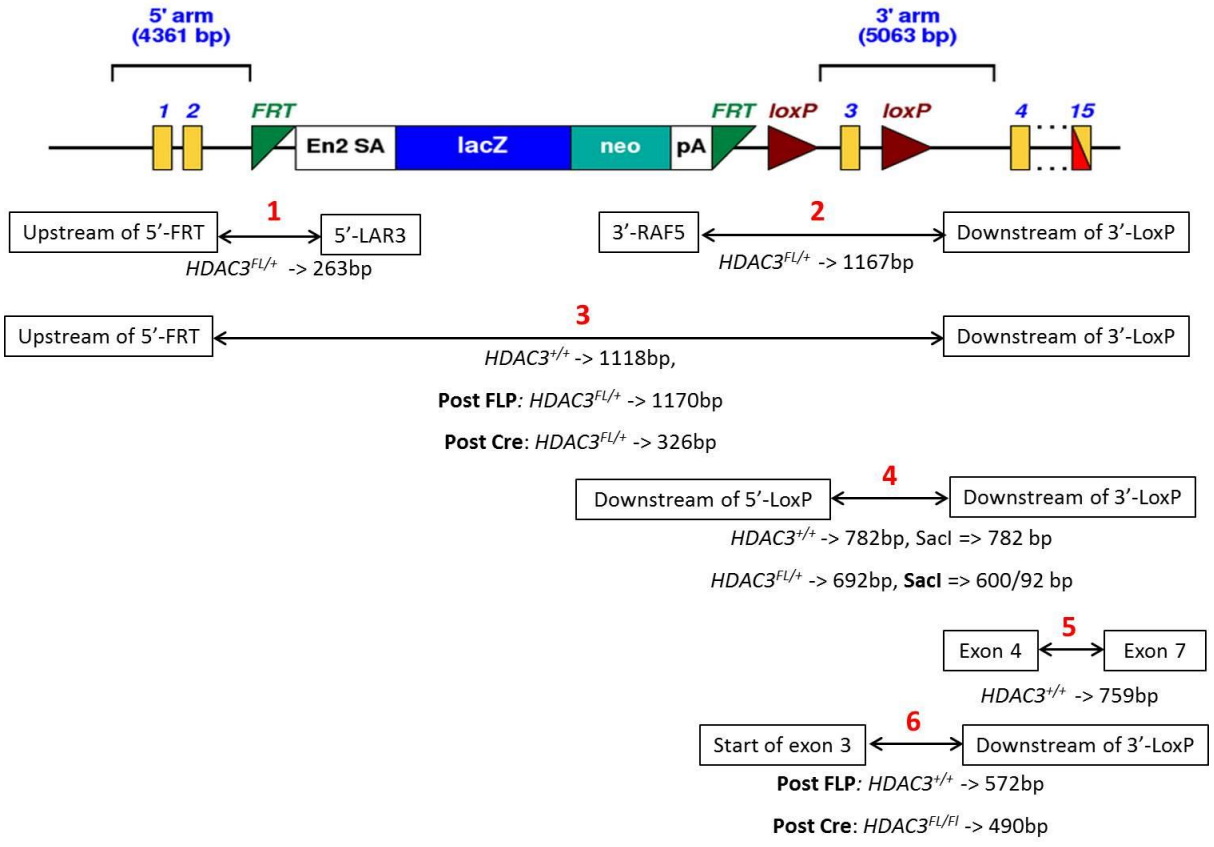

Figure 2.2. HDAC3 transgene and primer pairs used for genotyping mice.

Numbers in red indicate the primer pairs as shown in **Table 2.7**. Double arrows indicate the size of the PCR amplicon.

F1 heterozygous mice were then bred with Col2-Cre mice to generate (F2) heterozygous *HDAC3(+/Fl); FLP(+); Col2-Cre(+)* mice. In F3 generation *HDAC3(+/Fl); FLP(+); Col2-*

Cre(+) heterozygous mice were used for the final breeding step that would generate the conditional knockout mouse model. Genotyping results were obtained using primer pairs 3 and 6 to confirm Cre recombination and HDAC3 exon 3 deletion. Real-time PCR was also used to quantify Col2α1-Cre expression of the F5 mice and normalised to type X collagen expression levels (**Figure 2.4**).

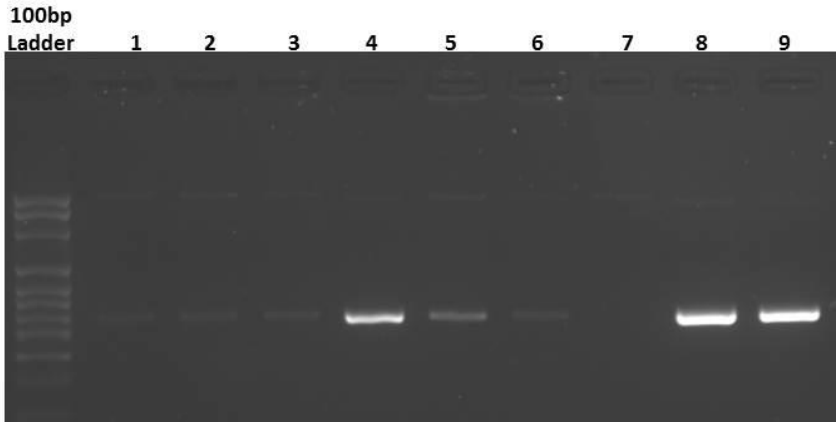

Figure 2.3. FLP presence was confirmed with PCR which would give a band at 234bp.

Animals 4, 5, 8 and 9 were FLP positive, while all the other animals (1, 2, 3, 6 and 7) did not inherit the FLP recombinase gene. bp: base pairs

Pair	Primer Name	Primer sequence (5'-3')	Annealing Tm
Pair 1	Forward- Upstream of 5'-FRT Reverse- 5'-LAR3	TGAGTCTGATGATGGCTCAAG CACAACGGGTTCTTCTGTTAGTCC	65
Pair 2	Forward- 3'-RAF5 Reverse- Downstream of 3'-LoxP	CACACCTCCCCCTGAACCTGAAAC CAGTCATGGGCCTCCTCACAG	65
Pair 3	Forward- Upstream of 5'-FRT Reverse- Downstream of 3'-LoxP	TGAGTCTGATGATGGCTCAAG CAGTCATGGGCCTCCTCACAG	65
Pair 4	Forward- Downstream of 5'- LoxP Reverse- Downstream of 3'- LoxP	GCCGTGGTATTGGGAATGTCT CAGTCATGGGCCTCCTCACAG	65
Pair 5	Forward- Exon 4 Reverse- Exon 7	GTGATGTAACCCTGAGTCTTG AGTCATGACCCGGTCAGTGAG	65
Pair 6	Forward- Start of exon 3 Reverse- Downstream of 3'-LoxP	CAGGTCTTCAAGCCTTACC CAGTCATGGGCCTCCTCACAG	65
FLP	Forward- FLP Reverse- FLP	GGACCGGCAATTCTTCAAGCA CCACGGCAGAAGCACGCTTAT	65

Table 2.7. Sequences of primers used for genotyping mice.

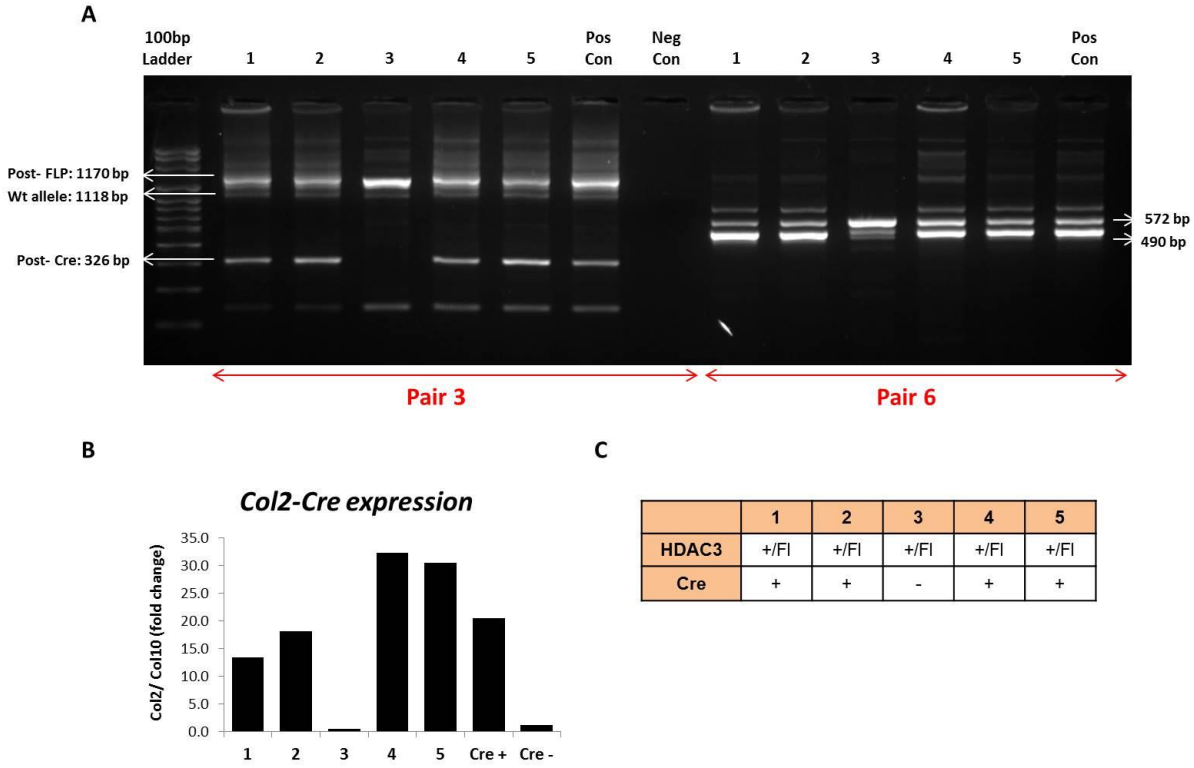

Figure 2.4. Primer pairs 3 and 6 were used to confirm Post-FLP and Post-Cre recombination of the HDAC3 target locus.

A. Primer pair 3 was used to confirm Cre recombination of the Post-FLP allele. The Wt allele amplicon is 1118bp long, whilst the HDAC3 target locus allele recombined by Cre is 326bp long. There is still a band for the Post-FLP HDAC3 target allele amplicon at 1170bp, indicating Cre recombination is not 100% efficient. Primer pair 6 could also be used to demonstrate the presence of the floxed allele, since it amplifies a region around exon 3 (see **Figure 2.2**), which is smaller by 82bp in comparison to the Wt allele. **B.** Cre expression was quantified using qRT-PCR and normalised to type X collagen expression. **C.** Genotyping results from A & B show that animals number 1, 2, 4 and 5 are heterozygous for the HDAC3 (Fl/+) and have also inherited Cre recombinase (Cre positive, Cre+), while animal number 3 is Cre negative (Cre -).

2.2.12.1 Housing and care of animals

Mice were housed at the Comparative Biology Centre (CBC) in Newcastle University, in compliance with the Animals (Scientific Procedures) Act 1986 and its associated Codes of Practice. Mice were ear/notched at postnatal day 21 and separated into males/females after the weaning period. Up to 6 mice were housed together in special containers (300cm^2, 12cm height) to allow enough space for physical activities/ exercise. In cases where single housing had to be performed, close visual monitoring of the activity of the animals was maintained. In the case of breeding, one male was introduced to one or two females and re-introduction of

the breeders to already established groups was avoided in order to avoid problems of incompatibility and disrupted social relationships. Cleaning of the containers was performed by the technical staff in the CBC twice a week. All animals always had access to food and drinking water. Detailed record keeping of each animal used in this study was performed using the AniBio software system and returns of procedures (for Home Office) including severity limits and protocols performed annually.

2.2.12.2 Genotyping mice

Genotypes of the HDAC3 mice used in this study were determined using the Phire Tissue Direct PCR Master Mix (F170S, Thermo Scientific, Leicestershire, UK).

Method

DNA extraction was performed following the manufacturer's protocol. Briefly, an ear notch was obtained from each mouse and incubated in a 20µl mix of Dilution buffer and 0.5µl DNA release additive. Next tissue extracts were incubated at room temperature for 5 minutes, vortexed, centrifuged for 1 minute at 13,000 rpm and incubated at 95°C for 5 minutes. Samples were next vortexed and centrifuged as above and then stored at 4°C or PCR was performed immediately.

All PCR preparations were performed at room temperature as the Phire Hot Start II DNA Polymerase is specific for hot start amplification. To a 0.2ml PCR tube 10µl Phire Hot Start II DNA PCR reaction mix was added together with 0.25µM of each forward and reverse primers (see **Table 2.7**) and 1µl tissue extract and dH_2O to give a 20µl total reaction. Thermocycling stages included: 94°C for 5 minutes followed by 35 cycles of 94°C for 30 seconds, 65°C for 30 seconds, 72°C for 1 minute and a final step of 72°C for 10 minutes. The produced amplicons were then loaded onto a 1.5% (w/v) agarose TAE (Tris-Acetate-EDTA) gel and determination of mouse genotype followed. Mice were not born at expected Mendelian ratios since no conditional knockout animals were found during this study (see Chapter 7, Tables 7.1 & 7.2). COL2-Cre expression was quantified using real-time RT-PCR and the primers sequences can be found at **Table 2.8**. **Figure 2.2** shows where the primers are located, the size of the amplicons produced depending on the genotype and if they were used following FLP or Cre recombination.

Gene	Primer	Primer sequence (5'-3')
Mouse *COL2*	Forward	TCGATGCAACGAGTGATGAGG
	Reverse	GAAACCATTTCCGGTTATTCAACTTGC
Mouse *COL10*	Forward	CTTCCTGTCAAGCTCATCC
	Reverse	TAGGATTGCTGAGTGCTCC

Table 2.8. Sequences of primers used for COL2-Cre quantification using real-time RT-PCR (SYBR Green).

2.2.12.3 Agarose gel electrophoresis

Reagents

- TAE buffer (0.04M Tris (pH 8), 5.7% (v/v) glacial acetic acid and 0.001M ethylenediaminetetraacetic acid (EDTA)
- Loading buffer (Tris 0.125M (pH 6.8), 10% (v/v) glycerol and 0.001% (w/v) bromophenol blue)

Method

Gels were prepared at 1.5% (w/v) agarose in TAE with the addition of final 0.2µg/ml ethidium bromide (EtBr) solution. The DNA was electrophoresed on the gel in loading buffer and bands visualised on a ChemiGenius II BioImager (Syngene, Cambridge, UK) using a GeneRuler^{TM} 100bp or 1kb DNA ladder to determine DNA band size.

2.2.12.4 Cloning

Cloning reactions using the TOPO® TA Cloning® Kit (Life technologies) and bacterial transformation were performed according to manufacturer's instructions to check the sequence of the amplicons produced. Briefly reactions were prepared using 2µl of the PCR product produced as described above, 1µl of TOPO® vector and made up to 6µl with H_2O. The reaction was gently mixed and incubated for 5 minutes at room temperature. After performing the TOPO cloning reaction, One Shot® Mach1™-T1R *E. coli* competent cells were transformed. For each transformation one LB plate containing 100µg/ml Ampicillin and 40mg/ml 5-bromo-4-chloro-3-indolyl-β-D-galactopyranoside (X-gal) diluted in Dimethyleformamide (DMF) were placed at 37^{o}C until ready for use. S.O.C medium was also warmed up at room temperature and one vial of One Shot cells was thawed on ice. (see also section **2.2.2** ***Generation and use of expression vectors***). 2µl of each TOPO cloning reaction was added into a vial of One Shot cells, mixed gently and incubated on ice for 30 minutes. The cells were then heat-shocked at 42^{o}C for 30 seconds and then immediately transferred on ice. 250µl of S.O.C medium was then added to the tube and the samples were then incubated at

37ºC for 1 hour at 225rpm. Following incubation 50µl from each transformation were spread onto a pre-warmed LB-agar ampicillin + x-gal selective plate and incubated at 37ºC for 16 hours. The next day individual white (or light blue) colonies were selected and incubated in 5ml of LB supplemented with ampicillin (100µg/ml) at 37°C with shaking at 225rpm. Plasmid DNA was then isolated and analysed as described in section **2.2.2** ***Generation and use of expression vectors***and the samples were sequenced by Sanger sequencing (Source BioScience Life Sciences, Nottingham, UK) using the M13 Forward (−20) and M13 Reverse primers, the sequence of which can be found on **Table 2.9**.

Primer	Sequence (5'-3')
M13 Forward	GTAAAACGACGGCCAG
M13 Reverse	CAGGAAACAGCTATGAC

Table 2.9. Primers used for sequencing.

2.2.13 Destabilisation of the medial meniscus (DMM) surgery

Pre-operation: Male mice at 10 weeks of age were used for the DMM surgery. Each mouse was anaesthetised separately using isoflurane (2.5-3.5%) 1L/min O_2 and then placed in a recumbent position with their head in the mask. The left knee was shaved and the area disinfected with chlorohexidine solution (ECOLAB, MN, USA). An ear notch was taken at this stage if not earlier for genetic identification; the animal was weighed and checked for any possible infection. Subcutaneous injection of buprenorphine (0.15ml, 3µg/ml solution) was then performed.

Operation: A scalpel was used to make a small vertical incision in the skin just left of the knee joint avoiding the patella ligament region. The incision was then increased using curved scissors and any blood vessels present were cauterised to avoid bleeding. The fat tissue was then removed with scalpel/ scissors pealing back and avoiding blood vessels. If necessary, blood vessels, coming from the fat pad, were cauterised to avoid excess bleeding. Identification of the medial collateral ligament and the patella ligament was then necessary and a small vertical incision was made (large scalpel) down the side of the patella ligament and extended to the left. The fat pad was cleared with two fine forceps to expose the medial meniscus with the white medial meniscotibial ligament (MMTL) lying horizontal extending towards and behind the patella region. Throughout the surgery, any veins were cauterized to

avoid bleeding. Using a small scalpel blade an incision of the medial meniscus was made. The skin was then hold together with forceps and clipped. The clips were checked later that day and every day post-surgery before removal seven days post-surgery.

Post-operation: The animals were located in clean cages and the cages placed at 27^{o}C until the animals reach consciousness. Another dose of pain relief (buprenorphine, 0.15ml, 3µg/ml solution) was subcutaneously injected to all mice the following day and the animals were closely watched thereafter to ensure successful recovery.

End of experiment: Eight weeks post-surgery the animals were euthanized using CO_2 or by dislocation of the neck and both knee joints harvested and fixed in formalin solution, neutral buffered 10% (contains formaldeyde 4% (w/v), SIGMA-Aldrich, Poole, UK) overnight at room temperature with rotation, before decalcification in Formica 2000 (Formic acid, EDTA, Decalcifier, #1340, Decal Chemical Corp, NY) for 16 hours at room temperature was performed.

2.2.14 Intra-articular injections

For intra-articular delivery of RNAi for HDAC3 *in vivo*, the AteloGene™ in vivo siRNA Transfection Kit (KKN-1395, Reprocell-Europe) was used according to manufacturer's instructions and diluted in 0.01% (w/v) of Evan's blue dye (SIGMA Aldrich, Poole UK) which was used to ensure accuracy of the injection. Animals were anesthetised using isoflurane (2.5-3.5%) 1L/min O_2 and prepared as described for the DMM surgery in section **2.2.13** ***Destabilisation of the medial meniscus (DMM) surgery*** Using a 0.5ml syringe and 27G needles, 10µl of the prepared solution was gently inserted in the joint space. The skin was then held together and clipped. The clips were checked later on the same day and removed at the end of the experiment either three or six days after the injections.

2.2.15 Histological Staining

2.2.15.1 Embedding and microtome sectioning

After fixation of mouse knee joints or cartilage discs/pellets produced by differentiated MSC in Formalin solution for 24 hours at room temperature with rotation, tissue was sent in Newcastle Biomedicine Biobank (Newcastle University, UK) for dehydration in an ethanol series. Following tissue processing the samples were placed in wax moulds and heated forceps used to position the limb/tissue for longitudinal sectioning. Wax embedded

joints/cartilage discs/pellets were sectioned at a thickness of 5μm using a rotary microtome. Coronal sectioning was performed for the DMM joints stained for Safranin-O (see **Figure 7.1** and **Figures 7.2-7.3**), while sagittal sectioning was performed for analyzing growth plate development (as shown in **Figure 7.10**). Sections were taken and placed on warm water (37°C), allowed to expand and then transferred to slides (placed as sister sections, 100 slides/ joint and 20 slides/ disc or pellet). Slides were then left to dry and then placed in an oven overnight at 37°C. The slides were then stored at room temperature until staining was to be performed. Prior to any staining procedure, slides were placed in an oven at 60ºC for approximately 30min-1h to allow excess wax to melt. For the DMM experiment, 20 sections from each mouse were scored by two independent scorers blinded to drug treatments and the scores were combined and averaged. For analyzing the development of the growth plate of the three-week old wild-type and heterozygotes *HDAC3(Fl/+)*, at least 3 mice from different litters with the same genotype were used and in total 27 sections were stained and analysed.

2.2.15.2 Haematoxylin and Eosin staining

Haematoxylin and Eosin staining (H&E) is one of the principal stainings in histology. In H&E staining, nuclei are stained black due to the binding of the haematoxylin-dye-complex to the DNA and cytoplasm is stained pink/red. Slides were dewaxed in xylene (2 times, for 5 minutes each) and then rehydrated through a series of ethanol concentrations (100%, 95%, 75% and 50%) and ddH_2O for 2 minutes each. Slides were then placed in Mayers haematoxylin solution (SIGMA Aldrich, Poole, UK) for 1.5min and then placed under running tap water for 2-3 minutes until tissue sections turned a purple- blue colour. Slides were then placed in 1% aqueous eosin (SIGMA Aldrich, Poole UK) for 2 minutes and then quickly rinsed in running tap water for 30sec. The slides were then dehydrated through a series of ethanol concentrations (50%, 75%, 95%, 100% and 100%) for 1min each. Finally slides were placed in xylene (2 times for 10 minutes each), before mounting in DPX mountant (SIGMA-Aldrich, Poole, UK) and left overnight in a dehumidifier chamber to dry.

2.2.15.3 Safranin-O staining

This method is used for the detection of cartilage, mucin and mast cell granules on formalin-fixed; paraffin- embedded tissue sections and may be used for frozen sections as well. The cartilage and mucin will be stained orange to red and the nuclei will be stained black. The cytoplasm is stained green. This method is recommended as a semi-quantitative scoring system following DMM surgery (see **Table 2.10** and **Figure 2.5**). Two independent and blind

scorers assessed cartilage damage following eight weeks of the DMM surgery. Briefly, slides were de-waxed and rehydrated as described in section **2.2.15.2 Haematoxylin and Eosin staining**. Slides were then placed in Weigert's iron haematoxylin working solution (SIGMA-Aldrich, Poole, UK) for 10min and then briefly washed under running distilled water. Slides were then dipped briefly in acid alcohol (70% (v/v) EtOH, 1% (v/v) HCl) to remove excess haematoxylin and then rinsed in running tap water to stop the reaction. Slides were then placed in 0.06% (w/v) Fast Green solution (SIGMA-Aldrich, Poole, UK) for 5 minutes and then quickly rinsed in 1% (v/v) acetic acid solution (SIGMA-Aldrich, Poole, UK) for no more than 10-15 seconds. Finally, slides were stained in 0.1% Safranin O solution for 5 minutes before they dried to absorb excess staining and then transferred to 95% of ethanol for 1 minute and then to two 100% ethanols for 2 minutes each. Finally slides were placed in xylene (2 times for 10 minutes each), before mounting in DPX mountant (SIGMA-Aldrich, Poole, UK) and left overnight in a dehumidifier chamber to dry.

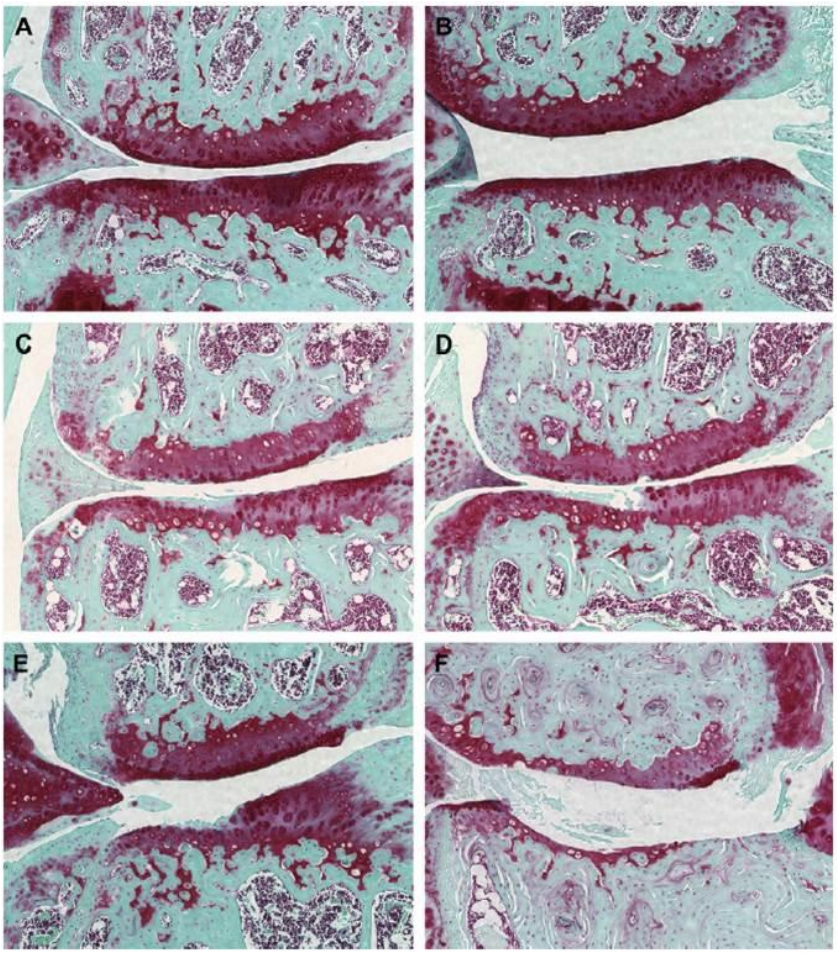

Figure 2.5. Safranin-O photomicrographs showing the medial femoral chondyle (MFC- above) and medial tibial plateu (MTP- below) and the medial meniscus (left), displaying a variety OA severity and semi-quantitive scores.

First score represents MFC, second score is MTP; **A.** 0, 0.5; **B.** 0, 1; **C.** 0.5, 2; **D.** 3, 3; **E.** 0, 4; **F.** 5, 6 [taken from (Glasson et al. 2010)].

Grade	Osteoarthritic damage
0	Normal
0.5	Loss of Safranin-O without structural changes
1	Small fibrillations without loss of cartilage
2	Vertical clefts down to the layer immediately below the superficial layer and some loss of surface lamina
3	Vertical clefts/erosion to the calcified cartilage extending to <25% of the articular surface
4	Vertical clefts/erosion to the calcified cartilage extending to 25- 50% of the articular surface
5	Vertical clefts/erosion to the calcified cartilage extending to 50- 75% of the articular surface
6	Vertical clefts/erosion to the calcified cartilage extending >75% of the articular surface

Table 2.10. The recommended semi-quantitative scoring system for assessing cartilage damage on DMM mouse joints [taken from (Glasson et al. 2010)**].**

2.2.15.4 Masson's trichrome staining

This method is used for the detection of collagen fibres in tissues such as skin, heart, knee, etc. on formalin-fixed, paraffin-embedded sections and may be used for frozen sections as well. The collagen fibres will be stained blue and the nuclei will be stained black and the background is stained red. De-waxing and rehydration of slides was performed as described above (in **2.2.15.2 Haematoxylin and Eosin staining**). Slides were stained in Weigert's iron haematoxylin working solution (SIGMA-Aldrich, Poole, UK) for 10min and then rinsed in running tap water for 10min and washed in distilled H_2O. Sections were subsequently differentiated in phosphomolybdic-phosphotungstic acid solution (SIGMA Aldrich, Poole, UK) for 10-15min until collagen was not red. Slides were then transferred directly to aniline blue solution and stained for 5-10min before rinsed briefly in dH_2O and differentiated in 1% acetic acid solution for 2-5min. Finally slides were washed in dH_2O, dehydrated very quickly in 95% ethanol, 100% ethanol for 1-2 minutes and cleared in xylene before mounting in DPX mountant (SIGMA-Aldrich, Poole, UK) and left overnight to dry.

2.2.15.5 Alcian Blue staining

This method was used to stain sulphated proteoglycans in cartilage. At pH 0.75 Alcian Blue specifically stains sulphated proteoglycans and this pH is recommended for staining cartilage. At pH 2.5 it stains most acid mucins (except some of the strongly sulphated groups),

at pH 1.0 it will stain only weakly and strongly sulphated acid mucins, and at pH 0.2 it will only stain strongly sulphated acid mucins. De-waxing and rehydration of slides was performed as described above (in **2.2.15.2 Haematoxylin and Eosin staining**). Slides were stained in alcian blue solution (SIGMA Aldrich, Poole, UK) for 10 minutes, washed twice with distilled H_2O for 5 minutes each time and then placed in fast red solution for 3-5 minutes (SIGMA Aldrich, Poole, UK). Finally slides were washed in dH_2O, dehydrated very quickly in 95% ethanol, 100% ethanol for 1-2 minutes and cleared in xylene before mounting in DPX mountant (SIGMA-Aldrich, Poole, UK) and left overnight to dry.

2.2.15.6 Toluidine Blue staining

This method is used to stain polysaccharides in cartilage (purple), since it is a basic dye with affinity for acidic tissue components. De-waxing and rehydration of slides was performed as described above (in **2.2.15.2 Haematoxylin and Eosin staining**). Slides were then placed in toluidine blue O solution (0.04g toluidine blue in 0.1M acetate buffer) (SIGMA Aldrich, Poole, UK) for 10 minutes, washed twice with distilled H_2O for 5 minutes each time and then placed in fast red solution for 3-5 minutes (SIGMA Aldrich, Poole, UK). Finally slides were washed in dH_2O, dehydrated very quickly in 95% ethanol, 100% ethanol for 1-2 minutes and cleared in xylene before mounting in DPX mountant (SIGMA-Aldrich, Poole, UK) and left overnight to dry.

2.2.15.7 Alizarin red/Alcian blue staining of one day old mouse skeletons

One-day old pups were sacrificed, and the skin and intestines were removed. The skeletons were then fixed in 95% EtOH for three days and then placed in alcian blue solution (15mg + 80ml 95% EtOH + 20ml HAc, pH 0.75) for 24 hours to stain cartilaginous tissues. The skeletons were then rinsed twice using 95% ethanol and placed in 95% ethanol for 48 hours before clearing with 1% (w/v) KOH for 6 hours was performed. Alizarin red solution (50mg/l 2% (w/v) KOH) was subsequently used to stain bone and the skeletons were then placed in 2% (w/v) KOH for 24 hours following by incubation in 80:20 2% KOH: glycerol, 60:40 2% KOH: glycerol, 40:60 2% KOH: glycerol and 20:80 2% KOH: glycerol for 24 hours each.

2.2.16 Immunohistochemistry (IHC)

Method

Sections were de-paraffinised and rehydration was performed as described above (in **2.2.15.1 Embedding and microtome sectioning**). For heat-induced epitope retrieval the sections were placed in sodium citrate buffer pH 6.0 and microwaved for 2 x 5 minutes. The endogenous peroxidase activity was quenched by incubating the slides in 0.3% (v/v) H_2O_2 in dH_2O for 30 minutes. Sections were then blocked in 2% (v/v) normal horse blocking serum for 30 minutes before 1 hour incubation with a 1:100 dilution of primary antibody for anti-acetyl Lysine, 1:1000 dilution for anti-HDAC3, 1:50 dilution for anti-acetyl α-tubulin and 1:100 dilution for Ki67 antibody (diluted in PBS with 2% (v/v) normal horse blocking serum) (dilutions optimised by Sharon Watson, Newcastle University). Slides were then incubated with Biotin-conjugated secondary antibody for 30 minutes followed by further 30 minutes incubation with Avidin/Biotin Complex (ABC). Peroxidase substrate 3,3'-diaminobenzidine (DAB) demonstrated peroxidase activity. Sections were washed in running tap water for 5 minutes and were counterstained with haematoxylin followed by dehydration through graded concentrations of ethanol for 5 minutes each: 50%, 70%, 95% (x2) and 100% (x2) with a final 5 minutes in xylene (x2). All incubation steps were carried out at room temperature and sections were washed thoroughly in between each step; all washing steps used PBS for 2 x 5 minutes unless otherwise stated. Slides were mounted with D.P.X. mounting medium and covered with glass coverslips for visualisation under a Leica DM4000B microscope (Leica, Milton Keynes, UK). IHC experiments were carried out by Sharon Watson, Musculoskeletal Research Group (Institute of Cellular Medicine, Newcastle University, Newcastle, UK).

2.2.17 Image analysis

All images were taken using a Leica SCN 400 slide scanner and viewed with the Slide Path software (Leica, Milton Keynes, UK). A scale bar was automatically included in each image at scanning and is given in μm. Quantification of the immunoblotting (IB) bands and immunohistochemistry (IHC) staining was performed using ImageJ software and compared to the positive loading control used in each experiment (either GAPDH or β-catenin for IB).

Briefly, the images were saved as .jpeg or .tiff files and opened with ImageJ software. Then for IB quantification the brightness/contrast was adjusted by the Image -> Adjust -> Brightness/Contrast menu. The rectangular selection tool was then selected and a rectangular drawn around the first band to be quantified. Then Analyse -> Gels-> Select first lane was

selected. The first rectangular was then dragged to the second gel band to be quantified and then Analyse-> Gels-> Select next lane. The second lane box was dragged to the third gel band and then Analyse-> Gels-> Select next lane and this process was repeated for all the bands present in the gel. To finish this step go back to Analyse-> Gels-> Plot lanes. This will bring up a graphical depiction of band intensity for each band selected in the image. Then the straight line tool was selected from the tool menu and a straight line was marked under the peak for the first lane and the same process was repeated for all the lanes. Then the wang tool was selected from the tool menu and each band peak was selected. The areas under the peaks were then measured and the results copied to Microsoft Office Excel for further normalisation with reference to the loading control used.

For IHC quantification, the area of interest was determined using an area cut off. The image was calibrated based on a colour threshold by selecting Image-> Adjust -> Colour threshold. Thresholding method was set to 'Default', Threshold colour to 'Red', and the colour space was set to HSB (Hue, Saturation, Brightness). The risk area was then selected and background excluded from the analysis by adjusting the brightness and saturation of the image and clicking on select to apply the filter. Two filters were applied, one to define the area of interest, and a second filter to select the positive (brown) stained cells present in the already defined by the first filter area. Both filtered areas were then measured and a percentage of the positive stained cells was calculated with reference to the whole area.

2.2.18 Flow cytometry

To study the effect of HDAC3 and/or E2F1 knockdown in cell cycle progression of the SW1353 cells DNA quantitation and flow cytometry analysis was performed. Propidium Iodide (PI) binds the DNA present in the cell. Cells that are in S phase will have more DNA than cells in G1 phase and will take up proportionally more dye and will fluoresce more brightly. Once the G1 cells have doubled their DNA content and in G2 phase they will be approximately twice as bright as the ones in G1.

Reagents

- 70% (v/v) Ethanol
- 50µg/ml Propidium Iodide diluted in PBS (P4170, SIGMA Aldrich, Poole, UK)
- 100µg/ml Ribonuclease I diluted in H_2O (R6513, SIGMA Aldrich, Poole UK)

Method

One million SW1353 cells were plated in 10cm culture dishes and the following day transfected with siRNA as described in section **2.2.7** ***RNA interference (RNAi)*****.** Next, serum starvation followed to achieve cell cycle synchronisation, growth restriction in the G0/G1 phase and induce quiescence (Rosner et al. 2013). The following day, cells were harvested by trypsinisation, washed twice in PBS and fixed in cold 70% ethanol to allow entry of the dye which is otherwise actively pumped out by living cells. The ethanol was added dropwise while vortexing to avoid cell clumping. Samples were then stored at 4^{o}C for at least 30 minutes, pelleted by brief centrifugation at 2,000 rpm to discard the ethanol, washed twice with PBS and centrifuged each time at 2,000rpm for 5 minutes. To ensure that only DNA is stained, cells were treated with Ribonuclease I (100µg/ml), and PI at a final concentration 50µg/ml was added to each sample.

For analysis the FACSCanto II analyser (Flow cytometry unit, Newcastle university, UK), was used and at least 10,000 single cell-reads were taken for each sample. Two biological repeats were performed to ensure statistical significance and reproducibility. First forward and side scatter were measured to identify single cells and pulse processing was used to exclude cell doublets from the analysis, this was achieved by using pulse area versus pulse width. PI has a maximum emission at 605nm so can be measured in either FL2 (585/42 filter) or FL3 (650LP filter) and 400 voltage. While running the cytometer the following plots were displayed; forward and side scatter to identify the cells, pulse area versus pulse width to identify clumps and doublets, forward scatter versus PI signal and PI histogram as shown in **Figure 2.6 A**.

For analysis, first a gate was set on the single cell population using pulse width versus pulse area, then this gate was applied to the scatter plot and obvious debris was gated out. The gates were then combined and applied to the PI histogram plot, as shown in **Figure 2.6 B**. By using markers set within the analysis program, the number of cells in each cell cycle phase was quantified (**Figure 2.6 C**). Next, using FlowJo, an algorithm which attempts to fit Gaussian curves to each phase was used and a more objective quantitation of the percentage of cells in each cell cycle phase was acquired (**Figure 2.6 D**).

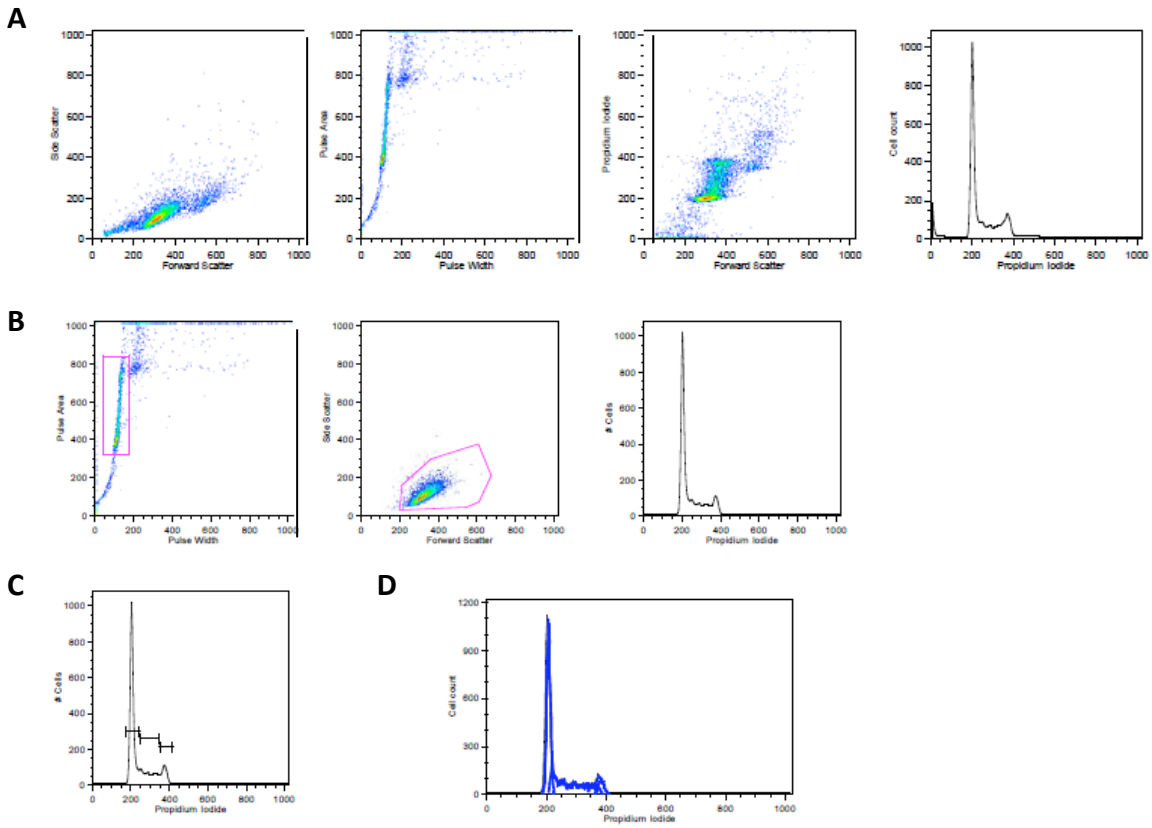

Figure 2.6. Flow cytometry analysis and cell gating following DNA staining using Propidium Iodide.

A. From the left to the right the following plots are displayed: Forward and side scatter to identify the cells, Pulse area versus pulse width to identify clumps and doublets, Forward scatter versus PI and finally the PI histogram plotting cell counts relative to PI emission. **B.** Gating was first performed to set on the single cell population using pulse width versus pulse area, then this gate was applied to the scatter plot and obvious debris was gated out. The gates were then combined and applied to the PI histogram plot. **C.** Next, markers set within the analysis program were used to quantify the number of cells in each cell cycle phase. **D.** Using FlowJo, the Watson pragmatic algorithm was used to fit in Gaussian curves to each phase of the cell cycle.

2.2.19 RNA microarray analysis

A gene expression array experiment was performed to identify differentially expressed genes following *HDAC3* gene silencing or inhibition after Apicidin treatment in SW1353 cells (as described in sections **2.2.7** ***RNA interference (RNAi)*** and **2.1.7** ***Histone Deacetylase Inhibitors*** respectively). Two independent IL-1 stimulation time-points were performed including IL-1 stimulation for 1 hour and for 6 hours and compared with the basal-no IL-1 stimulation time-point. Three biological replicates were included per time-point and treatment. Following RNA extraction using the RNeasy mini kit (Qiagen, West Sussex, UK) according to manufacturer's instructions, RNA quality was checked using real-time RT-PCR and the samples analysed by the Central Biotechnology Services (Cardiff University) for analysis using the Illumina platform. For total RNA assays using an Agilent 2100 bioanalyzer, the ribosomal ratio of 28S and 18S were determined, giving an indication on the integrity of the RNA sample. In humans, 28S rRNA has ~5070 nucleotides, and 18S has 1869 nucleotides, which gives a 28S/18S ratio of ~2.7. A high 28S/18S ratio is an indication that the purified RNA is intact and has not degraded. Usually, a 28S/18S ratio of >2 is taken to mean that the purified total RNA is of high quality. Additionally, the RNA integrity number (RIN) was utilized to estimate the integrity of total RNA samples based on the entire electrophoretic trace of the RNA sample, including the presence or absence of degradation products. The data obtained were also displayed as a densitometry plot, creating a gel-like image. Numbers from '1' to '10' were used as labels. '10' stands for a perfect RNA sample without any degradation products, whereas '1' marks a completely degraded sample. The labels in-between are used to indicate progressing degradation states of the RNA sample. **Figure 2.7** shows typical representatives of the rRNA ratio and RIN number for one out of the 36 samples included in this microarray experiment. RNA integrity and quality of all samples presented similar ratios/RIN.

Following RNA quality and degradation assessment, RNA was fluorescent labelled and hybridisation followed. Briefly, the samples were allowed to hybridize onto the same microarray glass slide containing millions of copies of identical oligonucleotides that correspond to a gene. At this point any RNA sequence in the sample will hybridize to specific copies on the glass slide based on complementarity. The amount of bound RNA to a copy will be directly proportional to the initial number of RNA molecules present for that gene in a sample. Following the hybridisation step, the hybridized microarray is excited by a laser and scanned at suitable wavelengths to detect the fluorescent dyes. The amount of fluorescence emitted upon excitation corresponds to the amount of bound nucleic acid.

The Illumina BeadChip HT12-v4 array was used, which is based on the GRCh37 human assembly. Raw data (IDAT files) from the Illumina scanner were summarised into a sample probe profile and control probe profile using Illumina's Genome Studio. In this process, replicate bead measurements are collapsed to ascertain average signal intensity and bead standard error, which allows for a more reliable measure of signal intensity. The raw data was normalised in R using robust spline normalisation (RSN), and variance stability transformation (VST), which is a more sophisticated method to quantile. Normalisation functions were used from the Lumi library (Lu et al. 2008). A bead level filtering step is implemented to remove any probes that fail detection p value in more than 50% of samples.

Differentially expressed gene lists were finally obtained and a final cut off of ± 1.5-fold change and a p-value ≤ 0.05 were applied. Differential expression was performed using a linear model framework and Bayesian adjustments from the Limma package (Ritchie et al. 2015). Additional analysis were performed using GATHER (A Gene Annotation Tool to Help Explain Relationships) (Chang and Nevins, 2006), a bioinformatic tool that has the capacity to discover novel functions and predict transcription factor binding sites and pathways affected by a specific gene group.

Other bioinformatic tools used in this study include STRING (a functional protein association network) (Szklarczyk et al. 2015) that predicts protein-protein interactions, PROMO (Messeguer et al. 2002; Farre et al. 2003) was used to predict transcription factor binding sites to the MMP promoters and Ingenuity Pathway Analysis (IPA) was used to identify upstream regulators, mechanistic networks, pathways and microRNA that might have caused the results observed in the microarray. VENNY was used to create all the venn diagrams in this thesis (Oliveros, 2007-2015) and the Open Targets platform (Koscielny et al. 2017) was used to identify OA and cartilage disease related genes.

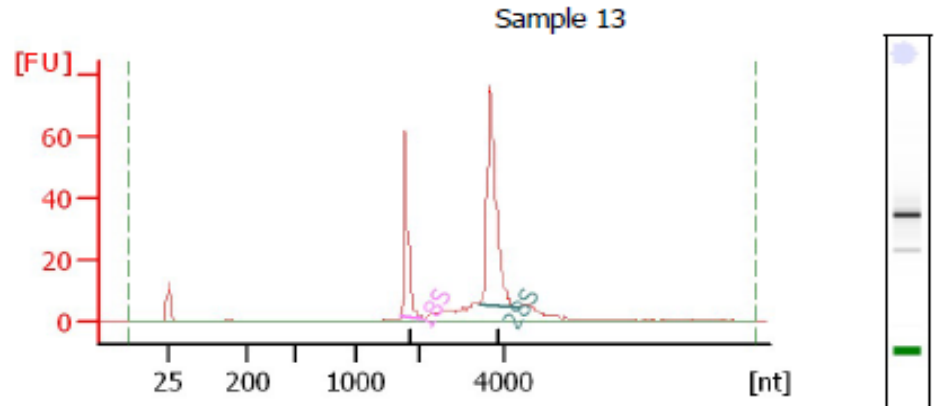

Overall Results for sample 1 : Sample 13

RNA Area:	281.5
RNA Concentration:	298 ng/µl
rRNA Ratio [28s / 18s]:	2.2
RNA Integrity Number (RIN):	10 (B.02.07)
Result Flagging Color:	
Result Flagging Label:	RIN:10

Fragment table for sample 1 : Sample 13

Name	Start Size [nt]	End Size [nt]	Area	% of total Area
18S	1,719	2,049	55.4	19.7
28S	3,428	4,393	122.6	43.6

Figure 2.7. Representatives of the rRNA ratio [28S/18S] and RNA Integrity Number (RIN) (red box) for sample 13. The densitometry plot on the right shows the integrity of 28S (top band) and 18S (bottom band) in a gel-like image.

Two differential expression tests were carried out using a cut off of ± 2 fold change and a p-value ≤ 0.01.

(i) Knockout comparisons: siHDAC3 versus siCON and Apicidin versus DMSO for each time point and

(ii) Time point comparisons: no IL1 versus IL1- 1 hour or IL1- 6 hours of stimulation for each treatment.

2.2.20 Chromatin Immunoprecipitation (ChIP)

Reagents

- ChIP Lysis buffer: 50mM HEPES-NaOH pH 7.5, 140mM NaCl, 1mM EDTA pH 8.0, 0.1g SDS, 0.1g Sodium Deoxycholate, 1ml Triton X-100, 2 tablets protease inhibitors (cOmplete^{TM} Protease inhibitor cocktail), add up to 100ml with ddH_2O
- RIPA Buffer: 50mM Tris-HCl pH 8.0, 150mM NaCl, 2mM EDTA pH 8.0, 1ml NP-40, 0.1g SDS, 0.5g Sodium Deoxycholate, 2 tablets protease inhibitors, add up to 100ml with ddH_2O
- Low Salt Buffer: 0.1g SDS, 2mM EDTA pH 8.0, 20mM Tris-HCl pH 8.0, 150mM NaCl, 1ml Triton X-100, add up to 100ml with ddH_2O
- High Salt Buffer: 0.1g SDS, 2mM EDTA pH 8.0, 20mM Tris-HCl pH 8.0, 500mM NaCl, 1ml Triton X-100, add up to 100ml with ddH_2O
- LiCl Salt Buffer: 0.25M LiCl (SIGMA-Aldrich, L4408), 1mM EDTA pH 8.0, 10mM Tris-HCl pH 8.0, 1ml NP-40, 1g Sodium Deoxycholate, add up to 100ml with ddH_2O
- Elution Buffer: 1g SDS, 100mM $NaHCO_3$, add up to 100ml with ddH_2O
- TE Buffer: 10mM Tris-HCl pH 8.0, 1mM EDTA pH 8.0, add up to 100ml with ddH_2O
- TBS Buffer: 50mM Tris-HCl pH 7.5, 150mM NaCl, add up to 100ml with ddH_2O
- Proteinase K (P6556, SIGMA-Aldrich)
- Glycogen (AM9516, Invitrogen)

Method

Cross- linking and cell harvesting: First 2-3 x 10^6 SW1353 cells were plated in T75 flasks or 150cm^2 tissue culture dishes and incubated for 5 days at 37ºC in 5% (v/v) CO_2. Cross-linking was performed in confluent flasks (10^7 -5 x 10^7 cells) by adding formaldehyde dropwise to a final concentration of 0.75% with rotation for 10 minutes. Then 125mM glycine was added to the flask and rotation for 5 minutes at room temperature followed. The cells were then rinsed twice using ice- cold PBS, harvested by trypsinisation and immediately transferred to a 50ml cold tube. Centrifugation then followed at 4ºC for 5 minutes at 1,000 x g to pellet the cells and remove supernatant. The cell pellets were then suspended in ChIP Lysis buffer (750µl per 10^7 cells) and incubated on ice for 10 minutes. The chromatin was then either stored at -80ºC or sonication and IP followed immediately.

Sonication: Sonication was performed using Bioruptor (Diagenode) and optimised as different cells require different sonication times. 12 cycles (30 seconds ON: 20 seconds OFF each cycle) were chosen for SW1353 cells (see also Chapter 5, **Figure 5.11**), since after 12 cycles

of DNA sonication, there was the highest amount of 200-500bp sonicated chromatin which is considered to be ideal for real-time PCR analysis. The samples were then centrifuged for 10 minutes at 4^{o}C at 800 x g to pellet cell debris. Supernatant was transferred to a new tube and used for immunoprecipitation.

Immunoprecipitation: First the amount of chromatin to be used for IP was determined and 1-10% input was also included for each antibody used. Pre-clearing of the sonicated chromatin was performed as previously described (section **2.2.10** ***Immunoprecipitation (IP)***). 10^6 cells were used for 1µg of E2F-1 antibody and 3 x 10^6 cells for 4µg of HDAC3 antibody (see also **Table 2.1**) and incubated at 4^{o}C for 1 hour with rotation. An equal volume of Protein A and G beads were prepared and washed three times with 1ml RIPA Buffer, centrifuged each time at 10,000 x g, at 4^{o}C for 1 minute. Then 20µl of beads in RIPA buffer were added per 0.2-2µg of primary antibody used and incubated overnight at 4^{o}C with rotation. The following day the complex of sonicated chromatin- primary antibody-beads was collected by centrifugation at 2,000 x g for 1 minute at 4^{o}C and the supernatant was discarded. The bead pellet was then washed 3 times once with low salt buffer, second with high salt buffer and finally with LiCl buffer and centrifuged each time at 2,000 x g for 1 minute at 4^{o}C.

Elution and reverse cross-linking: After the last wash, the DNA was eluted from the beads by washing with elution buffer and rotating at room temperature for 30 minutes. The samples were centrifuged at 4^{o}C for 1 minute at 2, 000 x g and then supernatant was transferred to a new tube. The input was included at this stage. 400µl TBS and 5µl 20mg/ml Proteinase K were added to each sample and heat at 65^{o}C overnight with rotation.

DNA extraction using phenol-chloroform: An equal volume of organic phase of phenol-chloroform was added to each sample and then vortexed for 30 seconds. Centrifugation for 5 minutes at 13, 000 rpm followed and the upper phase transferred to a new tube. To this twice the volume of 100% ethanol was added together with 10µl of 5mg/ml glycogen, vortexed for 20 seconds and incubated at -20^{o}C for 30 minutes. Centrifugation for 30 minutes at 4^{o}C, at 13,000 rpm followed to remove the ethanol and then 200µl of 70% ethanol was added to each sample. The samples were centrifuged again for 5 minutes at 13,000 rpm to remove the ethanol and let to evaporate for 15 minutes at room temperature. DNA was diluted in 20-50µl of dH_2O and NanoDrop ND-1000 spectrophotometer was used to define the exact amount of DNA present in each sample. At least 10ng of each sample were used for each real-time RT-PCR and the primers used can be found in **Table 2.11**. Reactions were performed as described in section **2.2.11.3 Taqman® Probe-Based Real- time qRT-PCR.**

Primers used in ChIP experiments	Sequence (5'-3')	Size of amplicon (bp)	Probe
P1M13	GCCATTACAGTTGTTCCGTTCC TGGCATGACCTCTCGACAAA	98	SYBR Green
P2M13	TCTGCGGAAAGACAACAGTC GCCCGACAATGAGTCCAG	96	#35
P3M13	TTGAGCTGGACTCATTGTCG GGAGGTCTTCCTCAGACAAATC	76	#9
P4M13	CAAGATGCGGGGTTCCTGAT TGAGGTATTCTCGGCAACCAT	220	SYBR Green
P5M13	GAAAAAGTCGCCACGTAAGC CGACAATGAGTCCAGCTCAA	198	SYBR Green
P1M1	GAAGAGCCCCTTTCACTATTTTC GGTGCGGCAGAGACCAAAGAACA	74	#59
P2M1	ACGCTCAGTCTCTTTCCAGC GATAACTCCCCACCCCTTGC	108	SYBR Green
P3M1	CAGGGTCCCTCTCTGTTGC AAGAGGTGGGAGGATCACTTGG	94	#19

Table 2.11. Primers used for real-time RT-PCR in ChIP experiments.

2.2.21 Statistical analysis

Luminescence values were normalised against *Renilla* values and combined technical replicates values from each experiment were given as mean ± standard error of the mean (SEM).

The statistical test used in the microarray experiment is a moderated t-test, implemented in the Limma package, with an additional empirical Bayes moderation. P values were adjusted for multiple testing using a Benjamini Hochberg correction, and thresholded at 0.01 for significance filtering. An additional significance filter was applied for magnitude of change, by only keeping observations with a fold change > 2.

2.2.22.1 Real-time RT-PCR analysis

The 18S ribosomal RNA (rRNA) gene was used as the housekeeping gene, as an endogenous control for normalisation and to allow analysis of the relative expression of the target gene. Real-time RT-PCR results were analysed using the relative quantification method ($2^{-\Delta CT}$). C_T values of controls and different treatments were averaged. Normalised values were obtained using 18S rRNA C_T values as a reference, and then the ΔC_T values were calculated (ΔC_T: Difference of the C_T values = C_T of sample – C_T of 18S). Relative expression levels of

controls and treated samples were then compared and formulated into a bar graph. Data from at least 2 experimental repeats were combined and values given as mean + standard deviation of the mean (SD). A One-way analysis of variance (one way ANOVA) with a Bonferroni multiple comparison test was performed using Graph Pad PRISM to compare the means of more than two groups of samples, to determine the statistical significance of the different data sets and a p-value of $\leq$ of 0.05 was considered significant. Alternatively, an unpaired Student's t-test was performed to compare the means and determine any statistical significance between two independent sample groups. Statistical significance is shown as:

* $p \leq 0.05$, ** $p \leq 0.01$ and *** $p \leq 0.001$.

Chapter 3. HDAC3 regulates collagenases expression and NF-κB in chondrocytes.

3.1 Introduction

Besides their role in collectively being able to degrade every component of the extracellular matrix (ECM), the matrix metalloproteinases (MMPs) also play an important role in tissue repair after injury and in pathological disorders such as in arthritis and cancer metastasis (Clark et al. 2008). Many MMPs are regulated at the level of transcription by a variety of chemokines, growth factors and cytokines, including Interleukin-1 (IL-1) and oncostatin M (OSM). (Rowan & Young 2007) Modulation of the acetylation state of chromatin by histone deacetylases (HDACs) has also been suggested to affect the expression of inducible MMPs (Clark et al. 2008). However, specific inhibition of these enzymes has not proven notably useful for the treatment of various diseases and therefore an alternative therapeutic approach is to try to understand and control the expression of these genes.

Interestingly, histone deacetylase inhibitors (HDACi), trichostatin A (TSA) and sodium butyrate (NaBy) have been shown to inhibit collagen breakdown from cartilage explants and *in vitro* these compounds inhibit cytokine induced (IL-1) *MMP* expression. The induction of aggrecan degrading enzymes such as the 'a disintegrin and metalloproteinase with thrombospondin motif 4' (*ADAMTS4*), 5 (*ADAMTS5*), and 9 (*ADAMTS9*) was also abrogated in chondrocytes following cytokine stimulation and HDACi treatment, making these molecules potential therapeutic agents for patients with arthritis. Some of these HDACi, such as TSA, act on specific regions, altering the acetylation state of the adjacent chromatin and allowing or not specific protein binding. For instance, the identification of an Sp1 binding motif in Timp-1 promoter constructs shed some light on the differential regulation of TSA upon *Timp-1* expression. (Young et al. 2005) A role for class I HDACs and in particular for HDAC3 in activating TGF-β-dependent signalling pathways and subsequent gene expression regulation of the disintegrin and metalloproteinase domain-containing protein 12 (*ADAM12*) and the tissue inhibitor of metalloproteinases-1 (*TIMP1*) in mouse C3H10T1/2 fibroblasts has also been proposed. (Barter et al. 2010)

Of particular relevance to MMP transcription, the c-Jun N-terminal kinases (JNKs) and the extracellular signal regulated kinases (ERKs) phosphorylate and activate the activating protein-1 (AP-1) transcription factors to drive transcription of numerous genes. One AP-1 family member in particular, c-Jun, which dimerizes with c-Fos, drives transcription of

multiple MMPs. It has also been shown that the ERK pathway regulates the activity of erythroblastosis-26 (Ets) transcription factor, which co-operate with AP-1 proteins on many MMP promoters. Another major cytokine-induced signalling pathway includes the translocation of the nuclear factor κB (NF-κB) family members from the cytoplasm to the nucleus. Upon phosphorylation and subsequent ubiquitination of the inhibitor of κB (IκB), p50/p65 NF-κB dimers are free to translocate to the nucleus and transactivate several genes including selected MMPs. When NF-κB is maintained in the cytoplasm due to constitutive levels of IκB, reduced expression of *MMP1*, *MMP3* and *MMP13* is observed in cytokine-stimulated cells. (Vincenti & Brinckerhoff 2002)

Reports about the chondroprotective role of HDACi also comes from the destabilisation of the medial meniscus (DMM) mouse model, where osteoarthritis was surgically induced in nine weeks old male mice and cartilage erosion assessed eight weeks post- surgery. *In vivo* efficacy of TSA in blocking cartilage erosion was observed in the mice undergoing either DMM surgery, in comparison to the mice that underwent sham surgery and were used as vehicle control. In addition to, TSA, valproic acid and MS-275 (two class I HDACi) significantly repressed the IL-1 induced levels of *MMP1* and *MMP13* expression in human articular chondrocytes (HACs) and RNA interference (RNAi) studies for class I HDACs confirmed these findings in the SW1353 cells. The use of TSA and MS-275 also inhibited cartilage degradation of a bovine nasal cartilage (BNC) explant assay. As such a class I HDAC- mediated mechanism of collagenase gene expression regulation has been proposed following these findings. (Culley et al. 2013)

When this project started, the role of the class I HDACs and in particular of Histone Deacetylase 3 (HDAC3) in gene regulation was only poorly understood. Therefore, the first step to be taken was to confirm the aforementioned findings by using the TSA and MS-275 HDACi in SW1353 chondrocyte-like cells and determine the effect on collagenase expression. To decide whether HDAC3 is important for MMP expression, a selective HDAC3 inhibitor, Apicidin, and RNA interference (RNAi) against HDAC3 were used and MMP expression determined using the SW1353 cell-line. As the effect of HDAC3 on MMP expression may be indirect and might involve other intermediate signalling molecules, transcription factors and/or pathways, the wider effect of TSA, MS-275, Apicidin and HDAC3 RNAi on the Immediate Early Genes (IEG) expression, essentially AP-1 factors, and on a NF-κB luciferase reporter construct was also examined.

3.2 Aims

- To determine the effect of HDAC inhibition or *HDAC3* gene depletion or specific inhibition in gene expression programmes associated with cartilage degeneration using a chondrocyte-like cell line
- Determine whether HDAC3 is involved in cell signalling pathways associated with osteoarthritis.

3.3 Results

3.3.1 MMP13 and MMP1 are responsive to IL-1 cytokine stimulation.

To explore whether *MMP13* and *MMP1* genes are responsive to IL-1 cytokine stimulation an initial experiment, where the levels of *MMP13* and *MMP1* gene expression following IL-1α cytokine stimulation for 1, 3, 6 and 24 hours were quantified, was performed. Human chondrosarcoma SW1353 cells were used for this experiment as these cells have been shown to have a similar gene expression profile as primary human articular chondrocytes (HACs) following IL1-β treatment and can be used to study protease expression, a phenomenon also seen in chondrocytes (Gebauer et al. 2005). Cells were seeded onto 96- well culture plates and following overnight serum starvation, IL-1 stimulation over a time-course was performed. *MMP13* and *MMP1* gene expression was quantified by qRT-PCR. Both MMPs are responsive to IL-1α with a significant increase in expression observed after 6 and 24 hours of stimulation (**Figure 3.1**). Therefore, and for the needs of this study 6h of IL-1α stimulation was chosen and used for subsequent experiments.

3.3.2 Histone deacetylase inhibition affects collagenase expression.

3.3.2.1 The effect of HDAC inhibition on acetylation of histones and α-tubulin.

HDAC inhibitors induce histone acetylation predominantly through the inhibition of HDACs. In the current study the activities of three different HDACi on gene expression were compared. TSA, a broad-spectrum HDACi, which inhibits all HDACs in the nM range, the benzamide MS-275, which exhibits EC_{50} values in the nM range against HDAC1 and is less potent (in the μM range) for HDAC2, 3 and 9 and the selective HDAC3 inhibitor Apicidin (**Table 2.2**) were used. The concentrations of the HDACi used here were not toxic, as shown in **Figure 2.1**, and were carefully selected based on the HDAC inhibitory IC_{50} (see section **2.1.7** ***Histone Deacetylase Inhibitors***) and previous literature (Culley et al. 2013). The effect upon acetylation of total histone H3 and α- tubulin in SW1353 cells was then assessed by immunoblotting. HDAC5 and HDAC6 are reported to deacetylate α-tubulin and therefore an increase in its acetylation is likely to indicate inhibition of these two HDACs. Treatment of SW1353 cells with all three HDACi resulted in a significant increase of the acetylation of histone H3. In particular, TSA increased acetylation by 90% in comparison to the ethanol control; while treatment with MS-275 and Apicidin resulted in 20% and 15% increase in acetylation respectively compared with the DMSO control (**Figure 3.2 top lane**). Acetylation of α- tubulin on the other hand, was only increased following HDAC inhibition by TSA

(**Figure 3.2 second lane**). This observation indicated that TSA alone inhibits the catalytic activity of HDAC5 and/or HDAC6, supporting in this way its status as an HDAC "pan-inhibitor".

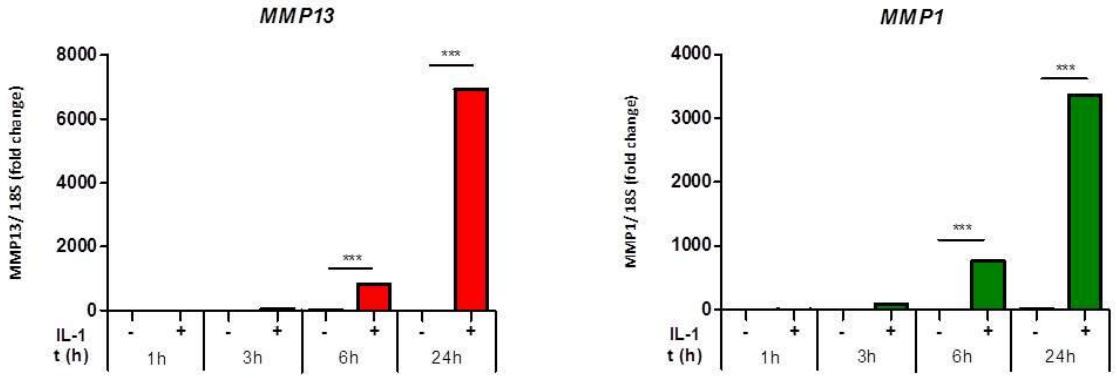

Figure 3.1. *MMP13* and *MMP1* gene expression after a time-course of IL-1α cytokine stimulation.

SW1353 cells were stimulated with IL-1α (0.5ng/ml) for 1, 3, 6 or 24 hours, or left unstimulated following an overnight serum starvation. Total RNA was extracted, reverse transcribed to cDNA and MMP expression measured by quantitative Real-time PCR (qRT- PCR). Results are shown relative to 18S ribosomal RNA expression. Significance was compared with respect to non-stimulated cells (-) for each time point. Figure shows two independent experiments (n=4 per experiment) and bars show the mean of eight biological replicates +SD. For statistical analysis, one-way ANOVA with a Bonferroni multiple comparison test was performed. *** $p<0.001$

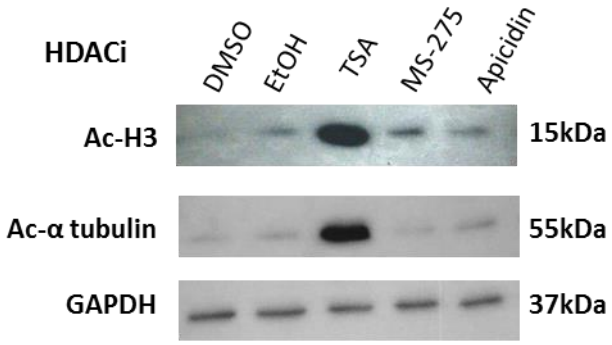

Figure 3.2. Inhibition of HDACs increased the acetylation of histone H3 and α-tubulin.

SW1353 cells were treated with TSA (330nM) or EtOH control (0.1%), MS-275 (10μM), Apicidin (160nM) or DMSO control (0.2%) for 6.5h before cells were harvested, lysed and total protein extraction was performed. Immunoblotting was performed with an anti-acetylated Histone H3 antibody, an anti-acetylated alpha tubulin antibody and GAPDH served as a loading control. EtOH was the control for the TSA-treated samples, while DMSO was the control for the MS-275 and Apicidin- treated samples. Quantification of immunoblotting was performed using ImageJ software and with reference to the GAPDH loading control.

3.3.2.2 The effect of TSA, MS-275 and Apicidin on the induction of gene expression by IL-1.

As IL-1α stimulation induced *MMP13* and *MMP1* expression, the effect of HDAC inhibition on collagenase expression was then examined. SW1353 serum-starved cells were incubated for 30 minutes with the indicated concentrations of TSA (20ng/ml=66nM, 50ng/ml=165nM, 100ng/ml=330nM and 250ng/ml=756nM), MS-275 (1μM, 2μM, 5μM and 10μM) or Apicidin (20ng/ml=32nM, 50ng/ml=80nM, 100ng/ml=160nM and 250ng/ml=401nM) or treated with DMSO (0.25%), before IL-1α stimulation (0.5ng/ml) was performed. IL-1 induces the expression of synergistic cytokines such as IL-6, IL-8 and IL-17, which augments the catabolic effects of IL-1β and TNF-α in cartilage (Mueller & Tuan 2011). Therefore, gene expressions of *IL-6* and *IL-8* were also measured, following IL-1 induction and histone deacetylase inhibition using TSA, MS-275 or Apicidin inhibitors.

TSA treatment of SW1353 cells showed similar pattern of repression of the induced expression of both *MMPs* and *IL-6* (**Figure 3.3 A-C**), but significantly increased *IL-8* induced expression at 250ng/ml concentration (**Figure 3.3 D**). Maximum repression of *MMP1*, *MMP13* and *IL-6* was observed following treatment with 100ng/ml of TSA, with significant inhibition also at 250ng/ml, suggesting this is an HDAC-mediated event. The levels of *MMP1* and *MMP13* expression remained low in the basal (no stimulation) condition and no significant effect of TSA was found, while *IL-6* and *IL-8* expression were not detected in unstimulated cells, confirming the induction following IL-1 stimulation.

HDAC inhibition using the class I HDACi MS-275 also decreased the IL-1 - induced levels of *MMP13*, *MMP1* and *IL-6* (**Figure 3.4 A-C**), strongly indicating that class I HDACs, including HDAC1, HDAC2 and HDAC3 are important for regulating the expression of these genes. However, MS-275 did not significantly change *IL-8* induced expression (**Figure 3.4 D**). MS-275 blocked the induction of *MMP13* and *IL-6* expression at concentrations of 5μM and above, although inhibition at the higher concentration (10μM) was more pronounced for *MMP1*. Basal expression of all genes remained low and was not significantly changed following MS-275 treatment.

Apicidin inhibited the IL-1 induced expression of *MMP13*, *MMP1* and *IL-6* in a concentration-dependent manner (**Figure 3.5 A-C**). On the contrary, apicidin did not alter the induced expression of *IL-8* (**Figure 3.5 D**). In the absence of IL-1 stimulation, apicidin had no significant effect on the expression of any of the aforementioned genes.

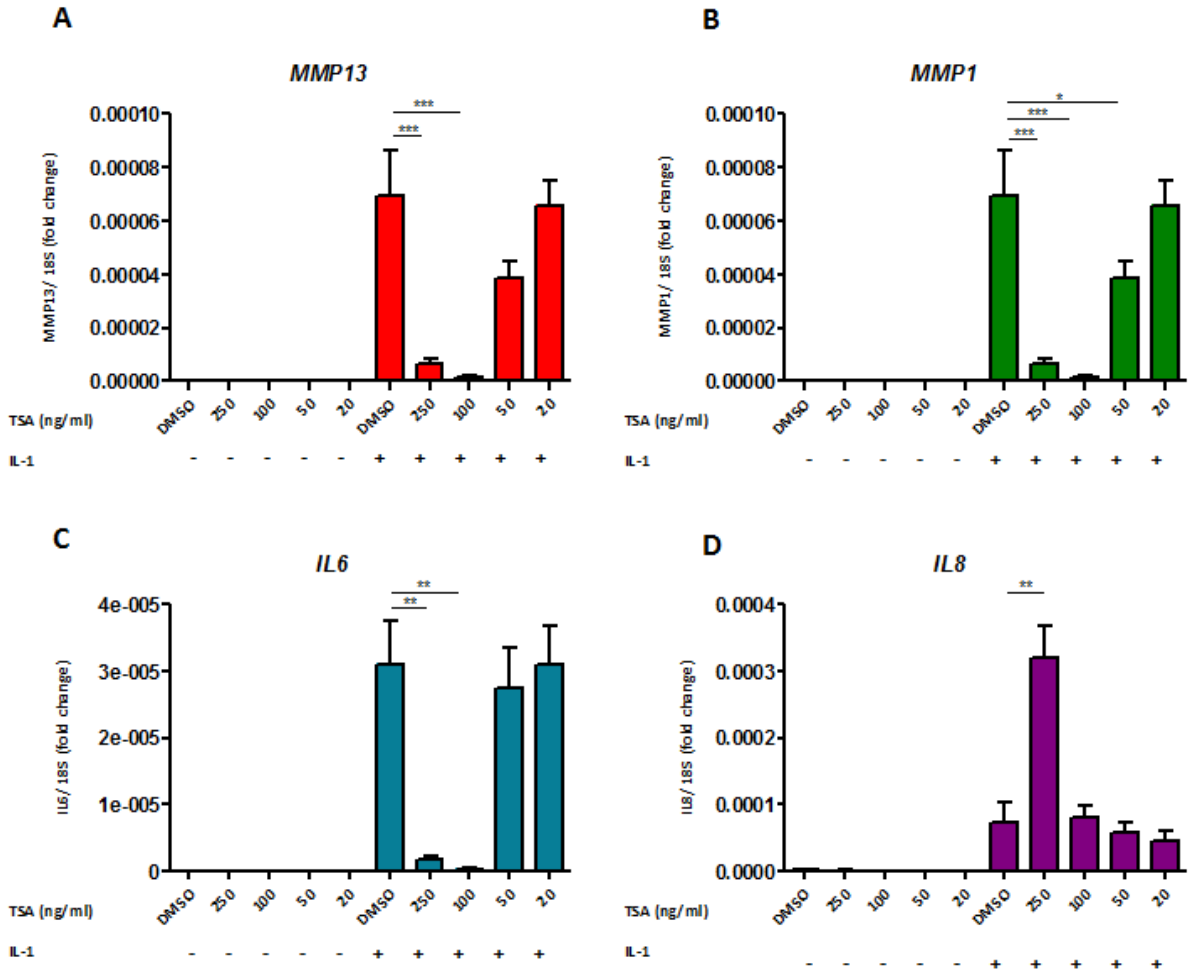

Figure 3.3. Regulation of gene expression by TSA HDACi

SW1353 cells were incubated for 30min with increasing concentrations of TSA (20- 250ng/ml) or DMSO (0.25%), before IL-1 (0.5ng/ml) stimulation for 6h was performed, following an overnight serum starvation. Total RNA was extracted using the cells-to cDNA lysis buffer, reverse transcribed to cDNA and *MMPs*, *IL-6* and *IL-8* expression quantified by qRT-PCR. Results are shown relative to 18S ribosomal RNA expression. Significance was compared with respect to the DMSO control treated cells in the basal and IL-1 induced level. Figure shows two independent experiments and bars represent the mean of eight biological replicates +SD. For statistical analysis, one-way ANOVA with a Bonferroni multiple comparison test was performed. ***p<0.001, **p<0.01, *p<0.05

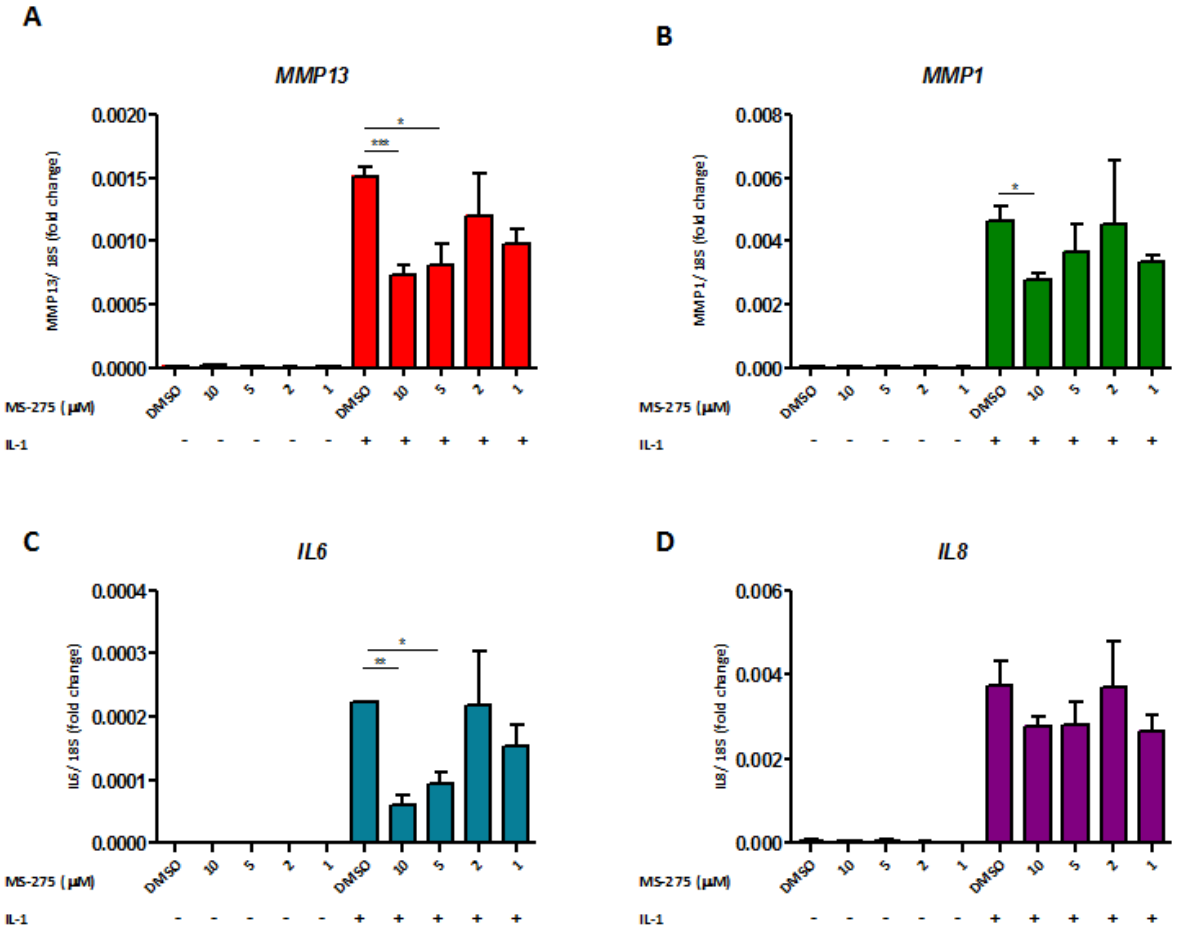

Figure 3.4. Regulation of gene expression by the class I HDACi MS-275.

SW1353 cells were incubated for 30min with increasing concentrations of MS-275 (1-10µM) or DMSO (0.25%), before IL-1 (0.5ng/ml) stimulation for 6h was performed, following an overnight serum starvation. Total RNA was extracted using the cells-to cDNA lysis buffer, reverse transcribed to cDNA and *MMPs*, *IL-6* and *IL-8* expression quantified by qRT-PCR. Results are shown relative to 18S ribosomal RNA expression. Significance was compared with respect to the DMSO control treated cells in the basal and IL-1 induced level. Figure shows two independent experiments and bars represent the mean of eight biological replicates +SD. For statistical analysis, one-way ANOVA with a Bonferroni multiple comparison test was performed. ***p<0.001, **p<0.01, *p<0.05

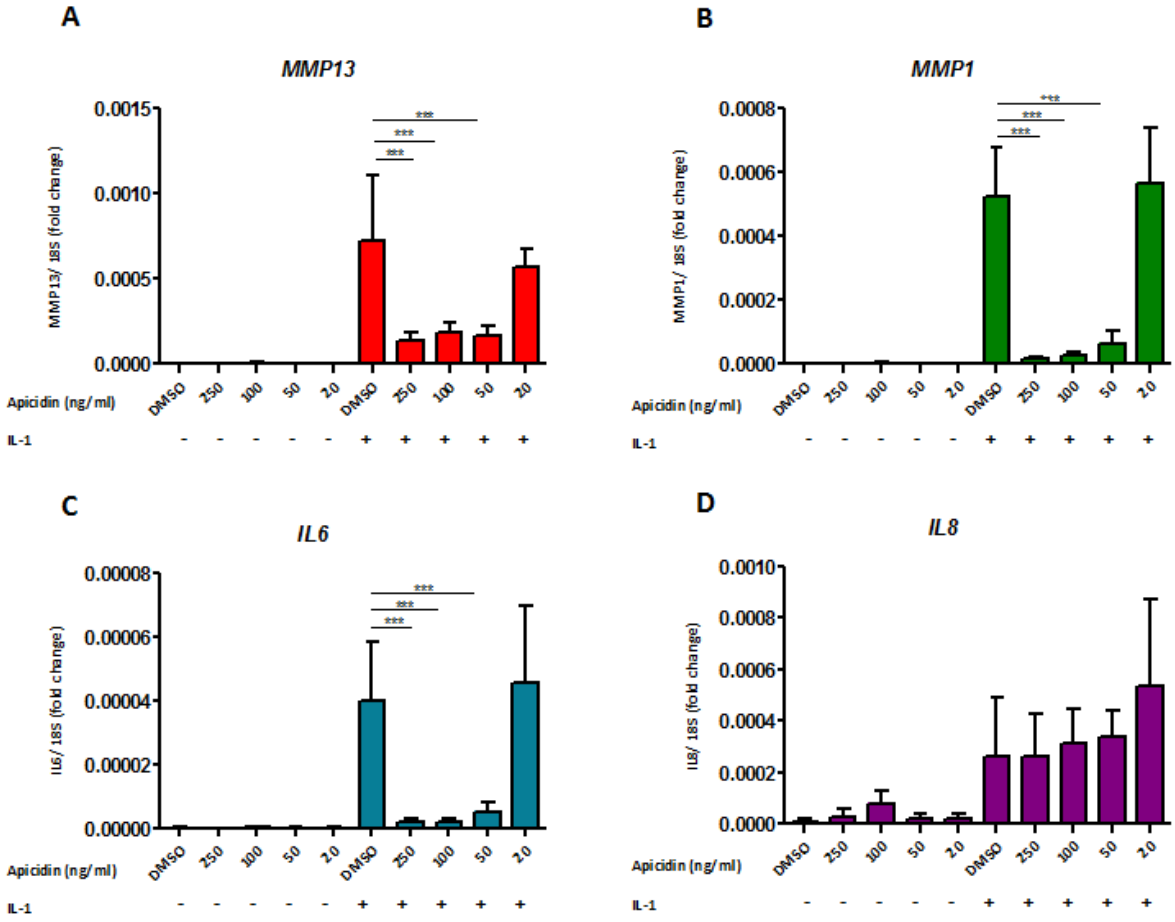

Figure 3.5. Regulation of gene expression by the selective HDAC3 inhibitor Apicidin.

SW1353 cells were incubated for 30min with increasing concentrations of Apicidin (20-250ng/ml) or DMSO (0.25%), before IL-1 (0.5ng/ml) stimulation for 6h was performed, following an overnight serum starvation. Total RNA was extracted using the cells-to cDNA lysis buffer, reverse transcribed to cDNA and *MMPs*, *IL-6* and *IL-8* expression quantified by qRT-PCR. Results are shown relative to 18S ribosomal RNA expression. Significance was compared with respect to the DMSO control treated cells in the basal and IL-1 induced level. Figure shows two independent experiments and bars represent the mean of eight biological replicates +SD. For statistical analysis, one-way ANOVA with a Bonferroni multiple comparison test was performed. ***$p<0.001$

3.3.2.3 Collagen release after addition of HDACi to IL-1α/OSM treated bovine nasal cartilage.

It is known that bovine and human cartilage in explant culture respond to pro-inflammatory cytokines stimulation with both an increase in the expression activation of collagenases (eg. MMP1, MMP8, MMP13). More particularly, in bovine nasal cartilage (BNC) explants, more than 90% of collagen release is observed after 14 days of culture, with little, if any, collagen release seen before 7 days of culture. (Barksby et al., 2006; Cawston et al., 2003) Herein, BNC explants were cultured with/without IL-1α and/or oncostatin M (OSM). Cartilage was treated with different HDAC inhibitors including the pan-HDACi TSA and the selective HDAC3 inhibitor Apicidin. Collagen levels were determined by assay of hydroxyproline following 14 days of culture. **Figure 3.6 A** shows the levels of collagen release remain unchanged when no cytokine stimulation occurs, in the presence of all the different HDACi. This suggests that no extra cartilage breakdown happens in the presence of each HDACi when compared to the control and cytokine stimulation is required for the increased expression and activation of procollagenases and subsequent collagen release. The addition of TSA to the IL-1α stimulated cartilage, significantly decreased collagen breakdown (**Figure 3.6 B**). In **Figure 3.6 C** not only TSA but also apicidin partially blocked the breakdown of collagen from IL-1α + OSM treated bovine cartilage. Taken together, these results suggest that pro-inflammatory cytokine stimulation is required for cartilage collagen breakdown and HDACi including TSA and apicidin can protect, at least in part, collagen breakdown. It also predicts a novel- specific role for the class I HDAC3, in mediating cartilage degradation and in particular collagen breakdown.

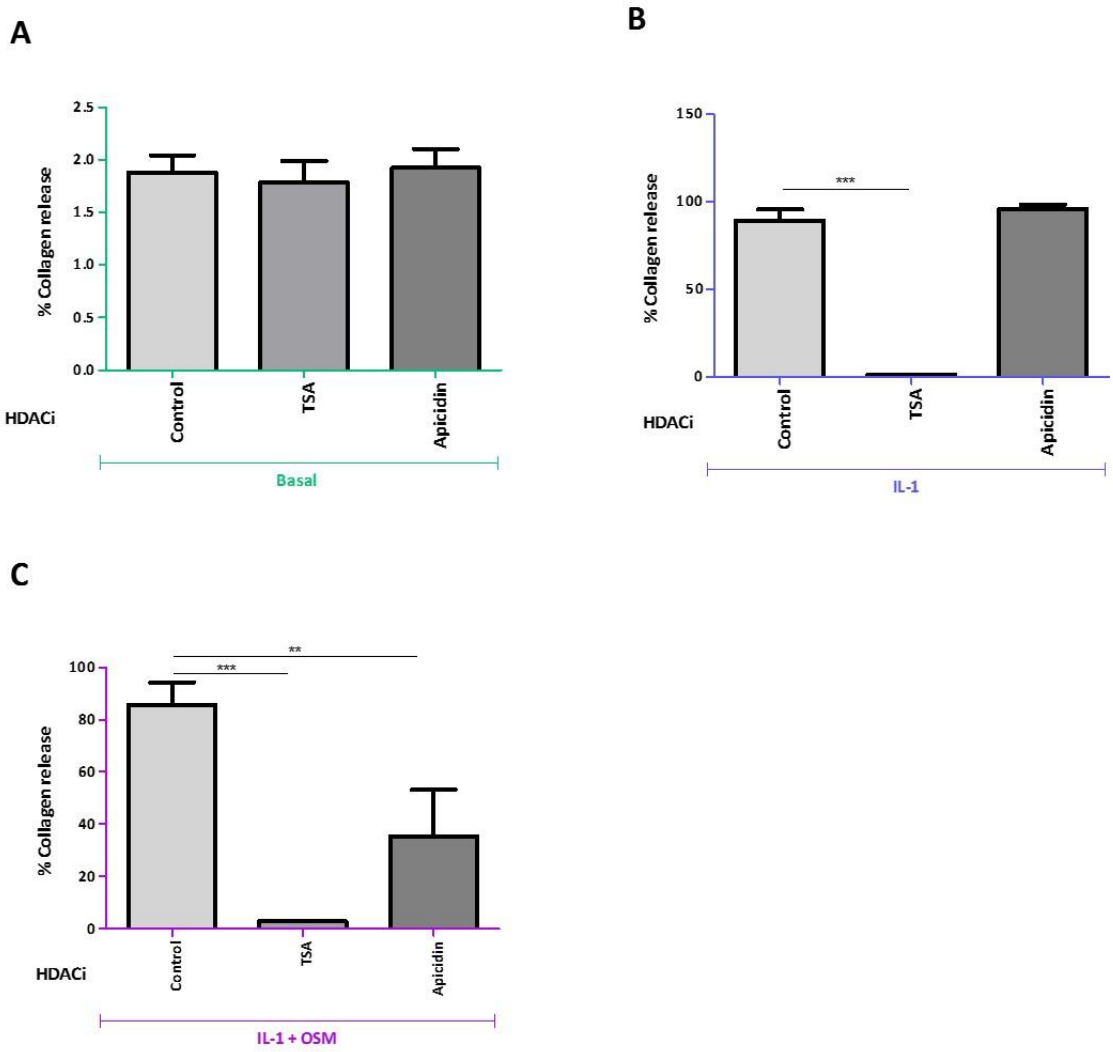

Figure 3.6. Addition of HDAC inhibitors (HDACi) to Interleukin-1α ± Oncostatin M (IL-1α ± OSM) treated bovine nasal cartilage (BNC).

BNC was cultured in medium with or without HDACi: TSA (250ng/ml), Apicidin (100ng/ml) or DMSO-Control at Day 0, and either stimulated with IL-1α (10ng/ml) and/or IL-1α (4ng/ml) plus OSM (20ng/ml), or left unstimulated (Basal). Combined media from Day 7 and Day 14 as well as papain digested day 14 cartilage were collected and collagen release was quantified by measuring the levels of hydroxyproline. For statistical analysis, one-way ANOVA with a Bonferroni multiple comparison test was performed. *** $p<0.001$, ** $p<0.01$

3.3.3 The effect of HDAC3 RNAi on the induction of collagenase expression by IL-1.

3.3.3.1. The effect of RNAi on HDAC3 mRNA and protein levels.

The inhibition of IL-1- induced collagenase expression by the selective HDAC3 inhibitor apicidin and the blockage of collagen breakdown following apicidin treatment and IL-1 + OSM stimulation in a BNC assay suggested a specific role for the class I HDAC3. Therefore, RNAi-mediated gene depletion of *HDAC3* was used to study the effect of HDAC3 in the induction of *MMP1* and *MMP13* expression by IL-1. The optimal transfection procedure and duration of siRNA incubation is described in section **2.2.7** ***RNA interference (RNAi)***. Transfection of SW1353 cells with different concentrations of siRNA targeting HDAC3 were used starting from 5-100nM and knockdown efficiency was determined using quantitative real-time PCR and immunoblotting. Transfection with 50nM and 20nM concentration of siHDAC3 reduced HDAC3 mRNA levels by >80% in the basal (**Figure 3.7 A**) and by >60% in the IL-1 induced level (**Figure 3.7 B**) and 5nM of siHDAC3 concentration halved HDAC3 mRNA levels in the basal level (**Figure 3.7 A**). Protein levels of HDAC3 (quantified using ImageJ software) were decreased following siRNA transfection at 100nM by 68%, at 50nm by 52% and at 20nM by 46% (**Figure 3.7 C**).

3.3.3.2 The effect of HDAC3 RNAi on the induction of collagenase expression by IL-1.

Initially the effect of depleting HDAC3 on gene expression using 5-50nM concentration of siRNA was examined. *HDAC3* gene depletion significantly decreased the induction of *MMP13*, *MMP1*, *IL-6* and *IL-8* expression by IL-1 at 50nM compared to the non-targeting control siRNA levels (**Figure 3.8 A-D**). *MMP1* induced expression was also blocked at 20nM of siRNA concentration. RNAi-mediated depletion of *HDAC3* had no effect on the basal levels of *MMP1*, *MMP13*, *IL-6* and *IL-8* expression.

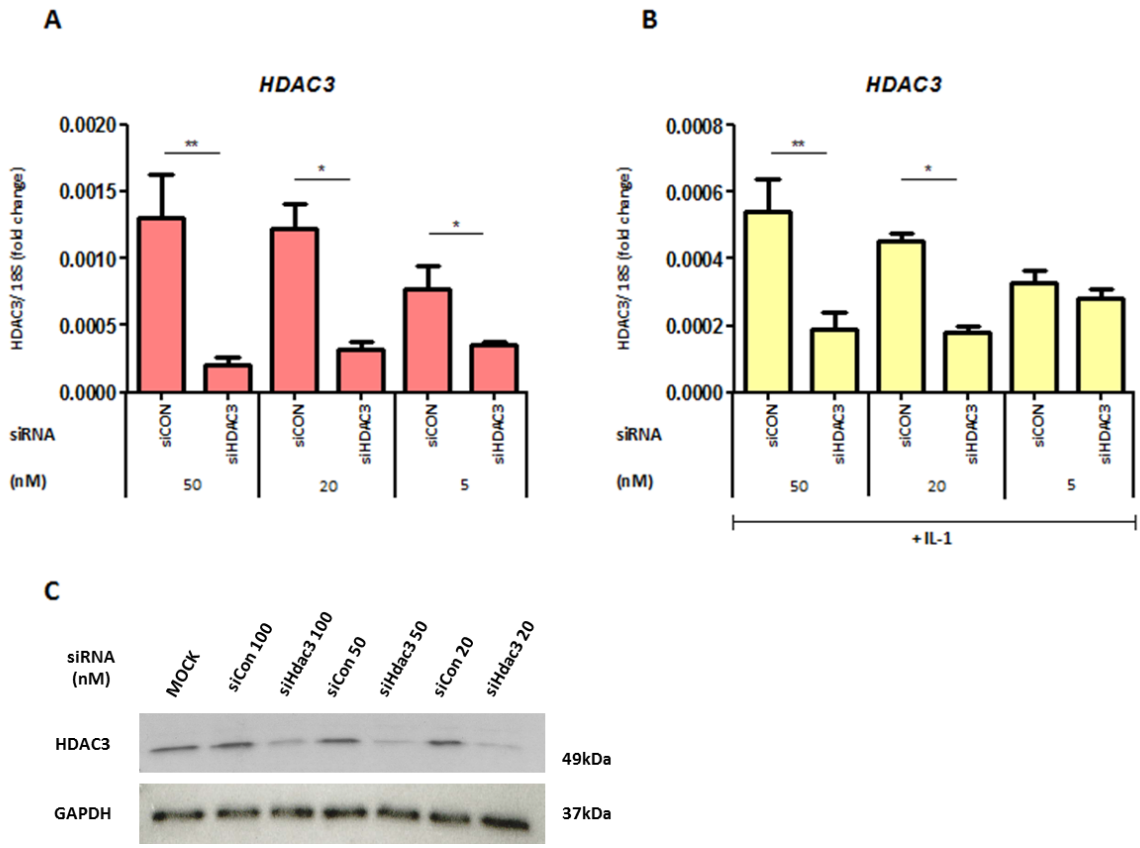

Figure 3.7. Gene silencing of *HDAC3* expression using a HDAC3-specific siRNA.

SW1353 cells were transfected with decreasing concentrations (nM) of a non-targeting siRNA control (siCON) or a HDAC3-specific siRNA (siHDAC3) for 24h. The following day, the cells were serum starved for 16h and then stimulated with IL-1α (0.5ng/ml) (B) or left unstimulated (A). A- B. Total RNA was extracted, reverse transcribed to cDNA and *HDAC3* expression measured by qRT- PCR. Results are shown relative to 18S ribosomal RNA expression. Significance was determined with respect to siCON treated cells in comparison to the siHDAC3 treated cells, both in the basal and IL-1 induced level. Figure shows the mean of two independent experiments each with four biological replicates +SD. For statistical analysis, one-way ANOVA with a Bonferroni multiple comparison test was performed. C. HDAC3 protein levels were quantified following a 24h transfection with decreasing concentrations of siRNA. Cell lysate was harvested the next day, proteins were quantified and immunoblotting for an anti-HDAC3 specific antibody was performed. GAPDH served as a loading control. ** $p<0.01$, * $p<0.05$

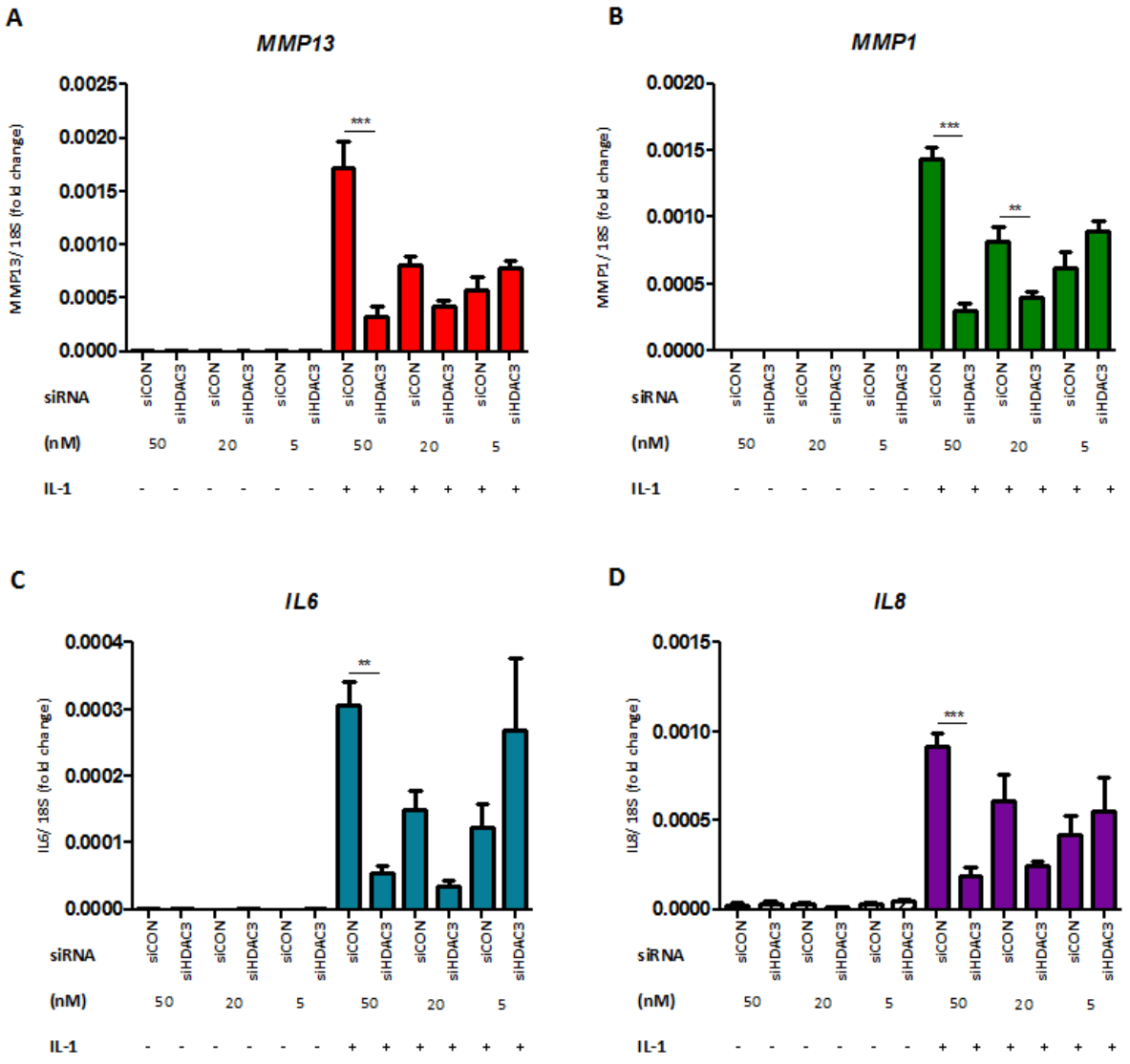

Figure 3.8. Gene expression regulation following *HDAC3* gene silencing.

SW1353 cells were transfected with decreasing concentrations (nM) of a non-targeting siRNA control (siCON) or a HDAC3-specific siRNA (siHDAC3) for 24h. The following day, the cells were stimulated with IL-1α (0.5ng/ml) following an overnight serum starvation. Total RNA was extracted, reverse transcribed to cDNA and *MMPs*, *IL-6* and *IL-8* expressions measured by quantitative Real-time PCR. Results are shown relative to 18S ribosomal RNA expression. Significance was determined by comparing the siCON with the siHDAC3 treated cells, both in the basal and IL-1 induced level. Figure shows two independent experiments and bars represent the mean of eight biological replicates +SD. For statistical analysis, one-way ANOVA with a Bonferroni's multiple comparison test was performed. *** $p<0.001$, ** $p<0.01$

3.3.4 The effect of HDAC inhibition or RNAi for HDAC3 on the induction of Immediate Early Genes expression.

3.3.4.1 Immediate Early gene expression following IL-1 stimulation.

Immediate Early Genes (IEG) encode for transcription factors that control cell proliferation, differentiation and survival by controlling specific transcriptional programs (Hargreaves et al. 2009). Two of the most well characterised IEG include the FOS and JUN family of transcription factors, binding sites of which have been found in both MMP1 and MMP13 promoters, suggesting these are potential regulators of *MMP1* and *MMP13* expression (Vincenti & Brinckerhoff 2002). Initially an experiment to test whether IEG expression is induced following IL-1 stimulation for 30, 60 and 120 minutes was performed and compared to non-stimulated cells. *IL-6* and *IL-8* gene induction were included in the analysis as their expression has been shown to be induced following IL-1 stimulation (**Figure 3.9 A-B**). From the genes studied (**Figure 3.9**) only *FRA1* (**Figure 3.9 C**), *cFOS* (**Figure 3.9 E**), *FOSB* (**Figure 3.9 G**) and *JUND* (**Figure 3.9 J**) were significantly induced after 60 and 120 minutes of IL-1 stimulation, suggesting a potential role for these genes on the induced collagenase expression regulation in chondrocytes. Other genes studied include *ATF2*, *JUNB*, *FRA2*, *cJUN* but no significant induction of their expression was found in the SW1353 cells, hence the effect of HDACi on the induction of these genes was not studied.

3.3.4.2 The effect of HDAC inhibitors on selected IL-1- regulated IEG.

To determine the effect of TSA, MS-275 and Apicidin on the IL-1 induced expression of IEG, SW1353 serum starved cells were treated with the indicated HDACi before IL-1 stimulation was performed. mRNA quantification followed, and only *FRA1* induced expression was significantly decreased by HDACi; after 60 and 120 minutes of IL-1 stimulation when treated with TSA (**Figure 3.10 A**) and after 30 and 120 minutes of IL-1 stimulation when treated with Apicidin (**Figure 3.10 C**). A modest but not significant decrease was also found at 30 minutes of the TSA and MS-275 treated cells (**Figure 3.10 B**), yet no effect of MS-275 was observed following further IL-1 stimulation. The induced expression of no other IEG was significantly changed following HDACi treatment (**Figure 3.10 D-I**).

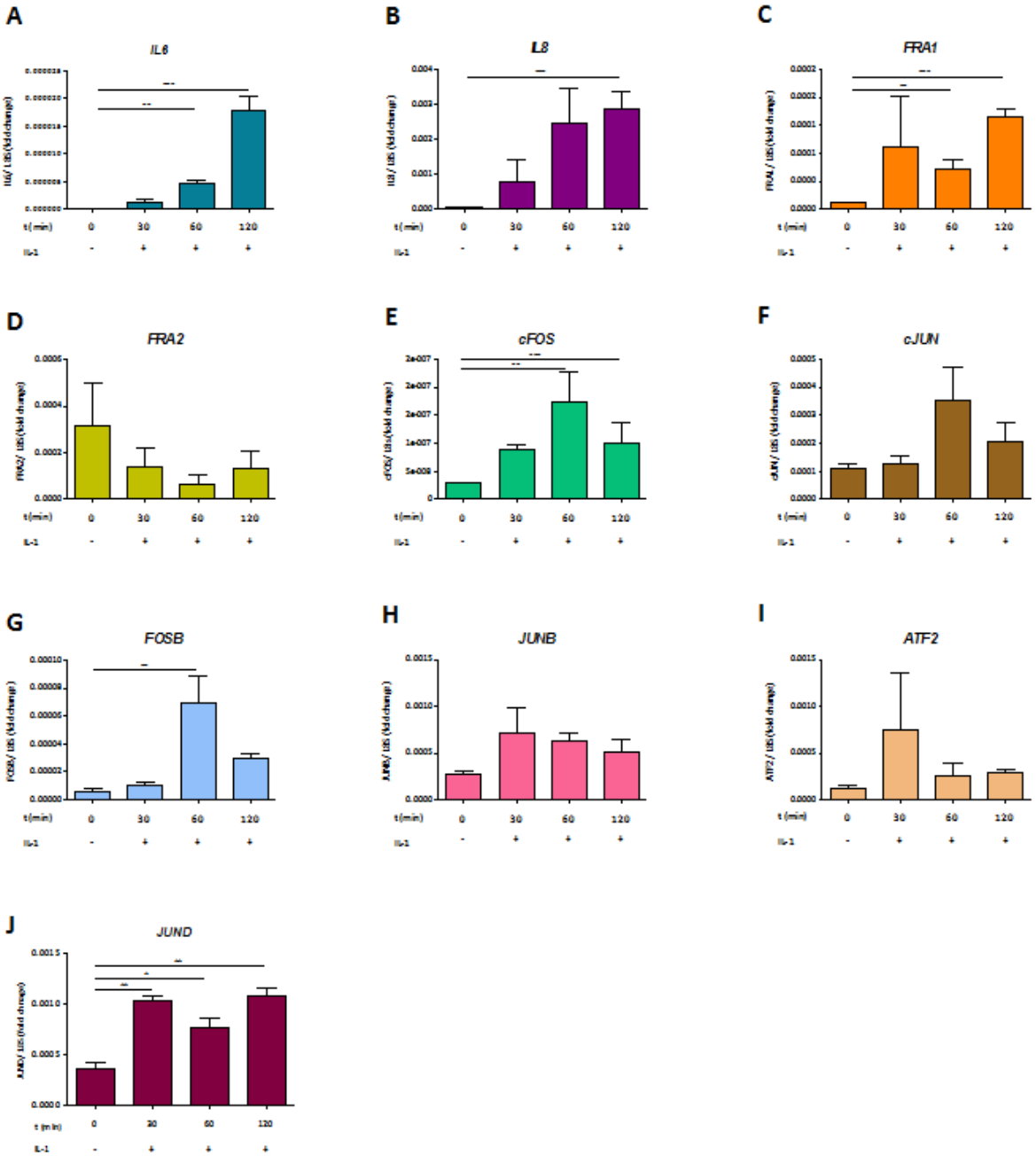

Figure 3.9. Immediate early genes (IEG) expression following IL-1 cytokine stimulation.

SW1353 cells were stimulated with IL-1α (0.5ng/ml) for different times (30, 60 and 120 minutes), following an overnight serum starvation. Total RNA was extracted, reverse transcribed to cDNA and IEG expressions measured by qRT- PCR. Results are shown relative to 18S ribosomal RNA expression. Significance was determined by comparing the unstimulated with the IL-1 treated cells. Figure shows one independent experiment and bars represent the mean of four biological replicates +SD. For statistical analysis, one-way ANOVA with a Bonferroni multiple comparison test was performed. *** $p<0.001$, ** $p<0.01$, * $p<0.05$

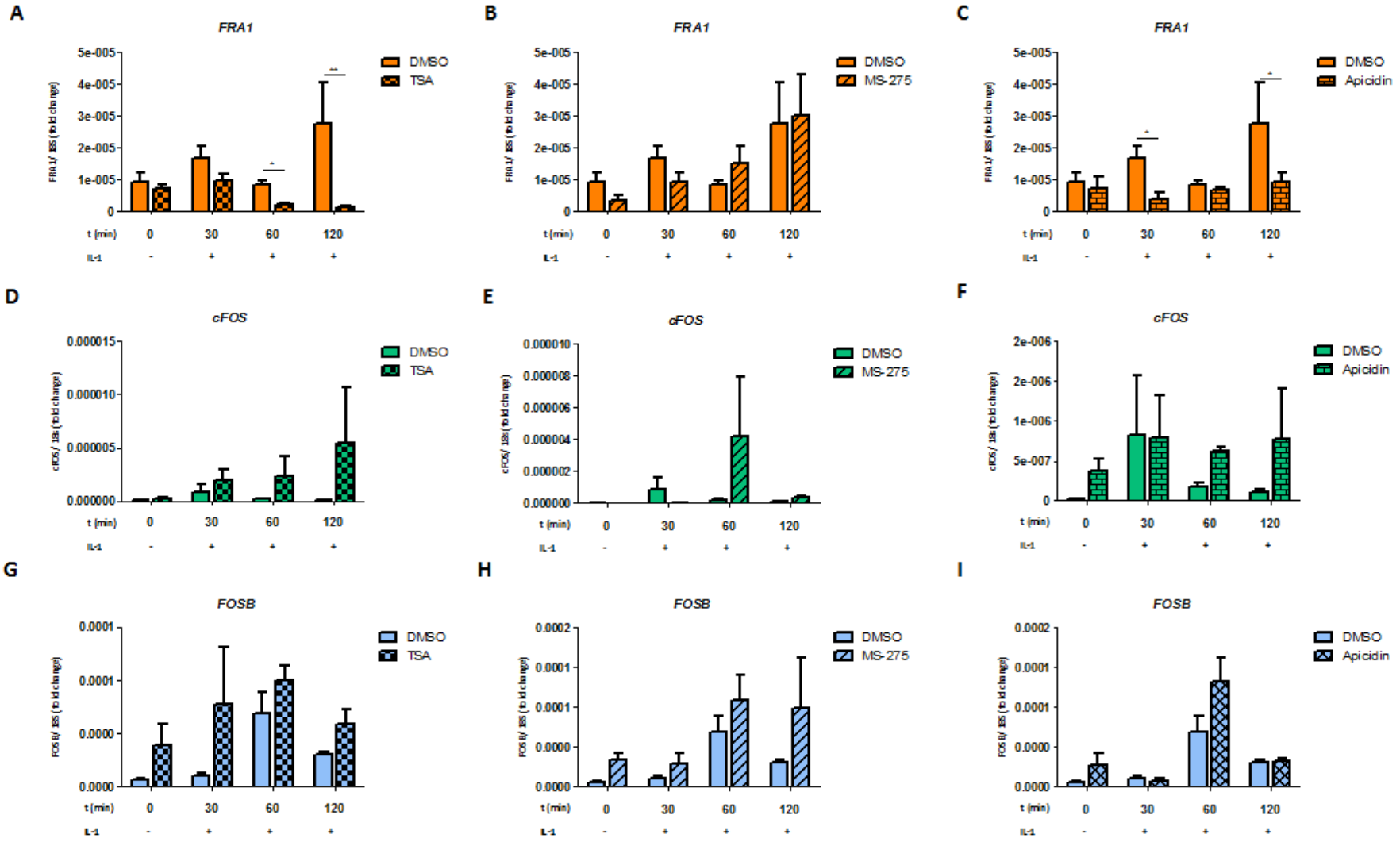

Figure 3.10. Regulation of IEG gene expression by HDAC inhibitors.

SW1353 cells were incubated for 30min with HDAC inhibitors: TSA (100ng/ml) (A, D, G), MS-275 (10μM) (B, E, H) and Apicidin (100ng/ml) (C, F, I), before IL-1α (0.5ng/ml) stimulation for different times (30, 60 and 120 minutes) was performed, following an overnight serum starvation. Total RNA was extracted, reverse transcribed to cDNA and IEG expression measured by qRT- PCR. Results are shown relative to 18S ribosomal RNA expression. Significance was compared with respect to the DMSO control treated cells in the basal and IL-1 induced levels. Figure shows one independent experiment and bars represent the mean of four biological replicates +SD. For statistical analysis, two-way ANOVA with a Bonferroni post- test to compare replicate means by row was performed. ** $p<0.01$, * $p<0.05$

3.3.4.3 The effect of HDAC3 RNAi on selected IL-1-regulated Immediate Early Genes.

HDAC inhibitory treatment with TSA and apicidin suggested *FRA1* IEG had a similar expression pattern with *MMP1* and *MMP13* following IL-1 stimulation. Knowing that binding sites for these genes have been found in the promoters of both MMPs (Weiss et al. 2003), *FRA1* renders a good candidate for regulating expression of collagenases in cartilage. To examine the specific effect of *HDAC3* on *FRA1* induced expression, RNAi targeting HDAC3 was used, *HDAC3* was subsequently depleted and *FRA1* induction was measured following IL-1 stimulation. *HDAC3* expression was significantly blocked following siRNA treatment (**Figure 3.11 A**.). *FRA1* induction was prevented following *HDAC3* depletion and IL-1 stimulation at 60 minutes (**Figure 3.11 B**), but did not change at earlier or later time-points of IL-1 induction.

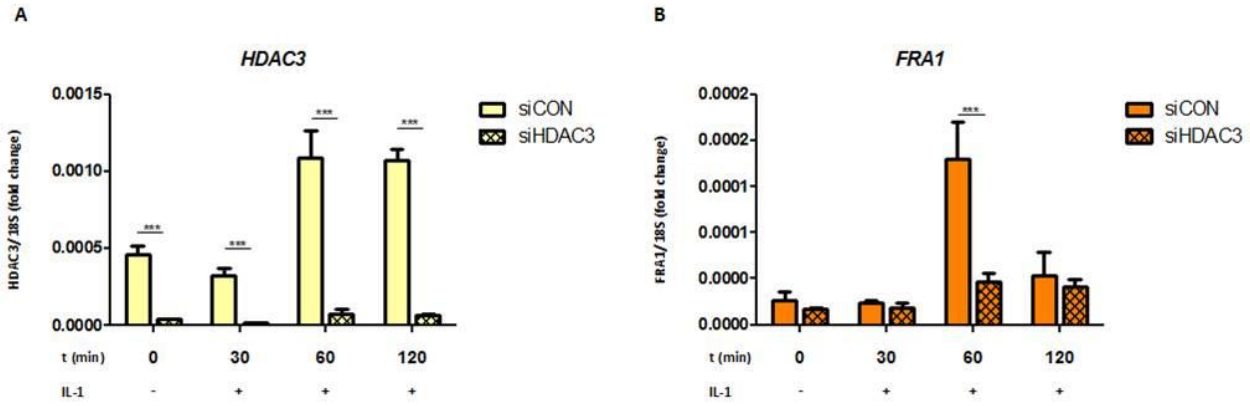

Figure 3.11. Regulation of FRA1 gene expression following HDAC3 gene silencing.

SW1353 cells were transfected with a non-targeting siRNA control (siCON) or the HDAC3-specific siRNA (siHDAC3) for 24h. The following day the cells were stimulated with IL-1α (0.5ng/ml) for different times (30, 60 and 120 minutes), following an overnight serum starvation. Total RNA was extracted, reverse transcribed to cDNA and *HDAC3* (A) and *FRA1* (B) expression measured by qRT-PCR. Results are shown relative to 18S ribosomal RNA expression. Significance was compared with respect to the siCON control treated cells in the basal and IL-1 induced levels. Figure shows one independent experiment and bars represent the mean of four biological replicates +SD. For statistical analysis, two-way ANOVA with a Bonferroni post- test to compare replicate means by row was performed. *** $p<0.001$

3.3.5 Effect of HDAC inhibition on the activation of NF-κB signalling pathway.

Most of the immune and inflammatory genes induced by IL-1 are NF-κB regulated, making it a key regulator of IL-1 effects in cells. (O'Neill & Greene 1998) To clarify the impact of HDACs in the activation of NF-κB signaling pathway, a luciferase reporter assay was performed. SW1353 cells were transfected with a NF-κB responsive firefly luciferase reporter and a control *Renilla* expression vector before HDACi treatment with 100ng/ml TSA or 10μM MS-275 or 100ng/ml Apicidin was performed (as described in section **2.2.7**). After stimulation with interleukin-1 (IL-1), luciferase activity was measured and normalised to *Renilla*. Optimal stimulation conditions were previously described in section **2.2.7**. The reporter assay determined that HDAC inhibition using TSA or class I HDAC inhibition using MS-275 significantly reduced both basal and IL-1-induced NF-κB activity compared to the control. (**Figure 3.12**) Interestingly, the selective HDAC3 inhibitor apicidin also blocked luciferase transactivation of NF-κB activity, indicating HDAC3 as a potential mediator of the NF-κB regulated gene expression.

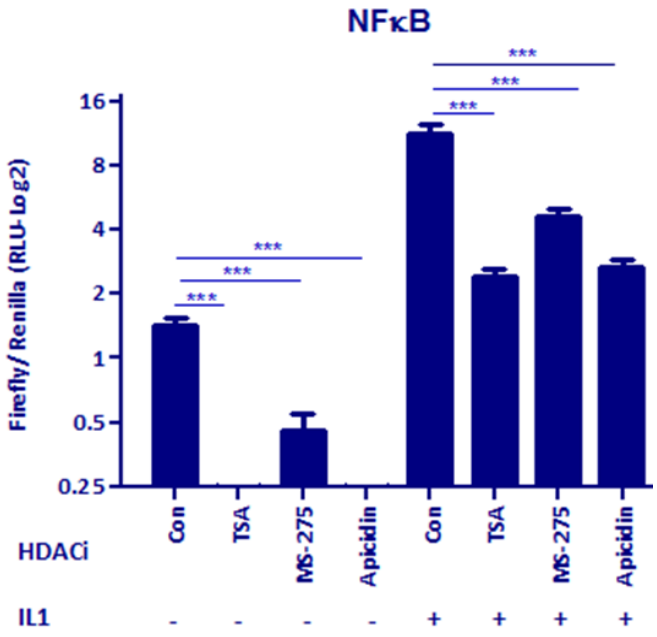

Figure 3.12. NFκB luciferase reporter activity is repressed following HDACi treatment.

SW1353 serum-starved cells were incubated with TSA (100ng/ml), MS-275 (10μM) or Apicidin (100ng/ml) for 30min before IL-1 (0.5ng/ml) stimulation for 6h was performed. Luciferase expression was quantified using the Dual-Glo® Luciferase Assay system (Promega) and normalised to Renilla on a GloMax®- Multi Luminescene Module (Promega). Significance was compared with respect to the DMSO control treated cells in the basal and IL-1 induced levels. Assays were performed at least 3 times, containing six repeats per treatment per biological repeat. Bars show the average ± SD of two experiments. *** $p \leq 0.001$

3.4 Discussion

The nucleosomal histones can be modified by reversible acetylation by histone acetyltransferases (HAT) and deacetylases (HDACs). The general model supports that HATs induce hyperacetylation causing nucleosomal relaxation which is associated with transcriptional activation. HDACs on the other hand, form co-repressor complexes which negatively regulate gene transcription. (Dangond et al. 1998) Histone deacetylase inhibitors (HDACi) enhance acetylation by preventing removal of acetyl groups by HDACs inducing gene transcription. (Clayton et al., 2006) It has been shown that treatment of chondrocytes with TSA, MS-275 or valproic acid was able to dose-dependently induce the acetylation of H3 histone and H4 histone and demonstrated similar efficacy across the tested doses. (Culley et al. 2013) In the current study, treatment of SW1353 cells with HDAC inhibitors TSA, MS-275 and Apicidin resulted in an increase in the acetylation of total histone H3 (**Figure 3.2**). TSA, but not MS-275 or Apicidin induced acetylation of α-tubulin, confirming that only the former could inhibit the activity of HDAC5 and/or HDAC6. (Cho & Cavalli 2012; Hubbert et al. 2002)

Although diminished histone acetylation generally correlates with gene silencing, there is also evidence that HDACs can activate some genes. (Kim & Bae 2011) HDAC inhibition for example using TSA was found to cause both the induction and repression of a large number of genes in pancreatic cancer cell lines, although the number of genes whose expression was up-regulated was greater than the number of genes that were down-regulated. When categorised into cellular functions, the differentially expressed genes were found to be involved in a variety of cellular processes including cell proliferation, signalling, regulation of transcription and apoptosis. (Moore et al. 2004) Similarly, many differentially regulated genes following TSA treatment were identified in hepatoma cells, with decreased expression to be linked to the development of hepatomas. (Chiba et al. 2004) Other studies demonstrated that apoptosis of human multiple myeloma cells was induced following treatment with suberoylanilide hydroxamic acid (SAHA), due to down-regulation of members of the insulin growth factor (IGF)/ IGF-1 receptor and IL-6 receptor (IL-6R) signalling cascade, anti-apoptotic molecules, oncogenic kinases, DNA repair enzymes and transcription factors including E2F-1 and XBP-1. (Mitsiades et al. 2004) Interestingly, histone deacetylase inhibitors TSA and sodium butyrate (NaBy) have been also shown to block *MMP* and aggrecan degrading enzymes expression *in vitro* and reduced collagen breakdown from cartilage explants. (Young et al. 2005) A role for class I HDACs and in particular for HDAC3 in activating TGF-β-dependent signalling pathways and subsequent gene expression

regulation of *ADAM12* and *TIMP1* in mouse C3H10T1/2 fibroblasts has also been proposed. (Barter et al. 2010)

The main aim of this chapter was to investigate the role of HDACs and in particular of HDAC3 in regulating gene expression in chondrocytes. Parallel experiments were designed and gene expression of collagenases, IEG and NF-κB signaling pathway activation was determined following HDAC inhibition or *HDAC3* specific depletion and IL-1 stimulation. A BNC assay also determined how HDACi affect collagen release in the presence or absence of stimulus. The results presented in this chapter imply a role for HDACs and particularly HDAC3 in regulating collagenase and *FRA1* IEG expression in chondrocytes as well as in positively regulating the activation of NF-κB signalling and collagen release in a cartilage assay.

3.4.1 HDACi and RNAi for HDAC3 abrogate IL-1-induced collagenase expression.

TSA, MS-275 and Apicidin could all abrogate the IL-1 induced expression of *MMP1* and *MMP13*, both of which are key collagenases involved in cartilage degradation in human articular chondrocytes (**Figure 3.3** and **Figure 3.4** and **Figure 3.5**). IL-1-induced *IL-6* expression was also blocked using all three HDAC inhibitors, supporting a role for class I HDACs and HDAC3 in particular in regulating its expression. RNA interference targeting HDAC3 mRNA also significantly decreased *MMPs* and *IL-6* expression (**Figure 3.8**). Similar findings using TSA, valproic acid and MS-275 have previously shown a down-regulation in the expression of both *MMPs* and knockdown of each class I HDAC blocked the IL-1 induced expression of *MMP1* and *MMP13*, while knockdown of *HDAC2* showed statistically significant repression of *MMP13* expression in the basal level. (Culley et al. 2013) A number of mechanisms might have accounted for these results. Some of these HDACi may act on specific genomic regions altering the acetylation state of the adjacent chromatin and allowing or preventing specific transcription factor binding or protein-DNA interactions. For instance, the identification of an Sp1 binding motif in Timp-1 promoter constructs shed some light on the differential regulation by TSA on *Timp-1* expression. (Young et al. 2005) Moreover, transcription factor half-life, stability, subcellular localisation or transcriptional potential may be impaired. HDACi mediated increase in acetylation in critical DNA regions, including the promoters of the above genes, might block the tissue-specific interaction of transcription factors necessary for inducing gene transcription.

Other reports supported that HDACi could affect intermediate negative regulators such as MCPIP1, which is a negative regulator of *IL-6* expression and is expressed at low levels in human osteoarthritis cartilage. Treatment of OA chondrocytes with SAHA robustly induced the expression of MCPIP1 and inhibited the expression of *IL-6* and secretion of IL-6 following IL-1β stimulation. This effect was mediated by recruitment of the CEBPα transcription factor to the hyperacetylated MCPIP1 promoter following SAHA treatment. (Makki & Haqqi 2015) Therefore, HDAC inhibition or HDAC3 specific depletion could prevent the induction of selected genes by activating their negative regulators.

Normal signal transduction or protein-protein interactions could also be impaired following HDAC inhibition. It is known that IL-1 activates numerous pathways involved in cartilage destruction and dedifferentiation of chondrocytes. p38MAPK and/or PI3K/JNK signalling pathways have been identified as being crucial for IL-1 induced IL-6 secretion by chondrocytes and the down-regulation of aggrecan mediated by p38MAPK and/or ERK1/2. (Radons et al. 2006) HDACi treatment could impinge upon IL-1 mediated induction of *IL-6* expression by inhibiting signal transduction or protein-protein interaction of intermediate molecules of the aforementioned pathways. Involvement of ERK-, p38- and JNK- MAPK as well as AP-1, ATF2 and NF-κB transcription factors have been suggested to be involved in aggrecanase expression in chondrocytes. (Sylvester et al. 2012) And MS-275 and TSA treatment suppressed MAPK- mediated activation of RUNX2, ADAMTS5 and MMP3 in human articular chondrocytes. (Saito et al. 2013) Therefore, histone deacetylation may be necessary for facilitating normal signal transduction and HDAC inhibitors may render novel therapeutic agents against degenerative joint diseases such as osteoarthritis.

Additionally, RNAi of HDAC3 would impact on the large multi-component subunit that contains HDAC3, the NCoR and SMRT co-repressors, which are necessary for HDAC3 activity, modulating in this way its repressive effect. Interestingly, through interactions with these co-repressors, HDAC3 can associate with other class II HDACs including HDAC4, HDAC5 and HDAC7 and due to the presence of nuclear import and export signals it can translocate to the cytoplasm, where it is phosphorylated by Src. (Longworth & Laimins 2006) Therefore, *HDAC3* depletion could not only affect its repressor- deacetylase activity, but also its subcellular localisation and interaction with other HDACs.

Other evidence indicated that inhibition of class I, II HDACs or class III sirtuin HDACs potently block the production of IL-6 and TNF-α by macrophages from healthy donors and patients with rheumatoid arthritis (RA). Importantly, inflammatory and angiogenic cytokine production in intact RA synovial biopsy explants was also suppressed by HDACi treatments.

Two HDACi, TSA and nicotinamide, selectively induced macrophage apoptosis by downregulating the anti-apoptotic protein Bfl-1/A1, and inflammatory stimuli enhanced this HDACi-induced apoptosis. (Grabiec et al. 2010) It is therefore possible that TSA and the other HDACi used in this study have a similar effect in inducing apoptosis and hence downregulating cytokine production and an inflammatory response.

Regarding *IL-8* expression, this was not affected by MS-275 or Apicidin HDAC inhibition, but was significantly increased by TSA in the IL-1-induced level and instead decreased following siRNA-mediated *HDAC3* depletion and IL-1 stimulation. Strong up-regulation of *IL-8* was previously found in MCF-7 breast cancer cells following TSA treatment and this up-regulation was dose- and time- dependent. This transcriptional activation involved mainly the NF-κB site of the IL-8 promoter and blocking NF-κB abolished IL-8 induction. (Chavey et al. 2008) In concordance with our findings TSA but not any other HDACi such as apicidin, MS-275, valproic acid, butyrate, and depudecin increased the IL-1 induced expression of *IL-8* in A549 human lung epithelia cells. (Kallsen et al. 2012)

One of the most remarkable properties of IL-8 expression is the variation of its expression levels. In healthy tissues it is barely detectable, but it is rapidly induced in response to pro-inflammatory cytokines such as tumor necrosis factor or IL-1, bacterial or viral products and stress. For IL-8 to be generated, a combination of de-repression of its gene promoter, transcriptional activation by the NF-κB and JNK pathways and finally stabilization of IL-8 mRNA by the p38-MAPK pathway need to take place. As a result cells fine-tune the amounts of secreted IL-8. (Hoffmann et al. 2002) Hence, the effect upon *IL-8* expression following HDAC3 depletion is probably independent of the regulatory effects of the broad-spectrum HDACi TSA, and suggests IL-1 specific functions for HDAC3. The stimulatory function of HDAC3 for inflammatory gene expression involves a mechanism that uses binding to NF-κB p65 and its deacetylation at various lysines. NF-κB p65-deficient cells stably reconstituted to express acetylation mimicking forms of p65 (p65 K/Q) had largely lost their potential to stimulate IL-1-triggered gene expression, implying that the co-activating property of HDAC3 involves the removal of inhibitory NF-κB p65 acetyl groups from K122, 123, 314 and 315. (Ziesché et al. 2013; Sun et al. 2013) These data describe a novel function for HDAC3 as a co-activator in inflammatory signaling pathways and especially in the regulation of *IL-8* expression.

3.4.2 Effect of HDAC inhibitors on cytokine induced collagen release in vitro using cartilage explants.

The ability of different HDACi to abrogate collagen degradation *in vitro* was assessed in a BNC assay. Although, collagen breakdown remained unchanged in the basal level after the addition of the different HDACi, TSA significantly rescued collagen release following IL-1 and IL-1 + OSM stimulation. Apicidin also showed inhibition of collagen breakdown in the IL-1 + OSM stimulated cartilage explants (**Figure 3.6**). These results suggest that pro-inflammatory cytokine stimulation is required for cartilage collagen breakdown and HDACi including TSA and apicidin can protect, at least in part, collagen breakdown. It also predicts a novel- specific role for the class I HDAC3, in mediating cartilage degradation and in particular collagen breakdown. Previous reports confirm these findings at least as far as the TSA HDACi is concerned (Young et al. 2005) and also measurement of gene expression in a BNC assay following MS-275 inhibition showed repressed levels of *MMP1*, *MMP13*, *ADAMTS4* and *ADAMTS5*. (Culley et al. 2013) In the same study proteoglycans (GAG) loss was also studied as a marker of cartilage degradation and following MS-275 HDAC inhibition, GAG loss was prevented. Taken these data together, we have shown that class I HDAC3 selective inhibitor apicidin can in part reduce cartilage destruction in a manner similar to that of the broad-spectrum TSA and the class I HDACi MS-275.

3.4.3 HDACi and RNAi for HDAC3 inhibit IL-1-induced IEG-FRA1 expression.

The transcriptional program induced following growth factor or cytokine stimulation is classically described in two stages as follows: the rapid protein synthesis and independent induction of immediate early genes (IEG) followed by the subsequent protein synthesis-dependent induction of secondary response genes. In this study, the effect of HDACi and HDAC3 RNAi upon the activating protein-1 (AP-1) family of IEG expression was determined, since the promoters of MMP1 and MMP13 (and most other MMPs) contain multiple AP-1 binding sites that may contribute to gene expression. (Tullai et al. 2007; Vincenti & Brinckerhoff 2002)

From the genes studied, it was demonstrated that only *FRA1*, *cFOS*, *JUND* and *FOSB* were significantly up-regulated following early IL-1 stimulation (**Figure 3.9**) and out of these four genes only *FRA1* expression was responsive to HDACi or RNAi for *HDAC3* (**Figure 3.10** & **Figure 3.11**). Induction of *FRA1* expression was determined following IL-1 stimulation and down-regulation of its expression followed after TSA and Apicidin treatment. Further one-

way ANOVA analysis for the MS-275 treated cells concluded in a modest but not significant reduction of the 30 minutes IL-1 induced *FRA1* expression, but no further effect was demonstrated. siRNA-mediated depletion of *HDAC3* also prohibited *FRA1* expression following 60 minutes of IL-1 stimulation. It has been reported that *FRA1* expression requires dynamic changes in histone acetylation which is catalysed by lysine acetyltransferases and HDACs. Moreover, FRA1 is induced by several signal transduction pathways, resulting in the activation of MSK protein kinase and phosphorylation of histone H3 at Ser10 of the upstream promoter and regulatory region of the target gene. (Khan & Davie 2013) Interestingly, HDAC inhibition using TSA or Apicidin prevented *FRA1* induction and the association of HDAC1, HDAC2 or HDAC3 with the gene body. The mechanism of HDAC recruitment to the gene body is thought to be via RNAPII which is required to transfer HDAC to the coding region of the gene. As the HDAC inhibitors prevented the initiation of transcription, RNAPII is not present to do this task. However, HDACi did not prevent the nucleosomal response but enhanced acetylation of histones at the upstream FRA1 promoter. (Khan & Davie 2013) Consistent with our results, others have shown that HDAC inhibitors can attenuate transcriptional initiation possibly by abrogating the binding of RNAPII and other transcription factors to promoter regions. (Yamaguchi et al. 2005; Rascle et al. 2003; Wolter et al. 2008) Furthermore, acute short term depletion of all or some specific HDACs differs significantly to the depletion of one HDAC for over 48 hours. Therefore, dynamic acetylation required for transcriptional initiation of IEG *FRA1* would be opposed by HDAC inhibition. These reported findings support our data and suggest that *FRA1* is among the genes that are down-regulated by HDACi or RNAi for specific HDACs. These results demonstrate that inhibition of all HDACs or specific depletion of HDAC3 can hinder transcription possibly via dynamic protein acetylation on the upstream promoter region.

However, the effect of FRA1 gene on either *MMP1* or *MMP13* expression was not studied here, (for limitations of the study and future work, see **Chapter 8: General Discussion**). Nevertheless, there are reports supporting a role for FRA1 on regulating many MMPs, including MMP1, MMP2, MMP9 (Henckels & Prywes, 2013; Adiseshaiah et al. 2008; Belguise et al. 2005; Ho et al. 2008; Singh et al. 2010; Kimura et al. 2011). In particular, Kimura et al (2011) demonstrated that phosphorylated c-Jun and FRA1 bind to the AP-1 element in the proximal promoter of MMP1 and are essential for its expression in 143B osteosarcoma cells. Differential expression of *MMP1* has repeatedly correlated with tumorigenesis and metastasis. Henckels &Prywels (2013) showed that *MMP1* expression is regulated by an AP1 element and FRA1 can differentially bind this element to regulate *MMP1*

expression in the MDA-MB-231 breast cancer cells. *FRA1* expression and protein levels were higher in the metastatic cells, which in turn resulted in an induction of *MMP1* and *MMP9* expression. (Henckels & Prywes, 2013; Belguise et al. 2005) Knockdown of *FRA1* in lipopolysaccharide (LPS)-induced primary monocytes resulted in diminished MMP1 expression, while over-expression of *FRA1* increased *MMP1* expression. (Ho et al. 2008) Adiseshaiah et al. also showed that ectopic expression of *FRA1* stimulated *MMP9* and *MMP2* expression, which induced lung epithelial cell growth and invasion (Adiseshaiah et al. 2008).

3.4.4 HDAC inhibition abrogates NF-κB signalling pathway activation.

Transactivation by NF-κB in the presence/absence of HDACi and IL-1 stimulation was assessed by luciferase assay (**Figure 3.12**). The reporter assay determined that HDAC inhibition using TSA, or class I HDAC inhibition using MS-275 significantly reduced both basal and IL-1-induced NF-κB activity in the SW1353 cells. Interestingly, the selective HDAC3 inhibitor apicidin also blocked luciferase transactivation of NF-κB activity.

The relation of HDACs to NF-κB pathway is complicated and evidence has recently accumulated supporting that acetylation and deacetylation events are implicated in the regulation of NF-κB transcriptional activity. First, acetylation of histones regulates the NF-κB-dependent transcription factor gene accessibility. Second, acetylation events modulate temporally the IKK activity and subsequently the duration of NF-κB presence, translocation and transcriptional activation in the nucleus. Third, direct acetylation of the NF-κB subunits p65 and p50 regulates different NF-κB functions, including transcriptional activation, DNA-binding affinity and IκBα assembly. It has been suggested that HDAC3 can deacetylate lysines 122, 123, 314 and 315 of NF-κB p65 to induce inflammatory gene expression. (Ziesché et al. 2013) In particular, it was shown that de-acetylation of K122 and K123 by HDAC3 is required for stable association of p65 with chromatin and subsequent p65-dependent gene activation, yet does not affect nuclear translocation of p65. Elsharkawy et al. (2010) also showed that the p50 subunit of NF-κB can associate with HDAC1 is specific inflammatory gene promoters including *CCL2*, CXCL10, *GM-CSF* and *MMP13* to inhibit transcription. Interestingly these genes were over-expressed in *nfκb1* (p50) deficient mice suffering from chronic hepatitis and in inflammatory hepatic stellate cells isolated from *nfκb1*$^{-/-}$ liver. The same study indicated that p50 was required for HDAC1 recruitment to the κB sites in the MMP13 promoter, and ChIP assays identified binding sites for HDAC1 in the promoters of the other inflammatory genes. (Elsharkawy et al. 2010)

In addition, acetyltransferases and deacetylases interact directly with several proteins involved in the NF-κB signaling pathway, including NF-κB itself, IκBα, IKKα and IKKγ. These interactions probably allow acetylation of NF-κB itself, of other transcription factors and of histones associated with NF-kB regulated genes. (Quivy & Van Lint 2004) It has been reported that MS-275 and SAHA suppressed lipopolysaccharide (LPS)- induced NF-κB p65 nuclear accumulation, IL-6, IL-18 and TNFα secretion in THP-1 monocytic cells. The same study showed that Nitric Oxide (NO) secretion was inhibited and cell cycle arrest at the G0/G1 phase was induced. (Choo et al. 2010) These results taken together with the findings of this study imply a possible role for HDACi in suppressing NF-κB nuclear accumulation that would possibly impact upon reduced MMP expression in chondrocytes.

While some studies support a synergistic role between HDACs and NF-κB to suppress gene expression, (Zhou et al. 2013), others propose an HDACi- mediated NF-κB activation of p65/RelA (Rosato et al. 2010). It is becoming therefore clear that further experiments are needed to additionally validate the role of HDACs and in particular HDAC3 in relation to NF-κB activity in chondrocytes. RNAi for different HDACs should be used and NF-κB transcriptional activation or DNA binding potential should be tested.

3.5 Conclusions

In SW1353 cells:

- HDAC inhibition using TSA, MS-275 or Apicidin blocked IL-1-induced collagenase expression *in vitro*.
- HDACi decreased collagen release following cytokine stimulation in BNC assay.
- RNAi for HDAC3 abrogated *MMP1* and *MMP13* IL-1-induced expression.
- HDACi and HDAC3 RNAi suppressed the induction of the IEG *FRA1* by IL-1.
- NF-κB transactivation was reduced following HDAC inhibition both in the basal and IL-1 induced level.

Chapter 4. Identification of differentially regulated genes by HDAC3 using RNA microarray analysis.

4.1 Introduction

A previous microarray analysis identified the molecular changes taking place after HDAC3 depletion in osteoblast progenitor cells (using Osterix-Cre mediated knockout of Hdac3 in mice). Of the genes identified, 43 genes were significantly upregulated and 21 genes were down-regulated, with the most upregulated gene being a cyclin dependent kinase inhibitor (Cdkn1a), a known HDAC regulated gene. (Sambucetti et al. 1999; Richon et al. 2000; Han et al. 2000) Gene ontogeny analysis of the 64 differentially regulated genes identified 11 pathways as being affected by *Hdac3* depletion. These pathways include signal transduction pathways such as Wnt, Akt, G-proteins, cell cycle and DNA damage pathways and cytoskeletal/ cell adhesion. Thus, it became apparent that HDAC3 modulates pathways crucial for the development and function of the osteoblast pathways. (Razidlo et al. 2010) Very recently, Hdac3- deficient chondrocytes exhibited increased expression of cytokine and matrix-degrading genes and a decrease in expression of genes related to ECM production, bone development and ossification. Histone acetylation was increased at the near genes that had increased expression, including *Il-6, Mmp3, Mmp13* and *Saa3*, and increased cytokine signalling promoted activation of NF-κB and JAK-STAT pathways. (Carpio et al. 2016)

In addition cardiac-specific deletion of Hdac3 results in cardiac hypertrophy due to the upregulation of genes associated with fatty acid uptake, fatty acid oxidation, myocardial lipid accumulation and elevated triglyceride levels. These abnormalities were attributed to excessive activity of the nuclear receptor PPARα. (Montgomery et al. 2008) Sun and colleagues have also demonstrated that Hdac3 conditional knockout in the mouse liver, upregulated many lipogenic genes and resulted in severe hepatosteatosis. An increase in histone acetylation was profound as indicated by increased H3K9ac and H3K27ac, although HDAC3 target genes were not upregulated, indicating that hyperacetylation is insufficient to induce gene transcription. However, it was shown that while HDAC3 is the primary HDAC enzyme present in NCoR/SMRT complexes, other HDACs can be also recruited in a transcription factor- dependent or context- dependent manner, altering in this way gene expression programmes. (Sun et al. 2013)

Gene profiling studies have demonstrated only a relatively small number of genes (2-10%) modulated by HDAC inhibitors and data obtained from the previous chapter indicated that

HDAC3 may mediate IL-1 induced collagenase and *FRA1* IEG gene expression and NF-κB pathway activation in a chondrocyte-like cell line. However, one question became immediately obvious: How does HDAC3 work at the molecular level to regulate specific gene expression programmes in chondrocytes? To determine the gene expression changes that result from *HDAC3* gene depletion or selective inhibition, the gene expression patterns in SW1353 cells were determined by microarray analysis and confirmed by qPCR.

Data in the previous chapter indicated that HDAC3 selective inhibition or gene depletion mediates IL-1 induced collagenase and *FRA1* immediate early gene expression. It was also proposed that HDACs in general and HDAC3 in particular may positively activate NF-κB. A number of possible mechanisms were introduced, yet herein a whole genome expression array was utilized to identify specific pathways, transcription factor binding sites and biological functions affected by HDAC3 knockdown or inhibition prior to and following IL-1 cytokine stimulation in the SW1353 cells.

4.2 Aims

- To reveal mechanistic information regarding the types of genes, pathways and transcription factor binding sites that are altered following HDAC3 selective inhibition or gene depletion in chondrocytes.

4.3 Results

4.3.1. Cell treatments, RNA quantification and differential expression tests performed for the gene expression array experiment.

The different treatments performed in the microarray experiment are shown in **Table 4.1** and have been previously described (in section **2.2.19** ***RNA microarray analysis***). Briefly, SW1353 cells were transfected with siRNA targeting *HDAC3* mRNA or a non-targeting siRNA was used as control. Following 24 hours of transfection and an overnight serum starvation, cells were induced with IL-1α for 1 or 6 hours. Independent of *HDAC3* gene depletion, HDAC3 was also selectively inhibited using the HDACi Apicidin, with DMSO used as vehicle control. In this case, serum starved cells were incubated with the inhibitor for 30 minutes before an IL-1α stimulation for 1 or 6 hours was performed. Unstimulated cells having been transfected with siRNA/ HDACi were also included in this study.

The principal component analysis to assess gene expression variation between different samples, leveraging all probes was constructed by Andrew Skelton, (Bioinformatics Support Unit, Newcastle University, Newcastle, UK) and can be found in **Figure 4.1**.The first principal component identified in my microarray experiment which explains the largest driver of variation is between the HDACi and siRNA treated samples and is plotted on the x axis. The second principal component (second biggest driver of variation) is plotted on the y axis and is explained based on if the samples had IL-1 stimulation or not.

By profiling, the global gene expression changes of 23,739 genes and transcript variants were identified, but a subset of the significantly gene expression changes ($p<0.01$ and fold change ±2) were taken into account as shown in **Figure 4.2**- heatmap. K-mean clustering was used to identify subsets of genes that present similar gene expression across the IL-1 stimulation and siHDAC3/siCON or Apicidin/DMSO treatments (**Figure 4.3**), because it was hypothesized that there might be a common mechanism of their gene expression regulation. The number of K-clusters was set to 24 and among the groups of co-regulated genes, there were clusters of genes that were induced at 1 hour of IL-1 stimulation but no further induced at 6 hours and RNAi for HDAC3 (**Figure 4.3 A**); clusters of genes that were induced across IL-1 stimulation and further induced following siHDAC3 (**Figure 4.3 B**) and genes which expression remained stable, independent of the treatment and/or IL-1 induction (**Figure 4.3 C**-siHDAC3 & **D**-Apicidin treatment). The list of genes in each cluster is given in **Appendix A.**

.

Two differential gene expression tests were carried out including: i) 'knockout' comparisons, by comparing the siHDAC3-treated to the siCON-treated samples or the Apicidin-treated to the DMSO-treated samples for each IL-1 stimulation time-point independently (**Figure 4.4 A & C**) and ii) time-point comparisons, by comparing the differentially IL-1 treated samples which had the same RNAi or HDACi treatment (**Figure 4.4 B & D**).

IL-1α stimulation (0.5 ng/ml)								
No- IL-1			IL-1 for 1 hour			IL-1 for 6 hours		
Vehicle control	**Treatment**	**c (nM)**	**Vehicle control**	**Treatment**	**c (nM)**	**Vehicle control**	**Treatment**	**c (nM)**
siCON	siHDAC3	50	siCON	siHDAC3	50	siCON	siHDAC3	50
DMSO (0.25%)	Apicidin	160	DMSO (0.25%)	Apicidin	160	DMSO (0.25%)	Apicidin	160

Table 4.1. Treatments performed for gene expression array experiment and IL-1 stimulation time-points.

Figure 4.1. Principal component analysis of technical replicates for microarray experiment.

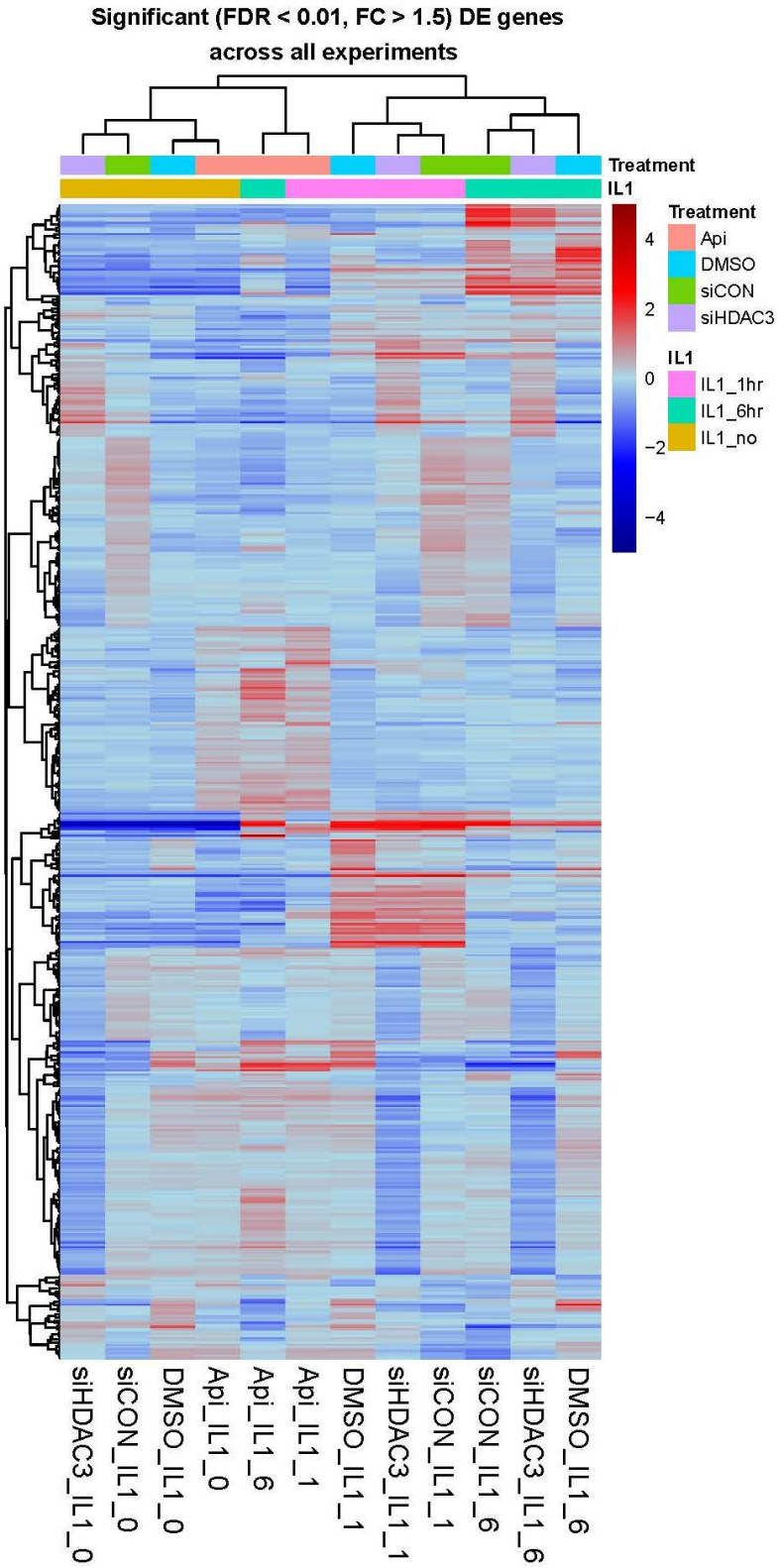

Figure 4.2. Heat-map showing the expression profile of IL-1 induced- HDAC3 regulated genes at 1 hour, 6 hours after IL-1 stimulation and basally (no IL-1).

Blue or red represents increase or decrease in gene expression relative to vehicle (either DMSO or siCON) treated cells respectively. Only genes that display significant changes in expression levels (fold change> 1.5, $p<0.01$) as compared to vehicle treated controls of three technical replicates are shown.

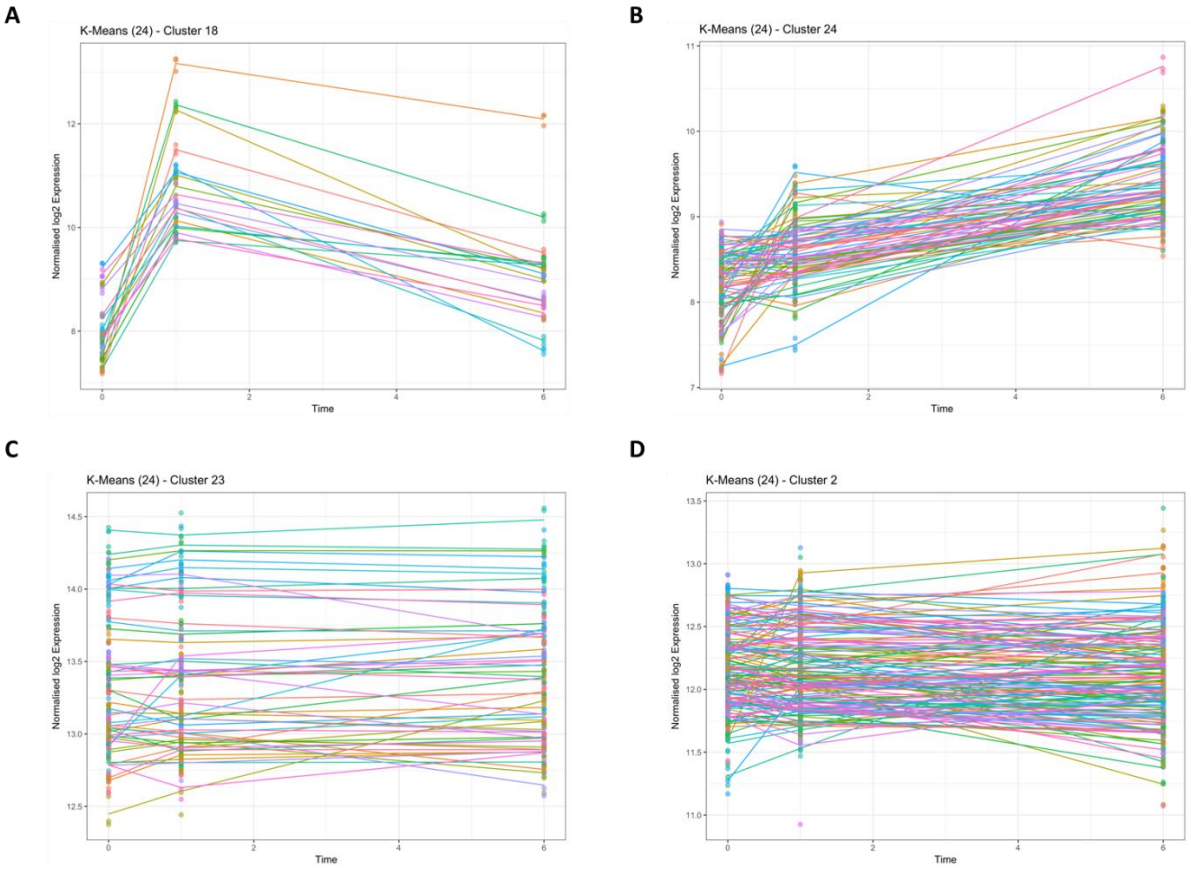

Figure 4.3. K-mean clustering was used to identify subset of genes with similar expression patterns across the IL-1 stimulation and Apicidin or siHDAC3 treatment.

A. Genes induced at 1 hour of IL-1 stimulation but no further induced at 6 hours and siHDAC3, **B.** Genes that were induced across IL-1 stimulation and further induced following siHDAC3, **C.** Genes whose expression remained stable across the IL-1 stimulation and siHDAC3 and **D.** Genes whose expression remained stable across the IL-1 stimulation and Apicidin treatment.

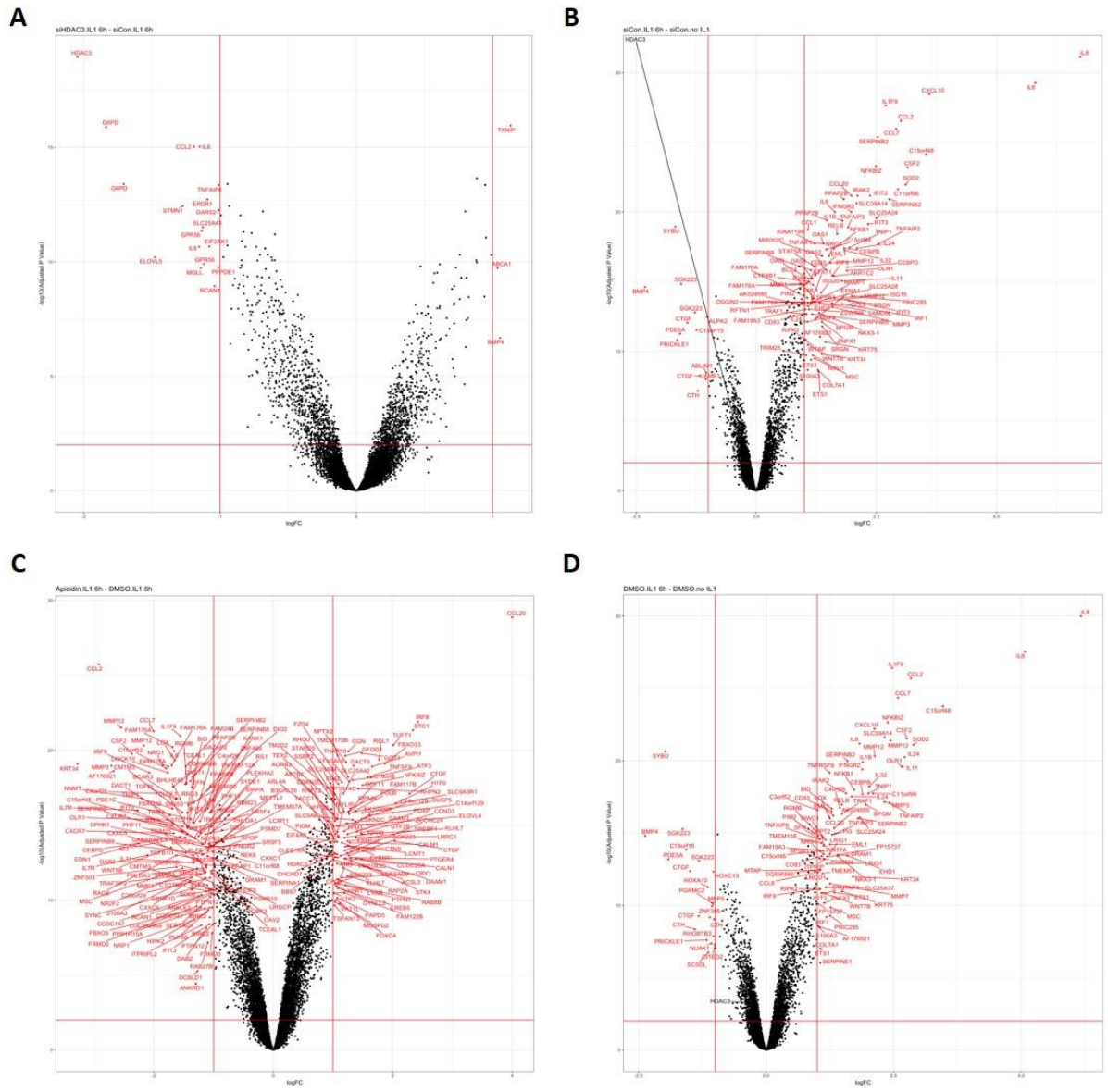

Figure 4.4. Volcano plots of two differential expression tests performed in the microarray experiment.

***A*- C.** Knockout comparison: siHDAC3 versus siCON and Apicidin versus DMSO treated samples following 6 hours of IL-1 stimulation and

***B*- D.** Time-point comparison: siCON/DMSO treated cells at 6 hours of IL-1 stimulation versus no IL-1.

Red dots: significantly changed gene expression, Black dots: Non- significant changed gene expression. HDAC3 gene is shown in all different comparisons.

After validating the quality and degradation of the RNA samples (see section **2.2.19** ***RNA microarray analysis***), quantitative real-time RT-PCR was used and gene expression measured to confirm the previous effect of siRNA depletion or Apicidin inhibition and IL-1 induction. In particular, *HDAC3* depletion was confirmed with qRT-PCR as shown in **Figure 4.5**. *MMP1* and *MMP13* expression were significantly induced following IL-1 stimulation and as expected downregulated following siHDAC3 depletion or Apicidin treatment (**Figure 4.6)**, confirming the results presented in Chapter 3.

The log_{FC} values ($log_{\text{fold change}} = log_{FC}$) obtained from the microarray were as below: for MMP1 (= -0.864) and for MMP13 (= -0.487) in the Apicidin treated samples after 6 hours of IL-1, and for MMP1 (= -0.571) and for MMP13 (= -0.412) in the siHDAC3 treated samples after 6 hours of IL-1. Additionally, *FRA1* (= -1.5967), *IL-6* (= -1.14965) and *IL-8* (= -1.15432) gene expressions were measured by qRT-PCR (results not shown here) and the effect of HDAC3 depletion/inhibition upon their expression was confirmed as previously described in Chapter 3.

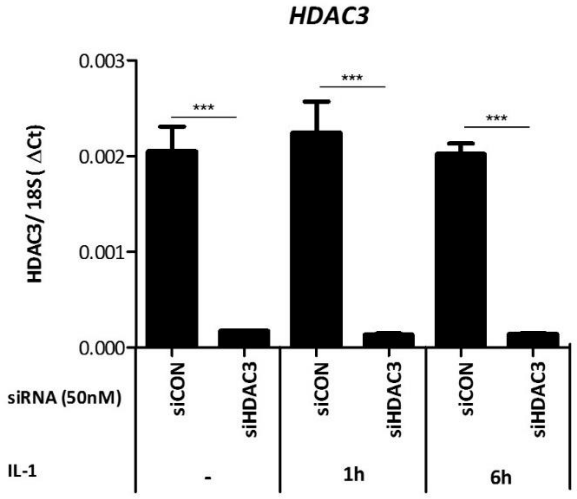

Figure 4.5. HDAC3 gene expression following RNAi for HDAC3 and IL-1α cytokine stimulation.

SW1353 cells were transfected with 50nM of non-targeting siRNA control (siCON) or a HDAC3-specific siRNA (siHDAC3) for 24h. Following an overnight serum starvation, the cells were stimulated with IL-1α (0.5ng/ml) for 1 hour, 6 hours or left unstimulated. Total RNA was extracted, reverse transcribed to cDNA and HDAC3 expression measured by qRT- PCR. Results are shown relative to 18S ribosomal RNA expression. Significance was determined by comparing the siCON with the siHDAC3 treated cells in the basal and IL-1 induced level. Bars represent the mean of three biological replicates +SD. For statistical analysis, an unpaired two-tailed student's t-test was performed. *** $p < 0.001$

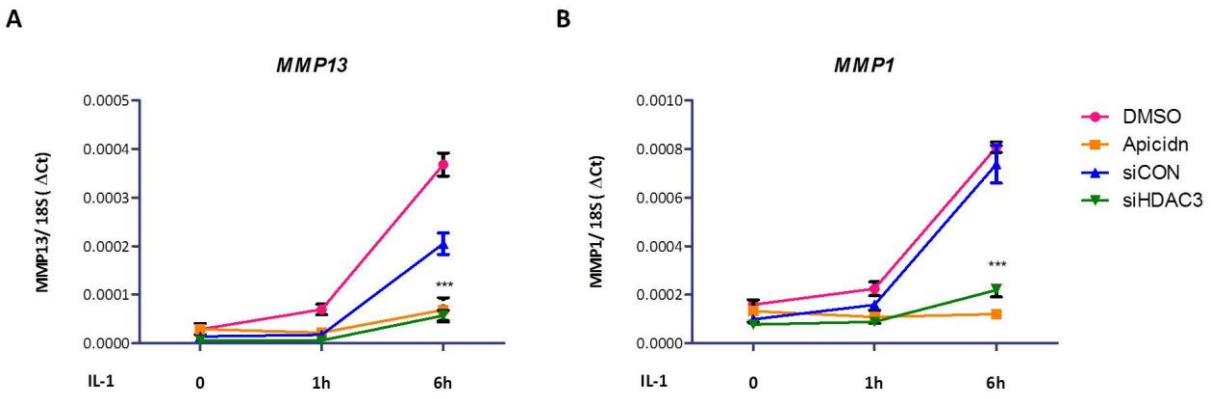

Figure 4.6. MMP13 and MMP1 gene expression following RNAi or HDACi and IL-1α cytokine stimulation.

SW1353 cells were transfected with 50nM of non-targeting siRNA control (siCON) or a HDAC3-specific siRNA (siHDAC3) for 24h. Following an overnight serum starvation, the cells were stimulated with IL-1α (0.5ng/ml) for 1 hour, 6 hours or left unstimulated. Alternatively, serum starved cells were incubated for 30min with Apicidin (100ng/ml= 160nM) or DMSO (0.25%), before IL-1α (0.5ng/ml) stimulation was performed. Total RNA was extracted, reverse transcribed to cDNA and *MMP1/13* expression measured by qRT- PCR. Results are shown relative to 18S ribosomal RNA expression. Significance was determined by comparing the siCON with the siHDAC3 treated cells, or the Apicidin with the DMSO treated cells both in the basal and IL-1 induced level. Bars represent the mean of three technical repeats ±SD. For statistical analysis, a two-way ANOVA with a Bonferroni post-test was performed. *** $p < 0.001$

4.3.2 Genes and pathways induced by IL-1 following 1 or 6 hours of stimulation.

The gene lists produced from the gene expression array and with final cut off of ±1.5 fold change (log_{FC} = 0.58) and a p-value ≤ 0.05were analysed for gene ontology, KEGG pathways and transcription factor binding sites using GATHER (Chang & Nevins 2006). In the first instance, the genes significantly up-regulated by IL-1 stimulation were identified. A total of 62 genes were significantly upregulated following IL-1 stimulation for 1 hour, while 290 genes were induced following IL-1 stimulation for 6 hours in the DMSO-treated control samples. In the siCON-treated samples 78 genes were induced by IL-1 after 1 hour of stimulation, while 268 were induced after 6 hours. Out of these genes, 45 and 190 were common between the DMSO and siCON treated samples following 1 or 6 hours of IL-1 stimulation respectively (see **Figure 4.7 A**, IL-1 for 1 hour timepoint; and **Figure 4.8 A**, IL-1 for 6 hours timepoint).

As expected the most inducible gene was an immediate early gene, FOS (log_{FC} = 0.99) which has been reported as being induced by IL-1 stimulation and previously linked to MMP expression and OA. (Cawston et al. 2003; Vincenti & Brinckerhoff 2002) The list of the 45 common genes between the DMSO and siCON- treated samples was found to be significantly associated with three pathways including apoptosis, focal adhesion and the Toll-like receptor signaling pathway. The top ten biological functions and transcription factor binding sites are also shown in **Figure 4.7 B** and **C**. Among these, AP-1 binding sites come in the top of the list and NF-κB transcription factor was present twice. The latter could be associated with the IκB kinase/NF-κB cascade gene ontology annotation that was predicted. Interferon regulatory factors that are known mediators of the JAK-STAT signaling pathway and the FOXP3 transcription factor which has been linked to immunodeficiency syndromes were also determined. The above predicted transcription factor binding sites, in combination with the prediction of the serum response factor (SRF), which can bind to the promoter regions of target genes could regulate important cellular physiological processes. For instance, the SRF can bind to the serum response element to regulate the activity of many IEG such as c-FOS and therefore participates in cell cycle regulation, apoptosis, cell growth and cell differentiation. (Johansen & Prywes 1994) This gene is the downstream target of MAPK signaling pathway, suggesting that other biological functions for example transcription factor –nucleus import, protein transportation or signal transduction may be altered following IL-1 stimulation.

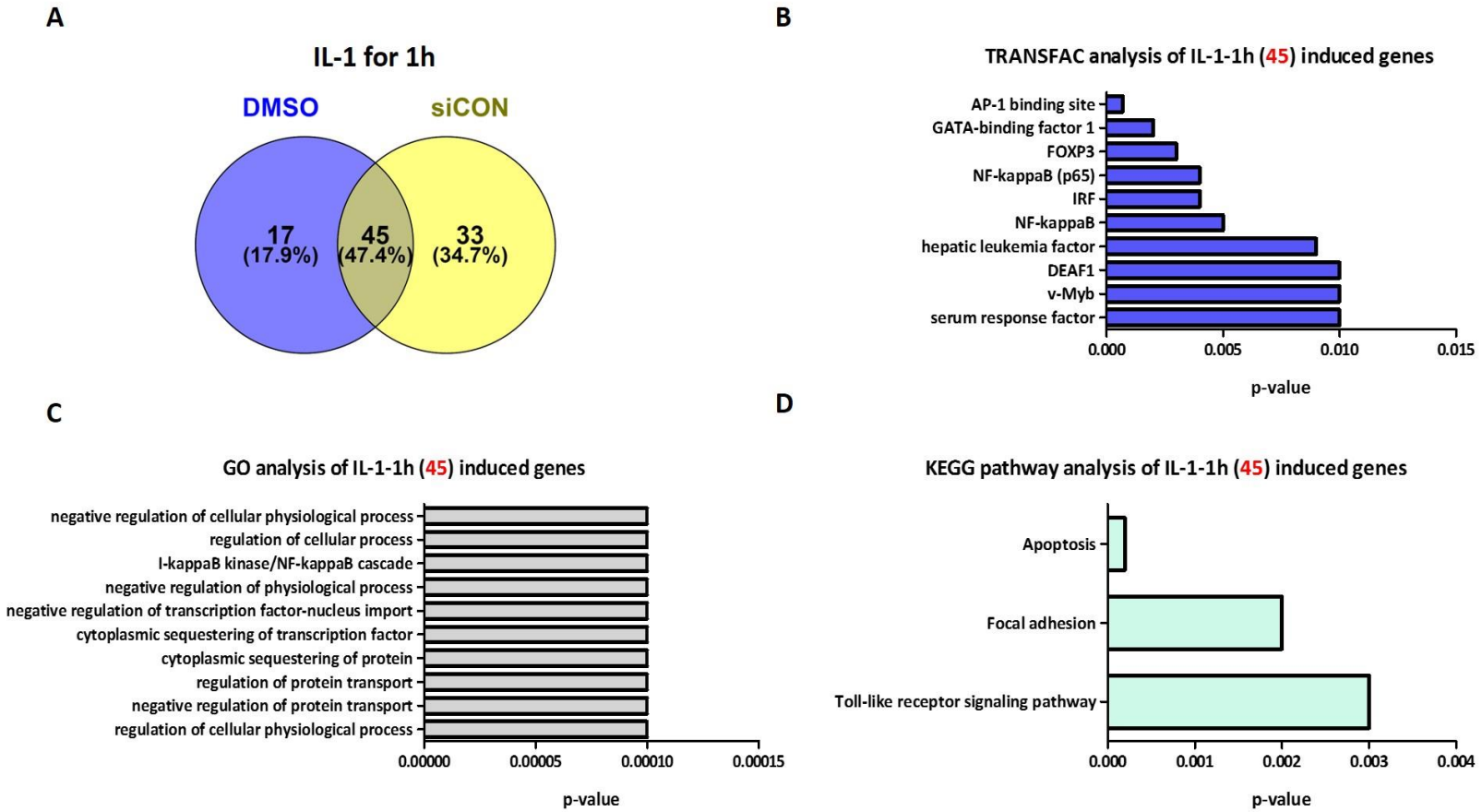

Figure 4.7. Differentially induced genes following 1 hour of IL-1α (0.5ng/ml) stimulation.

A. Venn diagram of genes induced after 1 hour of IL-1 stimulation in the siCON-treated or DMSO treated samples. Only 45 genes were identified as up-regulated in common between the two treatments. **B.** Top 10 transcription factor binding sites (TRANSFAC) analysis, **C.** Top 10 gene ontology (GO) analysis and **D.** KEGG pathway analysis of up-regulated genes (45) were performed using GATHER.

The most upregulated gene following 6 hours of IL-1 stimulation in both the DMSO and siCON-treated samples was CXCL8 (C-X-C Motif Chemokine Ligand 8, also known as IL-8) with $\log_{FC} = 6.17$, a member of the CXC chemokine family and a major mediator of the inflammatory response. A more comprehensive examination (**Figure 4.8**) suggests that most of the genes induced are related to an immune response or response to stimulus as would be anticipated following IL-1 stimulation. However, gene ontology analysis (**Figure 4.8 C**) predicts many other biological processes including cell cycle regulation, cell death and proliferation, cell signalling, signal transduction, lipid metabolism and cell migration are also affected by the IL-1 stimulation. NF-κB transcription factor binding sites are the predominant binding motifs identified in the 190 common up-regulated genes (**Figure 4.8 B**) confirming NF-κB factor as the key mediator of IL-1 cytokine response. Furthermore, four pathways (**Figure 4.8 D**) were significantly associated with the IL-1 induced genes including cytokine-cytokine receptor interaction, Toll-like receptor signalling pathway, apoptosis and JAK-STAT signalling pathway.

The Open Targets platform (https://targetvalidation.org/) (Koscienly et al. 2017) was used to identify OA and/or cartilage related genes among the IL-1 induced genes and the results can be found in **Table 4.2**.

IL-1 for 1 hour (9 out of 45 from Figure 4.7 A)	**IL-1 for 6 hours (54 out of 190 from Figure 4.8 A)**					
BMP4	*CCL2*	*CXCL8*	*IL6ST*	*MMP7*	*SERPINA1*	*TNIP1*
CDKN1A	*CCL20*	*EGFR*	*IRF1*	*MT2A*	*SERPINB2*	*TRIB1*
F3	*CCL8*	*FBXO32*	*KRT75*	*NAMPT*	*SERPINE1*	*VEGFC*
IL1B	*CD44*	*IFIH1*	*LIF*	*NFKBIA*	*SERPINE2*	*XBP1*
IL24	*CD82*	*IFIT1*	*LOX*	*OLR1*	*SMAD3*	
LDLR	*CDK6*	*IL11*	*LTB*	*PI3*	*SOD2*	
NLRP3	*CEBPB*	*IL1B*	*MAP2K3*	*PIK3CD*	*TNC*	
RHOB	*CEMIP*	*IL24*	*MMP1*	*RIPK2*	*TNFAIP3*	
TNFRSF10B	*CSF2*	*IL32*	*MMP12*	*SAT1*	*TNFAIP6*	
	CXCL10	*IL6*	*MMP3*	*SDC4*	*TNFRSF1B*	

Table 4.2. OA and cartilage related genes were identified among the IL-1-induced genes following 1 or 6 hours of stimulation.

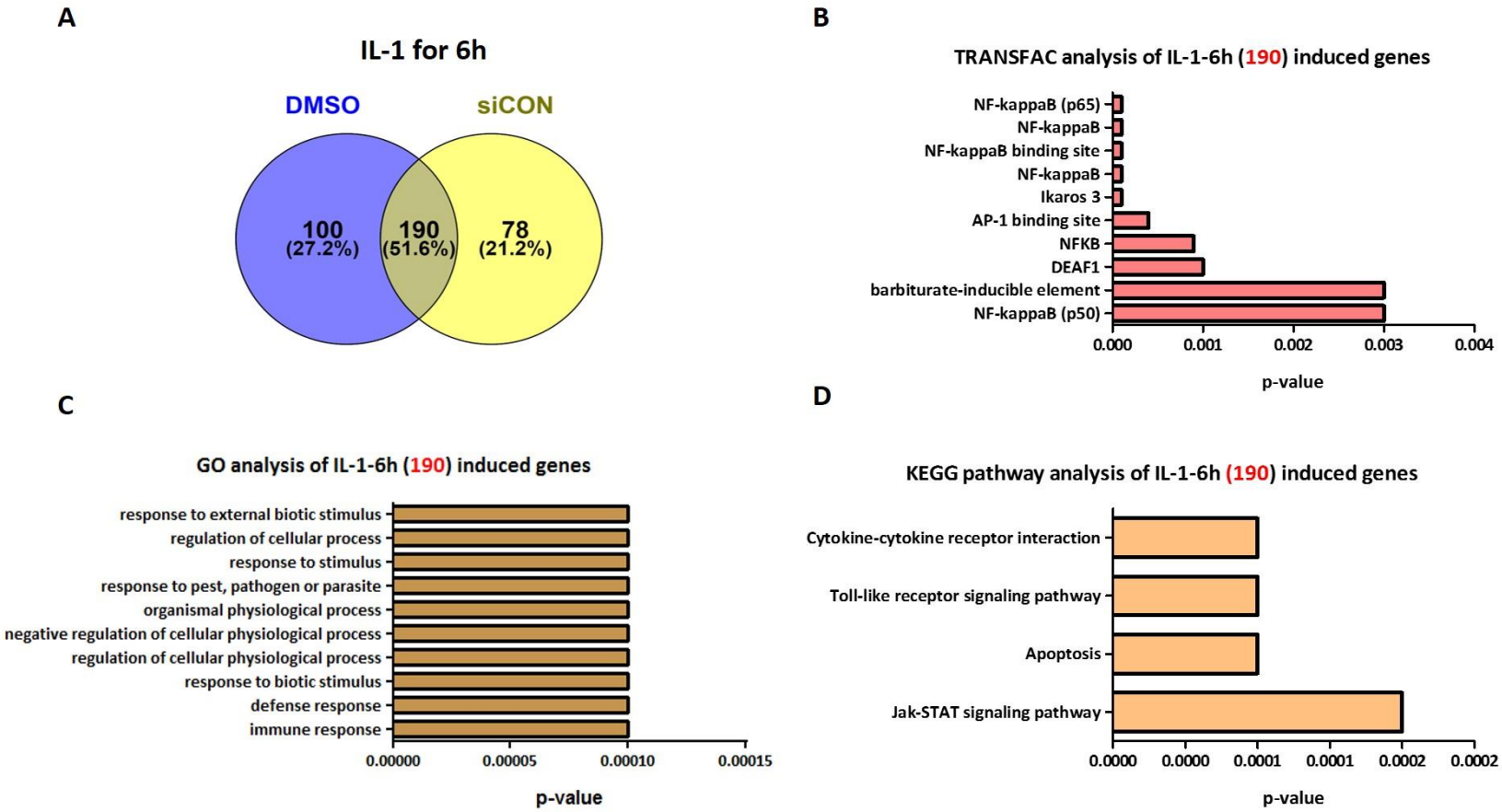

Figure 4.8. Differentially induced genes following 6 hours of IL-1α (0.5ng/ml) stimulation.

A. Venn diagram of genes induced after 6 hours of IL-1 stimulation in the siCON-treated or DMSO treated samples. 190 genes were up-regulated in both treatments. **B.** Top 10 transcription factor binding sites (TRANSFAC) analysis, **C.** Top 10 gene ontology (GO) analysis and **D.** KEGG pathway analysis of up-regulated genes (45) were performed using GATHER.

4.3.3 Differentially expressed genes following HDAC3 selective inhibition and IL-1 stimulation.

Next, an identification of the differentially expressed genes following IL-1 induction and Apicidin treatment followed. At the basal level, 43 genes were repressed by Apicidin, while 51 genes were induced. Most of the repressed genes were associated with having a role in regulation of transcription and metabolism, organogenesis and mesoderm development and linked to two pathways important for normal growth and development, the TGF-β (p-value = 0.0006) and Wnt (p-value = 0.003) signalling pathways. Regarding the 51 induced genes, these were associated with protein-nucleus import (p-value= 0.01), negative regulation of cyclin dependent phosphorylation, negative regulation of transcription and KEGG pathway analysis identified methionine metabolism (p-value= 0.002) and Notch signaling pathway (p-value= 0.007). Transcription factor binding sites predicted for the induced gene list included X-box binding protein RFX1, ATF3, PAX5 and KROX transcription factors.

However, and because ECM modifying enzymes are regulated at the level of transcription by cytokines, and inducible MMPs were repressed following Apicidin treatment, a need for understanding how the IL-1 induced and further repressed by Apicidin genes are regulated became apparent. Therefore, the focal point of this study was to identify pathways and transcription factors of the inducible repressed genes that could clarify the molecular basis of the HDAC3-mediated gene regulation.

The results obtained from the gene expression array regarding the selective HDAC3 inhibitor Apicidin are summarised in **Figure 4.9**. In total, we identified 121 genes significantly induced by IL-1 after 1 hour of stimulation, and 290 genes significantly induced after 6 hours of stimulation. A heatmap (**Figure 4.9 A**) shows the top 20 induced and most repressed by Apicidin genes at 6 hours of IL-1 stimulation and their expression in the basal level and 1 hour of IL-1 is also shown as a comparison. Pie charts in **Figure 4.9 B & D** show almost half of the genes induced by IL-1 are no longer induced in the presence of the HDACi Apicidin, whereas the other half is further induced. Among them, OA/ cartilage related genes were identified and the results can be found in **Table 4.3**. The molecular network analysis of the no longer induced genes (**Figure 4.9 C & E**) identified three pathways in common, following 1 or 6 hours of IL-1 stimulation, and these involved cytokine-cytokine receptor interaction, JAK-STAT signalling pathway and apoptosis, whilst MAPK and Toll-like receptor signalling pathways appeared only in the 1 hour list, suggesting a role for these pathways and their downstream targets early after a cytokine induction. The molecular functions of the down-

regulated genes were also assessed and the results indicate a great diversity of biological processes such as immune response and response to stimulus, cell-cell signalling, regulation of cell proliferation and negative regulation of cellular physiological processes (**Figure 4.9 G & I**). With regards to the TRANSFAC analysis, NF-κB binding sites appeared multiple times in the list of down-regulated genes, together with AP-1 and ICSBP (Interferon Consensus Sequence Binding Protein, also known and IRF-8) sites (**Figure 4.9 F &H**). Other transcription factors identified in the analysis include the Ikaros 3, Maz related factor, CP2, TAL1 and MRF2, yet none of these have been linked to directly binding or regulating matrix modifying enzymes. MTF1 transcription factor was also predicted; MTF1 has been previously associated with zinc dependent-regulation of catabolic transcription in osteoarthritis. In particular, it was shown that the zinc importer ZIP8 was upregulated in osteoarthritic cartilage from humans and mice, and Zn^{+2} influx increased transcriptional activity and promoted nuclear localization of MTF1 transcription factor, which in turn resulted in an increased expression of many MMPs including, *MMP3*, *MMP9*, *MMP12*, *MMP13* and *ADAMTS5*. (Kim et al. 2014)

IL-1 (for 1 hour) -induced and repressed by Apicidin genes (20 out of 63 from Figure 4.9 B)		**IL-1 (for 6 hours) -induced and repressed by Apicidin (41 out of 137 from Figure 4.9 D)**				
CCL2	*LDLR*	*CCL2*	*IL11*	*MMP1*	*SERPINB2*	*XBP1*
CCL20	*LIF*	*CCL8*	*IL1B*	*MMP12*	*SMAD3*	
CSF2	*NLRP3*	*CDK6*	*IL24*	*MMP3*	*SOCS1*	
CXCL8	*OLR1*	*CEBPB*	*IL32*	*MMP7*	*SOD2*	
EDN1	*SOD2*	*CEMIP*	*IL6*	*NAMPT*	*TNFAIP6*	
IL11	*SPRY2*	*CSF2*	*IL6ST*	*NFKBIA*	*TNIP1*	
IL1B	*TNF*	*DDIT4*	*IRF1*	*OLR1*	*TRIB1*	
IL24	*TNFAIP3*	*EGFR*	*LIF*	*PLAUR*	*TUBB6*	
IL32	*TRIB1*	*FBXO32*	*LOX*	*PTPRK*	*UCN2*	
KLF6	*LDLR*	*IFIH1*	*LTB*	*SERPINA1*	*VEGFC*	

Table 4.3. OA and cartilage related genes were identified following IL-1 stimulation and HDAC3 selective inhibition using Apicidin.

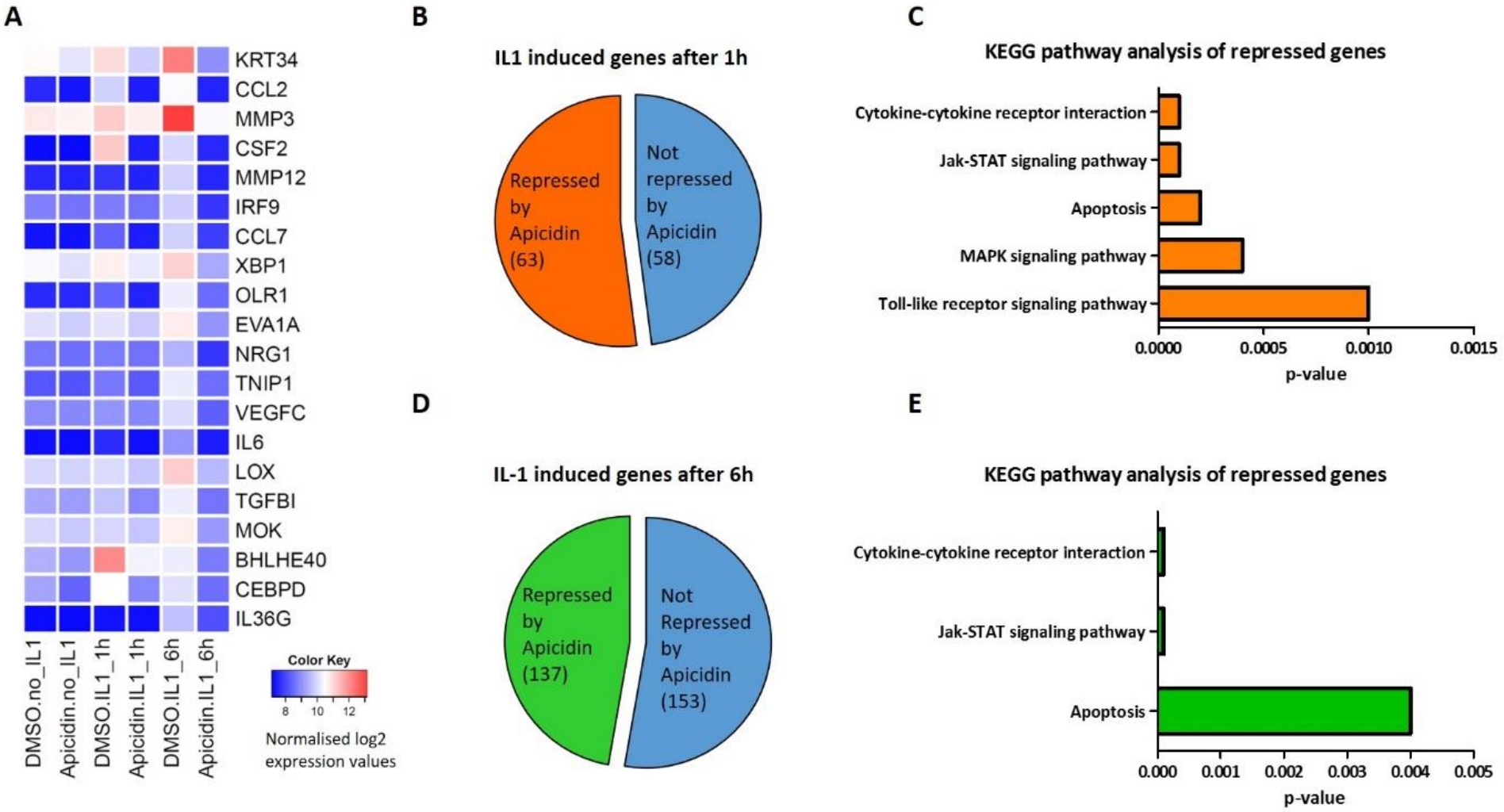
A
KRT34
CCL2
MMP3
CSF2
MMP12
IRF9
CCL7
XBP1
OLR1
EVA1A
NRG1
TNIP1
VEGFC
IL6
LOX
TGFBI
MOK
BHLHE40
CEBPD
IL36G
DMSO.no_IL1
Apicidin.no_IL1
DMSO.IL1_1h
Apicidin.IL1_1h
DMSO.IL1_6h
Apicidin.IL1_6h
Color Key
8 10 12
Normalised log2 expression values
B
IL1 induced genes after 1h
Repressed by Apicidin (63)
Not repressed by Apicidin (58)
C
KEGG pathway analysis of repressed genes
Cytokine-cytokine receptor interaction
Jak-STAT signaling pathway
Apoptosis
MAPK signaling pathway
Toll-like receptor signaling pathway
0.0000 0.0005 0.0010 0.0015
p-value
D
IL-1 induced genes after 6h
Repressed by Apicidin (137)
Not Repressed by Apicidin (153)
E
KEGG pathway analysis of repressed genes
Cytokine-cytokine receptor interaction
Jak-STAT signaling pathway
Apoptosis
0.000 0.001 0.002 0.003 0.004 0.005
p-value

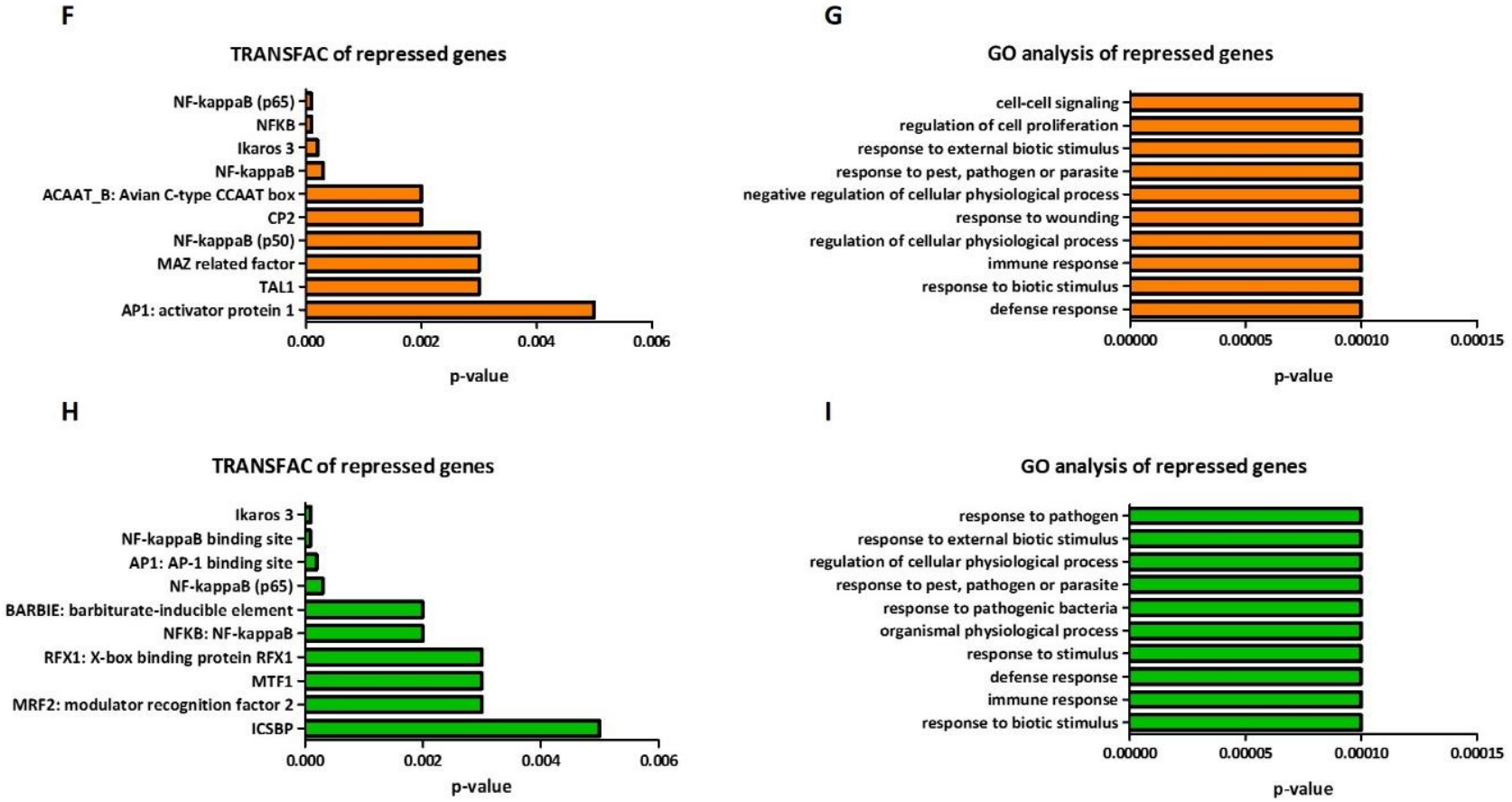

Figure 4.9. Gene expression profiling following IL-1α (0.5ng/ml) stimulation and Apicidin (160nM) treatment in SW1353 cells.

A. Top 20 genes induced by IL-1 after 6 hours and repressed by Apicidin. **B, D.** Size-dependent pie charts of genes induced by IL-1 (**B**) after 1 hour or (**D**) 6 hours and repressed by Apicidin. **C.** KEGG pathway analysis of the IL-1 induced (1 hour) and Apicidin- repressed genes. **E.** KEGG pathway analysis of the IL-1 induced (6 hours) and Apicidin- repressed genes. **F, G.** TRANSFAC and GO analysis of the IL-1 induced (1 hour) and Apicidin- repressed genes. **H, I.** TRANSFAC and GO analysis of the IL-1 induced (6 hours) and Apicidin- repressed genes.

4.3.4 Differentially expressed genes following HDAC inhibition and IL-1 stimulation.

In the current study, data obtained from another gene expression array analysis performed by Dr Matthew Barter (Newcastle University, Newcastle, UK) was taken into account. In this microarray SW1353 cells were treated with 756nM (250ng/ml) of the pan-HDACi TSA for 30 minutes before IL-1 stimulation for 6 hours followed. RNA extraction and microarray analysis were then performed as previously described (see section **2.2.19**). The results obtained from this microarray were compared to the data obtained from the Apicidin treated cells basally (no IL-1) (**Figure 4.10**) and following 6 hours of IL-1 stimulation (**Figure 4.11**). The lists of induced and repressed by both HDACi genes with/without IL-1 stimulation were subjected to GO, KEGG pathway and TRANSFAC analysis using the same cut off of ± 1.5 fold change as before.

In the basal level (no IL-1), 231genes were induced only by TSA-mediated HDAC inhibition and 35 genes were induced only by Apicidin (**Figure 4.10 A**). Between the two treatments 13 genes were induced in common and these were associated significantly with three pathways, including methionine metabolism (p-value= 0.0002), aminoacyl-tRNA biosynthesis (p-value= 0.0003) and selenoamino acid metabolism (p-value= 0.0003). The most significant identified GOs included methionyl-tRNA aminoacetylation (p-value= 0.0003), negative regulation of cyclin dependent protein kinase activity (p-value= 0.0009), odontogenesis (p-value= 0.002), bone mineralization/ remodelling (p-value= 0.003) and ossification (p-value= 0.008). TRANSFAC analysis indicated enrichment for E2F, Pax3, Nuclear factor Y-binding box, ELF1, SMAD4 and Ras-responsive binding element transcription factors.

Furthermore, 141 genes were repressed only by TSA and 27 genes only by Apicidin when no IL-1 stimulation was performed. Seven genes were decreased by both HDACi and these were also subjected to GO (**Figure 4.10 C**), TRANSFAC (**Figure 4.10 D**) and KEGG pathway analysis (**Figure 4.10 E**). GO analysis predicted B-cell differentiation and activation, lymphocyte differentiation/ activation, haemopoiesis, immune cell activation and cell growth, while Wnt signalling and focal adhesion pathways are predicted following KEGG analysis. Both of these pathways have been previously associated with osteoarthritis and rheumatoid arthritis. (Corr 2008; Shahrara et al. 2007; Prasadam et al. 2013; Luyten et al. 2009)

Following IL-1 stimulation, 23 genes were further induced by TSA and 141 by Apicidin, while 12 genes were in common between the two treatments (**Figure 4.11 A**). The top 4 GO terms predicted were linked to mating/reproductive behaviour (p-value< 0.001) and the next terms were associated with regulation of viral genome replication, immune response and

regulation of apoptosis (all had p-value< 0.01). Cytokine- cytokine receptor interaction (p-value= 0.001), Toll-like receptor signalling pathway (p-value= 0.005) and tight junction (p-value= 0.006) were among the pathways affected by these 12 genes, whereas the most prevalent transcription factor identified was NF-κB (p-value <0.0001).

Interestingly, of the 85 repressed by TSA and the 110 by Apicidin, 27 genes were no further induced in the presence of both HDACi. Except for the GO terms immune response, response to biotic stimulus and response to wounding and inflammatory response, which were previously described in the Apicidin section, collagen catabolism is a newly predicted biological function in the GO analysis (**Figure 4.11 C**), fortifying the involvement of HDACs in regulating critical for this process enzymes. With reference to the pathway analysis (**Figure 4.11 E**), the results were similar to the inducible genes that were no longer induced by Apicidin (**Figure 4.9 E**) and contained cytokine-cytokine interaction, apoptosis, Toll-like receptor and JAK-STAT signalling pathways. These results suggest that HDAC3 may act through specific signalling pathways and by associating with specific transcription factors controls important gene expression programs in chondrocytes. As far as the TRANSFAC analysis is concerned interferon regulatory transcription factors come at the top of the list with ICSBP first and IRF second (**Figure 4.11 D**). NF-κB and AP-1 binding motifs are also predicted, but for the first time the no longer induced by both HDACi genes are predicted to be enriched for E2F and E2F-1 transcription factor binding sites.

The Open Targets platform predicts the OA/cartilage related genes among the lists of repressed genes in the basal and IL-1 induced level as shown in **Table 4.4**.

TSA and Apicidin repressed genes (no IL-1, 1 out of 7 from Figure 4.10 A)	IL-1 (for 6 hours) -induced and repressed by TSA & Apicidin (10 out of 27 from Figure 4.11 A)
KLF6	*CCL8*
	CSF2
	IFIH1
	IL1B
	IL24
	IL6
	LTB
	MMP1
	MMP12
	MMP3

Table 4.4. OA and cartilage related genes were identified following HDAC inhibition with TSA or Apicidin in the presence or absence of IL-1 stimulation.

A

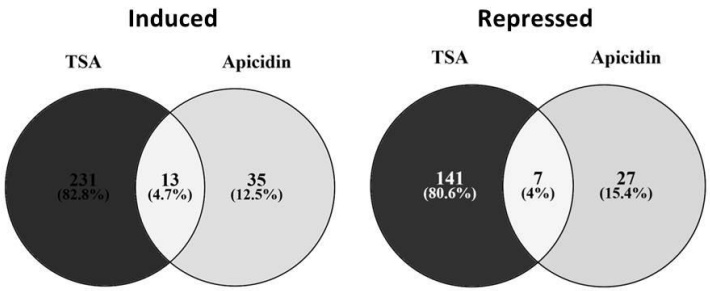
No IL-1
Induced
TSA
Apicidin
231
(82.8%)
13
(4.7%)
35
(12.5%)
Repressed
TSA
Apicidin
141
(80.6%)
7
(4%)
27
(15.4%)

B

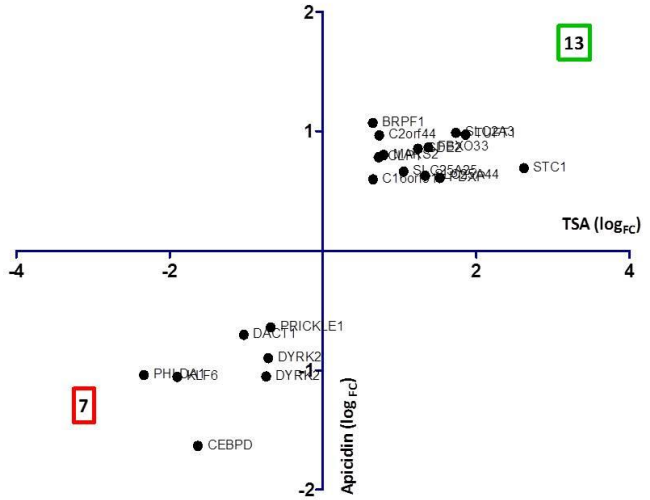
Genes induced or repressed by HDACi
13
7
BRPF1
C2orf44
STC1
PRICKLE1
DACT1
DYRK2
DYRK1
CEBPD
TSA (log FC)
Apicidin (log FC)
2
1
-1
-2
-4
-2
2
4

C

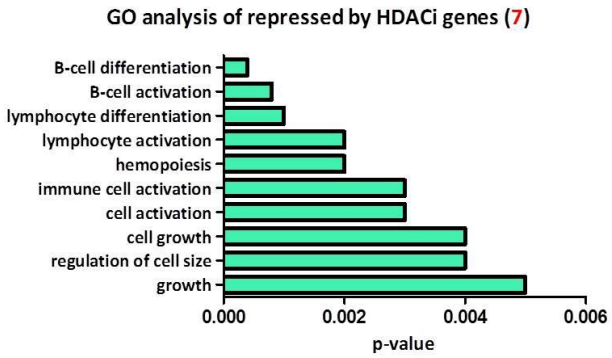
GO analysis of repressed by HDACi genes (7)
B-cell differentiation
B-cell activation
lymphocyte differentiation
lymphocyte activation
hemopoiesis
immune cell activation
cell activation
cell growth
regulation of cell size
growth
0.000
0.002
0.004
0.006
p-value

D

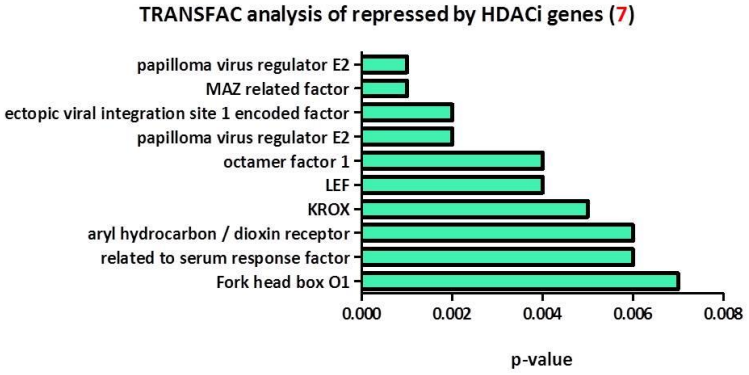
TRANSFAC analysis of repressed by HDACi genes (7)
papilloma virus regulator E2
MAZ related factor
ectopic viral integration site 1 encoded factor
papilloma virus regulator E2
octamer factor 1
LEF
KROX
aryl hydrocarbon / dioxin receptor
related to serum response factor
Fork head box O1
0.000
0.002
0.004
0.006
0.008
p-value

E

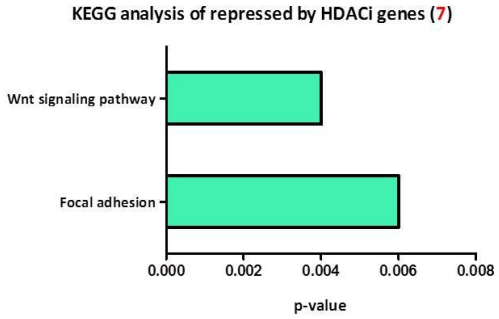
KEGG analysis of repressed by HDACi genes (7)
Wnt signaling pathway
Focal adhesion
0.000
0.002
0.004
0.006
0.008
p-value

Figure 4.10. Differentially expressed genes following TSA (756nM) or Apicidin (160nM) treatment in SW1353 cells.

A. Venn diagrams of genes induced or repressed by the HDACi. **B.** X-Y scatter plot of the total number of induced or repressed by the HDACi genes. **C.** Top 10 gene ontology (GO) analysis of the repressed genes. **D.** Top 10 TRANSFAC analysis of the repressed genes and **E.** KEGG pathway analysis of the repressed genes were performed using GATHER.

A

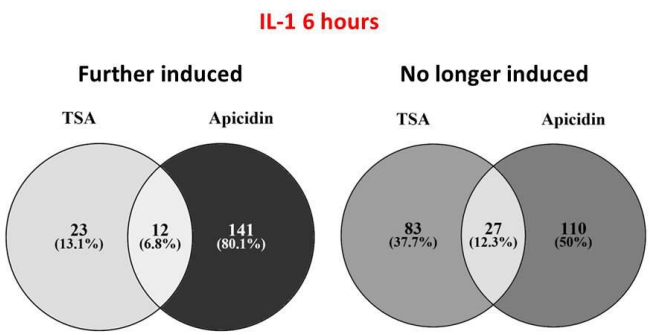
IL-1 6 hours
Further induced
No longer induced
TSA
Apicidin
TSA
Apicidin
23
(13.1%)
12
(6.8%)
141
(80.1%)
83
(37.7%)
27
(12.3%)
110
(50%)

B

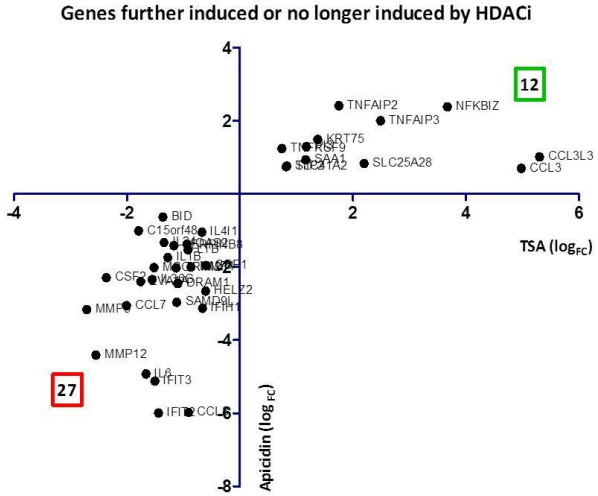
Genes further induced or no longer induced by HDACi
12
27
TNFAIP2
NFKBIZ
TNFAIP3
KRT75
RSF9
SAA1
SLC25A28
CCL3L3
CCL3
BID
C15orf48
IL4I1
IL1B
CSF2
BRAM1
HELZ2
SAMD9L
MMP9
CCL7
MMP12
IL6
TFIT3
TSA (log FC)
Apicidin (log FC)

C

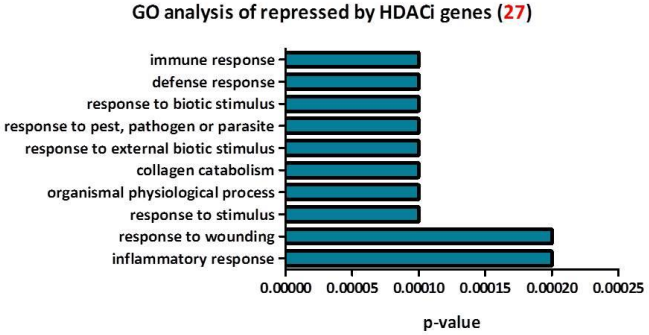
GO analysis of repressed by HDACi genes (27)
immune response
defense response
response to biotic stimulus
response to pest, pathogen or parasite
response to external biotic stimulus
collagen catabolism
organismal physiological process
response to stimulus
response to wounding
inflammatory response
0.00000
0.00005
0.00010
0.00015
0.00020
0.00025
p-value

D

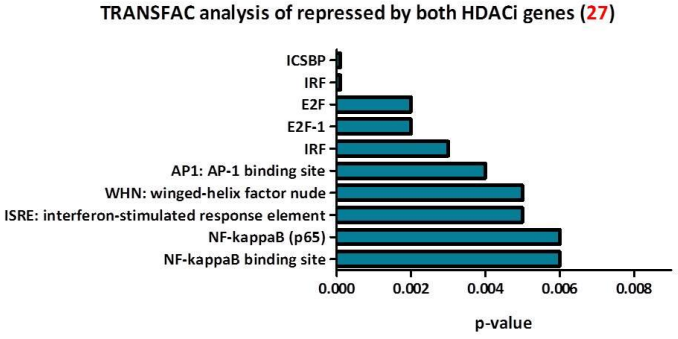
TRANSFAC analysis of repressed by both HDACi genes (27)
ICSBP
IRF
E2F
E2F-1
IRF
AP1: AP-1 binding site
WHN: winged-helix factor nude
ISRE: interferon-stimulated response element
NF-kappaB (p65)
NF-kappaB binding site
0.000
0.002
0.004
0.006
0.008
p-value

E

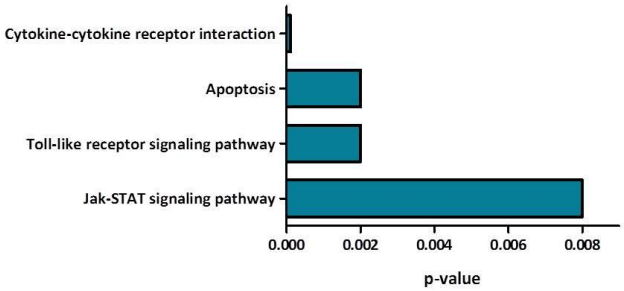
KEGG analysis of repressed by both HDACi genes (27)
Cytokine-cytokine receptor interaction
Apoptosis
Toll-like receptor signaling pathway
Jak-STAT signaling pathway
0.000
0.002
0.004
0.006
0.008
p-value

Figure 4.11. Differentially expressed genes following IL-1α (0.5ng/ml) stimulation for 6 hours and TSA (756nM) or Apicidin (160nM) treatment in SW1353 cells.

A. Venn diagrams of IL-1 induced genes and further induced or repressed by the HDACi genes. **B.** X-Y scatter plot of the total number of induced or repressed by the HDACi genes. **C.** Top 10 gene ontology (GO) analysis of the IL-1 induced and further repressed genes. **D.** Top 10 TRANSFAC analysis of the IL-1 induced and further repressed genes and E. KEGG pathway analysis of the IL-1 induced and further repressed genes were performed using GATHER.

4.3.5 Differentially expressed genes following RNA interference for HDAC3 and IL-1 stimulation.

To further improve our understanding of the role that HDAC3 plays in chondrocytes we specifically depleted HDAC3 using RNA interference in the SW1353 chondrosarcoma cells. At the basal level, 118 genes were down-regulated following gene depletion, with HDAC3 being at the top of this list (log_{FC} = - 2.0667, p-value<0.0001). Regulation of the cell cycle, UDP- glucose metabolism, isoprenoid biosynthesis and metabolism, mitosis checkpoint, co-enzyme metabolism and nucleotide-sugar metabolism are some of the predicted gene ontology annotations of the repressed by the siHDAC3 genes. Interestingly, these genes are enriched mainly for E2F-1 transcription factor binding sites; the same factor came up four times in the list of the top ten predicted factors (see **Appendix B** for list of transcription factors predicted). Moreover, cell cycle, isoprenoid biosynthesis and nucleotide sugars metabolism are the pathways associated with the repressed gene list. However, 28 genes were significantly induced following HDAC3 depletion. These genes were mainly associated with muscle development and maintenance, myelination, ionic insulation of neurons, nerve maturation and organ development. In terms of pathways, coagulation cascades and focal adhesion were predicted.

However, following IL-1 stimulation and *HDAC3* gene depletion only a small number of genes are no longer induced, with most of them being significantly up-regulated. In particular, after 1 hour of IL-1 stimulation only 2 inducible genes are suppressed by the siHDAC3 (**Figure 4.12 B**). These genes included the *CSF2* and *HMGCS1*. CSF2 is a cytokine which controls production and differentiation of granulocytes and macrophages, while HMGCS1 is involved in the regulation of cholesterol biosynthesis. *HMGCS1* gene expression has been shown to depend on HDAC3 to regulate cholesterol or fatty acid biosynthesis (Bhaskara et al. 2011). Both *CSF2* and *HMGCS1* were recently found to be upregulated in a different microarray analysis performed in two prostate cancer cell lines, after HDAC inhibition (Lin et al. 2016). Interestingly, 151 genes were repressed by the siHDAC3, but not induced by IL-1 stimulation. When these genes were analysed for TRANSFAC, E2F-1 came up four times in the top 10 list of transcription factors predicted by GATHER with a p-value <0.0001 (see **Appendix B**).

Following 6 hours of IL-1 induction 29 IL-1-induced genes are no longer induced by the siHDAC3 (**Figure 4.12 C**). A heatmap (**Figure 4.12 A**) shows the top 20 induced and most repressed by siHDAC3 genes after 6 hours of IL-1 stimulation and their expression in the basal level at 1 hour of IL-1 is also shown as a comparison. Cytokine-cytokine receptor

interaction and JAK-STAT signalling pathway were predicted following analysis of the no longer induced genes at the IL-1- 6 hours timepoint. Moreover, Toll-like signalling pathway, C21 steroid hormone metabolism and nucleotide sugars metabolism are associated with the IL-1-6 hours induced and siHDAC3 repressed genes (**Figure 4.12 E**), while HDAC3 role in inflammatory response and cell-cell signalling is also manifested after 6 hours of cytokine stimulation. The no longer induced by siHDAC3 genes appear to negatively regulate cellular physiological processes and are enriched for ISRE (Interferon Stimulated Response Element) and E2F-1 binding sites (**Figure 4.12 D**). Interestingly, previous reports support a role of the ISRE in immune-regulation by Toll-like receptors and other pattern recognition receptors (Honda & Taniguchi 2006). Additionally, 239 genes were repressed by the siHDAC3, but not induced by IL-1 stimulation and TRANSFAC analysis suggests these genes are enriched for E2F-1 transcription factor binding sites, similarly to the genes repressed by siHDAC3 at 1 hour of IL-1 and at the basal (no IL-1) level (see **Appendix B**). The OA/ cartilage related genes are shown in **Table 4.5**.

Nevertheless, 71 genes were further significantly upregulated following IL-1 induction (6 hours) and siHDAC3 treatment. Organogenesis, phosphate transport, fatty-acid beta oxidation, muscle contraction and development are among the GO predicted terms with p-values <0.01. KEGG pathway analysis identified TGF-β signaling pathway (p-value= 0.003), ECM receptor interaction (p-value= 0.003), focal adhesion (p-value= 0.003) and cell cycle (p-value= 0.004) to be accompanied with the induced gene list. Finally, the most common transcription factor identified was serum response factor (p-value= 0.007).

IL-1 (for 1 hour) -induced and repressed by siHDAC3 genes (1 out of 2 from Figure 4.12 B)	**IL-1 (for 6 hours) -induced and repressed by siHDAC3 (14 out of 29 from Figure 4.12 C)**	
CSF2	*CCL2*	*SERPINB2*
	CCL8	*STAT1*
	CSF2	*TNFAIP6*
	CXCL10	*UGDH*
	CXCL8	
	IFIT1	
	IL11	
	IL1B	
	IL6	
	MMP12	

Table 4.5. OA and cartilage related genes were identified following IL-1 stimulation and *HDAC3* gene depletion.

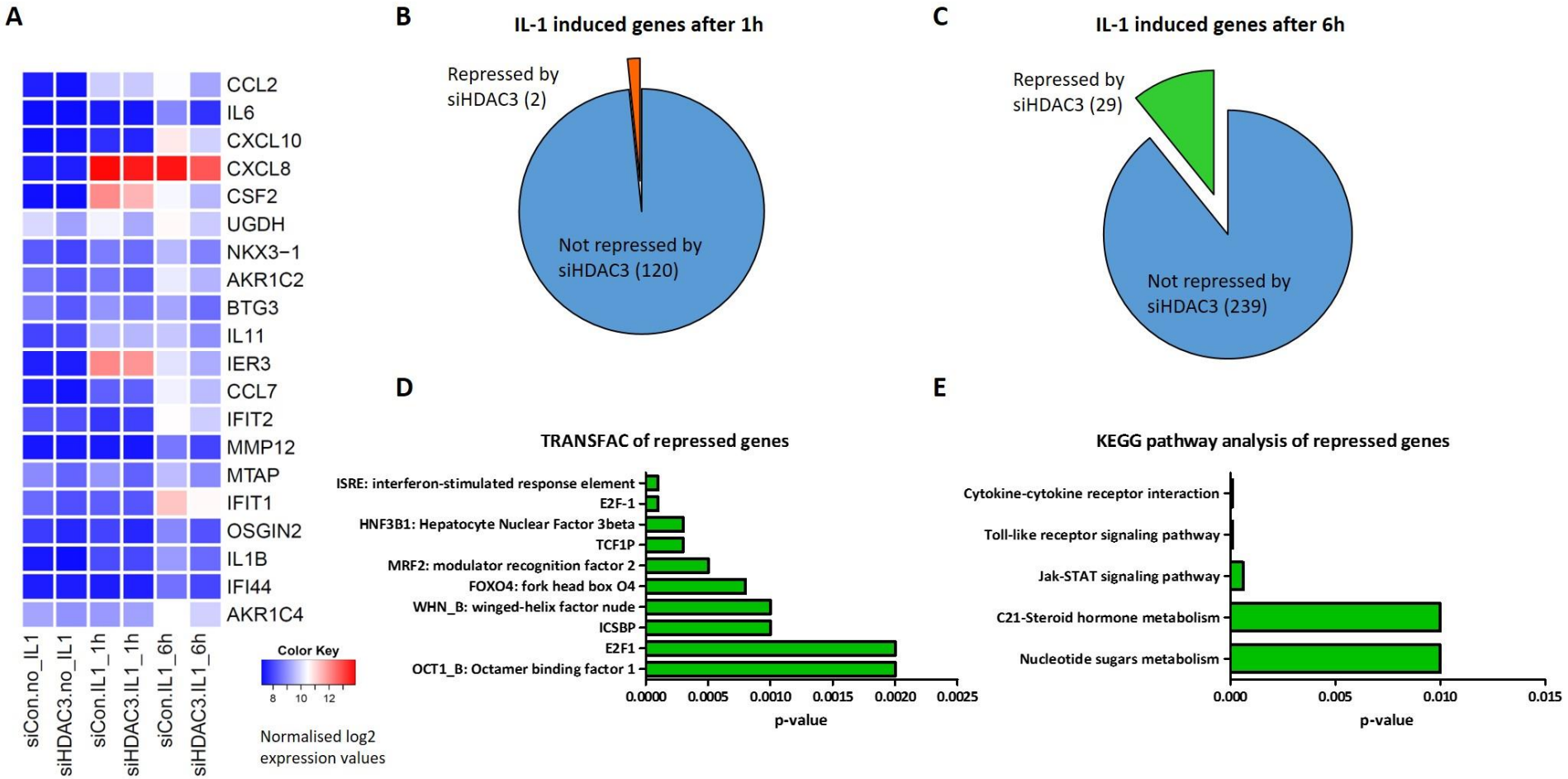
A
CCL2
IL6
CXCL10
CXCL8
CSF2
UGDH
NKX3−1
AKR1C2
BTG3
IL11
IER3
CCL7
IFIT2
MMP12
MTAP
IFIT1
OSGIN2
IL1B
IFI44
AKR1C4
siCon.no_IL1
siHDAC3.no_IL1
siCon.IL1_1h
siHDAC3.IL1_1h
siCon.IL1_6h
siHDAC3.IL1_6h
Color Key
8 10 12
Normalised log2 expression values
B
IL-1 induced genes after 1h
Repressed by siHDAC3 (2)
Not repressed by siHDAC3 (120)
C
IL-1 induced genes after 6h
Repressed by siHDAC3 (29)
Not repressed by siHDAC3 (239)
D
TRANSFAC of repressed genes
ISRE: interferon-stimulated response element
E2F-1
HNF3B1: Hepatocyte Nuclear Factor 3beta
TCF1P
MRF2: modulator recognition factor 2
FOXO4: fork head box O4
WHN_B: winged-helix factor nude
ICSBP
E2F1
OCT1_B: Octamer binding factor 1
0.0000 0.0005 0.0010 0.0015 0.0020 0.0025
p-value
E
KEGG pathway analysis of repressed genes
Cytokine-cytokine receptor interaction
Toll-like receptor signaling pathway
Jak-STAT signaling pathway
C21-Steroid hormone metabolism
Nucleotide sugars metabolism
0.000 0.005 0.010 0.015
p-value

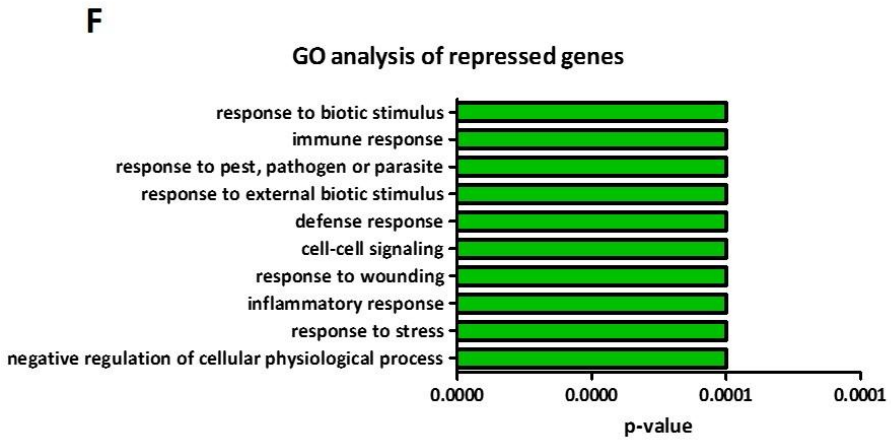

Figure 4.12. Gene expression profiling following IL-1α (0.5ng/ml) stimulation and RNAi (50nM) for HDAC3 in SW1353 cells.

A. Top 20 genes induced by IL-1 after 6 hours and further repressed by the siHDAC3. **B, C**. Size-dependent pie charts of the genes induced by IL-1 after 1 hour (**B**) or 6 hours (**C**) and further repressed by the siHDAC3. **D.** TRANSFAC analysis of the IL-1-induced and further repressed by siHDAC3 genes at 6 hours of IL-1 stimulation. **E.** KEGG pathway analysis IL-1-induced and further repressed by siHDAC3 genes at 6 hours of IL-1 stimulation. **F.** GO analysis of the IL-1-induced and further repressed by siHDAC3 genes at 6 hours of IL-1 stimulation.

4.3.6 Genes repressed by HDAC3 selective inhibition and gene depletion following 1 hour of IL-1 stimulation.

By comparing the genes repressed by the selective HDAC3 inhibitor Apicidin or the siRNA after 1 hour of cytokine IL-1 induction only one gene was identified to be suppressed by both. This gene was CSF2 (Colony stimulating factor 2), a cytokine that stimulates the growth and differentiation of haematopoietic precursor cells from various lineages, including granulocytes, macrophages, eosinophils and erythrocytes. The active form of this gene is found extracellularly as a homodimer. It has been localised to a cluster of related genes at chromosome region 5q31 which is known to be associated with interstitial deletions in the 5q syndrome and acute myelogenous leukaemia. Other genes in the cluster include those encoding for interleukins 4, 5 and 13 and thus pathway analysis predicts a role for JAK-STAT signalling pathway and for cytokine-cytokine receptor interaction. (Hamilton 2008) Active repression of this gene is linked to cellular defence response, response to wounding, immune response and response to biotic stimulus, as well as cell surface receptor linked signal transduction and development. (https://www.ncbi.nlm.nih.gov/gene/1437)

4.3.7 Genes repressed by HDAC3 selective inhibition and gene depletion following 6 hours of IL-1 stimulation.

Next, the genes repressed by the siHDAC3 depletion and the Apicidin inhibition, following IL-1 stimulation for 6 hours were examined (**Figure 4.13**). 13 genes were identified to no longer be induced by both treatments (**Figure 4.13 A**). KEGG pathway analysis showed three pathways were significantly associated with the repressed genes including cytokine-cytokine receptor interaction, JAK-STAT signalling pathway and Toll-like receptor signalling pathway (**Figure 4.13 B**). Most of the GO annotations have been predicted before and these include response to stimulus, immune/inflammatory response and cell-cell signalling (**Figure 4.13 D**).

Using TRANSFAC the 13 IL-1 repressed genes were enriched for E2F-1 transcription factor binding site as shown in **Figure 4.13 C** (in red boxes). By using a less stringent cut off (fold change < 0), all the genes that were significantly downregulated by both treatments were taken into account and analysed for transcriptional regulators using Ingenuity Pathway Analysis (IPA) software. In total 200 genes showed induction after IL-1 and decreased expression following siHDAC3 or Apicidin treatment and upstream transcriptional regulators analysis by IPA supports there is role for E2F-1 transcription factor (p-value $=7.37 \times 10^{-10}$) for the observed expression changes. The E2F-1 network with predicted transcription factors can be seen in **Figure 4.13 E**. The OA/cartilage related genes were identified as before and are presented in **Table 4.6**.

These findings suggest a possible common mechanism regulating the IL-1 induced and siHDAC3/ Apicidin repressed genes and E2F-1 transcription factor may play a key role in this process.

IL-1 (for 1 hour) - induced and repressed by Apicidin and siHDAC3 genes	IL-1 (for 6 hours) - induced and repressed by Apicidin and siHDAC3 (9 out of 13 from Figure 4.13 A)	All significantly induced by IL-1 and repressed by Apicidin and siHDAC3 genes (36 out of 200 that were subjected to IPA)			
CSF2	*CCL2*	*CCL2*	*IFIH1*	*LIF*	*SERPINB2*
	CCL8	*CCL8*	*IFIT1*	*LMNB1*	*SERPINE1*
	CSF2	*CCNA2*	*IL11*	*MGLL*	*TNFAIP6*
	IL11	*CDK4*	*IL1B*	*MMP1*	*TTK*
	IL1B	*CSF2*	*IL24*	*MMP12*	*TUBA1A*
	IL6	*DIO2*	*IL6*	*MMP13*	*TUBB4B*
	MMP12	*FAM46A*	*IRF1*	*OLR1*	*XBP1*
	SERPINB2	*FGF2*	*KLF6*	*RPL29*	*ZC3HAV1*
	TNFAIP6	*HMGB2*	*KRT75*	*RRM2*	*SERPINB2*

Table 4.6. OA and cartilage related genes were identified following IL-1 stimulation and HDAC3 inhibtion or gene depletion.

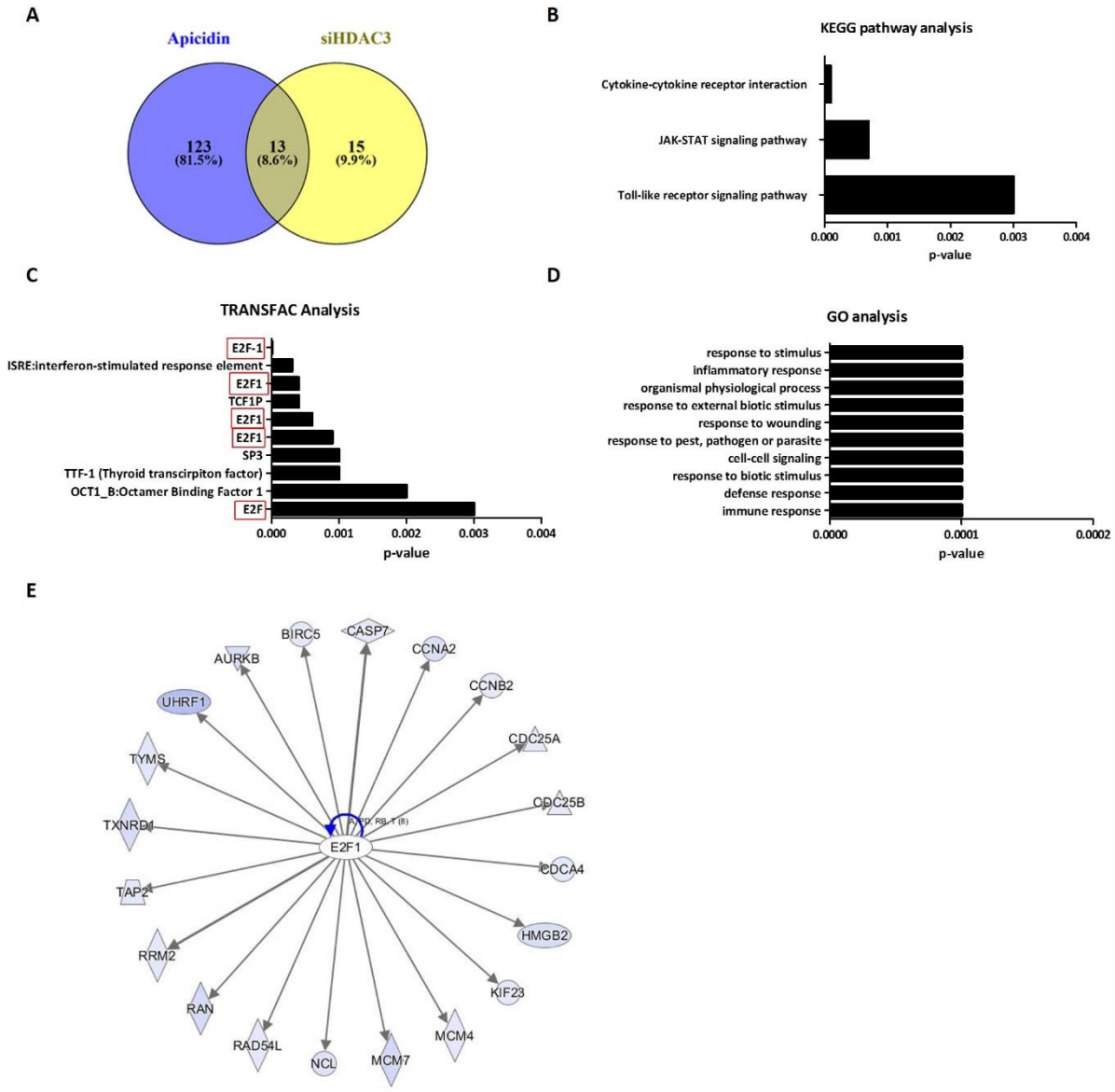

Figure 4.13. Genes induced by IL-1α (0.5ng/ml) after 6 hours of stimulation and repressed by Apicidin (160nM) treatment or siHDAC3 (50nM) gene knockdown.

A. Venn diagrams of the genes induced by IL-1 after 6 hours and repressed by the siHDAC3 or by Apicidin (13). **B.** KEGG pathway analysis, **C.** TRANSFAC analysis and **D.** GO analysis of the 13 repressed genes **E.** IPA upstream transcription regulator analysis of the genes induced by IL-1 and repressed by siHDAC3 or Apicidin (200 genes) identified E2F-1 as one of the potential transcription factors important for regulating expression of the repressed genes.

4.4 Discussion

Several studies have used HDAC3- deficient cells to compare gene expression changes targeting a specific gene set in the heart (Montgomery et al. 2008), liver (Sun et al. 2013) or skeleton (Razidlo et al. 2010). More recent reports suggest that embryonic deletion of HDAC3 in type II collagen alpha 1 (Col2α1) expressing chondrocytes is lethal, while postnatal deletion impaired endochondral bone formation, delayed secondary ossification centre formation and altered maturation of the growth plate (Carpio et al. 2016). In the previous chapter, the effect of HDAC3 on IL-1 induced matrix metalloproteinases and IEG genes expression was determined by qRT- PCR. This chapter aimed to comprehensively analyse gene expression changes following *HDAC3* gene depletion or inhibition in the SW1353 chondrosarcoma cell line. First, validation of the RNA used for microarray analysis was performed using qRT- PCR and the data obtained confirmed the results presented in Chapter 3, since both *MMP1* and *MMP13* followed identical expression patterns with significant induction by IL-1 and down-regulation following *HDAC3* knockdown or inhibition. Validation of the expression changes of other genes including *IL-6, IL-8* and *FRA1* using qRT- PCR was also performed and then our microarray data confirmed these expression changes.

4.4.1 Genes and pathways induced by IL-1 stimulation.

In total, 45 and 190 genes were up-regulated with a fold change ≥1.5, following IL-1 stimulation for 1 hour or 6 hours in both the DMSO and siCON treatments respectively. The datasets obtained by the 1 and 6 hours induced gene lists indicated the different gene ontology enrichment, networks and transcription factor binding sites predicted (**Figure 4.7** & **Figure 4.8**). Using GO analysis, cellular physiological processes, transcription factor nuclear import and protein transport appeared to be negatively regulated in the 1 and 6 hour list. Dynamic expression changes of the up-regulated genes showed gene ontology enrichment for NF-κB signaling, in accordance with previous reports (Ohne et al. 2016). As expected upon IL-1 stimulation an immune/ defense response is also predicted as well as a role in the cell cycle.

With regards to the network analysis, apoptosis and Toll-like receptor (TLR) signaling pathways were among the common pathways predicted in both the 1 hour and the 6 hours IL-1-induced genes list. Interestingly, the ability of IL-1β to induce apoptosis has been previously linked to nitric oxide generation (Dunger et al. 1996; Hoorens et al. 2001). However in human articular chondrocytes IL-1β has been shown to have an anti-apoptotic

activity, though NF-κB inhibition partially reversed the anti-apoptotic activity of IL-1, suggesting NF-κB may be part of the protective mechanism (Kuhn et al. 2000). Furthermore, TLRs can be classified into two subfamilies: the cell surface TLRs which recognize microbial cell membrane components and the intracellular TLRs which recognize nucleic acids from bacteria, viruses or self-nucleic acids in the case of auto-immunity. Toll- like receptors signals through the recruitment of specific ligands leading to the activation of NF-κB and MAPKs for the induction of inflammatory cytokine genes and IRFs which dictates innate immune responses. (Kawasaki & Kawai 2014) Cytokine-cytokine receptor interactions and JAK-STAT signaling pathways were only predicted in the 6 hour gene list while focal adhesion appeared in the 1 hour list.

In terms of the TRANSFAC analysis of the IL-1 induced genes, as expected NF-κB (p50/ p65) appear to be the main binding motifs together with AP-1 sites. NF-κB p50/ p65 can induce the expression of target genes including Interferon regulatory factor 1 (*IRF1*), heme oxygenase 1, nitric oxide synthase 2A (*iNOS*), coagulation factor III (*F3*), and proinflammatory cytokines such as *TNF-α*, *IL-6* and *IL-8* (Oeckinghaus & Ghosh 2009). Interestingly, AP-1 comes at the top of the list after only 1 hour of cytokine stimulation, confirming the immediate induction of these genes (Tullai et al. 2007). This is particularly interesting since *MMP1* and *MMP13* (and most other MMPs) gene promoters contain multiple AP-1 binding sites that may contribute to gene expression (Tullai et al. 2007; Vincenti & Brinckerhoff 2002) and a recent study has implied a role of ATF3 IEG on regulating *MMP13* expression in HACs (Chan et al. 2017).

4.4.2 Correlation of genes induced by IL-1 and repressed by HDACi.

An identification of the induced and repressed by Apicidin genes with/ without IL-1 followed. At the basal level, 43 genes were repressed by Apicidin, while 52 genes were induced. Most of the repressed genes were associated with having a role in regulation of transcription and metabolism, organogenesis and mesoderm development and two pathways important for normal growth and development were predicted following KEGG pathway analysis. The TGF-β and Wnt signalling pathways. With reference to the 52 induced genes, these were associated with protein-nucleus import, negative regulation of cyclin dependent phosphorylation, negative regulation of transcription. KEGG pathway analysis identified methionine metabolism and Notch signalling pathway. Transcription factor binding sites predicted for the induced gene list included X-box binding protein RFX1, ATF3, PAX5 and

KROX transcription factors. Of particular interest here is ATF3 transcription factor, which was shown to be necessary for activating transcription of *MMP13* in human articular chondrocytes. *ATF3* expression is AP-1 (cFOS/cJUN) dependent and can bind to the AP-1 binding motif of the proximal *MMP13* promoter of cytokine-induced (IL-1 +OSM) chondrocytes at time points that no longer support cFOS binding, indicating its importance in regulating *MMP13* expression (Chun et al. 2017). Also increased expression of ATF3 was found in synovial membranes from OA patients. (Zhang et al. 2016) Conditional deletion of Atf3 did not impair normal skeletogenesis or affect chondrogenesis, but alleviated the OA generated by surgically induced knee joint instability in mice. Moreover, IL-1 cytokine induction was found to induce expression of *ATF3* through NF-κB pathway in Atf3- deleted mice and human chondrocytes. (Iezaki et al. 2016)

In total, 121 genes were significantly induced after 1 hour and 290 after 6 hours of cytokine induction with around 50% of these genes being significantly down-regulated in each time-point. Interestingly, *MMP3* and *MMP12* are present in the top 20 IL-1 induced and Apicidin repressed gene list (**Figure 4.9**). In accordance to these results, it has been previously reported that in SW1353 chondrosarcoma cells, the majority of metalloproteinase genes that were robustly induced by IL-1+ OSM combination, were then repressed by HDACi including: *MMP1*, *MMP3*, *MMP7*, *MMP8*, *MMP10*, *MMP12*, *MMP13* and *ADAMTS9* (Young et al. 2005). MMPs were evolved from a single-domain protein which underwent successive rounds of duplication, gene fusion and exon shuffling events to generate the current functional diversity exhibited by MMPs and hence share the same regulatory elements. (Fanzul-Fernadez et al. 2010) The most obvious shared motif among inducible MMPs is an AP-1 site in the proximal promoter (Rowan and Young, 2007). However, it is probable that the effect of HDACi is on signalling pathways induced by these pro-inflammatory cytokines rather than on the MMP gene promoters themselves.

The molecular network analysis identified three pathways in common following 1 or 6 hours of IL-1 stimulation and these involved cytokine-cytokine receptor interaction, the JAK-STAT signaling pathway and cell apoptosis. These pathways were expected to be induced by cytokine stimulation and these results have been partly confirmed (Zhang et al. 2016). MAPK and Toll-like receptor signaling pathways appeared only in the 1 hour list, suggesting a role for these pathways and their downstream targets early after a cytokine induction.

Of particular relevance, the ERK MAPK pathways have been extensively studied in terms of its relevance in regulating matrix metalloproteinase gene expression (Q. Zhang et al. 2008). Also, the involvement of the ERK1/2 MAPK signalling pathway was demonstrated in

regulating the hypertrophic changes of normal articular cartilage chondrocytes induced by osteoarthritic subchondral osteoblasts. It was shown that osteoarthritic subchondral osteoblasts inhibited p38 phosphorylation and induced ERK1/2 signal phosphorylation in cultured articular cartilage chondrocytes. The ERK1/2 pathway inhibitor PD98059 significantly attenuated the hypertrophic changes induced by conditioned medium from osteoarthritic subchondral osteoblasts, while the p38 inhibitor SB203580 resulted in up-regulation of hypertrophic genes in articular cartilage chondrocytes. (Prasadam et al. 2010) Wang et al. showed that ERK1/2 activation is involved in IL-1 mediated *MMP3*, *MMP13*, type II collagen and aggrecan expression in chondrocytes (Wang et al. 2011). Other studies reported that upregulation of *ADAMTS4*, *ADAMTS5* and many MMPs (including *MMP1*, *MMP3* and *MMP13*) in co-cultures of human articular chondrocytes with osteoarthritic subchondral bone osteoblasts correlated with activation of MAPK-ERK1/2 pathway. (Prasadam et al. 2012) Importantly, Barter et al. (Barter et al. 2010) showed that HDAC3 is required for activation of ERK and PI3K pathways by TGF-β and for subsequent gene target activation, such as *Timp1* and *Adam12*, dependent on ERK signalling. In addition another HDACi, vorinostat was shown to inhibit IL-1 induced ERK1/2 and p38 activation and blocked *MMP1* and *MMP13* expression as well as IL-1 induced NF-κB nuclear translocation. (Zhong et al. 2013)

Toll-like receptor ligands (TLR) have also been implicated in differentially regulating gene expression in chondrocytes. Ligands for TLR6/2 and TLR3 showed the greatest upregulation of MMP1 and MMP13 respectively, although all TLR ligands upregulated these MMPs. These inductions were dependent upon the NF-κB pathway, but were differentially inhibited by various MAPK inhibitors, with MMP13 induction most reliant on the extracellular signal-regulated kinase pathway. (Zhang et al. 2008)

Herein, the molecular functions of the Apicidin repressed genes were also analysed. Gene expression changes following HDAC3 inhibition resulted in a great diversity of biological functions to be affected including immune response and response to stimulus, cell-cell signalling, regulation of cell proliferation and negative regulation of cellular physiological processes. In accordance with these results, gene expression profiling was conducted to identify differential expressed genes in inflamed OA samples and up- and down-regulated genes were identified. Up-regulated genes were involved in inflammatory response, while down-regulated genes were involved in cell cycle. (Dong et al. 2015)

With reference to the TRANSFAC analysis NF-κB binding sites appeared multiple times in the list of down-regulated by Apicidin genes, together with AP-1 sites. ICSBP was also

identified and this constitutes an important regulator of macrophages differentiation and function. IRF-8 together with IRF-1 are involved in the onset of an innate immune response and *MMP9* promoter has been found to be responsive to exogenous IRF-8 expression. (Dror et al. 2007) Other transcription factors identified in the analysis include Ikaros 3 (IKZF1), Maz related factor, CP2, TAL1 and MRF2, yet none of these have been linked to directly binding or regulating matrix modifying enzymes. MTF1 transcription factor was also predicted and has been previously associated with zinc dependent-regulation of catabolic transcription in osteoarthritis (Kim et al. 2014).

In this study, a previous microarray study performed by Dr Matt Barter at Newcastle University was taken into account. This array compared gene expression changes following HDAC inhibition using the TSA HDAC pan-inhibitor with/ without IL-1 stimulation.

In the basal level (no IL-1), 231genes were induced only by TSA-mediated HDAC inhibition and 35 genes were induced only by Apicidin (**Figure 4.10**). Between the two treatments 13 genes were induced by both TSA and Apicidin. These were associated significantly with three pathways, including methionine metabolism, aminoacyl-tRNA biosynthesis and selenoamino acid metabolism. Accordingly, the most significant GO terms identified were methionyl-tRNA aminoacetylation, negative regulation of cyclin dependent protein kinase activity, odontogenesis, bone mineralization/ remodelling and ossification. TRANSFAC analysis indicated enrichment for Pax3, Nuclear factor Y-binding box, ELF1, SMAD4 and Ras-responsive binding element transcription factors.

Furthermore, 141 genes were repressed only by TSA and 27 genes only by Apicidin when no IL-1 stimulation was performed. Seven genes were decreased by both HDACi and these were also subjected to GO (**Figure 4.10 C**), TRANSFAC (**Figure 4.10 D**) and KEGG pathway analysis (**Figure 4.10 E**). Our hypothesis here was that the genes repressed by both TSA pan-HDACi and the selective HDAC3i will be regulated by a common mechanism. GO analysis predicted B-cell differentiation and activation, lymphocyte differentiation/ activation, haemopoiesis, immune cell activation and cell growth, while Wnt signalling and focal adhesion pathways are predicted following KEGG analysis.

Both of these pathways have been previously associated with osteoarthritis and rheumatoid arthritis. (Corr 2008; Shahrara et al. 2007; Prasadam et al. 2013; Luyten et al. 2009) Products of the Wnt- signalling pathway, Frizzled, secreted Frizzled related protein (sFRP), Dickkopf and LDL- receptor related protein gene families have been implicated in the development and maintenance of bone, cartilage and joints. In addition, increased levels of β-catenin have been found in degenerative cartilage, suggesting Wnt signalling might contribute to cartilage loss.

Polymorphisms in sFRP have been associated with an increased susceptibility to the development of OA and higher levels of the Wnt inhibitor Dickkopf-1 was linked to slowed progression of OA. (Corr 2008) Loughlin et al. also found that non-synonymous SNPs in the *FRZB* gene, a Wnt antagonist are associated with hip OA in females. (Loughlin et al. 2004) The association of FRZB with susceptibility for OA was confirmed in a number of other cohorts (Lane et al. 2006; Valdes et al. 2007) including a differential association between hip OA and osteoporosis (Lories et al. 2006). Deactivated focal adhesion kinase pathway was implicated in morphological abnormalities of cytoskeletal structure, focal adhesions, increased apoptosis, altered osteocyte specific gene expression and increased *MMP2* and *MMP9* expression of osteocytes cultured in normal or OA-derived ECMs. (Prasadam et al. 2013)

Comparison between the IL-1 induced and TSA or Apicidin treated samples identified 27 genes were no longer induced in the presence of both HDACis and novel GO annotations were predicted including collagen catabolism (**Figure 4.11**). Indeed, the role of HDACs in regulating the expression of matrix degrading enzymes was indicated when using HDAC inhibitors including TSA and sodium butyrate. Both HDACi reduced cytokine-induced metalloproteinase expression at the mRNA and protein level, in the chondrosarcoma cell line SW1353 and also in primary human articular chondrocytes (HACs). In addition to that, in a bovine nasal cartilage (BNC) explants assay, the same compounds were shown to inhibit cytokine-induced cartilage degradation via the reduction of MMP expression (Young *et al.,* 2005). Moreover, the chondroprotective role of HDAC inhibitors is also supported in *in vivo* models of osteoarthritis (Culley *et al.,* 2013; Chen *et al.,* 2010). With the use of selective HDAC inhibitors, class I HDACs were implicated in the regulation of MMP expression, and RNAi studies introduced HDAC3 as a potentially key regulator of their expression (Culley *et al.,* 2013).

Moreover, the identification of the JAK-STAT signalling pathway in all the IL-1 induced and then HDACi and siHDAC3 repressed gene lists analysed here, was one of the main pathways predicted. While originally it was thought that STAT proteins only translocate to the nucleus upon JAK-mediated phosphorylation and dimerization following cytokine-mediated induction of JAK kinases, other studies have revealed that STATs can exist in the cytoplasm as stable non-phosphorylated dimers without cytokine stimulation (Mitchell & John 2005). However, upon cytokine induction, phosphorylated STATs translocate to the nucleus and together with other transcription factors regulate specific transcriptional programs. It has been proposed that for maximal transcription activation by STATs, chromatin remodelling by histone

acetylases/deacetylases is required. Although the role of HDAC3 is still not clear, cytokine induction of STAT1, STAT2 and STAT5 signalling requires chromatin recruitment of histone deacetylases and HDAC inhibition by TSA, SAHA or butyrate inhibits transcriptional activation by these STAT, IFN-γ induced JAK1 activation, STAT1 phosphorylation, its nuclear translocation and STAT1 dependent gene activation (Klampfer et al. 2004; Rascle et al. 2003). HDACs may also negatively regulate the duration and magnitude of STAT transcriptional activation by the recruitment to the STAT transcriptional complex via the nuclear co-repressor protein, SMRT, which directly associates with the coiled-coil domain of STAT5 (Nakajima et al. 2001).

It has been also shown that HDAC1 is essential for the transcription of interferon-responsive genes, via association with STAT1 and STAT2 activators of transcription and antiviral response is inhibited in the absence of HDAC1 (Nusinzon & Horvath 2003). Gene silencing experiments of HDAC1, HDAC2 and HDAC3 decreased IFN-γ driven gene activation, while over-expression of each one of them enhanced STAT1-dependent transcriptional activity and downstream signalling (Klampfer et al. 2004). Therefore previous findings and our data imply a role for HDAC3 in mediating JAK-STAT signalling, although more experiments are needed to better clarify the role of each HDAC in JAK-STAT signalling pathway and downstream target gene transcription.

Furthermore STAT3 was shown to be acetylated at a specific Lysine in the carboxyl-terminal, Lys^{685}, and HDAC1 could reverse the p300-mediated STAT3 acetylation at this site. Yuan et al. demonstrated that acetylation at Lys^{685} is critical for STAT3 ability to form stable dimers required for cytokine induced-DNA binding and transcriptional regulation, to enhance transcription of cell-growth related genes and to promote cell cycle progression in response to treatment with oncostatin M. (Yuan et al. 2005) STAT3 can be modified by acetylation both *in vitro* and *in vivo* and HDACi results in increased STAT3 nuclear localization. (Wang et al. 2005)

Regarding the TRANSFAC analysis of the IL-1 induced and further HDACi repressed genes, an enrichment for interferon-related transcription factor binding sites such as IRF-8, IRF-1 and ISRE as well as NF-κB and AP-1 were found. The use of HDACi have revealed an essential role for HDACs in the transcription of interferon- responsive genes, since such inhibitors have been shown to repress IFN- stimulated gene expression (Chang et al. 2004; Genin et al. 2003; Sakamoto et al. 2004). In addition to these factors enrichment for E2F family factors and in particular for E2F-1 is also predicted, and this prediction becomes more dominant when comparing the genes repressed by both siHDAC3 and Apicidin.

4.4.3 Correlation of genes induced by IL-1 and repressed by the HDAC3 RNAi.

To further define the molecular pathways and genes of HDAC3- mediated gene expression regulation, RNAi-mediated gene depletion was performed and gene expression changes were identified. Although only a small number of genes were induced by IL-1 at 1 hour and repressed by the siHDAC3, after 6 hours of stimulation approximately 12% of genes were no longer induced in the presence of the siHDAC3 when compared to the control siCON. Many of these genes are immune response-related genes: *CCL2*, *IL-6*, *CXCL10*, *CXCL8*, *CSF2*, *IL-11*, *CCL7*, *IFIT2*, *IFIT1* and *IL-1β*. Interestingly, *MMP12* is present in the top 20 repressed gene list, reinforcing the notion of an HDAC3-mediated mechanism of its gene expression.

Based on the KEGG pathway analysis, cytokine-cytokine receptor interaction and JAK-STAT signalling pathway were predicted following analysis of the siHDAC3 down-regulated genes. Acetylation and deacetylation of the above signalling pathway components makes studying gene expression regulation a complex process. A typical example of this complexity can be given with many inducible MMP genes such as *MMP1*, *MMP3*, *MMP7*, *MMP9*, *MMP10*, *MMP12* and *MMP13* which contain promoter proximal AP1 sites that are key features of their inducibility. In order for c-Jun to activate gene transcription, it requires phosphorylation by the Jun-N-terminal kinase (JNK) at serines 63/73 and threonines 91/93. A model whereby c-Jun phosphorylation mediates dissociation of an inhibitory complex containing HDAC3 has been proposed. Subsequent to this dissociation, c-Jun can then go on to activate target genes. This example made it clear that c-Jun can itself be the target of acetylation, which in turn may lead to altered transcription factor binding to MMP promoters. (Weiss et al. 2003)

Accordingly, TRANSFAC analysis of the siHDAC3 down-regulated genes appeared to be enriched for ISRE and E2F-1 binding sites. Interestingly, previous reports support a role of the ISRE in immune-regulation by Toll-like receptors and other pattern recognition receptors (Honda & Taniguchi 2006). Also, repression of E2F-regulated promoters was shown to be mediated by the Retinoblastoma protein (Rb), which often recruits a histone deacetylase complex (often relying on HDAC1 and HDAC2) (Nicolas et al. 2001).

4.4.4 Comparison of genes induced by IL-1 and repressed by Apicidin and the HDAC3 RNAi.

Finally, a comparison of the induced by IL-1 and repressed by both the HDAC3 selective inhibitor Apicidin and the siRNA for HDAC3 was performed (**Figure 4.13**). Following 6 hours of IL-1 stimulation, 13 previously IL-1 induced genes were identified as being significantly repressed by both treatments. TRANSFAC analysis predicts there are E2F-1 binding motifs on these genes, suggesting that HDAC3-regulated gene expression is potentially mediated through E2F-1 transcription factor. Adding to this hypothesis, an analysis for transcription regulators of all the genes that were significantly down-regulated by both treatments was performed. In total 200 genes were subjected to IPA and E2F-1 regulator was predicted again with a p-value = 7.37×10^{-10}. These results support that there is a common mechanism regulating the IL-1 induced and siHDAC3 or Apicidin repressed genes involving E2F-1 transcription factor.

Brehm et al. (Brehm et al. 1998) and Magnaghi et al. (Magnaghi-Jaulin et al. 1998) were the first to establish that hypophosphorylated Rb binds to the cell cycle regulator E2F and either blocks activation of E2F target genes or actively represses transcription by recruitment of a histone deacetylase. Auwerx's lab showed that Rb can directly interact with HDAC3 to suppress PPARγ (Peroxisome Proliferator-Activated Receptor γ) expression, a nuclear receptor pivotal for adipogenesis. Phosphorylation of Rb or inhibition of HDACs stimulated adipocyte differentiation. (Fajas et al. 2002) Moreover, histone deacetylase inhibition has been investigated on neuronal fate. Boutillier et al. (Boutillier et al. 2003) showed that HDACi TSA induces apoptosis in neurones, partly by activating the pro-apoptotic factor E2F-1. In the same paper, histone acetylation of the *E2F-1* promoter was investigated, but this modification was neither required, nor by itself sufficient, to induce transcription. Activation of transcription might thus occur through acetylation of non-histone proteins binding E2F-1 regulatory element. Nonetheless, others have shown that E2F-1 transcription factor can be acetylated at Lys^{117}, Lys^{120} and Lys^{125}, as well as deacetylated by the Rb-associated HDACs. Acetylation of E2F-1 occurs when it is not bound by Rb. In this Rb-free state acetylated E2F-1 may have three functional consequences: increased DNA binding activity, transactivation potential and protein half-life. It is also possible that acetylated E2F-1 can recognize a subset of promoters distinct from those normally bound by the repressor E2F-1- Rb complex. (Balbas et al. 2000)

A typical example whereby gene transcription is regulated in a complex fashion by a HDAC-Rb-E2F dependent pathway is given by Kimura et al. (Kimura et al. 2003). Herein, they showed that *DNMT1* (DNA Methyltransferase 1) promoter activity was decreased by expression of E2F-1 and Rb and this suppression was reversed in the presence of TSA. Another example is reported by Zhang et al. (Zhang et al. 2003), who showed that *EBP1*-mediated transcriptional repression depends on the presence of an E2F-1 consensus motif to the target core promoter and recruitment of HDAC activity, probably HDAC2. *In vitro* an EBP1 mutant lacking the HDAC binding domain in the C-terminal region failed to inhibit transcription. Most importantly, Johnson et al. (Johnson et al. 2012) suggest E2F transcription factors may play a role in promoting metastasis via regulating matrix metalloproteinase expression and targeting the Rb- E2F pathway is a promising approach for treating metastatic disease.

These reports in conjunction with our microarray data support a novel mechanism by which HDAC3 may co-operate with E2F-1 transcription factor to regulate specific gene expression programmes in chondrocytes. The possible relationship between HDAC3 and E2F-1 was further investigated and the results are presented in the next chapter.

4.5 Conclusions

- In total, 45 and 190 genes were induced following IL-1 stimulation for 1 hour or 6 hours in the control samples. Various GO terms and KEGG pathways were predicted, but most importantly the up-regulated genes were enriched for NF-κB and AP-1 binding sites, as would be anticipated.
- At the basal level (no IL-1), the genes repressed by both TSA and Apicidin were related to B-cell differentiation and activation, lymphocyte differentiation/ activation, haemopoiesis, immune cell activation and cell growth, while Wnt and focal adhesion signalling pathways are predicted following KEGG analysis, both of which have been previously associated with osteoarthritis.
- 13 genes were induced by both TSA and Apicidin treatments (no IL-1).
- Following IL-1 stimulation and HDACi, using either TSA or Apicidin, 27 genes were no longer induced. These were related to immune response and collagen catabolism. Network analysis also predicted cytokine-cytokine receptor interaction, apoptosis, Toll-like receptor signalling pathway and JAK-STAT signalling pathway were affected.
- All the genes repressed by siHDAC3 with/without IL-1 stimulation were enriched for E2F-1 transcription factor binding sites.
- Comparison of the IL-1 induced and siHDAC3 or Apicidin repressed genes are enriched for E2F-1 transcription factor, implying a role for this regulator on HDAC3-mediated gene regulation in chondrocytes.

Chapter 5. Regulation of *MMP1* and *MMP13* expression by HDAC3 involves the E2F-1 transcription factor.

5.1 Introduction

The retinoblastoma tumour suppressor protein, Rb, together with the E2F transcription factors are the main regulators of the mammalian cell cycle (Chen et al. 2009). Rb physically interacts with E2Fs 1-3 to repress their transcriptional activity, via binding to the activation domain and inhibiting nearby enhancer elements (Magnaghi-Jaulin et al. 1998; Brehm et al. 1998). Transcriptional repression by Rb is mediated partly through the recruitment of histone deacetylases and the Rb-associated histone deacetylase complex contains the RbAp48 protein, which directly interacts with HDAC1 and HDAC2 (Nicolas et al. 2001). However, Rb is inactivated in the G1 phase of the cell cycle leading to its dissociation from E2Fs 1-3. Hence, E2Fs 1-3 binding to DNA facilitates the expression of various genes that are necessary for DNA synthesis and cell cycle progression, including cyclin E, dihydrofolate reductase and DNA polymerase α. Not surprisingly mutations of the Rb-E2F pathway have been identified in human cancers, such as small cell lung carcinoma and osteosarcoma, indicating a major role for this pathway in cell cycle progression and oncogenesis. (Classon & Harlow 2002)

E2Fs are also important for proper execution of development, differentiation, apoptosis and DNA damage repair programmes (Attwooll et al. 2004; Singh et al. 2010). Interestingly, the different E2F family members show overlapping functions especially in the control of cell cycle progression, but also unique functions during development, tissue homeostasis and tumour formation. Earlier studies had shown that all 23 human MMP genes have potential E2F binding sites in their promoters and some, such as *MMP9*, *MMP14* and *MMP15* have multiple E2F binding sites and are regulated by the Rb-E2F pathway. In addition, ChIP assays and RNAi experiments supported that E2F-1 can associate with *MMP9*, *MMP14* and *MMP15* promoters and the genes are E2F responsive. (Johnson et al. 2012)

Moreover, gene expression arrays suggest that E2F-1 may also regulate cellular functions in addition to cell cycle, such as pathways involved in apoptosis, signal transduction, transcriptional control and membrane biology. Most surprisingly, E2F-1 expression repressed a number of genes, including *MMP5*, *MMP14* and *ADAMTS1*, suggesting that E2F-1 may have the potential to repress transcription (Ma et al. 2002). E2F-1 importance in regulating MMP expression has been also shown in a small cell lung cancer (SCLC) metastasis study of

a Chinese Han population. Knockdown of E2F-1 reduced *MMP9* and *MMP16* expression, which resulted in the down-regulation of migration and invasion in SCLC. Further study demonstrated that E2F-1 transcriptionally controlled the expression of other transcription factors such as Sp1 and p65, which in turn enhanced *MMP9* promoter activity. (Li et al. 2014)

Gene expression array data presented in the previous chapter revealed genes induced by IL-1 and repressed by HDAC3 inhibition or RNAi are enriched for E2F-1 transcription factor binding sites, implying a role for this transcription factor in mediating HDAC3 gene expression regulation. Herein, the relationship between HDAC3 and E2F-1 was further investigated and the effect on *MMP1* and *MMP13* expression and cell cycle progression determined.

5.2 Aims

- To investigate a possible interaction between HDAC3 and E2F-1 transcription factor.
- To determine the mechanism by which E2F-1 and by interaction with HDAC3 controls *MMP1* and *MMP13* expression in chondrocytes.

5.3 Results

5.3.1 MMP1 and MMP13 promoters have E2F-1 binding sites.

Microarray studies have suggested that *MMP* genes may be E2F responsive (Ma et al. 2002; Stanelle et al. 2002) and the data obtained from our gene expression array showed enrichment for the E2F-1 regulator on genes repressed by the siHDAC3 or Apicidin following IL-1 induction. To examine the possibility of *MMP1* and *MMP13* being regulated by E2F-1, the promoter region 2Kb upstream of the transcription start site (TSS) of both MMPs was analysed using PROMO (Messeguer et al. 2002; Farre et al. 2003). Putative E2F-1 binding sites were observed in both *MMP1* and *MMP13* gene promoters as shown in **Table 5.1**. MMP1 has three and MMP13 has five E2F-1 putative binding sites, upstream of the TSS within the 2Kb region, or downstream of the TSS within 600bp. Because MMP1 and MMP13 are the major collagenases in cartilage and one of the main aims of this study is to identify how HDAC3 regulates gene expression of these and other genes in cartilage, the relation between HDAC3/E2F-1 and the effect on MMP gene expression regulation were further studied.

Promoter	Number of E2F-1 binding sites	E2F-1 Binding sites relative to TSS	Sequence
MMP1	3	-1666 to -1659 -869 to -862 -751 to -744	TCTGCCGC TACTCCGC GCGGCACA
MMP13	5	-539 to -532 -8 to -1 176 to 183 277 to 284 407 to 414	GCGGTTGT GCGGAAAG GCGGTTGG GCGGGAAT GCGGGGTT

Table 5.1. PROMO analysis of E2F-1 putative binding sites on MMP1 and MMP13 promoters (-2Kb upstream of the Transcription Start Site (TSS) to 600bp downstream of the TSS).

5.3.2 In silico analysis predicts a direct protein-protein interaction between HDAC3 and E2F-1.

Based on the predictions that E2F-1 can bind to the MMP promoters, a possible association between E2F-1 and HDAC3 was examined using STRING, a protein-protein interaction tool (Franceschini et al. 2013). A novel interaction between HDAC3, E2F-1 and its coactivator DP1 is predicted and the Retinoblastoma protein 1 (Rb1) takes part in this predicted complex (p-value= 1.41 x 10^{-5}) (Figure 5.1). Using STRING, an extended view of the predicted network could be viewed with novel association molecules, which were predicted to be part of the HDAC3/ E2F-1/DP1/Rb network (Figure 5.1 B). STRING also predicts gene ontology, molecular functions and biological processes, and KEGG pathways for the protein association network and among the most significant biological processes predicted were negative regulation of transcription involved in G1/S transition of mitotic cell cycle, regulation of cellular protein localisation and negative regulation of fat cell proliferation. Transcription factor binding is the main molecular function associated with the predicted association network and cell cycle regulation as well as many cancer-related pathways arose from the KEGG pathway analysis. The complete list accompanied by the p-values can be found in **Table 5.2**.

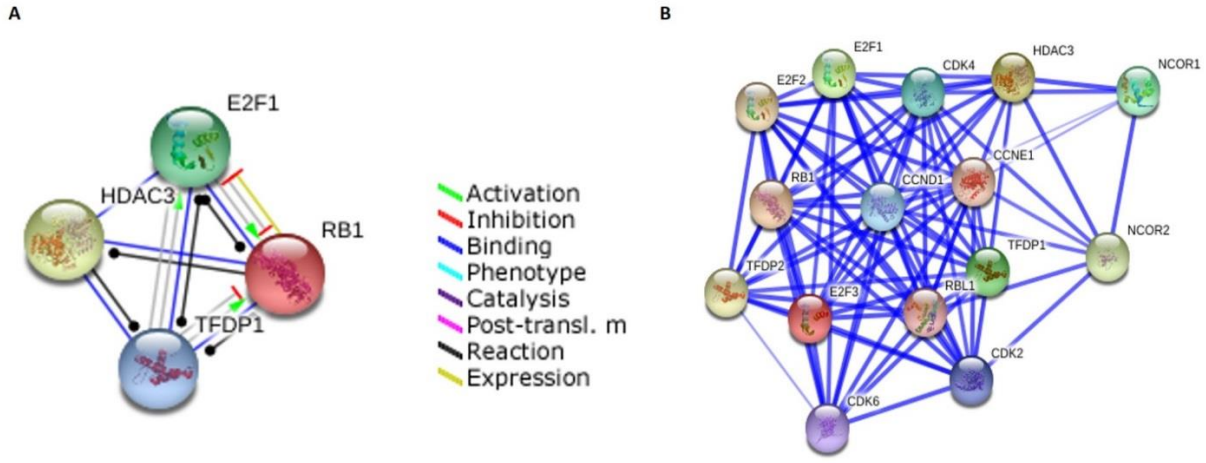

Figure 5.1. A. STRING analysis predicts a novel protein- protein interaction between HDAC3 and E2F-1/DP1 transcription factors which is possibly mediated through the Rb1 protein. **B.** Extended view of the predicted network shown in A predicts novel association molecules of the HDAC3/Rb/E2F-1/DP1 network. Stronger predicted associations are represented by thicker blue lines.

Biological process	**p-value**
negative regulation of transcription involved in G1/S transition of mitotic cell cycle	0.0011
regulation of cellular protein localization	0.0019
negative regulation of fat cell proliferation	0.0019
Notch signaling pathway	0.0028
G1/S transition of mitotic cell cycle	0.0043
positive regulation of transcription from RNA polymerase II promoter	0.0063
cell cycle process	0.0066
positive regulation of protein insertion into mitochondrial membrane involved in apoptotic signaling pathway	0.0085
epithelial cell apoptotic process	0.0085
cell cycle	0.0095
Molecular function	**p-value**
transcription factor binding	0.0005
KEGG pathway	**p-value**
Cell cycle	0.0002
Bladder cancer	0.0027
Pancreatic cancer	0.0027
Glioma	0.0027
Melanoma	0.0027
Chronic myeloid leukemia	0.0027
Non-small cell lung cancer	0.0027
Prostate cancer	0.0032
Small cell lung cancer	0.0032
Hepatitis B	0.0078

Table 5.2. Functional analysis of the predicted by STRING association network between HDAC3/ E2F-1/DP1 and Rb.

Gene ontologies involved two categories (Biological processes and molecular function) and KEGG pathway analysis was also performed.

5.3.3 In vitro co- immunoprecipitation analysis predicts a direct interaction between HDAC3 and E2F-1.

Given the STRING data prediction, co-Immunoprecipitation (co-IP) experiments were conducted in HEK293T cells to assess whether HDAC3 associates with E2F-1 and DP1 transcription factors *in vitro* (as described in section **2.2.9**). Over-expression of E2F-1 (**Figure 5.2**) was necessary, since endogenous levels could not be detected by immunoblotting. Endogenous IP's are often difficult with low expressed proteins such as transcription factors. Over-expression of the factors overcame this issue allowing for the addition of immunogenic tags for easier/better IP. After expressing each tagged protein, immunoprecipitation (IP) for FLAG (the tag of HDAC3 vector) was performed. The levels of the endogenous (lane 1) and over-expressed HDAC3, E2F-1 (lane 2) and HA tags (red arrows in lane 2- representing E2F-1 and DP1) were detected after immunoblotting (**Figure 5.3**). HDAC3 protein was immunoprecipitated as anticipated (lane 6, **Figure 5.3 A**). Immunoblotting for E2F-1 transcription factor confirmed its co- immunoprecipitated (lane 6) (**Figure 5.3 A**), supporting a direct interaction between HDAC3 and E2F-1. Similarly, the HA tag present on both DP1 and the E2F-1 were also detected in the FLAG co-immunoprecipitates (red square and arrows in lane 6), but not in the pcDNA3.1 control (compare lanes 5 versus 6 in **Figure 5.3 A**). There was no HDAC3, E2F-1 or HA present on the irrelevant IgG immunoprecipitates (lanes 3 and 4), which acted as the negative control, further establishing the specificity of this assay. Immunoprecipitation for HA (tag of E2F-1 and DP1 vectors) was also performed and confirmed the association between HDAC3 and E2F-1/DP1 as shown in **Figure 5.3 B** (lane 6).

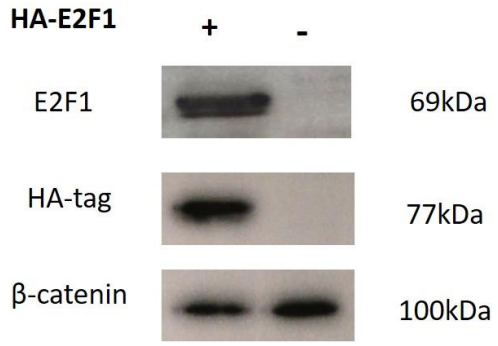

Figure 5.2. Expression of HA-E2F1 in HEK293 cells.

HEK293 cells were transfected with HA-E2F-1 (2µg). At 24 hours post-transfection cells were lysed, total proteins were extracted, and immunoblotting was performed with an anti-E2F-1 and an anti-HA antibodies. β-catenin served as a loading control. Molecular weights (MW) (kDa) are indicated.

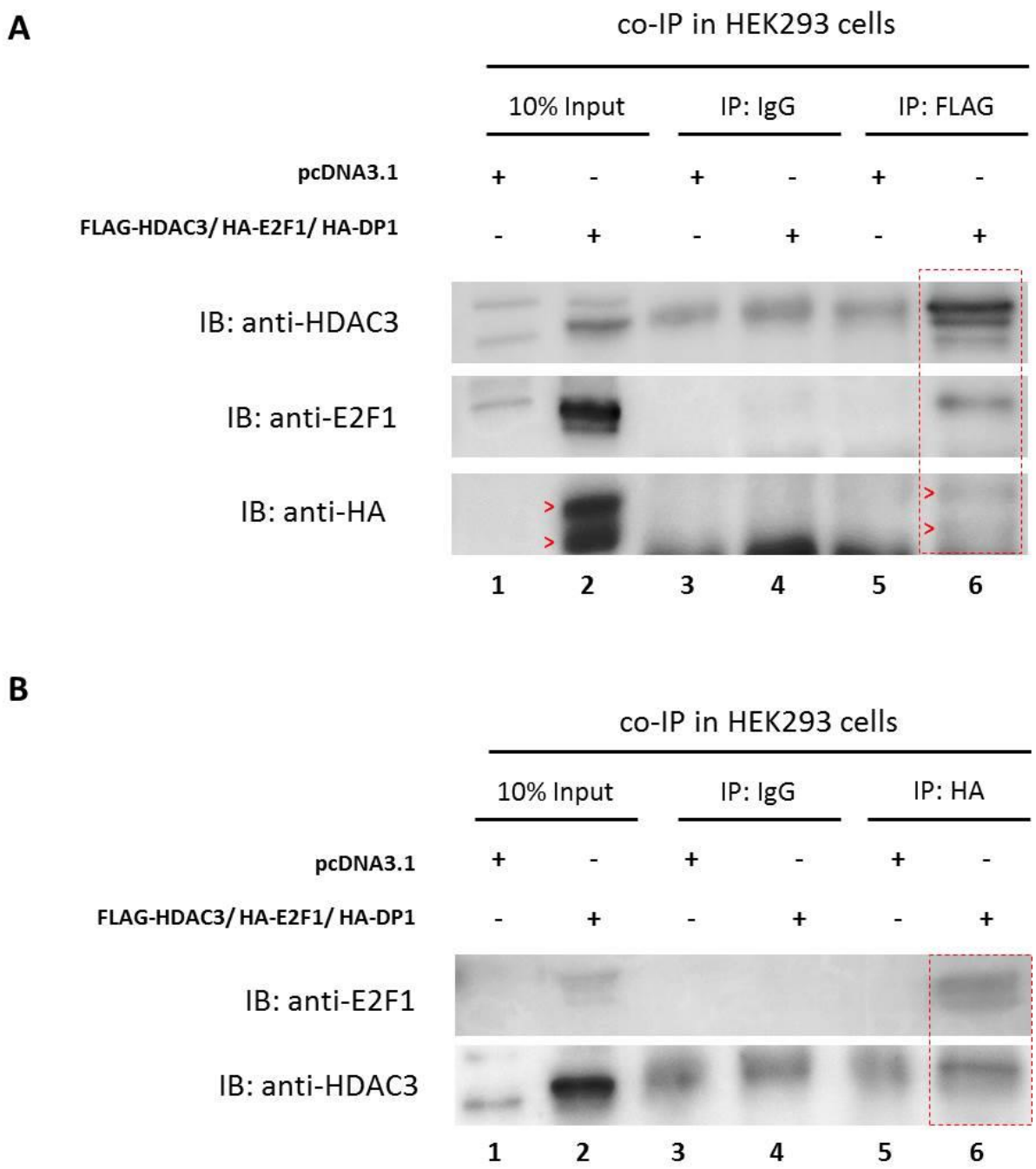

Figure 5.3. Co-Immunoprecipitation experiments suggest there is a direct association between HDAC3 and E2F-1.

A. HEK293 cells were transfected with FLAG-HDAC3 (2µg), HA-E2F-1 (2µg), and HA-DP1 (2µg) or pcDNA3.1 (6µg). At 24 hours post-transfection cells were lysed. Total proteins were extracted, pre-cleared, immunoprecipitated for FLAG or an irrelevant IgG antibody, resolved by SDS-PAGE and immunoblotted with an anti-HDAC3, an anti-E2F-1 and an anti-HA antibodies. Representative blots out of three independent experiments are shown. **B.** A reciprocal experiment was performed and IP for HA or an irrelevant IgG antibody was performed this time. Immunoblotting followed with an anti-HDAC3 and an anti-E2F-1 antibody.

5.3.4 The effect of E2F-1 RNAi on IL-1 induced gene expression.

Since *MMP1* and *MMP13* have putative E2F-1 binding sites in their promoters [see **Table 5.1** and (Johnson et al. 2012)], their expression was further studied following *E2F-1* gene depletion.

5.3.4.1 The effect of RNAi on E2F-1 mRNA and protein levels.

The gene expression array data (Chapter 4) support that the IL-1 induced and repressed (siHDAC3 or Apicidin) genes are enriched for E2F-1 transcription factor binding sites. STRING analysis and co-IP experiments also showed that HDAC3 and E2F-1 can directly associate *in vitro*, predicting a novel interaction network between the two molecules. The optimal transfection procedure and duration of siRNA incubation is described in section **2.2.6**. Transfection of SW1353 cells with 50nM of siRNA targeting E2F-1 was used and depletion efficiency was determined using quantitative real-time RT-PCR and immunoblotting. As shown in **Figure 5.4**, *E2F-1* expression was significantly reduced at the mRNA (Figure 5.4 A) and protein levels (Figure 5.4 B). *E2F-1* expression was very low in the SW1353 cells and although mRNA levels were detected with real-time PCR, endogenous protein levels could not be detected with immunoblotting; therefore over-expression of the protein and then RNAi confirmed the efficacy of the siRNA used in this study to silence *E2F-1* gene expression (Figure 5.4 B).

5.3.4.2 The effect of E2F-1 RNAi on the induction of MMP, IL-6 and IL-8 gene expression by IL-1.

siE2F-1 significantly increased the induction by IL-1 of *MMP1* and *MMP13* genes (Figure 5.5 A and 5.5 B respectively), yet had no effect on *IL-6* (Figure 5.5 C) and *IL-8* (Figure 5.5 D) expression. These results suggest the two major collagenases in cartilage, *MMP1* and *MMP13* may in fact be E2F-1 regulated. Nonetheless, RNAi-mediated depletion of *E2F-1* did not alter *MMP13*, *MMP1*, *IL-6* and *IL-8* basal gene expression.

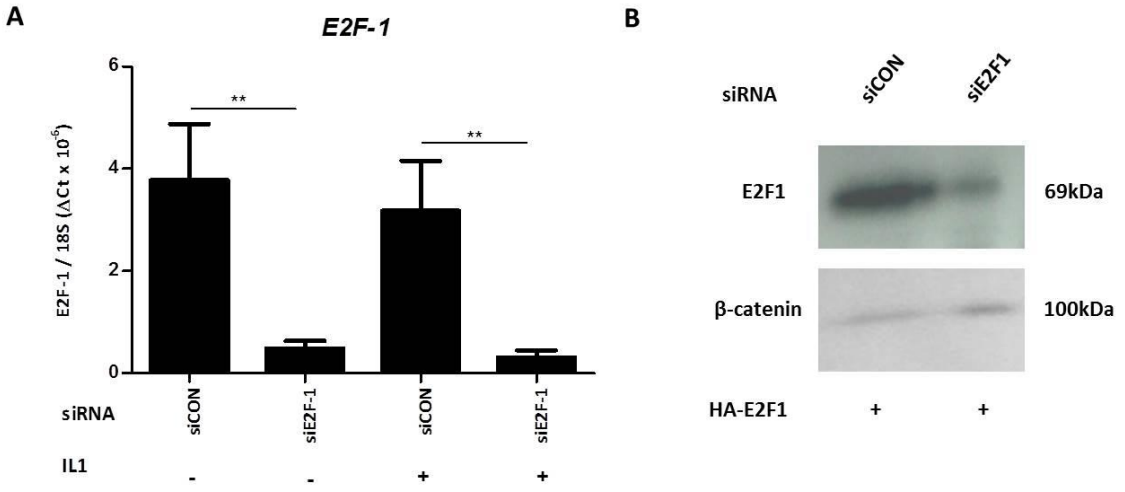

Figure 5.4. Gene silencing of E2F-1 expression using an E2F-1-specific siRNA

A. SW1353 cells were transfected with 50nM of a non-targeting siRNA control pool (siCON) or an E2F-1-specific siRNA pool (siE2F-1) for 24h. The following day, the cells were serum starved for 16h and then stimulated with IL-1α (0.5ng/ml) for 6 hours or left unstimulated. Total RNA was extracted, reverse transcribed to cDNA and E2F-1 expression measured by qRT-PCR. Results are shown relative to 18S ribosomal RNA expression. Significance was determined with respect to siCON treated cells in comparison to the siE2F-1 treated cells, both in the basal and IL-1 induced level. Figure shows two biological experiments and bars represent the mean of eight technical repeats +SD. For statistical analysis, one-way ANOVA with a Bonferroni multiple comparison test was performed. **B.** SW1353 cells were transfected with HA-E2F-1 (2µg) before a 24 hour siRNA (50nM) transfection was performed. Cell lysate was harvested the next day and protein levels quantified by SDS-PAGE and immunoblotting for an anti-E2F-1 antibody. β-catenin served as a loading control. ** $p<0.01$

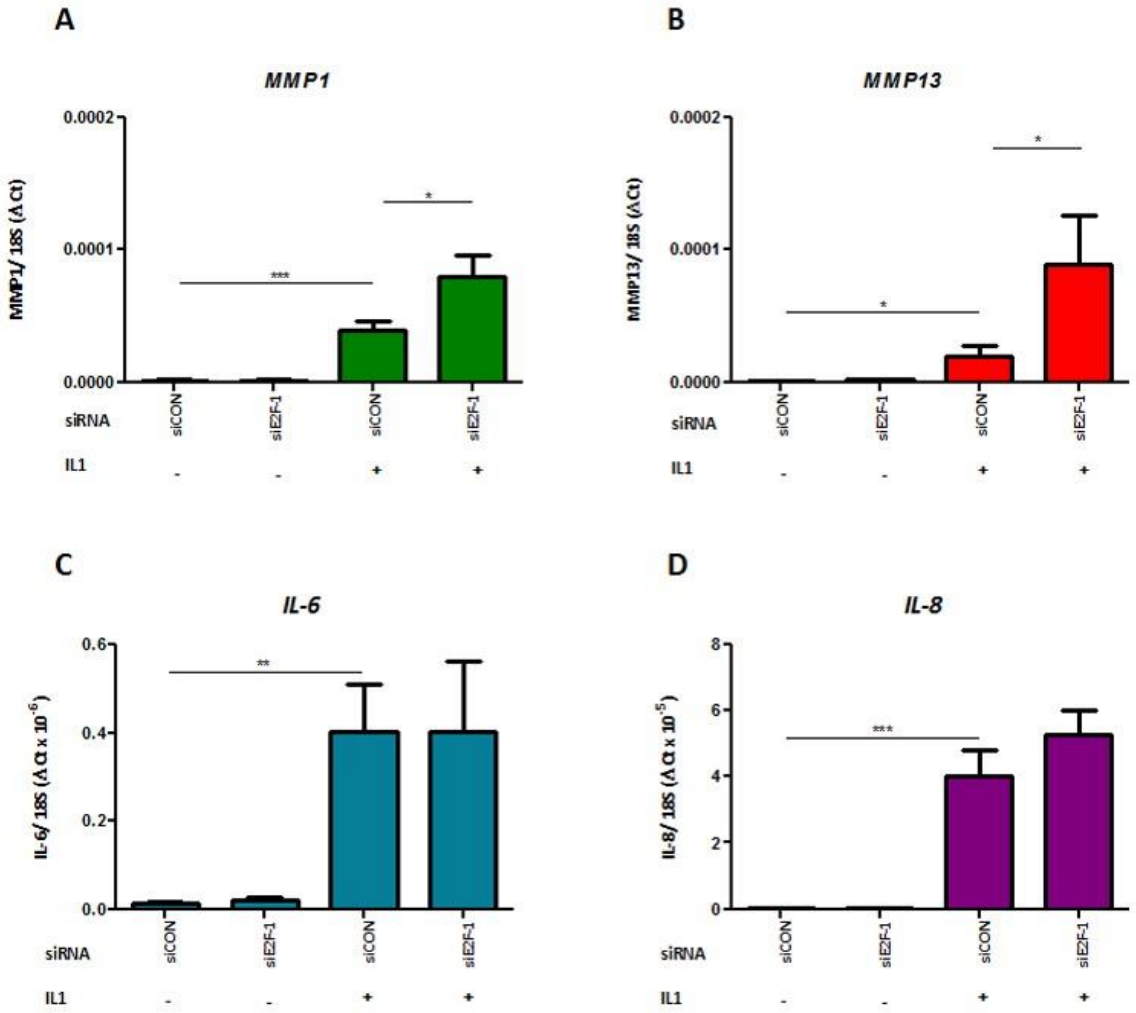

Figure 5.5. Gene expression regulation of MMP1, MMP13, IL-6 and IL-8 following E2F-1 gene silencing.

SW1353 cells were transfected with 50nM of a non-targeting siRNA control (siCON) or an E2F-1-specific siRNA (siE2F-1) for 24h. Following an overnight serum starvation, the cells were stimulated for 6 hours with IL-1α (0.5ng/ml). Total RNA was extracted, reverse transcribed to cDNA and MMP1 (A), MMP13 (B), IL-6 (C) and IL-8 (D) expression measured by qRT- PCR. Results are shown relative to 18S ribosomal RNA expression. Significance was determined by comparing the siCON with the siE2F-1 treated cells, both in the basal and IL-1 induced level. Figure shows two biological experiment and bars represent the mean of eight technical repeats +SD. For statistical analysis, one-way ANOVA with a Bonferroni's multiple comparison test was performed. * $p<0.05$, ** $p<0.01$, *** $p<0.001$

5.3.4.3 The effect of E2F-1 RNAi on the induction of genes identified in the microarray analysis.

So far, our results support a role for HDAC3 and E2F-1 on regulating gene expression in the SW1353 chondrosarcoma cells. A novel protein-protein interaction was also determined between E2F-1/HDAC3 and direct binding sites for E2F-1 transcription factor were predicted on both MMP promoters. Four other genes (out of the 13 showed in **Figure 4.11 A**), that had similar gene expression patterns with *MMP1* and *MMP13*, were identified in the gene expression array and further analysed. These genes included: the *WNT7B*, *CCL2*, *SERPINB2* and *TNFIP6*. E2F-1 binding sites were also predicted to be present in their promoters (data not shown), and *HDAC3* expression was also quantified following *E2F-1* depletion. All the genes analysed here (**Figure 5.6**), except for *HDAC3*, were significantly induced following IL-1 cytokine stimulation and a further significant increase was found only for *SERPINB2* (**Figure 5.6 C**) in the siE2F-1 treated samples when compared to the siCON samples. A trend towards increased expression was found for *WNT7B* (Figure 5.6 A), *CCL2* (**Figure 5.6 B**) and *TNFAIP6* (**Figure 5.6 D**), but these findings were not statistically significant. *HDAC3* expression (**Figure 5.6 E**) was not altered with or without IL-1 and/or in the presence of the siE2F-1. Interestingly, our microarray data showed that *E2F-1* expression also remained stable following *HDAC3* depletion and cytokine stimulation. These results indicate that E2F-1 and/or HDAC3 expression do not change when either is depleted, and therefore HDAC3 might impact upon E2F-1 binding affinity, cellular localisation or transactivation activity, which in turn may alter specific gene expression programmes in cartilage.

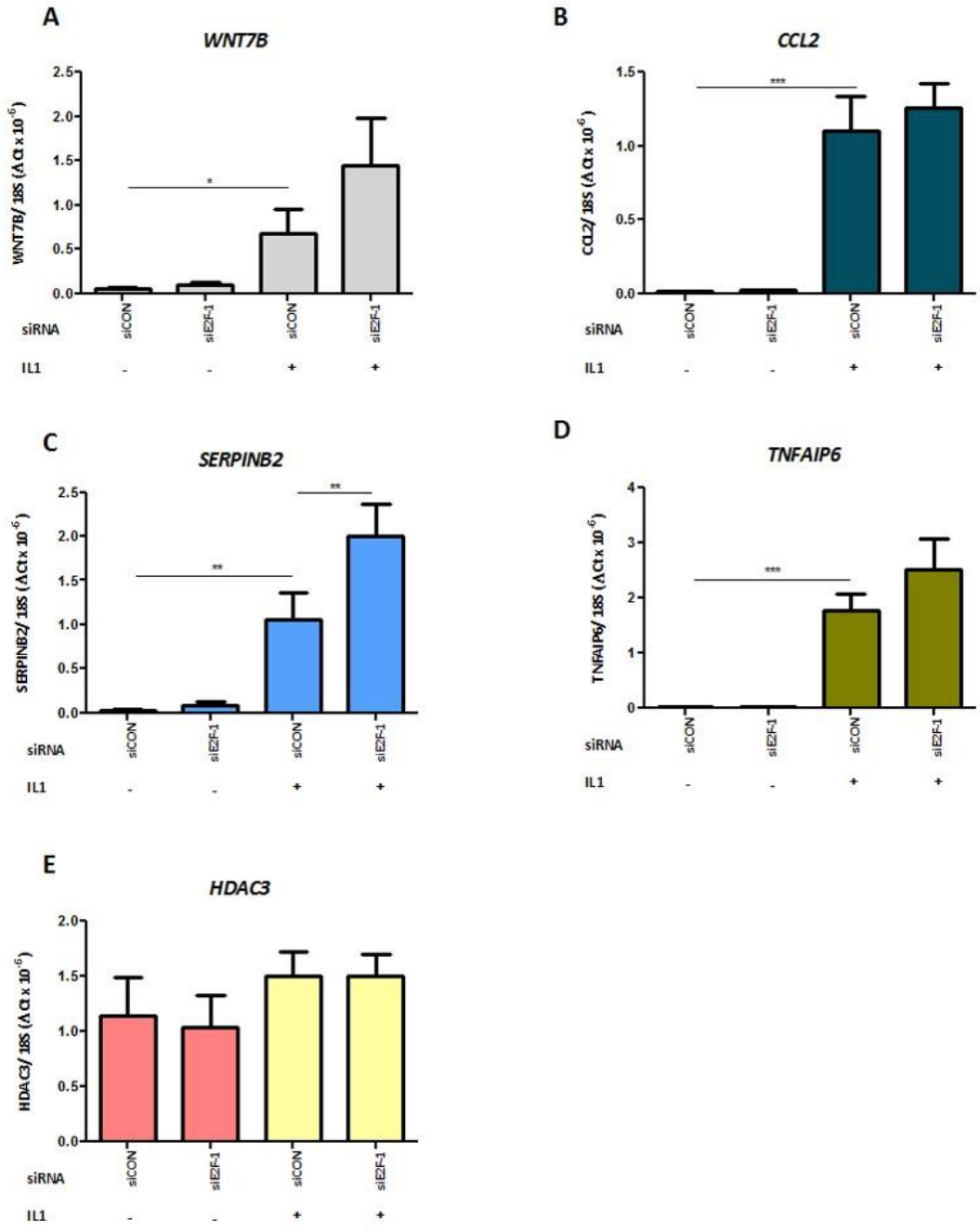

Figure 5.6. Gene expression regulation following E2F-1 gene silencing.

SW1353 cells were transfected with 50nM of a non-targeting siRNA control (siCON) or an E2F-1-specific siRNA pool (siE2F-1) for 24h. Following an overnight serum starvation, the cells were stimulated for 6 hours with IL-1α (0.5ng/ml). Total RNA was extracted, reverse transcribed to cDNA and WNT7B (**A**), CCL2 (**B**), SERPINB2 (**C**), TNFAIP6 (**D**) and HDAC3 (**E**) expression measured by qRT- PCR. Results are shown relative to 18S ribosomal RNA expression. Significance was determined by comparing the siCON with the siE2F-1 treated cells, both in the basal and IL-1 induced level. Figure shows two biological experiment and bars represent the mean of eight technical repeats +SD. For statistical analysis, one-way ANOVA with a Bonferroni's multiple comparison test was performed. * $p<0.05$, ** $p<0.01$, *** $p<0.001$

5.3.5. MMP promoters are responsive to E2F-1 expression and HDAC inhibition or RNAi.

5.3.5.1 The effect of E2F-1 over-expression on CDC6, MMP1 and MMP13 promoter activity.

Previous studies had demonstrated that MMP promoters including *MMP9*, *MMP14*, *MMP15* and *MMP16* are regulated by E2F family members such as E2Fs 1-3 and E2F-4, suggesting the MMPs may be a new class of E2F target genes. (Johnson et al. 2012; Li et al. 2014) Since E2F-1 putative binding sites were predicted on *MMP1* and *MMP13* promoters (**Table 5.1**), we next wanted to assess whether E2F-1 can regulate their promoters via luciferase reporter activation, using vectors containing part of the proximal promoters of each MMP, as previously described in section **2.2.8** ***Luciferase reporter assays***. SW1353 cells were transiently transfected with luciferase constructs with or without over-expression of HA- E2F-1 and its heterodimer HA- DP1 (**Figure 5.7**). Initially, the effect on an E2F-1- responsive promoter, namely CDC6 reporter was examined. E2F-1 and DP1 over-expression activated the CDC6 luciferase reporter (**Figure 5.7 A**), confirming previous reports (Ingram et al. 2011). On the other hand, over-expressing E2F-1 reduced the activation of all the MMP reporter vectors analysed here (**Figure 5.7 B**), suggesting that (overexpressed) E2F-1 binding to *MMP1* and *MMP13* promoters might suppress their transcriptional activation. Since E2F-1 decreased luciferase activation of both MMP13 constructs, only the 3.2 kb reporter, which contains the 1.6 kb (from the TSS) proximal promoter region plus an (1.5 kb) enhancer element (inserted immediately 5' to the promoter) was used in subsequent experiments.

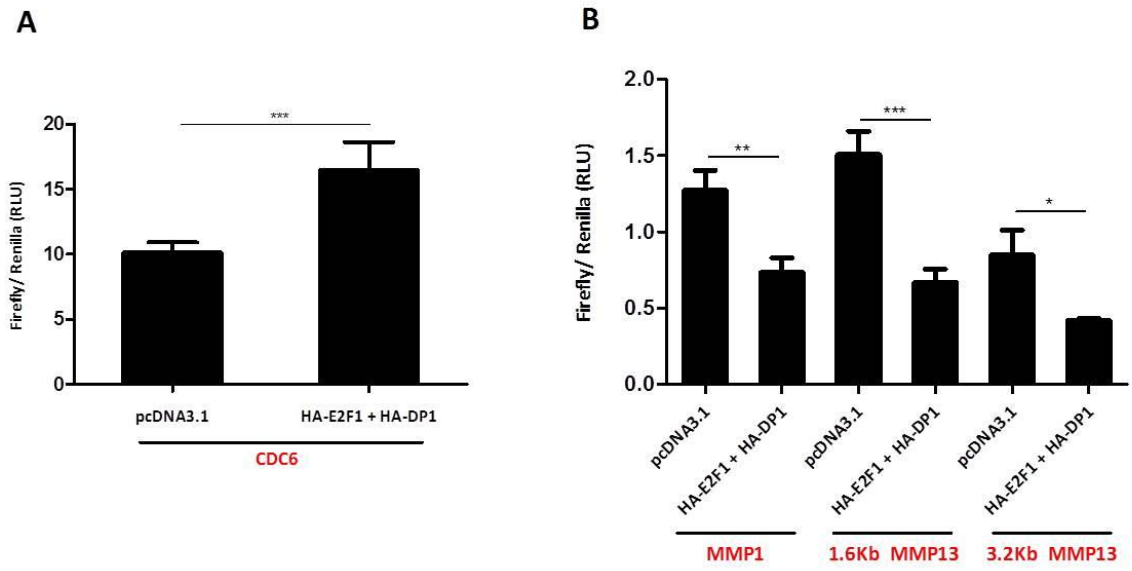

Figure 5.7. *CDC6, MMP1, MMP13* luciferase reporter activity following E2F-1/DP1 over-expression.

SW1353 cells were transfected with the indicated expression vectors (HA-E2F-1= 50ng, HA-DP1= 50ng) or an empty vector pcDNA3.1 (100ng) together with 1.5ng of Renilla reporter and the effect on (**A**) CDC6 (25ng) and (**B**) MMP1 (25ng), 1.6 kb (fromTSS) MMP13 (25ng), 3.2 kb (1.6 kb form TSS plus 1.5 kb enhancer) MMP13 (25ng) luciferase expression was measured. The luciferase activity was quantified using the Dual-Glo® Luciferase Assay system (Promega) and normalised to Renilla on a GloMax®- Multi Luminescene Module (Promega). Assays were performed once, containing six repeats per treatment per biological repeat. Bars show the average +SD of six samples. For statistical analysis an unpaired two-tailed student's t-test was performed. RLU: Relative Light Unit, * $p<0.05$, ** $p<0.01$, *** $p<0.001$

5.3.5.2 The effect of E2F-1 over-expression and HDAC inhibition or HDAC3 gene depletion on CDC6, MMP1 and MMP13 promoter activity.

Next, the effect of HDAC inhibition, using the TSA HDAC pan-inhibitor and E2F-1/ DP1 over-expression was determined on the same luciferase reporters as previously (section **5.3.5.1 The effect of E2F-1 over-expression on CDC6, MMP1 and MMP13 promoter activity.**). HDAC inhibition, using TSA, decreased the activation of the CDC6 reporter, even though E2F-1 and DP1 were over-expressed (**Figure 5.8 A**), but was still higher than the basal level. Activation of MMP1 and 3.2Kb MMP13 luciferase reporters was decreased following E2F-1/ DP1 exogenous expression and TSA treatment (**Figure 5.8 B**), suggesting there might be a direct interaction between E2F-1 and some HDACs on the promoters of both collagenases. Histone H4 de-acetylation of lysines 5 and 12 for instance has been linked to gene expression regulation by HDAC-1, which is stably bound to classical E2F target promoters during the G0 and G1 phase of the cell cycle. (Ferreira et al. 2001)

The MMP13 luciferase reporter activation was also decreased following Apicidin treatment and E2F-1/DP1 expression, as shown in **Figure 5.9 A**. MMP1 reporter presented a small but not significant decrease following HDAC3 inhibition with Apicidin (**Figure 5.9 A**). Also RNAi-mediated *HDAC3* depletion significantly reduced MMP1 and MMP13 reporter activation (**Figure 5.9 B**). These results introduce a novel mechanism by which *MMP1* and *MMP13* promoters may be regulated by a direct interaction/ binding of HDAC3 and E2F-1 transcription factor.

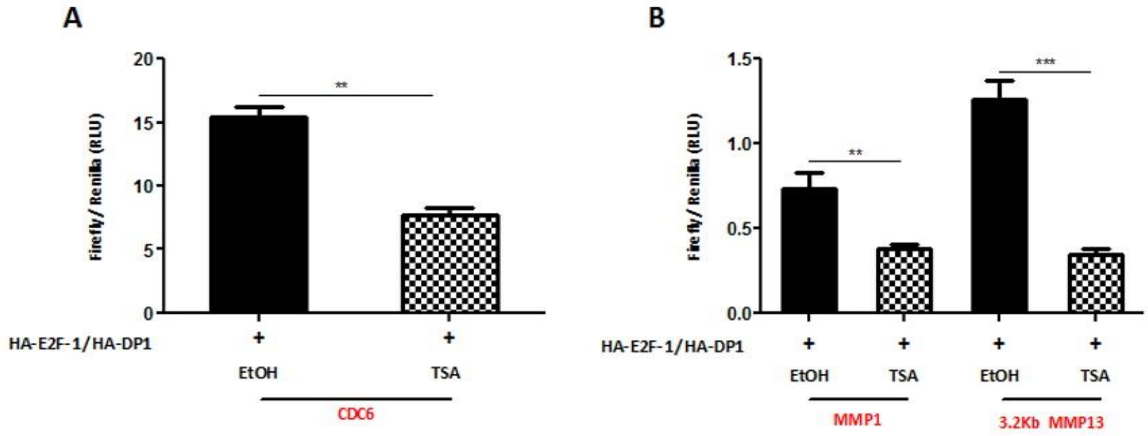

Figure 5.8. CDC6, MMP1 and MMP13 luciferase reporter activity following E2F-1/DP1 over-expression and HDAC inhibition using TSA.

SW1353 cells were transfected with the indicated expression vectors (HA-E2F-1= 50ng, HA-DP1= 50ng) or an empty vector pcDNA3.1 (100ng) together with 1.5ng of Renilla reporter. The following day the cells were incubated with 330nM TSA for 6.5 hours and the effect on (**A**) CDC6 (25ng), (**B**) MMP1 (25ng) and MMP13 (25ng) luciferase expression was measured. The luciferase activity was quantified using the Dual-Glo® Luciferase Assay system (Promega) and normalised to Renilla on a GloMax®- Multi Luminescene Module (Promega). Assays were performed once, containing six repeats per treatment per biological repeat. Bars show the average +SD of six samples. For statistical analysis an unpaired two-tailed student's t-test was performed. RLU: Relative Light Unit, * $p<0.05$, ** $p<0.01$, *** $p<0.001$

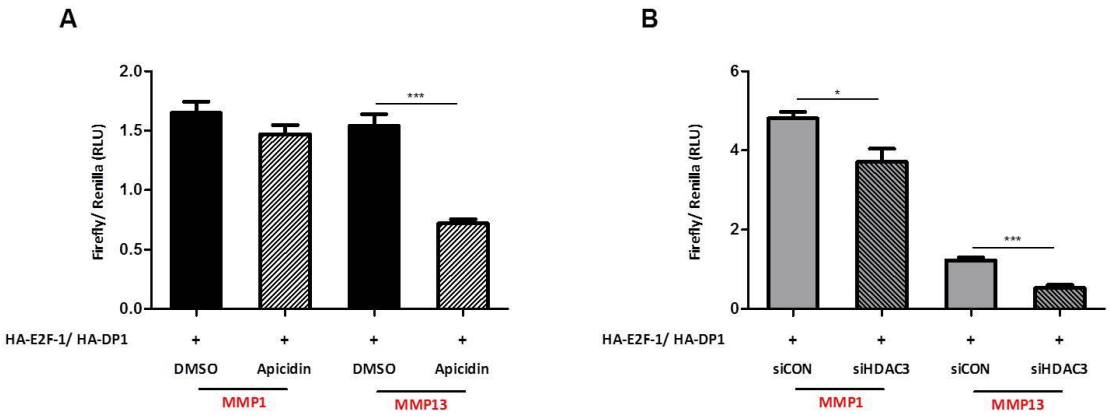

Figure 5.9. MMP1 and MMP13 luciferase reporter activity following E2F-1/DP1 over-expression and HDAC3 inhibition/ depletion by Apicidin or RNAi.

SW1353 cells were transfected with the indicated expression vectors (HA-E2F-1= 50ng, HA-DP1= 50ng) or an empty vector pcDNA3.1 (100ng) together with 1.5ng of Renilla reporter. The following day the cells were incubated with 160nM Apicidin in (**A)** or 50nM siRNA targeting HDAC3 in (**B**) and the effect on MMP1 (25ng) and MMP13 (25ng) luciferase expression was measured. The luciferase activity was quantified using the Dual-Glo® Luciferase Assay system (Promega) and normalised to Renilla on a GloMax®- Multi Luminescene Module (Promega). Assays were performed once, containing six repeats per treatment per biological repeat. Bars show the average +SD of six samples. For statistical analysis an unpaired two-tailed student's t-test was performed. RLU: Relative Light Unit, * $p<0.05$, *** $p<0.001$

5.3.6 E2F-1 and HDAC3 are necessary for normal cell cycle progression.

To understand the relationship between E2F-1 and HDAC3 in the cell cycle control, SW1353 cells were synchronised in the G0/ G1 phase by a 24- hour serum starvation and HDAC3 and/or E2F-1 were depleted by RNAi. The cells were then released to re-enter into the cell cycle (by stimulation with growth media containing 10% FBS). To test whether HDAC3 has a cell cycle related function, flow cytometry was used to determine whether *HDAC3* depletion can impair cell cycle progression. The cell cycle phase distribution was then analysed (**Figure 5.10**). As expected, *E2F-1* depletion led to a significant increase in the proportion of cells by 12.6% in the G1 phase when compared to the control treated cells. This increase was most likely due to the lack of the E2F-1 transcriptional induction of its G1– S transition target genes. As a consequence, the number of cells in the S and G2/M phase decreased by 4.8% and by 7.3% respectively. Interestingly, *HDAC3* depletion also significantly increased the number of cells in the G1 phase by 15.7% in comparison to the control. An increase of 3.1% of the proportion of cells in the G1 phase of the HDAC3 depleted cells in comparison to the E2F-1 depleted cells was also observed, though this increase was not statistically significant. Consequently, the percentage of cells in the S phase was reduced by 8.3%, as was the percentage of cells in the G2/M phase by 8.6%. The effect of *HDAC3* and *E2F-1* double depletion on cell cycle phase distribution was also analysed. No additive effect was observed following double gene depletion. The proportion of G1 cells increased by 14.4%, leading to a decrease in cells in the S phase by 7.6% and in the G2/M phase by 7.3% compared to control cells. The FACs gating data from one experiment can be found in **Appendix C**.

These results revealed that HDAC3 is necessary for normal cell cycle progression at the G1- S transition phase. As no cumulative effect was found when using both HDAC3 and E2F-1 siRNAs, it suggests HDAC3 could positively control the cell cycle through the E2F-1 regulatory pathway.

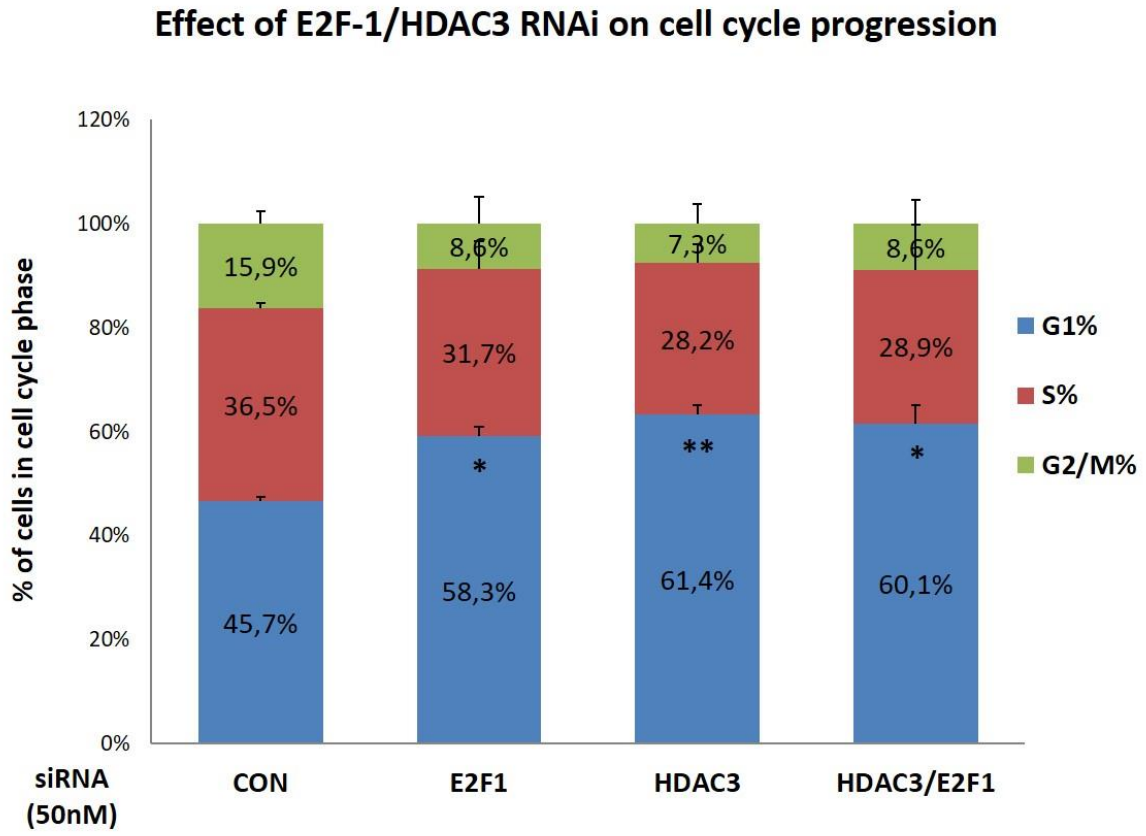

Figure 5.10. HDAC3 depletion induces cell accumulation in G1 phase.

SW1353 cells were synchronised by a 24-hour serum starvation, released and collected. Endogenous *HDAC3*, *E2F-1* or both were depleted and cell cycle analysis was performed using FlowJo. Assays were performed twice, containing four replicates per treatment per biological repeat. Bars show the average +SD of eight samples. For statistical analysis an unpaired two-tailed student's t-test for each cell cycle phase was performed. ** $p<0.01$, * $p<0.05$

5.3.7 HDAC3 recruitment of E2F-1 to MMP promoters.

Given the above results, a speculation on whether HDAC3 could act directly or indirectly on E2F-1 DNA binding ability in association with the chromatin within the E2F-1 binding region was tested. To answer this question, chromatin immunoprecipitation (ChIP) assays and real-time PCR were performed on SW1353 cells. Primers were designed based on the PROMO predicted E2F-1 binding sites (**Table 5.1**) and are depicted as arrows in **Figure 5.11 A**. An extra primer set (P6M13), which has been previously used in the literature (Bui et al. 2012) and amplifies a 198bp genomic region around the Transcription Start Site (TSS) of MMP13 was also utilised in this experiment. Sonication times were optimised for the SW1353 cell line (as described in section **2.2.19**) and 12 cycles were chosen as the optimum time (**Figure 5.11 B**). The sonicated samples were then de- cross-linked, DNA was extracted and all the primer assays tested with PCR to confirm correct size amplification as shown in **Figure 5.11 C**. All primer sets gave the correct size amplicons, while HBB (human haemoglobin) served as a positive control.

ChIP assays were conducted on asynchronously dividing SW1353 cells to assess whether HDAC3 and E2F-1 can directly associate with the *MMP1* and *MMP13* promoters. The cells were transfected with the HA-E2F-1/ HA-DP1 and FLAG-HDAC3 vectors and stimulated for 6 hours with IL-1α. Unstimulated cells were also used for comparison. ChIP was performed using an E2F-1 or HDAC3 antibody. 10% input of the sonicated chromatin was used in each ChIP assay for normalization of the adjusted Ct values obtained from the qRT- PCR. *CDC2* and *p21* genes were the positive controls for E2F-1 and HDAC3 respectively and were provided with the ChIP kits (see section **2.1.10**). However, no significant enrichment of either *CDC2* or *p21* promoters could be detected following IP for E2F-1 and HDAC3 with or without IL-1 stimulation (**Figure 5.12**). Hence the representative results (obtained using the indicative primer sets) presented in **Figure 5.13** should be viewed with caution. Non-specific binding to the irrelevant IgG antibodies was detected, generating doubtful results. Also the small fold enrichment found for CDC2 (+ IL-1) (**Figure 5.12 B**) and p21 (± IL-1) (**Figure 5.12 C-D**) is not in accordance with the fold enrichment suggested by the company, where 86.80 increase was reported for CDC2 and 14.45 increase for p21.

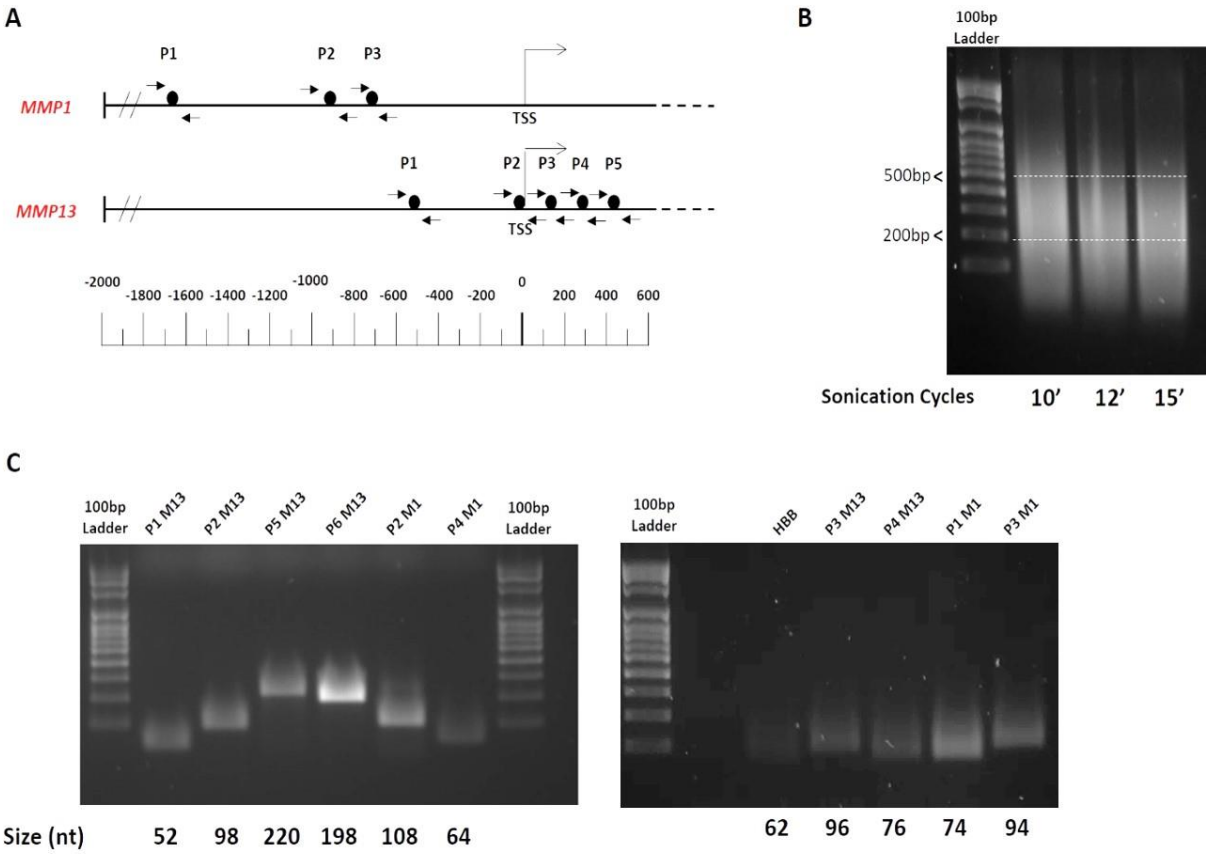

Figure 5.11. MMP promoters are responsive to E2F-1 transcription factor.

A. Schematic representation of *MMP1* and *MMP13* promoters showing potential E2F-1 binding sites as black circle symbols. The arrows represent the primers designed -2Kb to +600bp around the TSS, spanning E2F-1 binding sites, used in ChIP assays. **B.** SW1353 cell chromatin was used for ChIP assays (see **Figure 5.12**) and sonication time optimised following reverse-cross-linking and DNA extraction. **C.** The primer sets designed in A were tested using PCR. nt: nucleotides

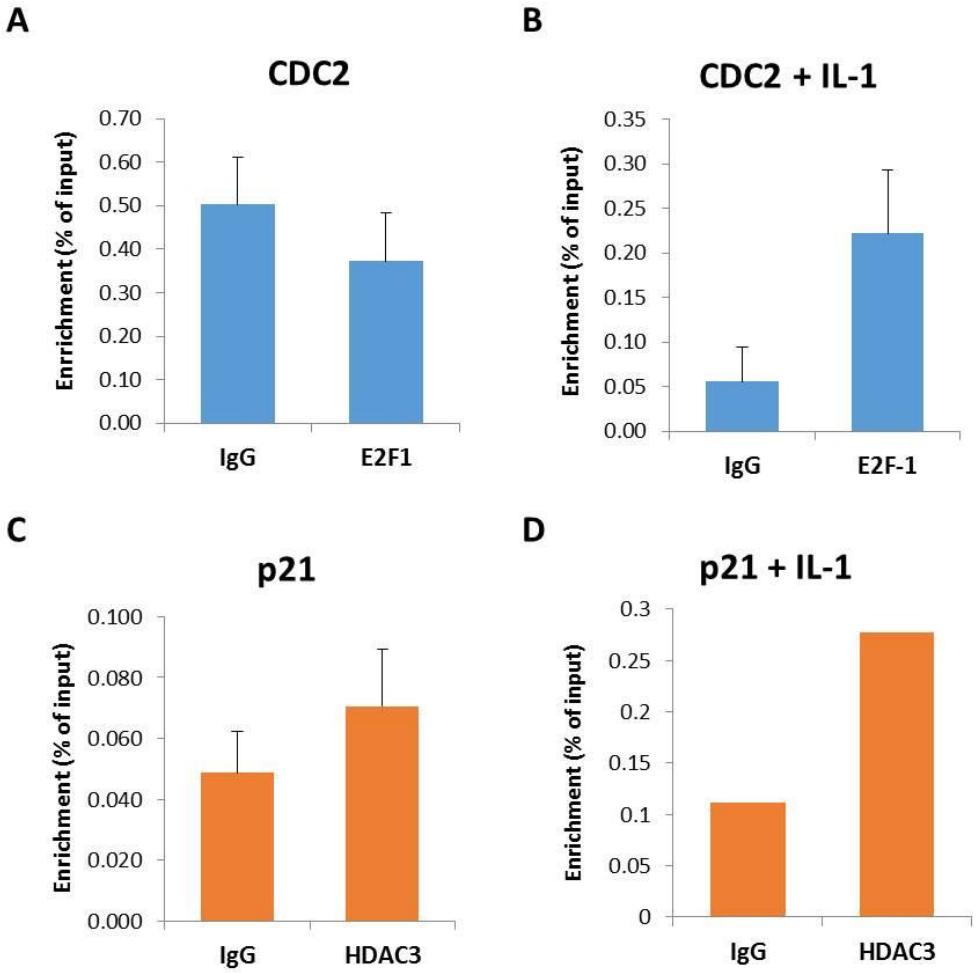

Figure 5.12. Chromatin immunoprecipitation (ChIP) assays failed to show enrichment of HDAC3 and/or E2F-1 on p21 and CDC2 promoters respectively with or without IL-1 stimulation.

SW1353 cells were transfected with FLAG-HDAC3 (2µg), HA-E2F-1 (2µg), and HA-DP1 (2µg). 24 hours post-transfection cells were stimulated with IL-1α (0.5ng/ml) for 6 hours or left unstimulated. Proteins were then cross-linked to DNA using formaldehyde for 10 minutes and cells harvested. Sonicated chromatin was pre-cleared and immunoprecipitation followed using an anti-E2F-1 or an anti-HDAC3 or an irrelevant IgG antibody. The following day the DNA was eluted from the beads and the cross-linking reversed by incubation at 65ºC including proteinase K. DNA was then extracted using phenol-chloroform and used for qRT-PCR. 10% input of the sonicated chromatin was used in each assay for normalization of the adjusted Ct values obtained from the qRT- PCR. **A-B.** *CDC2* served as the positive control for E2F-1 immunoprecipitates, while **C-D.** *p21* was the positive control for HDAC3.

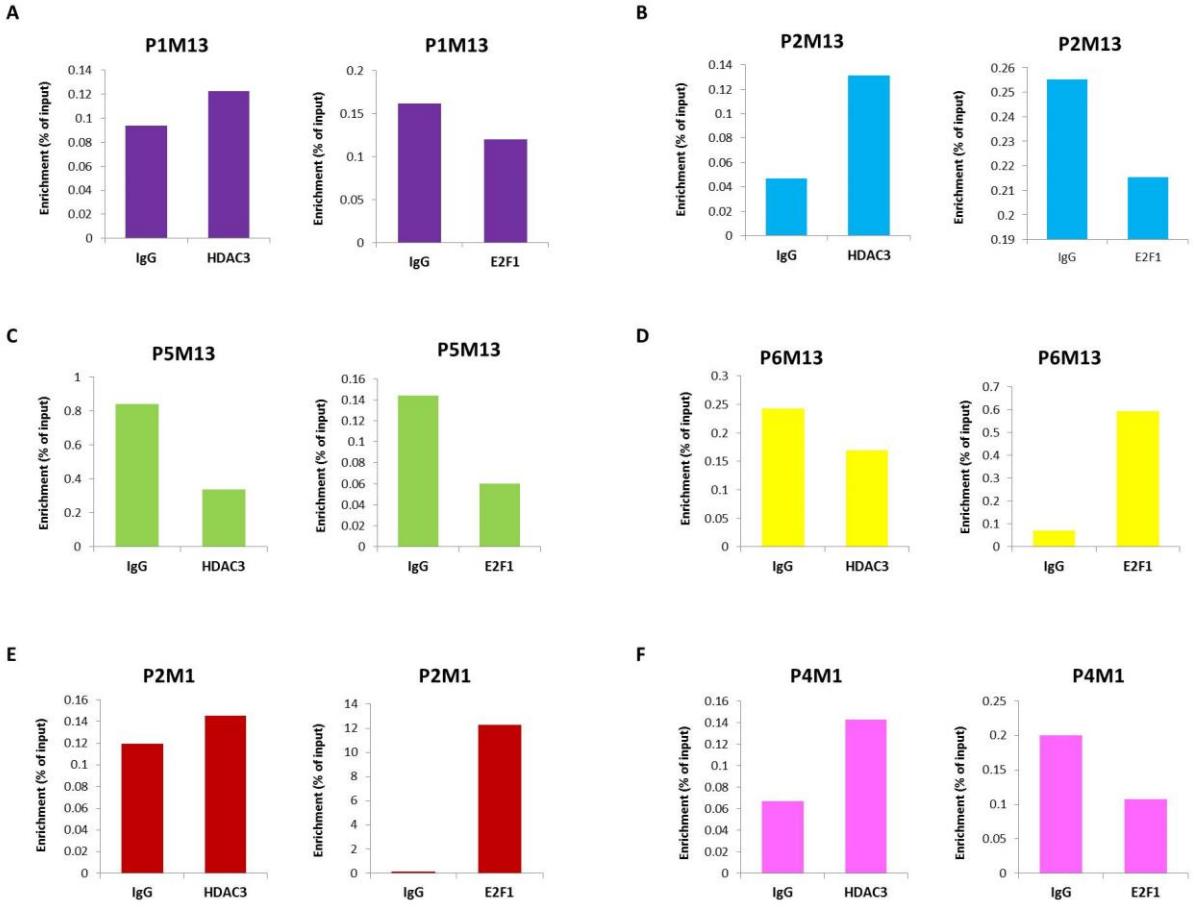

Figure 5.13. Chromatin immunoprecipitation (ChIP) assays failed to show a direct interaction of HDAC3 and/or E2F-1 on MMP1/13 promoters in the absence of IL-1 stimuli.

SW1353 cells were transfected with FLAG-HDAC3 (2μg), HA-E2F-1 (2μg), and HA-DP1 (2μg). ChIP assays were performed as previously described and 10% input of the sonicated chromatin was used in each assay for normalization of the adjusted Ct values obtained from the qRT- PCR. Indicative examples (no IL-1 stimulation) for primer sets (**A**) P1M13, (**B**) P2M13, (**C**) P5M13, (**D**) P6M13, (**E**) P2M1 and (**F**) P4M1 are shown**.**

5.4 Discussion

The E2F family of transcription factors have been implicated in a plethora of cellular and organismal functions, including cell cycle progression, DNA repair, apoptosis, development and tumorigenesis. (New et al. 2012) The ability of E2F family members to regulate these processes has been linked to their ability to regulate transcription of target promoters. A considerable amount of work has been dedicated to identifying novel E2F- regulated genes by gene expression arrays and chromatin immunoprecipitation arrays. (Lavrrar & Farnham 2004; Wells et al. 2002; Weinmann et al. 2001) Most of these studies aimed to identify proteins or enzymes involved in the metastatic spread of tumor cells which physically requires the degradation of the ECM. It is therefore intriguing that at least in cell lung cancer cell lines, E2Fs act as transcriptional activators of *MMP9*, *MMP14* and *MMP15*. (Johnson et al. 2012) In addition, many MMP promoters can be bound by Sp1, and E2Fs are well known to work co-operatively with Sp1 to regulate gene expression. (Clark et al. 2008; Li et al. 2014)

The gene expression array data presented in the previous chapter supports an important role for E2F-1 transcription factor in mediating the expression of the IL-1 induced and repressed by HDAC3 loss genes. Therefore, the purpose of this chapter was to investigate the relationship between HDAC3 and E2F-1 in regulating MMP expression and shed light on the regulatory mechanism.

5.4.1 E2F-1 binding sites are present on MMP1 and MMP13 promoters.

To identify whether *MMP1* and *MMP13* are potentially E2F-1 target genes, an analysis of the promoters within 2 Kb of the transcription start site (TSS) was performed using PROMO, since it has been suggested that most E2F-1, E2F-4 and E2F-6 binding sites are frequently located within 2Kb of the TSS in both normal and tumor cells. (Xu et al. 2007) We found that both *MMP1* and *MMP13* carry potential binding sites within their promoters (**Table 5.1**), confirming in this way previous reports which support that matrix metalloproteinase genes have E2F-1 binding motifs (Johnson et al. 2012). Interestingly, it has been demonstrated that the majority of E2F-1 binding sites (>80%) are located in core promoters and that >50% of these sites overlap with TSS. (Bieda et al. 2006) Only a small fraction of these sites possessed the E2F-1 consensus binding sequence (TTTSSCGC, where S is either a G or a C), suggesting that E2F-1 is recruited to promoters via a method distinct from recognition of the own consensus motif. (Bieda et al. 2006) These findings point toward a new understanding of

E2F-1 as a factor that potentially contributes to the regulation of a large fraction of human genes including MMPs.

ChIP-chip assays were used to demonstrate that the majority of active promoters (as defined by TAF1 or POLR2A binding) in both normal (GM06990 B lymphocyte cell line) and carcinoma (Ntera2) cells were also bound by an E2F member. (Xu et al. 2007) This very close relationship between E2F binding sites and binding sites for general transcription factors in both normal and carcinoma cells, suggests that a chromatin-bound E2F could indicate an active transcription region. Moreover, Xu and colleagues suggest that there is only modest cell type specificity of the E2F family and as a result it is difficult to assess the role of any E2F in transcriptional regulation, due to redundancy to target promoters. As a consequence, Rabinovich et al. (Rabinovich et al. 2008) propose three models of E2F recruitment to a core promoter lacking a consensus binding motif *in vivo*: i) indirect recruitment through another transcription factor, ii) looping to the core promoter mediated by an E2F bound to a distal motif and iii) assisted binding of E2F to a site that only weakly resembles an E2F binding site. These studies implied that examination of the binding and subsequent transcriptional regulation of any of the E2F family members is not as straightforward as it might have been anticipated.

5.4.2 HDAC3 directly interacts with E2F-1 transcription factor in vitro.

Next, a direct association between HDAC3 and E2F-1 was examined using both *in silico* and *in vitro* analysis. First, STRING protein-protein interaction prediction tool suggested that HDAC3 interacts directly with E2F-1 and its co-activator heterodimer the DP1 transcription factor, and Rb protein also takes part in this predicted complex (**Figure 5.1**). Second, co-IP experiments in HEK293 cells confirmed the above predicted association between HDAC3 and E2F-1, since IP for FLAG (a tag added to HDAC3 vector) resulted in both HDAC3 and E2F-1 to be immunoprecipitated. In addition to, IP for FLAG also resulted in the HA tagged E2F-1 and DP1 being co-immunoprecipitated (**Figure 5.3 A**). When an IP for HA (the tag of E2F-1 vector) was performed both HDAC3 and E2F-1 proteins were co-immunoprecipitated (**Figure 5.3 B**). Also, GO analysis of the predicted network supports a role in determining protein localisation and transcription factor binding (**Table 5.2**). These results suggest HDAC3 may bind directly to E2F-1 to alter its DNA binding potential or cellular localisation. It is also possible that HDAC3 is responsible for de-acetylating E2F-1 factor and therefore changing its transactivation capability. Rb may facilitate deacetylation of E2F-1 either by stimulating HDAC3 enzymatic activity or by facilitating the interaction between HDAC3 and E2F-1. As a

consequence, regulation of gene expression programmes may be altered or intermediate transcription factor binding/ localisation affected, which in turn impact on *MMP1* and *MMP13* expression.

To our knowledge this is the first time that a protein- protein interaction between HDAC3 and E2F-1 has been shown. Previous reports have concentrated on whether Rb can bind any HDAC during cell cycle progression. Indeed, it has been shown that Rb can associate with HDAC1 to repress E2F- regulated promoters, such as the gene encoding for the cell cycle protein *cyclin E*. Inhibition of HDAC activity by TSA only partly inhibited the Rb-mediated repression of E2F-regulated promoters, supporting there are possibly other HDACs taking part in this complex. (Magnaghi-Jaulin et al. 1998; Brehm et al. 1998) Nicolas and colleagues (Nicolas et al. 2001) have subsequently demonstrated that the Rb-associated histone deacetylase contain the RbAp48 protein which directly interacts with HDAC1 and HDAC2 and could favour the deacetylation of histones since it binds directly to histone H4. The same study has also indicated that transcriptional repression of the E2F activity requires the presence of RbAp48. HDAC3 was suggested to act as a bridge between RbAp48 and Rb and it is considered that it favours the recruitment of RbAp48 to Rb.

5.4.3 E2F-1 gene silencing up-regulates MMP1 and MMP13 expression following IL-1 induction.

Based on the above results which suggest the presence of multiple E2F-1 binding sites on *MMP1* and *MMP13* promoters, and a direct interaction between HDAC3 and E2F-1, depletion and over-expression experiments were conducted and the effect of E2F-1 on *MMP1* and *MMP13* expression was determined. First, the efficacy of E2F-1 siRNA was confirmed at the mRNA and protein level, as shown in **Figure 5.4**. Endogenous E2F-1 protein levels could not be detected with immunoblotting in the SW1353 cells, and thus an over-expression had to be performed for subsequent experiments. This could be due to very low transcription factor expression and hence low protein levels and perhaps loading more protein on a SDS-PAGE or exposing the membrane for longer could have proven beneficial. Another reason could be that the endogenous protein is folded in such a way that the antibody used here can no longer recognise the epitope. SDS-denaturing conditions were used here and this could have also impacted on E2F-1 structure and therefore detection by immunoblotting.

E2F-1 gene depletion significantly increased the IL-1 induced levels of *MMP13* and *MMP1* genes (**Figure 5.5**) yet had no effect on *IL-6* and *IL-8* expression or the basal levels of either

MMP. These results suggested the two major collagenases of cartilage degradation, *MMP1* and *MMP13* may in fact be E2F-1 regulated. Other genes identified by the microarray aspect of this study and predicted to be regulated by E2F-1 also showed a similar expression pattern with *MMP1* and *MMP13* following E2F-1 depletion (**Figure 5.6**). *HDAC3* expression was also analysed and no change was identified, indicating that E2F-1 and/or HDAC3 do not impact on the expression of each other. Therefore, E2F-1 and HDAC3 must affect gene regulator networks via a mechanism which does not alter each regulator's expression.

5.4.4 E2F-1 over-expression decreases MMP1 and MMP13 luciferase activity.

At the molecular level, ChIP experiments failed to show a direct binding of HDAC3 or E2F-1 to the positive controls used, *p21* and *CDC2* genes respectively (**Figure 5.12**). Therefore, examination of HDAC3 or E2F-1 binding to *MMP1* and *MMP13* promoters did not generate trustworthy results, although several sets of primers were used in the ChIP assays (**Figure 5.13**). [For the ChIP experiments, ChIP assay kits containing the positive controls primers and antibodies for immunoprecipitation were purchased from Millipore (Watford, UK). However, for future experiments, it is worth including more than one positive control and also a negative control in the assays. Alternatively, an antibody that has been previously optimised for IP experiments could also be used to decrease the possibility of non-specific binding.]

Nonetheless, the effect of over-expressing E2F-1 and its heterodimer the DP-1 transcription factor on MMP promoters was determined using luciferase constructs. Transient transfections of SW1353 cells with luciferase constructs driven by *MMP1* or *MMP13* promoters revealed that over-expressing E2F-1 abrogates the activation of each promoter (**Figure 5.7**). The effect on an E2F-1- responsive promoter, the CDC6 reporter was also examined and a significant induction of this promoter was found following E2F-1/DP1 over-expression, consistent with previous reports (Ingram et al. 2011). In the first place, these data imply that the E2F-1 predicted binding sites to *MMP1* and *MMP13* promoters are functional and secondly, E2F-1 binding to the promoters of these genes might suppress their transcriptional activation in chondrocytes.

Furthermore, HDAC inhibition by TSA decreased the E2F-1-mediated activation of the CDC6 reporter and further reduced MMP1 and MMP13 luciferase transactivation (**Figure 5.8**). In addition, when HDAC3 was selectively inhibited using Apicidin or depleted by RNA interference, MMP13 reporter activation was decreased (**Figure 5.9**). These results suggest a novel mechanism by which *MMP1* and *MMP13* promoters may be regulated by a direct

interaction/ binding of some HDACs, possibly including HDAC3 and E2F-1 transcription factor.

Previous studies support that E2F-1-mediated transcription is repressed partly by the Rb protein which recruits members from the HDAC family, but also by direct regulation by HDACs of two E2F-responsive elements in the *E2F-1* gene promoter. (Boutillier et al. 2003; Panteleeva et al. 2004). Interestingly, HDAC inhibition by TSA induced E2F-1 dependent apoptosis in neurons by caspase-dependent mechanisms. (Boutillier et al. 2003) Others have shown that the E2F-7 can interact with the co-repressor CtBP (C-terminal Binding Protein) and recruit HDAC1 to the E2F-1 and CDC6 promoters to repress transcription. Nevertheless, E2F-7 repression on E2F-1 and CDC6 was not rescued by siRNA-mediated depletion of *HDAC1*, suggesting that E2F7-mediated repression might include other HDACs. (Liu et al. 2013) HDAC1 has been suggested to be responsible for E2F-1 de-acetylation, which in turn affects DNA- binding activity and downstream target activation, and depletion of HDAC1 only partially rescued transcription factor activity. (Xiong & Xu 2014)

One hypothesis here is that HDAC3, as a chromatin associated factor, could localise to the E2F-1 target promoters and participate in their transcriptional regulation with or without any physical contact with E2F-1. Direct interaction between HDAC3 and E2F-1 may allow recognition of different sites from those normally bound and repressed by the typical Rb/E2F-1. Also there is evidence that certain E2F-1 regulated promoter elements act positively whereas other act negatively to regulate transcription. (Dyson 1998; Johnson et al. 2012) This could be an indicator of different E2F-1 binding specificity depending on the cell type or binding motif recognised, or whether or not E2F-1 is bound by other proteins such as HDAC3.

Another hypothesis that could explain an indirect effect of HDAC3 on E2F-1 binding to DNA is modulation of its post-translational modifications. Among them, acetylation of lysine residues 117, 120 and 125 by p300/CBP and/or the associated factor P/CAF has been shown to strongly enhance E2F-1 binding to its target genes and further enhance transcription factor stability and half-life. (Bauer et al. 2000) Acetylation of E2F-1 by P/CAF leads to an increased transcriptional activity, but whether this is due to increased binding activity or increased stability due to acetylation remains unclear. However, until now, acetylation of E2F-1 has only been observed in conditions of DNA damage where it has been shown that acetylated E2F-1 is recruited to specific target genes like *p73* (Pediconi et al. 2003), *APAF-1* (Wallace & Cotter 2009) or *Bim* (Zhao et al. 2005) to induce apoptosis. Additionally, the acetylated residues of E2F-1 do not directly take part in DNA binding (Bauer et al. 2000), yet

the close proximity of the acetylated residues to the N-terminal of the E2F-1 DNA binding domain makes it likely that a conformational change mediated by acetylation allows better access to DNA. De-acetylation of E2F-1 by HDAC3 is therefore a novel mechanism by which E2F-1 could be regulated.

Finally, another possibility is that HDAC3 by de-acetylating E2F-1 could decrease the proteins half-life or reduce stability, and hence alter transcription of E2F-1 target genes like *MMP1* and *MMP13*. It is possible that de-acetylation of E2F-1 by HDAC3 leads to E2F-1's degradation through a yet unknown mechanism and blocks binding to DNA or activation of other transcription factors. For example, E2F-1 protein levels are regulated by the ubiquitin-proteasome-dependent degradation pathway and tight control of E2F-1 levels is a prerequisite to allow for particular cell cycle transition (Campanero & Flemington 1997; Harper & Elledge 1999). Therefore, upon HDAC3 de- acetylation ubiquitin- proteasome -mediated degradation of E2F-1 could be triggered. Moreover, the effect of HDAC3 loss on *FRA1* immediate early gene expression was discussed in sections **3.3.4.2** and **3.3.4.3**, though whether E2F-1 affects *FRA1* expression, which in turn might regulate MMPs was not studied and is yet to be determined.

5.4.5 HDAC3 and E2F-1 are required for normal cell cycle progression.

In the present study, we extended the characterization of HDAC3 function and its existing relationship with E2F-1 transcription factor during the cell cycle. This is partly because of the KEGG Pathway and GO terms predicted in my microarray experiment which included apoptosis and regulation of cell proliferation annotations in addition to the well known role of E2F-1 in controlling cell cycle progression. Interestingly, we showed by flow cytometry that HDAC3 siRNA can mimic the effect of an E2F-1 siRNA on cell cycle progression, by blocking the G1/S phase transition of the cell cycle similar to E2F-1 interference (**Figure 5.10**). This could lead to a delay of cell growth, cell differentiation or chondrocyte maturation during endochondral ossification. Moreover, the lack of an additive effect of the double HDAC3/ E2F-1 depletion on cell cycle proliferation, suggests that these two proteins can be found in the same regulatory pathway. Altogether, HDAC3 participates in a positive regulation of the E2F-1- mediated G1/S transition. HDAC3 may be required for the recruitment of E2F-1 to its target gene promoters or modulate E2F-1 deacetylation status that could modify its binding properties to DNA. Another prospect is that HDAC3 depletion could abrogate the expression of a gene whose expression is required for E2F-1 binding to specific targets during the G1/S transition.

Cytokine or growth factor stimulation has been generally linked to activating CDK (Cyclin dependent kinases) which phosphorylate Rb, which in turn is released from E2F-1 or E2F-1/DP complexes. Free E2F-1 can induce transcription of several genes involved in cell cycle entry, induction or inhibition of apoptosis. (Ertosun et al. 2016) Furthermore, E2F-1 regulates expression of various cytokines and growth factor receptors, establishing positive or negative feedback mechanisms. (Ertosun et al. 2016) In particular, IL-1β has been suggested to cause growth arrest in human melanoma cell line A375-C6 by increasing phosphorylation of Rb protein, while over-expressing E2F-1 reverted growth inhibition. (Muthukkumar et al. 1996) While IL-1β obstruct E2F-1 function, E2F-1 seems to induce IL-1α release. In keratinocytes transformed with E7 protein or HPV-16, E2F-1 over-expression induced IL-1α release and apoptosis (Iglesias et al. 1998). E2F-1 was shown to be required for NF-κB- mediated IL-1β expression, and binding sites of both have been found on IL-1β. In particular, following E2F-1 siRNA depletion, the expression of four pro-inflammatory cytokines was impaired including CCL3, IL23A, IL-1β and TNF-α, indicating an adverse relationship between E2F-1 and IL-1β. (Lim et al. 2007)

5.5 Conclusions

- HDAC3 can interact with E2F-1 transcription factor *in vitro*. These findings imply a role for HDAC3 on modifying E2F-1 function.
- E2F-1 binding sites have been predicted on both *MMP1* and *MMP13* promoters and transient transfections of luciferase constructs support these sites are functional.
- Over-expressing E2F-1 reduced the transactivation of all MMP luciferase reporters, while HDAC3 inhibition or gene depletion also decreased luciferase activation.
- Gene silencing of E2F-1 up-regulated *MMP1* and *MMP13* expression.
- Finally, HDAC3 and E2F-1 are required for normal cell cycle progression, since loss of either or both induced cell cycle arrest at the G1 phase. Moreover, the lack of an additive effect of the double *HDAC3*/ *E2F-1* knockdown on cell cycle proliferation, suggests that these two proteins can be found in the same regulatory pathway.

5.6 Hypothetic model of HDAC3 and E2F-1 in the SW1353 cells.

Our hypothesis is that HDAC3 could be responsible for de-acetylating E2F-1 transcription factor and HDAC3 inhibition or depletion leads to an increase in acetylated E2F-1. So far, acetylated E2F-1 has only been linked to an induction of apoptosis, though it is likely that a conformational change mediated by increased acetylation allows better E2F-1 access to DNA. Acetylated E2F-1 could bind either directly to MMP1/13 promoters and block transcription or abrogate transcription of intermediate molecules required for MMP expression.

HDAC3 loss increases acetylation of E2F-1, which in turn might increase DNA binding and block transcription of MMP1/13.

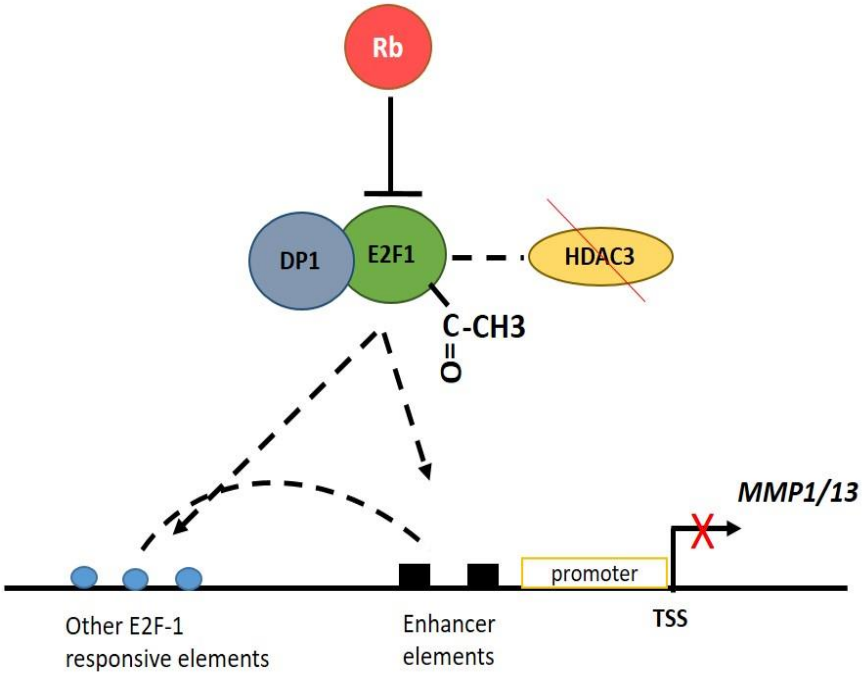

Chapter 6. The role of HDAC3 in chondrogenesis in a human mesenchymal stem cell model system.

6.1 Introduction

In vivo, human mesenchymal stem cells (MSC) are multipotent cells that can proliferate as undifferentiated cells but have the potential to differentiate into mesenchymal lineages including bone, cartilage, fat, tendon, muscle, and marrow stroma. (Ferrari et al. 1998; Jiang et al. 2002; Pittenger et al. 1999) This differentiation is regulated by specific intrinsic and extrinsic determinants that affect gene expression profiles, signal transduction pathways and epigenetic modifications. (Smith 2001) Thus specific growth factors that are contained in the respective media of MSCs in culture will induce the expression of genes, which will cause differentiation for a particular lineage. (Barry et al. 2001; Darfoul et al. 2006)

Briefly, for the initiation of the chondrogenic process, mesenchymal stem cells from the bone marrow aggregate to form high density condensations (Onyekwelu et al. 2009). Essential for this process are many transcription factors, especially SOX9 which will promote the expression of ECM genes including type II collagen and aggrecan (Akiyama 2008). *In vitro*, chondrocyte differentiation of MSCs can be achieved in a similar process driven by TGF-β stimulation over a 14-day differentiation period (Murdoch et al. 2007). However, in different cell models, for example the mouse embryonic carcinoma ATDC5 cells, induction of chondrogenesis is achieved by insulin and the cells require 14-21 days to differentiate into chondrocytes and 42 days for the maturation into hypertrophich chondrocytes. (Chen et al. 2005; Tare et al. 2005) Therefore, there is increasing interest for MSCs as a source to repair diseased or damaged tissues for new therapeutic strategies in regenerative medicine. In particular, osteoarthritis (OA) patients who experience severe cartilage damage may benefit from autologous MSC-derived *in vitro* preparations of cartilage. (Roelofs et al. 2013)

OA has a strong genetic component; however numerous studies have failed to identify genes that provide the full genetic susceptibility to the disease. This could be a result of low penetrance polymorphisms in the general population, but it is also suggested that in part, this could be accounted for by epigenetic modifications such as DNA methylation, histone modifications and microRNAs (miRNAs) (Barter et al. 2012). Regulation of histone acetylation/ deacetylation for example by HAT/ HDAC complexes holds promise in the field of OA. In addition to the HDACi studies in chondrocytes,(Young et al. 2005) (see also

Chapter 3),the role of HDACi was studied in MSC differentiation and chondrogenesis. HDACi have pleiotropic effects on cell homeostasis, and under distinct developmental conditions can promote either self-renewal or differentiation of embryonic stem cells. (Kretsovali et al. 2012)

Previous studies suggested that histone deacetylases regulate the expression of many ECM components produced by chondrocytes. In particular, it has been shown that short-term treatment of human bone-marrow derived MSCs with TSA, an HDAC pan-inhibitor, induced anabolic gene expression of *COL2α1*, *COL9α1*, and *ACAN* and enhanced cartilage matrix formation (El-Serafi et al. 2011). In contrast, extended treatment of primary articular chondrocytes with the same HDACi repressed many of these transcripts (Huh et al. 2007). However, others have suggested that treatment of human MSCs with TSA suppressed the TGF-β1- induced chondrogenic differentiation partly through inhibition of the TGF-β1-induced transcription factor Sp1 (Wang et al. 2011). More recently, Carpio et al. supported that HDAC3 is important for normal endochondral ossification and HDAC3 deficient chondrocytes exhibited reduced abundance of chondrogenic genes such as *COL2α1*, *Ihh*, *ACAN* and *COL10α1*. (Carpio et al. 2016)

This chapter aims to further establish the contribution of HDACs and particularly of HDAC3 in MSC-derived chondrogenesis over 7 or 14 days of differentiation. Herein, RNAi targeting HDAC3 and drug-inhibitory treatments including TSA and Apicidin will be used to define the role of inhibiting deacetylation early in cartilage development. Matrix deposition and cartilage disc composition will also be determined.

6.2 Aim

- To determine how HDAC inhibition, and particularly HDAC3 depletion or selective inhibition, affects chondrogenic differentiation *in vitro*, using human bone marrow-derived mesenchymal stem cells.

6.3 Results

6.3.1 Differential expression of HDACs in mesenchymal stem cells (MSCs) and MSC-differentiated chondrocytes.

MSCs were cultured in chondrogenic differentiation media either in transwell hanging cell culture inserts or V-bottomed cell culture plates/ tubes (**Figure 6.1 A**). RNA interference for HDAC3 or HDACi treatments were performed before the induction of chondrogenesis as described in sections **2.2.7** ***RNA interference (RNAi)***and **2.1.7** ***Histone Deacetylase Inhibitors*** respectively. A flexible, translucent cartilage disc or cell pellet was formed in each case. Gene expression data for cartilage ECM components and transcription factors in conjunction with proteoglycan quantification, histology and immunohistochemistry were used to assess chondrogenic differentiation, as previously described. (Murdoch et al. 2007; Barter et al. 2015)

RNA-seq analysis revealed all HDACs are differentially expressed in MSCs (Day 0 MSCs- before inducing chondrogenic differentiation) (**Figure 6.1 B**) (data provided by Kathleen Cheung, PhD student, Newcastle University). *HDAC1* and *HDAC2* are expressed at the highest level in MSCs (FPKM: fragments per kilobase of exon per million fragments mapped ~20-25), while *HDAC3*, *HDAC5*, *HDAC6*, *HDAC7* and *HDAC8* exhibited medium expression (FPKM ~ 15). *HDAC4*, *HDAC10* and *HDAC11* are present at lower levels (FPKM ~ 5), whilst *HDAC9* is barely detectable in MSCs (FPKM < 2). During chondrogenesis, class I HDACs including *HDAC1*, *HDAC2*, *HDAC3* and *HDAC8* are also expressed, with maximum *HDAC3* expression observed after 6 days of differentiation (**Figure 6.1 C**), after which it declined to its initial levels. *HDAC2* and *HDAC8* showed similar expression patterns with increased expression values during the first 3 days of the chondrogenic period and decrease of their expression thereafter. Finally, *HDAC1* was the most highly expressed class I HDAC at Day 0, yet showed decreased expression after the addition of TGF-β3 and the induction of chondrogenic differentiation. These results were also confirmed by microarray analysis for Day 0 and Day 14 (data provided by Dr Matt Barter, Newcastle University) (**Figure 6.1 D**).

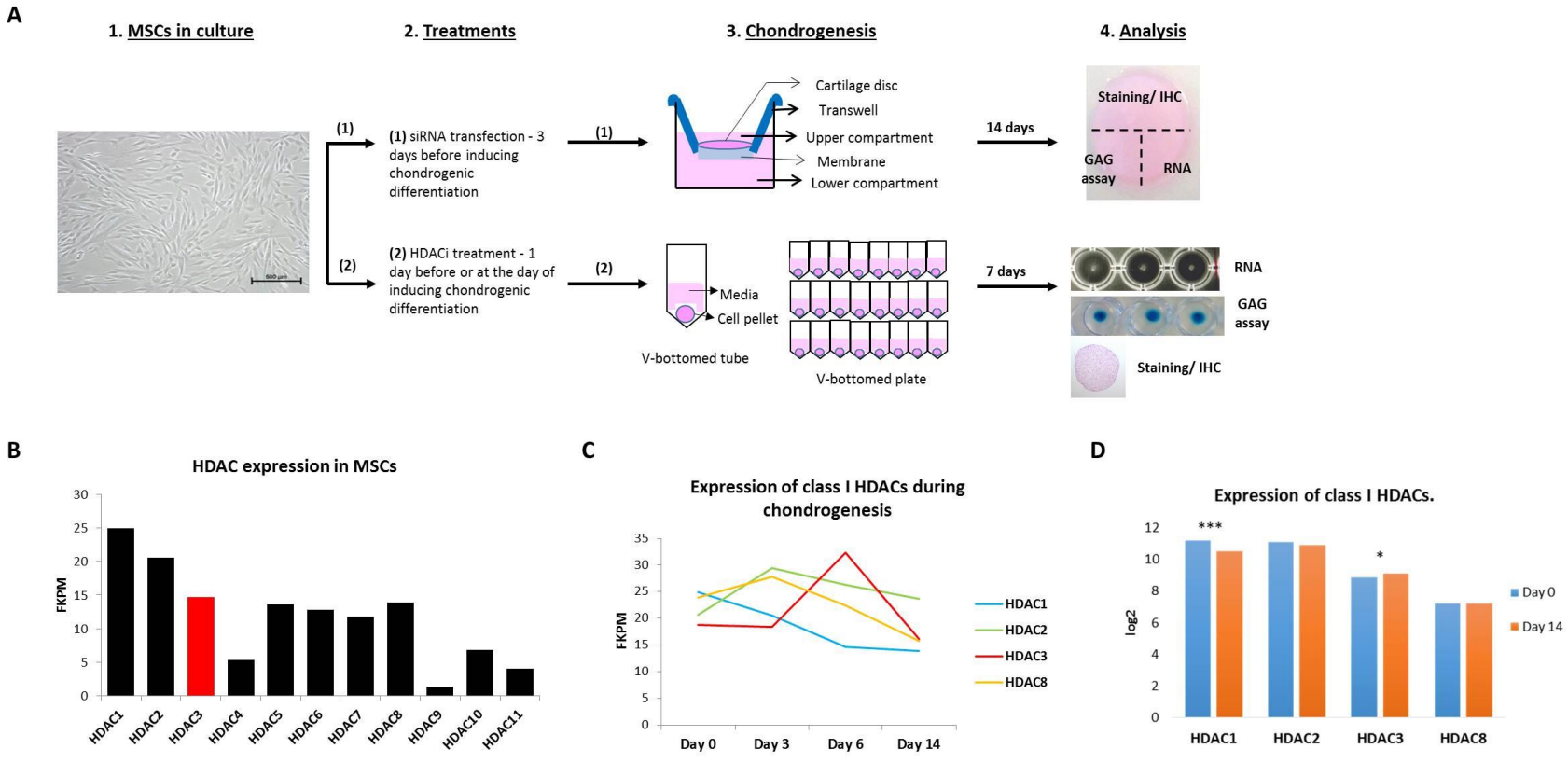

Figure 6.1. Differential expression of HDACs in human bone marrow- derived mesenchymal stem cells (MSCs).

MSCs were pre-treated with HDAC3 siRNA **(1)** or HDACi **(2)** before they were cultured in chondrogenic differentiation media over 14 or 7 days in hanging transwell inserts or cell culture tubes/ plates to form a cartilaginous disc or cell pellet respectively and analysed as indicated above. Bar= 500µm, **B.** MSCs were cultured in maintenance medium and RNA was isolated from confluent cells. RNA-seq was used to measure expression levels of HDACs. For each bar the gene counts (fragments per kilobase of exon per million fragments mapped, FPKM) and normalised expression are shown from one MSC donor. **C.** Class I HDAC expression at indicated time-points during MSC chondrogenesis. **D.** Relative expression values (log2) of class I HDAC expression at Day 0 and Day 14 during MSC chondrogenesis based on microarray data (n=3 per timepoint). * $p<0.05$, *** $p<0.001$

6.3.2 HDAC inhibition affects chondrogenic differentiation of human bone marrow-derived mesenchymal stem cells.

6.3.2.1 The effect of HDAC inhibition on the acetylation of lysine residues and α-tubulin.

Considering the fact that HDAC4 null mice have severe skeletal defects (Vega et al., 2004), while HDAC3 global knockout mice are embryonic lethal (Bhaskara et al., 2010) and bone-specific HDAC3 conditional knockout mice had impaired ossification, an investigation of whether MSCs respond to HDAC inhibitors (HDACi) such as TSA, a pan-HDACi, and Apicidin, a selective HDAC3 inhibitor was performed. First, immunohistochemistry was used to test whether HDAC inhibitors induce acetylation by using a total acetyl-α-tubulin antibody and a pan acetyl-lysine antibody. As anticipated, treatment of MSCs with 165nM TSA one day before inducing chondrogenesis (Day -1 treated MSCs) (**Figure 6.2 A-B**) or at the day of the induction of differentiation (Day 0 treated MSCs) (**Figure 6.2 C-D**) resulted in hyper-acetylation of α-tubulin and protein lysine residues. In particular, MSC treatment with TSA increased the percentage of acetylated lysines by 10% when treated at Day -1 (**Figure 6.2 B, top**) and by 11% when treated at Day 0 (**Figure 6.2 D, top**), while acetylation of α-tubulin was increased by 19% when treated at Day -1 (**Figure 6.2 A, top**) and by 6% when treated at Day 0 (**Figure 6.2 C, top**). In contrast, treatment of MSCs with 80nM Apicidin did not have any effect on the acetylation status of α-tubulin or changed the acetylation of protein lysine residues, as identified by immunohistochemistry for the indicated antibodies (**Figure 6.2 A-B-C-D, bottom**). Quantification of the DAB staining was measured using ImageJ software as previously described in section **2.2.17** ***Image analysis***.

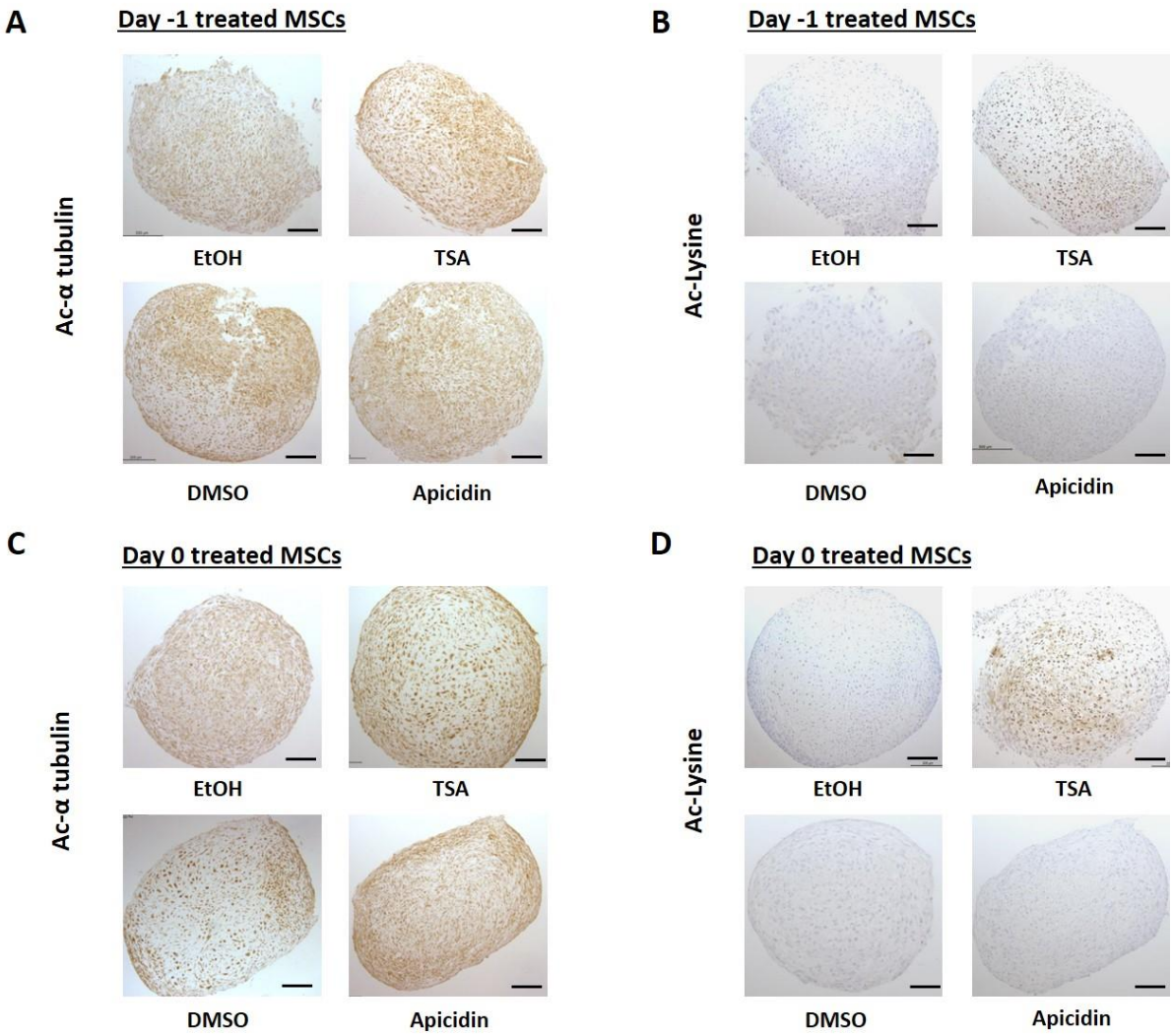

Figure 6.2. Effect of HDACi treatments on acetylation of MSCs.

MSCs were cultured in maintenance media and treated either with 160nM TSA or 80nM Apicidin, 24h before the addition of chondrogenic media (Day -1) (**A** and **B**), or at the day of inducing chondrogenesis (Day 0) (**C** and **D**). Chondrogenic differentiation was induced over 7 days in cell culture tubes and media was replaced after one day (Day -1 treated cells) or three days (Day 0 treated cells) and differentiation followed in the absence of HDACi. TSA was dissolved in ethanol (EtOH, 0.1%) and Apicidin was diluted in DMSO (0.2%), which served as vehicle controls. **A-C.** Immunohistochemistry was performed using an anti- acetylated α- tubulin antibody and, **B-D.** An anti-acetylated lysine antibody. Bar = 200μm

6.3.2.2 The effect of HDAC inhibition on cartilage gene expression and matrix deposition during MSC-derived chondrogenesis.

Next, the effect of the HDACi on ECM deposition and cartilage gene expression was determined. Three methods of chondrogenesis were performed: (i) cell pellets were formed in V-bottomed 96 well plates and used for RNA quantification, (ii) cell pellets were formed in 14ml falcon tubes and used for histology and (iii) micromass cell cultures were performed in 24-well plates and used for alcian blue staining.

MSCs from three different donors were cultured in V-bottomed 96-well plates to form smaller cell pellets (50,000 cells per pellet) and three pellets per treatment were formed (i). HDACi treatments were performed as described in section **6.3.2.1 The effect of HDAC inhibition on the acetylation of lysine residues and α-tubulin..** Chondrogenic differentiation was then performed over seven days. The media was replaced after one day (for the Day -1 treated cells) or after three days (for the Day 0 treated cells) and differentiation followed with the absence of HDACi. The smaller cell pellets were used for gene expression analysis using qRT-PCR. The expression of chondrogenic markers measured included type II collagen, aggrecan and the transcription factor *SOX9*. Alternatively, cells from the same MSC donors were cultured in V-bottomed tubes (14ml falcon tubes) in order to form cell pellets (500,000 cells per pellet) and used for histological scoring (ii). As above, cells were differentiated for seven days after HDACi treatments had been previously performed. In order to establish if there were any morphological differences among the HDACi treated cell pellets formed, H&E histologic staining was performed. Additionally, safranin-O staining for determining proteoglycan deposition and Masson's trichrome staining for the detection of collagen fibres were used to assess matrix composition of the newly differentiated/synthesized cartilage. Finally, micromasses of MSCs from one donor (250,000 cells/ micromass) were assessed with alcian blue staining as a marker of mucopolysaccharides formation (iii). MSCs were treated with HDACi one day prior to inducing chondrogenesis and allowed to differentiate for five days in the absence of HDACi.

No difference in the gross morphology of all the cell pellets was observed for the Day -1 treated or Day 0 treated controls; EtOH versus DMSO (**Figure 6.3 A-C**). Also there was no difference between the TSA and EtOH treated cell pellets or the Apicidin and DMSO treated pellets following seven days of chondrogenic differentiation, regardless as to whether the MSCs were treated one day prior to the induction of chondrogenesis or on the day of induction. The expression of selected chondogenic markers including *SOX9* gene were quantified at the end of the differentiation period. Results from three different donors were

combined and showed a trend towards decreased, but non- significant, *SOX9* expression (**Figure 6.3 B-D**). It is worth noting that *SOX9* expression has been shown to reach its maximum level as early as day one of this MSC- chondrogenesis model, and remains at the same levels, or lower, thereafter up to day fourteen. (Barter et al. 2015)

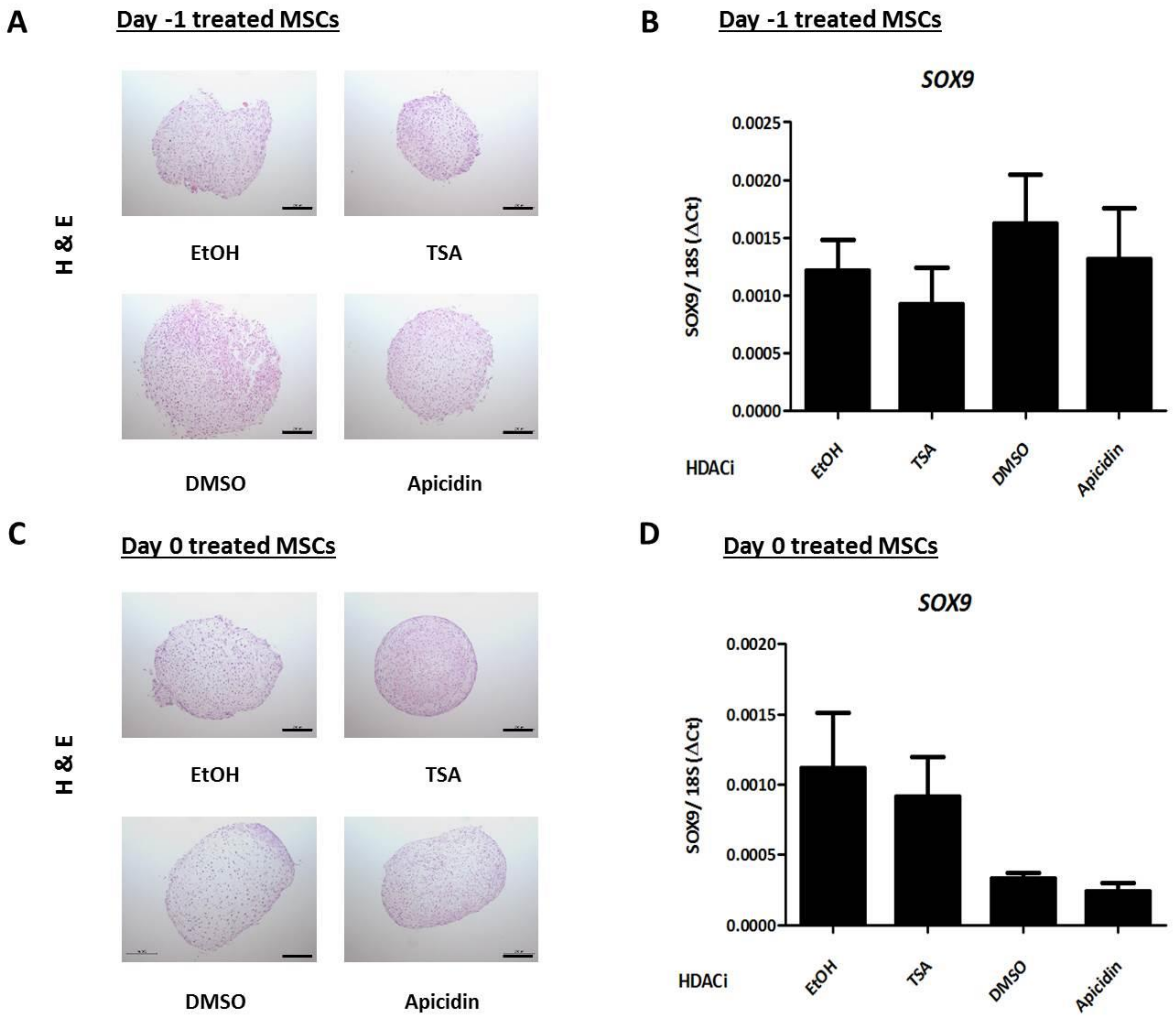

Figure 6.3. Effect of HDACi treatments on cell pellet morphology and gene expression of differentiated- MSCs.

MSCs were cultured in maintenance media before treatments either with 160nM TSA or 80nM Apicidin, 24h before the addition of chondrogenic media (Day -1 treated MSCs) (**A-B**), or on the day of inducing chondrogenesis (Day 0 treated MSCs) (**C-D**) were performed. Chondrogenic differentiation was induced over 7 days in cell culture plates/tubes and media was replaced after one day (for the Day -1 treated cells) or three days (for the Day 0 treated cells) and differentiation followed in the absence of HDACi. TSA was diluted in ethanol (EtOH, 0.1%) and Apicidin was diluted in DMSO (0.2%), which served as vehicle controls. **A-C.** Cell pellets were harvested at day 7, fixed, sectioned and stained for H&E. Bar= 200µm **B-D.** RNA was extracted from MSCs undergoing chondrogenic differentiation at day 7 and *SOX9* expression was assessed by qRT- PCR and normalized to 18S. Results are representative of the gene expression data pooled from three separate

MSC donors and bars show the mean +SD. For statistical analysis, an unpaired two-tailed student's t-test was performed.

However, histological staining for Safranin-O, that stains for cartilage proteoglycans (Goldring & Marcu 2009; Martel-Pelletier et al. 2008), revealed a difference in the Day 7 stained cell pellets. In particular, red staining (which corresponds to the amount of proteoglycans present in cartilage), was present in the EtOH and DMSO control cartilage formed after seven days of differentiation. HDAC inhibition reduced the amount of red staining at the indicated time-points (**Figure 6.4 A-C**). Furthermore, the TSA treated cell pellets were consistently smaller than the controls, indicating TSA may have impaired chondrogenesis (**Figure 6.4 A, top**). Because of the importance of aggrecan for cartilage (Martel-Pelletier et al. 2008), more emphasis was given to the expression of this gene. *ACAN* expression was significantly decreased at the Day -1 TSA treated MSCs ($p= 0.02$) when compared to the ethanol control, confirming the observations of the Safranin-O stained cell pellets (**Figure 6.4 B**). Apicidin treatment also showed decreased *ACAN* expression of the Day -1 treated MSCs, but these results were not statistically significant (**Figure 6.4 B**). The same observation towards reduced *ACAN* expression was found for the Day 0 TSA treated MSCs following seven days of differentiation (**Figure 6.4 D**). However, Apicidin had no significant effect in the expression of aggrecan. There is therefore very little evidence that inhibiting HDAC3 selectively before or after the initiation of the chondrogenic process alters chondrogenic gene expression.

Chondrogenesis can also be indicated by alcian blue staining, which stains mucopolysaccharides (mainly glycosaminoglycans (GAG)), and can be quantified by extracting alcian blue using guanidine hydrochloride (GuHCl) (see also **2.2.15.5 Alcian Blue staining**). MSCs were pre-treated with HDACi, as previously described, one day prior to inducing chondrogenesis. The cells were then seeded in micromasses in 24-well plates and differentiation was induced for five days in the absence of HDACi. As expected from the previous results, TSA treatment showed a decrease of alcian blue staining, while Apicidin treatment caused an increase, but neither significantly (**Figure 6.5 A-B**). These results were only validated using cells from one MSC donor.

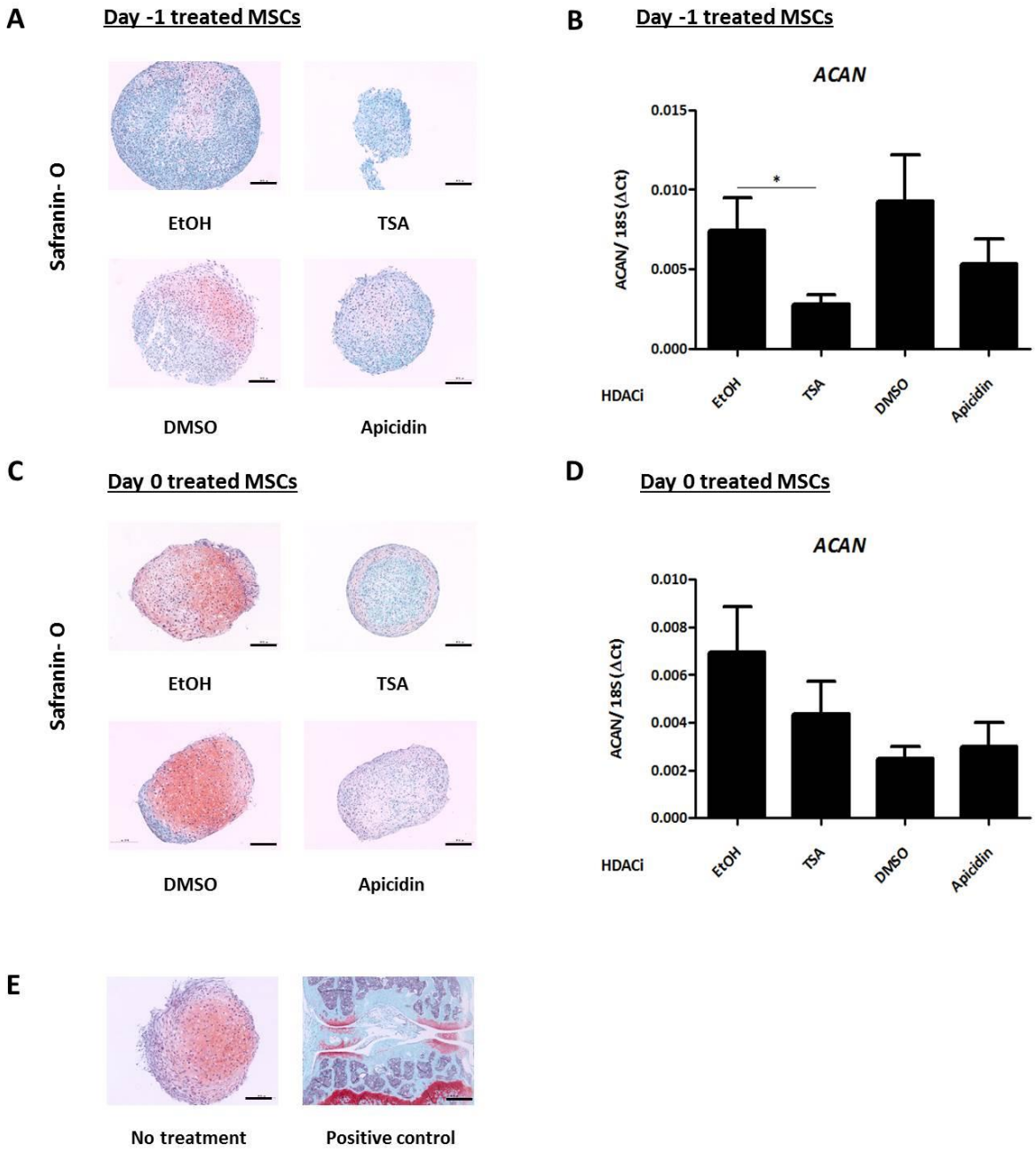

Figure 6.4. Effect of HDACi treatments on aggrecan gene expression and proteoglycan deposition of differentiated- MSCs.

MSCs were cultured in maintenance media before treatments either with 160nM TSA or 80nM Apicidin, 24h before the addition of chondrogenic media (Day -1 treated MSCs) (**A-B**), or at the day of inducing chondrogenesis (Day 0 treated MSCs) (**C-D**) were performed. Chondrogenic differentiation was induced over 7 days in cell culture plates/tubes and media was replaced after one day (for the Day -1 treated cells) or three days (for the Day 0 treated cells) and differentiation followed in the absence of HDACi. TSA was diluted in ethanol (EtOH, 0.1%) and Apicidin was diluted in DMSO (0.2%), which served as vehicle controls. **A-C.** Cell pellets were harvested at day 7, fixed, sectioned and stained for Safranin-O. Bar= 200μm **E.** A cell pellet that had no treatment was included in the experiment (Bar= 200μm) and a wild-type mouse knee joint section served as a positive control (Bar= 500μm) **B-D.** RNA was extracted from MSCs undergoing chondrogenic differentiation at day 7 and *ACAN* expression was assessed by qRT- PCR and normalized to 18S. Results are representative of

the gene expression data pooled from three separate MSC donors and bars show the mean +SD. For statistical analysis, an unpaired two-tailed student's t-test was performed. * $p<0.05$

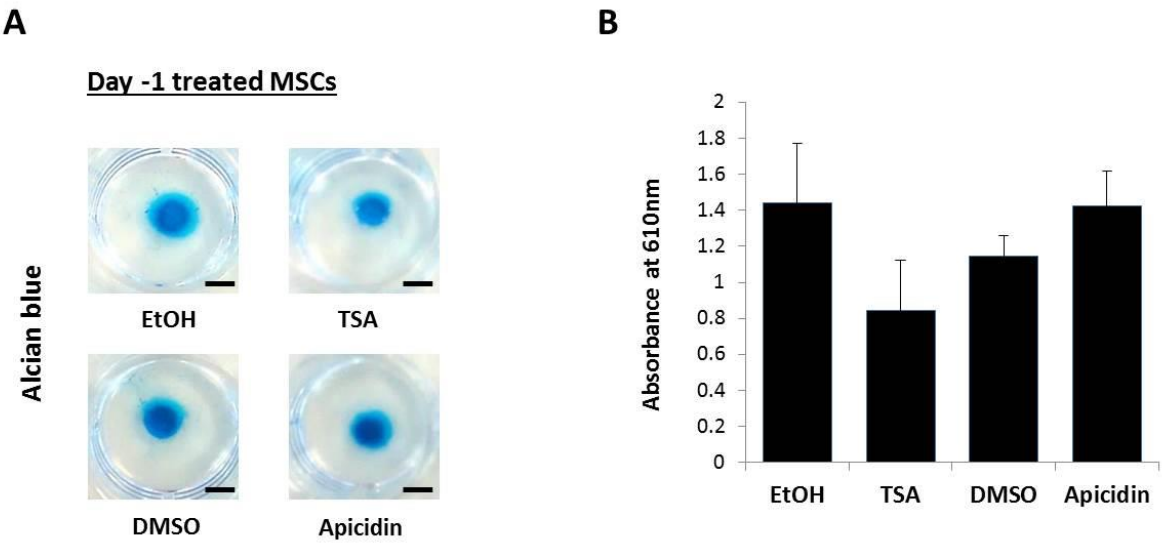

Figure 6.5. Alcian Blue staining was used as a marker of cartilage formation.

A. MSCs were cultured in maintenance media before treatments either with 160nM TSA or 80nM Apicidin or EtOH (0.1%) or DMSO (0.2%) were performed one day prior to inducing chondrogenesis. Chondrogenic differentiation was then induced over 5 days in tissue culture plates, the cells were seeded in micromasses and media was replaced every 2-3 days without any HDACi and up to day 5. Bar= 0.5cm **B.** Alcian blue was extracted using guanidine hydrochloride (GuHCl) and absorbance measured at 610nm. Data are representative of three biological replicates using cells from one MSC donor. For statistical analysis, an unpaired two-tailed student's t-test was performed.

Finally, Masson's trichrome staining was used to reveal collagen fibres present in the matrix of differentiated MSCs, following HDACi treatment. Type II collagen expression was also quantified with qRT- PCR. My results indicate there was no difference in collagen fibre presence in the Day -1 or Day 0- treated MSCs between the control and HDACi treated samples (**Figure 6.6 A-C**). Also, although there was a trend of decreased *COL2A1* expression in the TSA samples of the Day-1 treated MSCs these results were not significant. Moreover, no significant difference was found when comparing the DMSO to the Apicidin samples in both time points as well as in the TSA treated samples of the Day 0 MSCs (**Figure 6.6 B-D**).

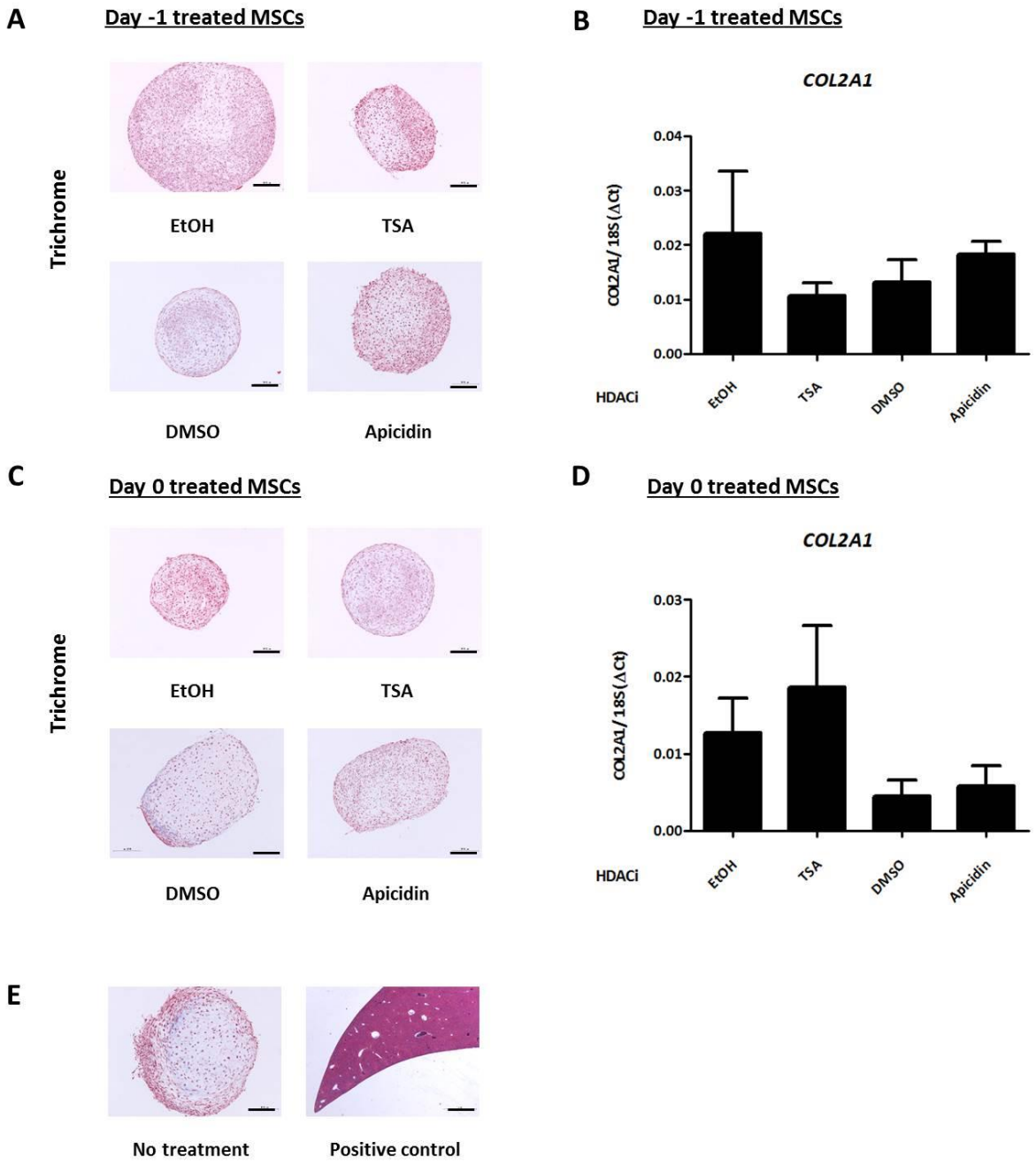

Figure 6.6. Effect of HDACi treatments on collagen fibres deposition and type II collagen gene expression of differentiated- MSCs.

MSCs were cultured in maintenance media before treatments either with 160nM TSA or 80nM Apicidin, 24h before the addition of chondrogenic media (Day -1 treated MSCs) (**A-B**), or at the day of inducing chondrogenesis (Day 0 treated MSCs) (**C-D**) were performed. Chondrogenic differentiation was induced over 7 days in cell culture plates/tubes and media was replaced after one day (for the Day -1 treated cells) or three days (for the Day 0 treated cells) and differentiation followed in the absence of HDACi. TSA was diluted in ethanol (EtOH, 0.1%) and Apicidin was diluted in DMSO (0.2%), which served as vehicle controls. **A-C.** Cell pellets were harvested at day 7, fixed, sectioned and stained for Masson's trichrome. Bar= 200µm **E.** A cell pellet that had no treatment was included in the experiment (Bar= 200µm) and a wild-type mouse liver section served as a positive control (Bar= 1mm) **B-D.** RNA was extracted from MSCs undergoing chondrogenic differentiation at day 7 and *COL2A1* expression was assessed by qRT- PCR and normalized to 18S. Results are

representative of the gene expression data pooled from three separate MSC donors and bars show the mean +SD. For statistical analysis, an unpaired two-tailed student's t-test was performed.

6.3.3 HDAC3 gene silencing increases anabolic gene expression in MSC chondrogenesis.

To further establish the role of HDAC3 in MSC chondrogenesis, a siRNA against HDAC3 mRNA was used to specifically deplete *HDAC3* from MSCs before the induction of chondrogenesis. MSCs from two independent donors were cultured in maintenance media in tissue culture plates and transfected at 40-50% confluency with 100nM of siHDAC3 or a non-targeting control siRNA (siCON) three days before the induction of chondrogenesis, as described in section **2.2.6**. Chondrogenic differentiation was then performed in hanging transwell filters (500.000 cells per transwell) over fourteen days and the media was replaced at day 3, 7, 10, 12 up to day 14 as described in (Barter et al. 2015). Two cartilage discs were formed for each time-point per MSC donor, and cells frozen at Day 0 were also included in all experiments. For each time-point transwell discs were harvested and either frozen for RNA extraction and gene expression quantification by qRT- PCR or fixed in 4% paraformaldehyde and processed into paraffin wax. Sections cut at 4 µm were either stained with H&E, Safranin O, or Masson's trichrome. A quarter of each disc was also used for glycosaminoglycans (GAG) quantification (GAG assay) and normalised to the disc's DNA content. Immunoblotting was also performed using a disc from each donor to establish HDAC3 protein levels following siRNA transfection during the differentiation period.

All discs formed had a normal morphology and no weight difference was detected between the siHDAC3 and siCON treated samples at Day 14 (**Figure 6.7 A**). *HDAC3* knockdown efficiency was confirmed with immunoblotting (**Figure 6.7 B**) and qRT- PCR (**Figure 6.7 D**) at Day 3, Day 7 and 14 during the differentiation period as well as with immunohistochemistry (**Figure 6.7 C**) at Day 14. Quantification of the immunohistochemistry with ImageJ software (as described in section **2.2.17** ***Image analysis***) showed there was 52% less HDAC3 staining in the siHDAC3 Day 14 cartilage discs when compared to the siCON discs.

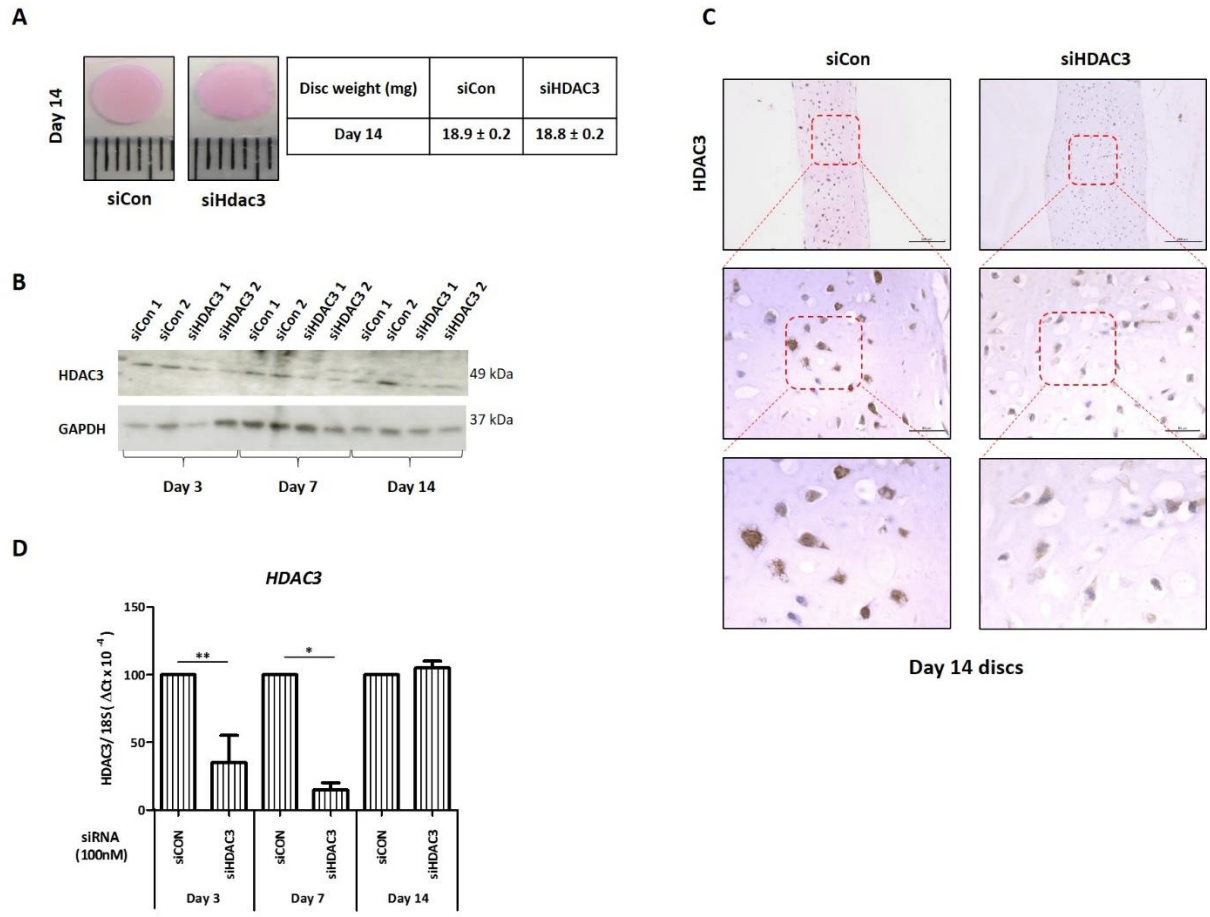

Figure 6.7. Effect of HDAC3 gene silencing on cartilage disc formation of differentiated-MSCs.

MSCs were transfected for 3 days with a HDAC3-targeting or a non-targeting control siRNA (100nM) prior to inducing chondrogenic differentiation for 14 days in hanging transwell inserts. **A.** Day 14 cartilage discs showed normal morphology and similar weight (average of 4 discs per treatment/ time-point from 2 independent MSC donors). **B.** Day 3, 7 and 14 cartilage discs were harvested, lysed and total protein extraction was performed. Immunoblotting was performed with an anti- HDAC3 antibody and GAPDH served as a loading control. **C.** Day 14 cartilage discs were harvested, fixed, sectioned and stained for an anti-HDAC3 antibody. Bar (top)= 200µm and Bar (bottom)= 50µm **D.** RNA was extracted from MSCs undergoing chondrogenic differentiation at the indicated time-points between Day 0 and Day 14 and *HDAC3* expression quantified by qRT- PCR. Results are shown relative to 18S ribosomal RNA expression. Significance was determined with respect to siCON treated cells in comparison to the siHDAC3 treated cells. Results are representative of the gene expression data pooled from two separate MSC donors and bars show the mean +SD. For statistical analysis, an unpaired two-tailed student's t-test was performed. ** $p<0.01$, * $p<0.05$

The cells in both the siCON and siHDAC3-treated discs had similar morphology as detected by H&E staining at the end of the differentiation period (Day 14) (**Figure 6.8 A**). However, *HDAC3*-depleted differentiated chondrocytes exhibited increased expression of genes related to extracellular matrix production including *ACAN* [**Figure 6.8 B (iii)**] at Day 14 and *COL2A1* [**Figure 6.8 B (ii)**] at Day 3 and Day 14. The chondrogenic marker SOX9 was also significantly increased at Day 14 [**Figure 6.8 B (i)**]. In accordance with the *ACAN* expression, proteoglycan deposition detected by Safranin-O staining showed higher deposition of proteoglycans of the Day 14 HDAC3-depleted cartilage discs in comparison to the siCON discs (**Figure 6.8 A**). Additionally, a significantly increased GAG content was found in the siHDAC3 treated discs when compared to the siCON discs at Day 7, while no significant difference was observed at Day 3 or Day 14 (**Figure 6.8 C**), indicating that *HDAC3* might play an important role in the regulation of genes such as aggrecan earlier rather than later in chondrogenesis. Nonetheless, Masson's trichrome staining for the detection of collagen fibres, shows a decrease of collagens, as the real-time results for *COL2A1* suggested. Increased expression for matrix-remodelling enzymes such as *MMP13* (**Figure 6.9 H)** was also detected in the siHDAC3 treated discs, following 14 days of differentiation.

Notably, none of the other genes analysed showed any significant difference in their expression as a result of *HDAC3* depletion, including the osteoblast markers *COL1A1* and RUNX2, hypertrophic and differentiation/maturation chondrocyte markers such as *COL10A1*, *COL11A1*, *COL9A1*, *MATN3* and the MSC-condensation marker *N-Cadherin* (**Figure 6.9 A-G**). Although these data did not show a significant statistical difference, all genes showed a trend towards increased expression up to Day 3 followed by a decrease at Day 14, suggesting that *HDAC3* knockdown increases the expression of matrix genes and cytokine-induced remodelling enzymes early in chondrocyte development and differentiation. Also the reduction of *COL1A1*, *COL11A1*, *COL9A1* and *COL10A1* expressions could explain the decreased trichrome staining found on the Day 14 siHDAC3 discs (**Figure 6.8 A**).

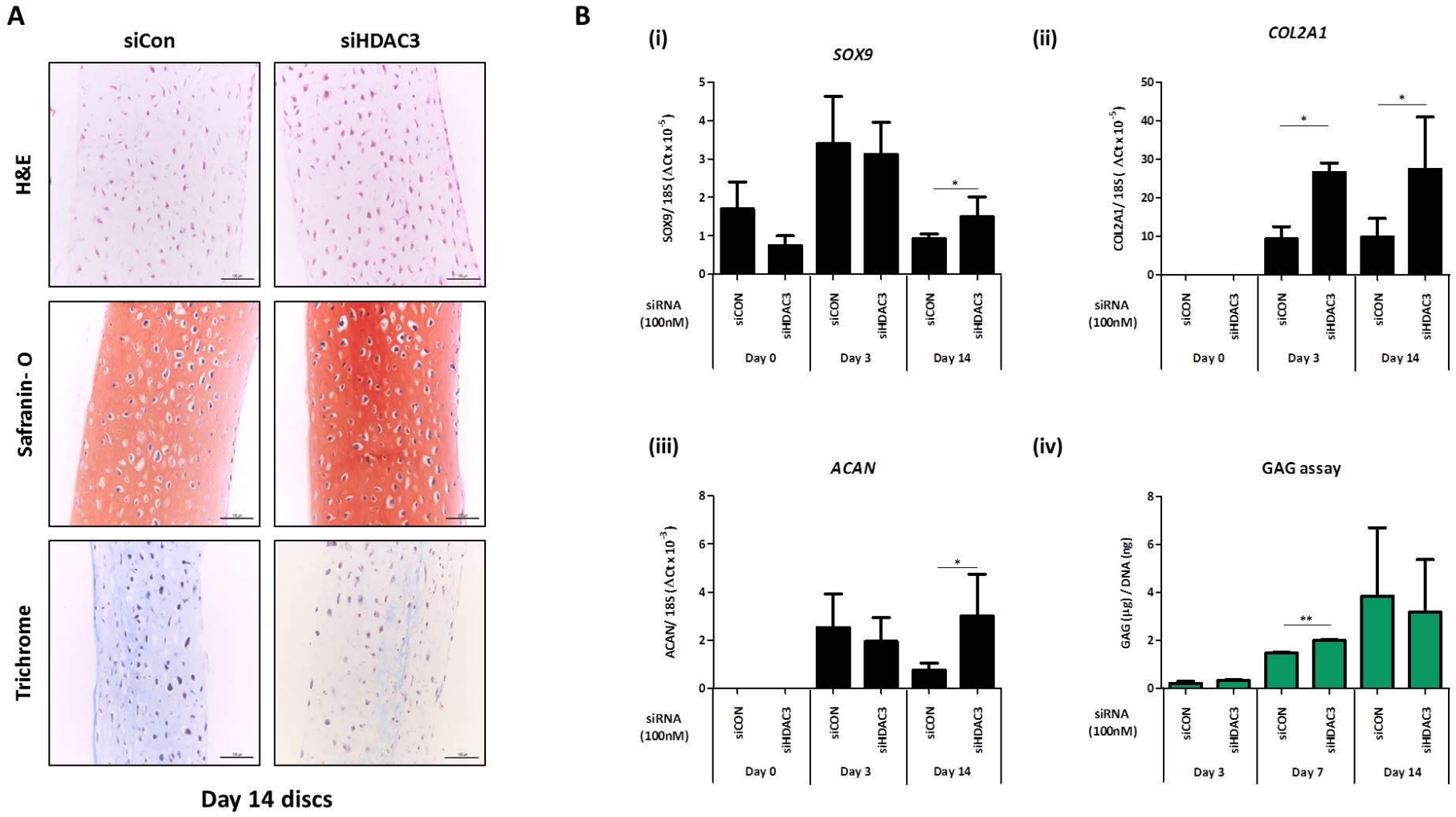

Figure 6.8. Effect of *HDAC3* gene silencing on matrix components deposition and cartilage gene expression of differentiated-MSCs.

MSCs were transfected for 3 days with a HDAC3-targeting or a non-targeting control siRNA (100nM) prior to inducing chondrogenic differentiation for 14 days in hanging transwell inserts. **A.** Day 14 cartilage discs were harvested, fixed, sectioned and stained for H&E, Safranin-O and Masson's trichrome. Bar= 100μm **B.** RNA was extracted from MSCs undergoing chondrogenic differentiation at the indicated time-points between Day 0 and Day 14 and gene expression quantified by qRT- PCR and normalised to 18S ribosomal RNA expression. Significance was determined with respect to siCON treated cells in comparison to the siHDAC3 treated cells. Results are representative of the gene expression data pooled from two separate MSC donors and bars show the mean +SD. For statistical analysis, an unpaired two-tailed student's t-test was performed. **C.** Quantification of cartilage GAG-bearing proteoglycans after performing papain digestion at 60^{o}C overnight to solubilize cartilage components. Dimethyl-methylene blue (DMB) was added and the results were read at 530nm. The results obtained from the GAG assay above were subsequently normalised with reference to the DNA levels contained to each sample and expressed as μg GAG/ ng DNA. **$p<0.01$, * $p<0.05$

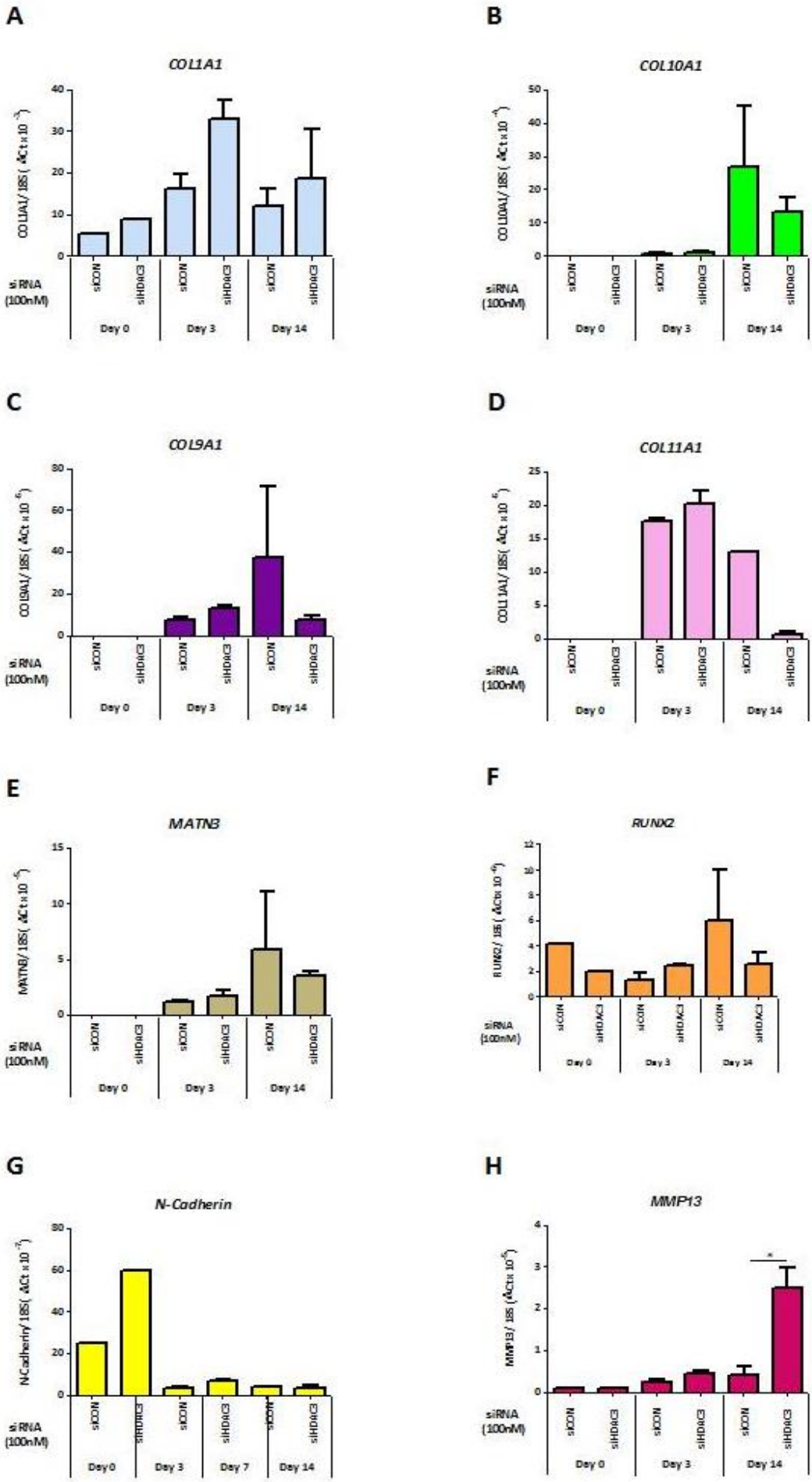
A
COL1A1
COL1A1/ 18S (ΔCt x 10 -3)
si RNA (100nM)
siCON
siHDAC3
Day 0
Day 3
Day 14
B
COL10A1
COL10A1/ 18S (ΔCt x 10 -4)
C
COL9A1
COL9A1/ 18S (ΔCt x 10 -6)
D
COL11A1
COL11A1/ 18S(ΔCt x 10 -5)
E
MATN3
MATN3/ 18S(ΔCt x 10 -5)
F
RUNX2
RUNX2/ 18S (ΔCt x 10 -6)
G
N-Cadherin
NCadherin/ 18S(ΔCt x 10 -7)
Day 7
H
MMP13
MMP13/ 18S (ΔCt x 10 -5)
*

Figure 6.9. Effect of *HDAC3* gene silencing on cartilage gene expression during MSC-chondrogenic differentiation.

MSCs were transfected for 3 days with a HDAC3-targeting or a non-targeting control siRNA (100nM) prior to inducing chondrogenic differentiation for 14 days in hanging transwell inserts. RNA was extracted from MSCs undergoing chondrogenic differentiation at the indicated time-points between Day 0 and Day 14 and gene expression quantified by qRT- PCR. Results are shown relative to 18S ribosomal RNA expression. Significance was determined with respect to siCON treated cells in comparison to the siHDAC3 treated cells. Results are representative of the gene expression data pooled from two separate MSC donors and bars show the mean +SD. For statistical analysis, an unpaired two-tailed student's t-test was performed. *$p<0.05$

6.4 Discussion

Histone deacetylases (HDACs) play a major role in chromatin remodelling, gene regulation and cellular signaling. While the role of each class of HDACs during normal development and chondrocyte differentiation is unclear, recent reports suggest HDAC inhibitors are embryo-toxic and can impair normal chondrogenesis and osteogenesis (Paradis & Hales 2015). More specifically, treatment of E12 embryonic forelimbs from COL2A1-ECFP, COL10A1-mCherry, and COL1A1-YFP CD1 reporter mice with the class I HDAC inhibitor MS-275 reduced the expression of *COL2A1*, *COL10A1* and *COL1A1*, suggesting gene expression regulatory effects of class I HDACs on both chondrogenesis and osteogenesis (Paradis & Hales 2015). Moreover, the bone-specific HDAC3 conditional knockout mouse model (Razidlo et al. 2010) and cartilage-specific HDAC3 inducible conditional knockout mouse model (Carpio et al. 2016) supported HDAC3 depletion interfere both with normal bone and cartilage formation.

Herein, an established chondrogenesis model (Barter et al. 2015) was used to determine how HDAC inhibition and *HDAC3* depletion or selective inhibition affects chondrogenic differentiation *in vitro*, using human bone marrow-derived mesenchymal stem cells. MSCs were transfected with a siRNA targeting HDAC3 for three days, before the induction of chondrogenesis with medium containing TGF-β3, and then cultured in hanging transwell inserts for up to 14 days. In this way the cells receive media from the top and bottom surface when a cartilage disc is starting to form, having more optimal nutrient access (Murdoch et al. 2007). Alternatively, MSCs were pre-treated with TSA or Apicidin one day before the induction of chondrogenesis or at the day of the induction. The cells were cultured in V-bottomed cell culture tubes/plates for up to 7 days for the formation of cell pellets which were then used for cartilage gene expression and matrix deposition analysis (**Figure 6.1 A**).

RNA-seq analysis revealed HDAC1-11 are differentially expressed in MSCs (**Figure 6.1 B**). In particular, *HDAC1* and *HDAC2* were expressed at highest expression in MSCs, while *HDAC3*, *HDAC5*, *HDAC6*, *HDAC7* and *HDAC8* exhibited medium expression. *HDAC4*, *HDAC10* and *HDAC11* are present in lower levels, whilst *HDAC9* is barely detectable in MSCs. The differential expression of HDACs and sirtuins have also been reported in adipose-derived MSCs by (Dudakovic et al. 2015). During chondrogenesis, class I HDACs including *HDAC1*, *HDAC2*, *HDAC3* and *HDAC8* are also expressed, with *HDAC3* maximum expression observed after 6 days of differentiation (**Figure 6.1 C**) and microarray analysis showed no class I HDAC exhibited significant differences in their expression between Day 0 and Day 14 in chondrogenesis (**Figure 6.1 D**).

6.4.1 HDACi agents including TSA and Apicidin negatively regulate the ability of MSCs to differentiate into cartilage.

My analysis revealed that HDACi treatment with TSA 24 hours prior to inducing chondrogenesis or at the day of the induction resulted in hyperacetylation of acetyl-α tubulin and acetyl-lysine residues (**Figure 6.2**) of the Day 7 cell pellets. As expected, Apicidin did not result in hyper-acetylation of α-tubulin, since it is a HDAC3 selective inhibitor (Khan & Davie 2013) and de-acetylation of α-tubulin is largely regulated by the catalytic activity of HDAC5 and HDAC6 (Cho & Cavalli 2012; Hubbert et al. 2002). Apicidin did not increase acetylation of lysine residues. In this study, histone acetylation at and near the genes analysed, such as aggrecan or type II collagen was not studied. However, data provided by Kathleen Cheung (PhD student, Newcastle University) for the H3K27Ac active enhancer marker showed an increase during chondrogenesis approximately 20Kb away from the *COL2A1* promoter and 10Kb from the *ACAN* promoter, which correlated to an increase in their gene expression during chondrogenesis (unpublished data). Similar experiments using MSCs-treated with vorinostat, another broad-spectrum HDACi revealed hyper-acetylation of histone-H3 (Xu et al. 2013), while human adipose derived MSCs-treated with SAHA, a class I HDAC inhibitor resulted in hyper-acetylation of both histone H3 and histone H4 (Dudakovic et al. 2015).

MSCs pre-treated with HDACi prior to inducing chondrogenesis showed decreased *ACAN* expression and proteoglycan deposition (**Figure 6.4** and **Figure 6.5**). In particular, Safranin-O staining revealed there was less peptidoglycans present at the TSA- and Apicidin- treated Day 7 cell pellets in comparison to the EtOH- and DMSO- treated control cells. Accordingly, aggrecan expression was significantly reduced in the TSA-treated cells, whilst the pellets formed were much smaller in size than those of the controls, suggesting HDAC pan-inhibition in MSCs might impair differentiation into the chondrogenic lineage. Apicidin treatment also showed decreased *ACAN* expression of the Day -1 treated MSCs and a slight increase when treated at Day 0, but these results were not statistically significant. As expected from the previous results, TSA treatment also decreased alcian blue staining, while Apicidin treatment had no effect (**Figure 6.5**). Moreover, no difference was found in cell morphology or the expression of the chondrogenic marker *SOX9* with neither HDACi at the end of the differentiation period (**Figure 6.3**). In accordance with these results, MSCs which were induced to undergo osteogenic or chondrogenic differentiation and treated with TSA, showed a slight but not significant increase in *RUNX2* and *SOX9* expression respectively. (Hye Joung et al. 2016) Furthermore, TGF-β1 induced chondrogenesis of MSCs was inhibited when cells

were exposed to TSA. Decreased chondrogenic gene expression of genes such as aggrecan, type II collagen and *SOX9* and chondrogenic proteins were found in the TSA-treated samples. (Wang et al. 2011) Also TGF-β1- mediated activation of Sp1 was suppressed in the presence of TSA, whereas when Sp1 was over-expressed the TSA-mediated inhibition of TGF-β1 induced chondrogenesis was abolished. (Wang et al. 2011)

Along with the aforementioned genes (aggrecan and SOX9), the expression of type II collagen was quantified using qRT- PCR and collagen content determined using Masson's trichrome staining. No significant effect on type II collagen expression was observed following pan-HDACi. Hye Joung et al., showed that TSA treatment alone failed to alter *COL2A1* expression, yet when TSA was combined with a hypo-methylating agent (HMA), 5-azacytidine (5-azaC), MSC chondrogenic and osteogenic differentiation were enhanced, as evidenced by increased type II collagen protein levels and increased calcium deposition and osterix expression respectively (Hye Joung et al. 2016). Based on these observations, the ability of the 5-azaC agent to induce chondro and osteo- differentiation was studied alone and it was shown that hypo-methylation plays a dominant role in enhancing MSC differentiation. (Hye Joung et al. 2016)

On the contrary, El-Serafi *et al.,* showed that pre-treatment of MSCs for 3 days with TSA, followed by culture in the absence of TSA enhanced cartilage matrix formation and chondrogenic structure, as indicated by increased *SOX9* and aggrecan expression 4 weeks after the induction of chondrogenesis (El-Serafi et al. 2011). In contrast, TSA decreased adipogenesis of bone-marrow derived MSCs when treated with 50 or 500nM for 2 days before the initiation of the differentiation. However the 500nM dose has proven to be cyto-toxic for the cells as it decreased cell proliferation. (Zych et al. 2013) Vorinostat an HDACi which is currently in a clinical phase III trial for multiple myeloma patients has been previously reported to cause bone loss. When the effect of vorinostat was tested on MSC-derived osteogenic differentiation, it was found that it inhibited the viability of MSCs in a dose-dependent manner, but it was also demonstrated that at lower concentrations it promotes osteogenic differentiation. (Xu et al. 2013) Also, administration of 100mg/kg vorinostat *in vivo* in mice for three weeks did not result in any bone loss. (Xu et al. 2013) Another study which utilized SAHA HDACi on adipose-derive MSCs showed that SAHA interfered with osteogenesis, adipogenesis and chondrogenesis. It also induced loss of differentiation potential of MSCs, by changing the expression of principal transcription factors that control mesenchymal or pluripotent states including *NANOG*, *OCT4*/*POU5F1*, and *SOX2*. In

addition, induction of the chondrogenic gene *SOX6* was not detected when SAHA was present, but clearly induced when the agent was removed. (Dudakovic et al. 2015)

Huh and colleagues found that HDAC activity in primary articular chondrocytes decreases during de-differentiation induced by monolayer culture and that HDAC activity recovered during re-differentiation induced by three-dimensional culture in a cell pellet. Inhibition of HDACs with TSA or PXD101, a class I HDAC selective inhibitor, was sufficient to block type II collagen expression in primary culture chondrocytes. HDAC inhibition also blocked the re-differentiation of de-differentiated chondrocytes by suppressing the synthesis and accumulation of type II collagen. HDAC inhibition promoted the expression of Wnt-5a, which is known to inhibit type II collagen expression, and knockdown of Wnt-5a blocked the ability of HDAC inhibitors to suppress type II collagen expression. In addition, the induction of Wnt-5a expression by HDAC inhibitors was associated with acetylation of the Wnt-5a promoter. Taken together, these results suggest that HDACs promote type II collagen expression in part by suppressing the transcription of Wnt-5a. (Huh et al. 2007)

To achieve better therapeutic strategies with the use of MSCs, it is a prerequisite to retain their pluripotency properties during *ex vivo* expansion. Although some studies have indicated that ageing of MSC in culture cause gradual loss of their differentiation potential (Lee et al. 2004; Li et al. 2011), more recently Han and colleagues demonstrated that an effective supplement for MSC pluripotency and differentiation potential is the TSA HDACi. In particular, it has been shown that in the presence of low concentrations of TSA (6.25nM), the acetylation of histone H3 at K9 and K14, particularly near pluripotent genes including *OCT4*, *SOX2* and *TERT* in passage 6 MSCs showed no significant difference compared to passage 1 MSC, which allowed them to retain their primitive pluripotency properties. Low doses of this HDACi markedly prevented the de-acetylation of histone H3 K9 and 14 and the appearance of ageing signs, whilst higher doses (200-300nM) were cyto-toxic. (Han et al. 2013)

My results indicate that the expression of chondrogenic genes *ACAN*, *COL2A1* and *SOX9* involves HDAC-dependent mechanisms, yet further studies are required to fully understand the molecular mechanisms of MSC differentiation. It is obvious that data regarding the effect of different epigenetic agents on MSC differentiation remains controversial. All of the discrepancies among the studies, including ours, may be associated with variations in experimental designs, with heterogeneity in the cells originating from various species such as humans, rats and mice or from different MSC sources including bone marrow, fat and cord blood could provide further explanation. Furthermore, variations in the type or dose of the HDACi used among the studies could also provide an explanation. In our study, cells were

exposed to the HDACi either 24h prior to inducing chondrogenesis or for 3 days after the induction. Other studies have included the epigenetic regulators throughout the differentiation period, therefore for slightly longer duration (Hye Joung et al. 2016). These influences of the individual epigenetic modifiers and for optimal doses and dose schedules could be researched and further optimized to achieve better differentiation for future studies. Another factor that we need to take into account is the half-life of each HDACi and hence its impermanent effect, which for example is 6.3 min for TSA it is upon peritoneal administration (Elaut et al. 2007), while for Apicidin is 0.8-1.1h upon intravenous injection (Shin et al. 2014).

Additionally, other epigenetic modifications may contribute differently in MSC chondrogenesis and/or progression of osteoarthritis. For example, one study showed that inhibition of lysine-specific demethylase 6A (UTX) and Jumonji domain- containing 3 (JMJD3) by GSK-J4 inhibitor abrogated expression of chondrogenic genes, such as *SOX9* and *COL2A1* in chondrogenic MSCs, and disrupted glycosaminoglycan and collagen synthesis. GSK-J4 also prevented cartilage destruction and expression of the OA-related genes *MMP13* and *PTGS2* in HACs. (Yapp et al. 2016) It is therefore important to understand how different epigenetic modifications modulate chondrogenesis and progression of OA. Additionally, whole genome ChIP revealed a large number of genes linked to MSC-properties are epigenetically pre-patterned by changes in H3K4me3 and H3K9ac near transcription start sites, but remained transcriptionally unaltered during chondrogenesis. Transcriptionally upregulated genes, more closely associated with chondrogenesis, are marked by H3K36me3 in gene bodies, increased H3K36me3 and H3K9ac on promoters and 5' end and increased H3K27ac and H3K4me1 marking in at least one enhancer region per upregulated gene. Within the 7-day differentiation period changes in promoter DNA methylation do not correlate significantly with gene expression changes. (Herlofsen et al. 2013). Histone modifications rather than DNA methylation may therefore provide the primary epigenetic control of early MSC chondrogenesis.

6.4.2 HDAC3 depletion enhances anabolic gene expression and proteoglycan deposition of MSC-derived cartilage.

Most of the research to date has focused on the effect of broad-spectrum HDACi in combination with de-methylating agents on MSC-derived chondrogenesis. However, the current study takes into account that independent HDACs may contribute differently to the induction of chondrogenic differentiation. To further determine the role of HDAC3 in human MSC-derived chondrogenesis, the RNA interference approach was taken to deplete MSCs of

HDAC3 prior to inducing chondrogenesis as described in (Barter et al. 2015). All cartilage discs formed presented normal morphology (**Figure 6.8 A- H&E staining**), and no weight difference was detected between the siHDAC3 and siCON discs at Day 14 (**Figure 6.7 A**). *HDAC3* knockdown efficiency was confirmed with immunoblotting, qRT- PCR and immunohistochemistry (**Figure 6.7 B-D**).

Interestingly, *HDAC3* knockdown resulted in increased chondrogenic gene expression, including genes such as aggrecan [**Figure 6.8 B (iii)**] at Day 14 and type II collagen [**Figure 6.8 B (ii)**] at Day 3 and Day 14. Besides these genes, the chondrogenic marker *SOX9* also presented a significant increase at Day 14 [**Figure 6.8 B (i)**]. In concordance with the aggrecan expression, proteoglycan deposition detected by Safranin-O staining showed higher content of proteoglycans at the Day 14 siHDAC3 discs when compared to the siCON discs (**Figure 6.8 A**). Additionally, a significantly increased amount of GAGs were found in the siHDAC3 treated discs at Day 7, yet no significant difference was observed at Day 3 or Day 14 (**Figure 6.8 C**). Nevertheless, trichrome staining for the detection of collagens, failed to show an increased abundance of collagens, as the real-time PCR data suggested for type II collagen. Notably none of the other genes studied (*COL1A1*, *RUNX2*, *COL10A1*, *COL11A1*, *COL9A1*, *MATN3*, *N-Cadherin*) showed any difference in their expression, except for *MMP13* (**Figure 6.9 H)** which was significantly induced in the siHDAC3 treated discs, following 14 days of differentiation. Finally, the reduction of *COL1A1*, *COL11A1*, *COL9A1* and *COL10A1* expressions could be an explanation of the decreased trichrome staining found on the Day 14 siHDAC3 discs (**Figure 6.8 A**).

Embryonic deletion of HDAC3 in type II collagen α1 expressing tissues is lethal as shown in the next chapter and also by (Carpio et al. 2016). However, postnatal deletion of HDAC3 in articular chondrocytes showed increased expression of cytokine and matrix-degrading genes such as *IL-6*, *MMP3*, *MMP13* and *Saa3* and activation of signalling pathways, classically related to inflammation. Reduced abundance of genes related to extracellular matrix production, bone development and ossification has also been observed in the same study, where *ACAN*, *COL2A1*, *Ihh* and *COL10A1* were reduced in contrast to our gene expression data, suggesting a role for HDAC3 in the final stages of chondrocyte maturation. (Carpio et al. 2016) Our results could be explained by the fact that when HDAC3 is lost, inhibition of deacetylation may result in altered affinity of transcription factors for DNA binding sites on target gene regulatory regions. It could also be a direct effect on signaling molecules responsible for the chondrogenic process and induction of chondrogenic genes, an altered interaction with other transcription factors or an altered protein half-life.

In a similar way, when Hdac3 was conditionally deleted from osteo-/chondro- progenitor mouse cells with Osx1-Cre, severe osteopenia was caused due to abnormal maturation of osteoblasts and decreased long bone length. (Bradley et al. 2013) To address this abnormal phenotypes the role of HDAC3 was evaluated in chondrocyte differentiation. This study demonstrated that HDAC3 was highly expressed in the resting and pre-hypertrophic zone of the growth plate chondrocytes as well as in articular chondrocytes. HDAC3-deficient chondrocytes entered hypertrophy sooner and were smaller than normal chondrocytes. ECM production was suppressed, evidenced by GAG secretion and production of aggrecan, osteoponin and matrix extracellular phosphoglycoprotein. These findings led to the hypothesis that Akt/mTOR pathway was repressed in Hdac3-deficient chondrocytes, because Akt promotes hypertrophy and matrix production in many tissues. Indeed, phosphorylation and activation of Akt, its substrate mTOR and the mTOR substrate, p70 S6 kinase were reduced in Hdac3-deficient chondrocytes. Constitutive expression of Akt restored phosphorylation of mTOR and p70 S6 kinase as well as matrix gene expression levels. Reduced expression of Akt in Hdac3-deficient chondrocytes and chondrocytes treated with HDACi correlated with increased expression of the phosphatase *Phlpp1* gene. It was found that HDAC3 associates with a *Phlpp1* promoter region containing Smad binding elements and was released after the addition of TGF-β in culture. These results demonstrated that HDAC3 plays an important role in chondrocyte hypertrophy and extracellular matrix production by repressing *Phlpp1* expression and facilitating Akt activity. (Bradley et al. 2013)

Injuries or age-related cartilage degeneration that occurs in osteoarthritic patients demands effective repair strategies. Thus the discovery and use of mesenchymal stem cells (MSCs) that can differentiate into specialised cartilaginous tissue could prove valuable for regenerative medicine purposes. My results suggest that HDAC3 loss prior to the induction of chondrogenesis could prove beneficial for autologous tissue regeneration and repair, since it promotes ECM production/ anabolic gene expression. After obtaining the tissue, cells could be treated in a similar way presented in this chapter and expanded in culture for 14 days for the formation of differentiated-functional chondrocytes. These chondrocytes can then be seeded onto a previously tested scaffold before transplantation back to the patient-donor can take place. Ideally these structures should be made of biocompatible and biodegradable materials capable to provide mechanical strength and to promote implant integration, uniform cell spreading and preserve phenotypes and functional characteristics of the transplanted cells.

6.5 Conclusions

- HDACs are differentially expressed in MSCs.
- HDAC inhibition using TSA, but not Apicidin, induced hyper-acetylation of α-tubulin and total lysines in MSCs.
- MSCs pre-treated with HDACi prior to the induction of chondrogenesis showed decreased anabolic gene expression and proteoglycan deposition as evidenced by safranin-O and alcian blue staining as well as gene expression data for aggrecan.
- No significant difference was found at the type II collagen levels or collagens deposition of the HDACi treated cells.
- *HDAC3* knockdown promoted anabolic gene expression of *SOX9*, *ACAN* and *COL2A1* and increased proteoglycan and GAG content after 14 days of differentiation.
- *HDAC3* knockdown also induced the expression of matrix remodelling enzymes such as *MMP13*.
- My results indicate that the expression of chondrogenic genes involves HDAC-dependent mechanisms, yet further studies are required to fully understand the molecular mechanisms of MSC-derived chondrogenic differentiation.

Chapter 7. The effect of Hdac3 loss in cartilage murine development.

7.1 Introduction

Osteoarthritis is a degenerative joint disease epitomised by articular cartilage loss and has yet no modifying therapies. HDAC inhibitors including TSA have been assessed *in vivo* in surgically induced- and drug induced- osteoarthritis mouse models and showed a chondroprotective role. (Culley et al. 2013; Cai et al. 2015) Cartilage damage was blocked in the presence of TSA and expression of OA-associated enzymes such as MMP1, MMP3 and MMP13 were reduced. (Culley et al. 2013; Cai et al. 2015) The role of TSA has also been assessed *in vivo* in rats, whereby knee joints were intra-articularly injected with mono-iodoacetate (MIA) to induce osteoarthritis. Reduced gene expression and protein levels of MMP1, MMP3, MMP13 and increased expression of *TIMP1* were observed in the TSA-treated group and safranin-O staining indicated cartilage retention, although not to the level of the sham-treated rats. (Qu et al. 2016) However, the exact mechanisms underlying this protective effect remain to be elucidated.

Mutant mice lacking individual HDACs are a powerful tool for defining the functions of individual HDACs *in vivo* and the molecular targets of HDACs inhibitors in disease. Several HDACs have been found to contribute to skeletal development. Deletion of Hdac1 in zebrafish for example causes a variety of skeletal defects. The specific target genes responsible for these phenotypes have not been defined, but it has been proposed that they are downstream of canonical and non-canonical Wnt signalling. (Cunliffe 2004; Cunliffe & Casaccia-Bonnefil 2006; M. Yamaguchi et al. 2005). While global Hdac1 knockout is embryonic lethal (Lagger et al. 2002), Hdac1 deletion in tissues such as the heart, brain, skeletal muscle and smooth muscle is well tolerated in mice, possibly due to functional redundancy with Hdac2 later in development and in post-natal life. (Montgomery et al. 2007) However, there is disagreement regarding the role of Hdac2 *in vivo*, with studies showing null mice are either viable (Trivedi et al. 2007)or show post-natal lethality (Montgomery et al. 2007). Global Hdac3 null mice die before E9.5 due to gastrulation defects and defective DNA- double stranded break repair. (Bhaskara et al. 2011) Deletion of Hdac3 in osteo/chondro- progenitor cells resulted in decreased bone density and severely impaired intramembranous and endochondral bone formation. (Razidlo et al. 2010)

Regarding the role of class II HDACs, Hdac4 deletion has been shown to cause premature ossification of the developing bones accompanied with ectopic hypertrophy of chondrocytes,

resulting in the conversion of cartilaginous skeletal elements to ossified bone, while its overexpression prevents chondrocyte hypertrophy and endochondral ossification. (Vega et al. 2004) Global Hdac6 deficiency modestly enhances trabecular bone formation (Y. Zhang et al. 2008), whereas global Hdac8 loss negatively affects intramembranous ossification (Haberland et al. 2009). Global Hdac7 deletion also leads to embryonic lethality, owing to a loss of integrity and endothelial-cell interactions and consequent rupture of blood vessels and heamorhaging. Furthermore, Hdac7 deletion caused increased expression of MMP10 and subsequent down-regulation of TIMP1 in endothelial cells. (Chang et al. 2006)

When this project was about to start the role of Hdac3 conditional deletion and/or selective inhibition in cartilage development *in vivo* had not been studied. Although previous studies have supported a role for the broad-spectrum inhibitor TSA in protecting cartilage damage in OA (Culley et al. 2013; Cai et al. 2015), Hdac3 selective inhibitors have never been tested for efficacy in preclinical OA models before. The first step to be taken here was to confirm the aforementioned findings by using TSA, but also try the selective Hdac3 inhibitor Apicidin in the destabilized of the medial meniscus (DMM) - surgically induced mouse model. Then, intra-articular delivery of a small interfering RNA for Hdac3 was also attempted in wild-type mice. Finally, the role of Hdac3 in type II collagen expressing tissues was assessed by developing a conditional knockout mouse model through selective breeding.

7.2 Aims

- Determine the consequence of Hdac3 inhibition on DMM-induced osteoarthritis, through the delivery of HDACi (TSA and Apicidin) via intra-articular injections.
- *In vivo* delivery of a siRNA targeting Hdac3 in the joint via intra-articular injections, and determine if there is any effect on cartilage morphology soon after the delivery.
- To establish a chondrocyte-specific Hdac3 conditional knockout mouse model that will be used to study cartilage development *in vivo*.

7.3 Results

7.3.1 The effect of Hdac3 inhibition on a DMM-induced osteoarthritis mouse model.

To define the role of HDAC inhibitors in OA *in vivo*, experiments were performed in wild-type C57BL-6J mice in accordance with the UK Home Office regulations. OA was induced in 10-week old mice, following surgical destabilization of the medial meniscus as described in section **2.2.12**. In this model, cartilage erosion develops primarily in the center of the load-bearing region of the medial tibial plateau and to a lesser extent to the medial femoral condyles, 8 weeks postoperatively (Glasson *et al.*, 2010). To test our hypothesis that HDAC inhibitors have a chondroprotective role *in vivo*, three groups of 6 mice underwent DMM surgery. The first group of mice received DMSO (control), the second one the non-selective HDACi TSA and the third the specific HDAC3i Apicidin. Both HDACi were diluted in DMSO at c= 10mg/ml and delivered immediately following the DMM surgery and via an intra-articular injection two weeks post-surgery. No sham surgeries were performed in this experiment. Four weeks post-DMM the mice were sacrificed and both knee joints were harvested for histologic examination and scoring as previously described (Glasson *et al.*, 2010) (see also **Table 2.10**). Scoring was carried out by two experienced independent scorers blinded to drug treatments and scores were combined and averaged.

Cartilage degeneration was not rescued by TSA or Apicidin treatment (**Figure 7.1**). On the contrary, there were no significant effects of both HDACi in the cartilage of the medial tibial plateau and the femoral condyle in the HDACi treated samples when compared to control-DMSO knee joints (**Figure 7.1 A-B**). However, due to obvious inflammation in three of the TSA treated mice, almost certainly due to an infection, the number of mice taken into account and averaged was reduced to three.

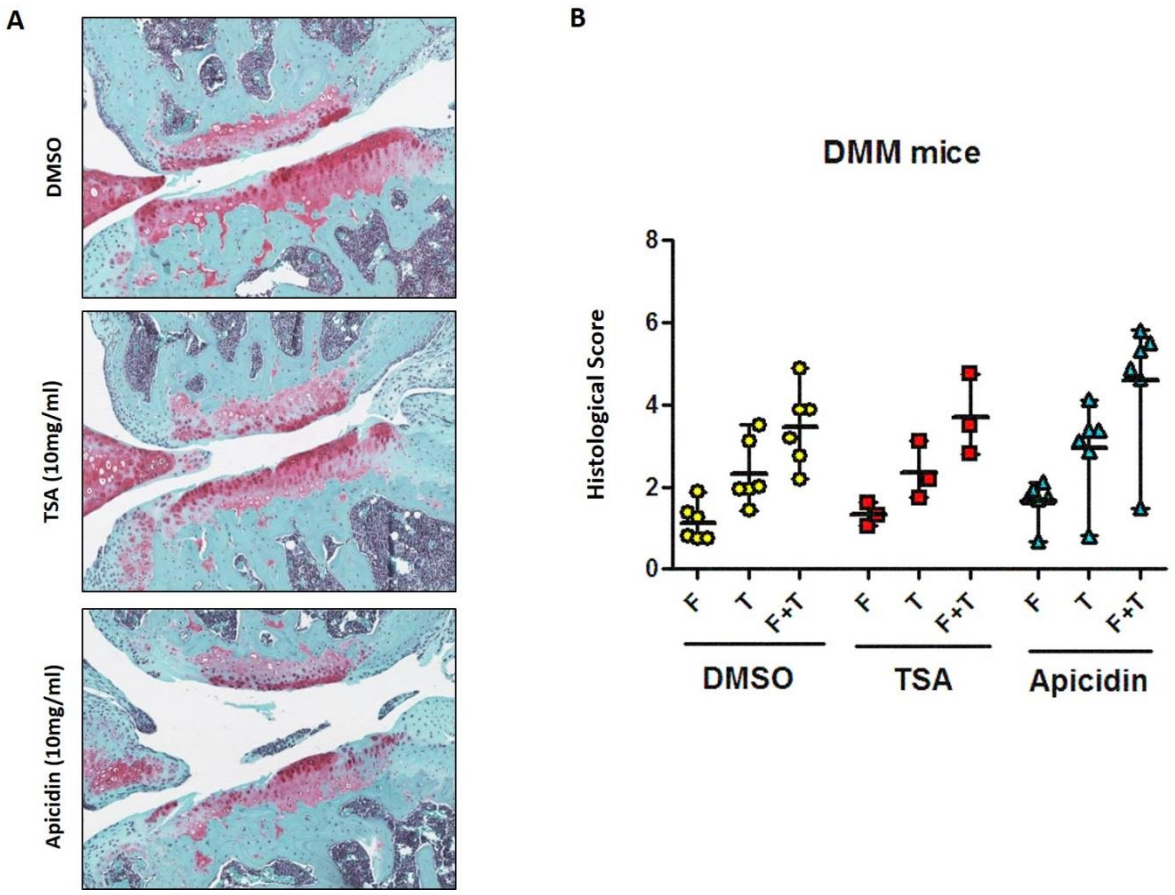

Figure 7.1. In vivo effects of TSA and Apicidin on blocking cartilage destruction in a destabilised of the medial meniscus (DMM) OA mouse model.

Osteoarthritis-like (OA) was induced in C57BL/6J mice following surgical DMM. TSA/Apicidin (10mg/ml) or vehicle control (DMSO) were injected during the surgery and two weeks after the surgery. **A.** Left: Representative coronal sections of the knee joint, stained for Saffranin O-Fast Green. **B.** Histologic scoring of OA (Glasson et al. 2010). Twenty sections from each mouse were scored in a blinded manner by 2 scorers, using a validated scoring system from 0 (normal knee) to 6 (vertical clefts, erosion to the calcified cartilage extending to 75% of the articular surface). Results at 4 weeks post-DMM are shown. Values are the mean +/- range of the maximum scores per 10 sections scored per mouse for the medial femoral chondyle (F), the medial tibial plateau (T) and the sum of the medial femoral chondyle and the tibial plateau (F+T) for each drug treatment (n=6 mice/group) and for TSA (n=3).

7.3.2 Intra-articular delivery of a siRNA targeting HDAC3 in C57Bl/6 mice joints

Next, AteloGene was combined with a siRNA suitable for *in vivo* transfections targeting Hdac3 as described in section **2.2.16**. Two groups of three mice were established, and three different treatments were performed in each group. The first mouse from each group received AteloGene combined with siHDAC3, the second mouse received siHDAC3 in PBS and finally the third mouse received siRNA buffer (siBuffer) plus PBS. All treatments were delivered through intra-articular injections on the left knee joint capsule of each mouse with 0.01% (w/v) Evans blue dye to confirm precision of the injection. The two groups of mice were sacrificed three or six days post- injections and knee joints were harvested, fixed, sectioned and stained with an anti-Hdac3 antibody. If siHdac3 was efficiently transfected to articular cartilage chondrocytes; reduced Hdac3 protein levels would be detected following immunohistochemistry. However, quantification of the staining did not reveal any significant difference among the three treatments neither at Day 3 (**Figure 7.2**) nor at day 6 (**Figure 7.3**), indicating siHdac3 intra-articular delivery was not efficient or it did not penetrate the joint tissue. In particular, 41% of positive staining was found in the siHdac3 + AteloGene treated mouse at day 3 (**Figure 7.2 A**), while 34% of positive stained cells were counted in the second siHdac3 + PBS mouse (**Figure 7.2 B**) and 30% in the third animal which had only siBuffer + PBS (**Figure 7.2 C**). In a similar manner, 48% of staining were observed in the siHdac3 + AteloGene treated mouse at day 6 (**Figure 7.3 A**), while 46% of Hdac3 staining was observed in the siHdac3 + PBS mouse (**Figure 7.3 B**) and 39% in the third siBuffer + PBS treated mouse (**Figure 7.3 C**).

siRNA delivery to the joint is only poorly established and AteloGene has not been widely used for local siRNA administrations and in particular intra-articular injections. This was a very preliminary experiment to decide whether or not AteloGene could be used to deliver siHdac3 *in vivo* in mice.

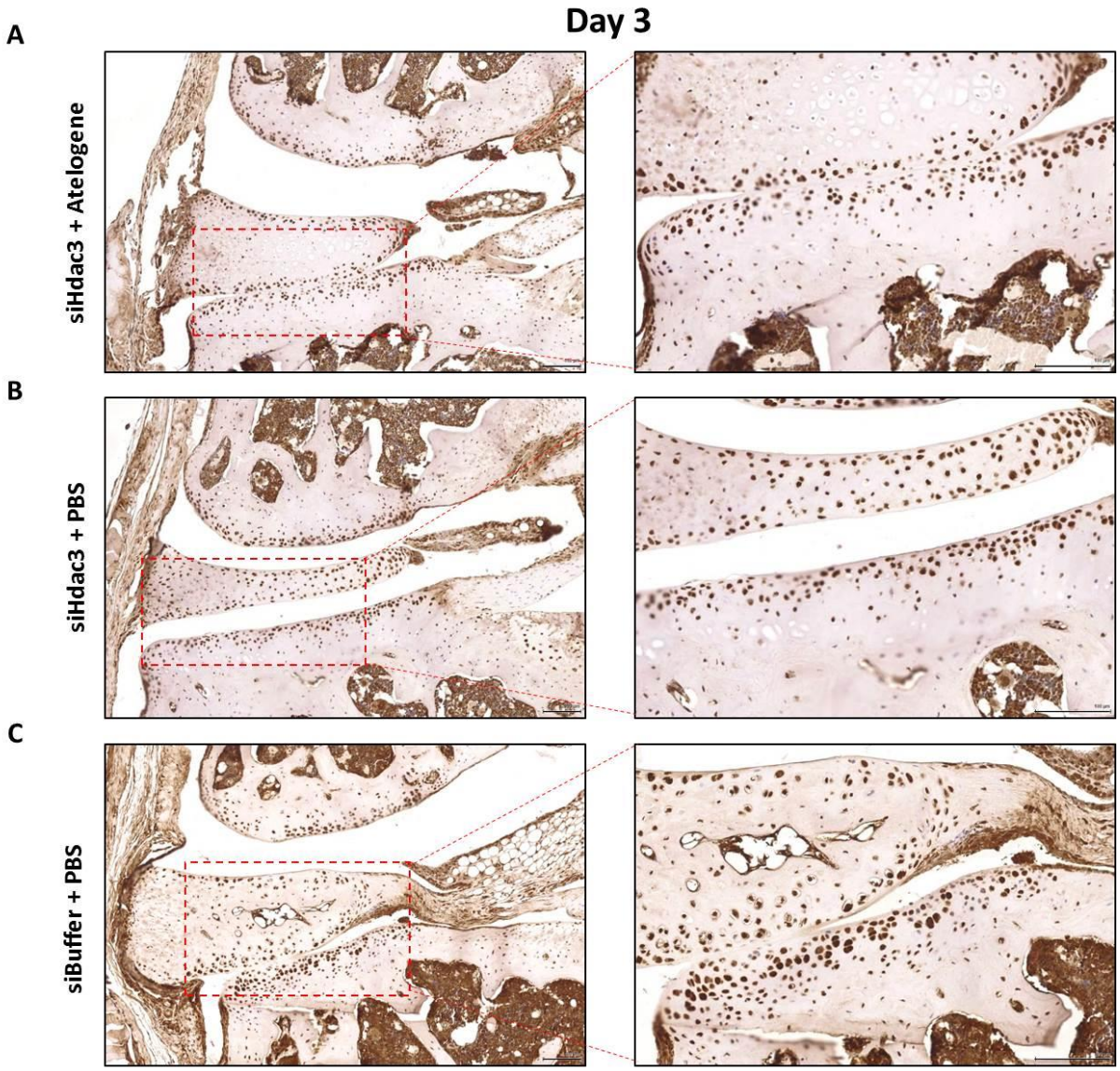

Figure 7.2. *In vivo* efficacy of the intra-articular delivery of a siRNA targeting Hdac3 on the mouse knee joint.

Adult C57BL/6J mice were anaesthetized and intra-articular injections performed in the left knee joint. Treatments included: **A.** siHdac3 (20µM) prepared in siRNA buffer (1.6x, provided in the AteloGene kit) and diluted in AteloGene containing 0.01% Evans blue dye (SIGMA Aldrich). **B.** siHdac3 (20µM) were prepared in siRNA buffer and diluted in PBS including 0.01% Evans blue dye **C.** siBuffer and PBS with 0.01% Evans blue dye were injected into the knee joint. For all treatments 15µl were injected into the joint capsule. Representative coronal sections of the knee joint, stained with an anti-Hdac3 antibody are shown in A-C. Three sections from each mouse were used for quantification.

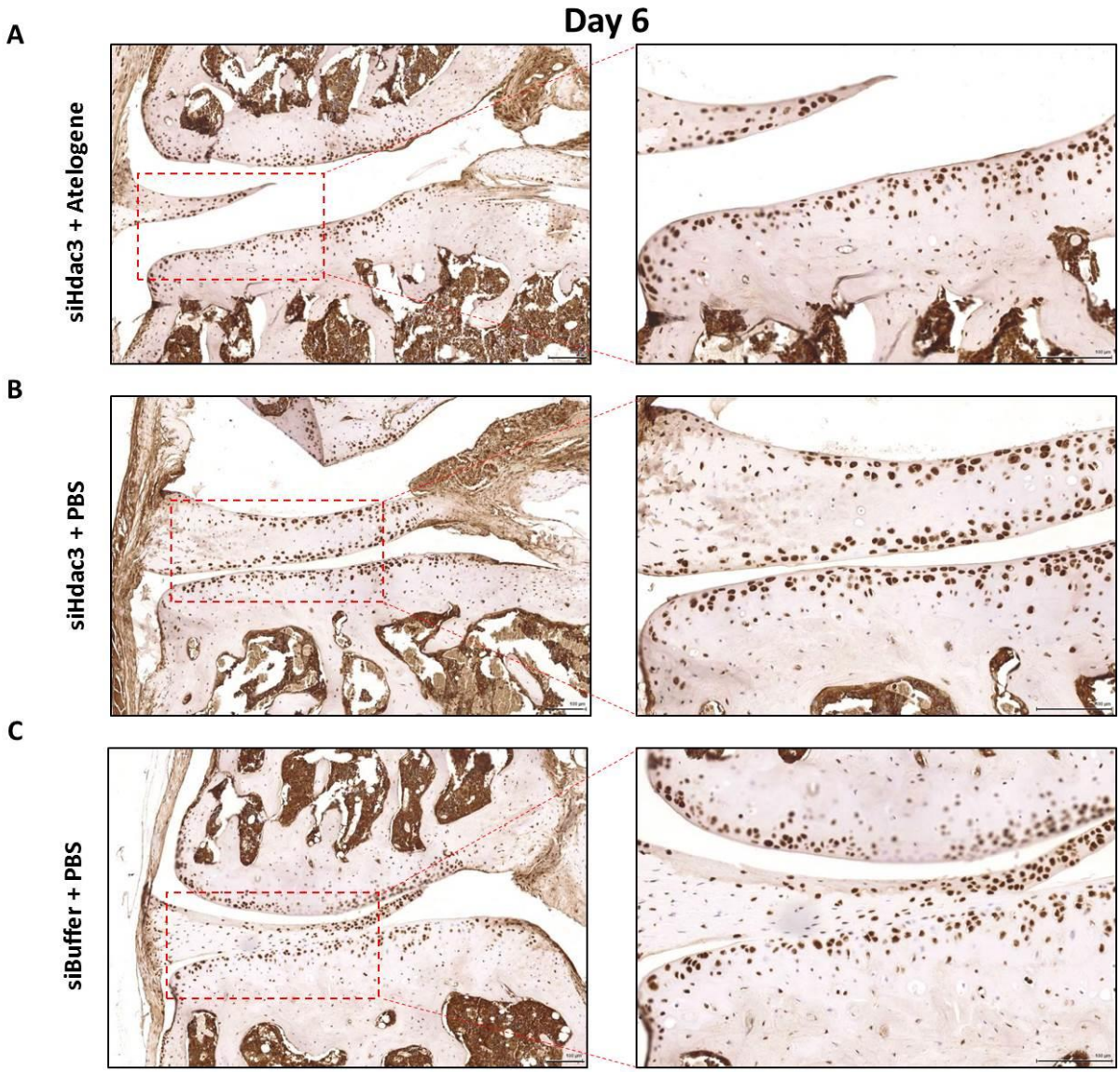

Figure 7.3. ***In vivo*** **efficacy of the intra-articular delivery of a siRNA targeting Hdac3 on the mouse knee joint.**

Adult C57BL/6J mice were anaesthetized and intra-articular injections performed in the left knee joint. Treatments included: **A.** siHdac3 (20μM) were prepared in siRNA buffer (1.6x, provided in the AteloGene kit) and diluted in AteloGene containing 0.01% Evans blue dye (SIGMA Aldrich). **B.** siHdac3 (20μM) were prepared in siRNA buffer and diluted in PBS including 0.01% Evans blue dye. **C.** siBuffer and PBS with 0.01% Evans blue dye were injected into the knee joint. For all treatments 15μl were injected into the joint capsule. Representative coronal sections of the knee joint, stained with an anti-Hdac3 antibody are shown in A-C. Three sections from each mouse were used for quantification.

7.3.3 Generation of a cartilage- specific Hdac3 conditional knockout (cKO) mouse model.

Previous studies showed that Hdac3 is expressed in proliferating and hypertrophic growth plate chondrocytes of one-month old mice. (Bradley et al., 2013) Further analysis also revealed that Hdac3 is detectable in these zones as early as E14.5. To further determine the role of Hdac3 in endochondral ossification, Hdac3 was conditionally deleted in cells expressing Cre recombinase under the control of type II collagen alpha 1 promoter [called *Hdac3(Fl/Fl); Col2-Cre(+)* or *Hdac3*$^{Cart\Delta Ex3}$]. The steps taken for the generation of the conditional knockout mouse model are summarised in **Figure 7.5** and also described in detail in section **2.2.11**.

Briefly, three males and three females Hdac3$^{tm1a(EUCOMM)Wtsi}$ targeted; knockout first allele (reporter-tagged insertion with conditional potential) mice, were obtained from the University of Veterinary Medicine, (Vienna, Austria). Detailed generation as well as phenotypic data are available from the International Mouse Phenotypic Consortium (IMPC, at http://www.mousephenotype.org/data/search/gene?kw="Hdac3"). In general no significant phenotype associations were found following x-rays, eye morphology and skin histopathology analysis and no association with a human disease found. These mice accounted for the parental line (P) and carried one Wild-type (Wt) allele and a Hdac3 target locus allele as shown in **Figure 7.4 A,** containing a lacZ-neomycin reporter cassette flanked by two 48bp FRT sites (5′-GAAGTTCCTATTCCGAAGTTCCTATTCTCTAGAAAGTATAGGAACTTC-3′) and a floxed exon 3 (one loxP site either side of exon 3). These mice are called *Hdac3(+/Fl)* hereafter. An initial experiment to compare endochondral ossification using Alizarin red/ Alcian blue staining of one day old (P1) mice was performed after breeding the parental line and results revealed endochondral ossification was normal and no significant difference of the length of femurs or tibias was found between the *Hdac3(+/Fl)* mice (n=3) and the Wt *Hdac3(+/+)* littermates (n=2) (**Figure 7.6**). Genotypes at this stage were confirmed using primer pairs 1, 2 and 5 as indicated in **Figure 7.4 B & C** (lanes 1-7).

The parental line *Hdac3(+/Fl)* was bred with mice expressing FLP recombinase (which recognises and cleaves at this site TCTAGAAA) (Rodriguez et al., 2000; Dymecki 1996), to promote site-specific DNA recombination and remove the lacZ-neomycin cassette. The mice generated formed the F1 generation of mice, were called *Hdac3(+/Fl); FLP(+)* and carried one Wt allele and a Post-FLP Hdac3 locus allele (**Figure 7.4 A**). For genotyping, primer pairs 3 and 4 were used to confirm FLP recombination and absence of the lacZ-neomycin reporter (**Figure 7.4 D & E**). Presence of FLP was also confirmed using PCR as described in section **2.2.11** and shown in **Figure 2.3**. Lane 8 for example (**Figure 7.4 D**) shows that when primer

pair 3 was used the Wt allele amplicon was 1118bp long, whereas the Hdac3 target locus allele recombined by FLP had 1170bp size. Therefore the Post-FLP allele amplicon was bigger by an FRT and two loxP sites in comparison to the Wt allele. Similarly, when primer pair 4 was used (lanes 10-13, **Figure 7.4 E**), the Post-FLP allele amplicon was 692bp long, while the Wt allele was 782bp long. In this case the Wt allele amplicon is slightly longer, because in order to introduce the Hdac3 target locus cassette into the mouse genome part of the wild-type sequence was removed, and although there is an extra loxP site in the Post-FLP allele, this is still smaller than the Wt amplification product.

F1 heterozygous mice were then bred with Col2-Cre mice (F2 generation in **Figure 7.5**) to generate heterozygous *Hdac3(+/Fl); FLP(+); Col2-Cre(+)* and promote recombination and exon 3 deletion via recognition of the loxP sites (5′-ATAACTTCGTATAGCATACATTATACGAAGTTAT-3′) by Cre recombinase (which recognises and cleaves at this site GCATACAT). Col2α1 is expressed in embryonic cartilaginous tissues as early as E10.5 and in developing skeletal structures at E13.5. (Chen et al. 2007; Nakamura et al. 2006) *Hdac3(+/Fl); FLP(+); Col2-Cre(+)* heterozygous mice were born at expected ratios and used for the final breeding step (F4 generation) that would generate the conditional knockout mouse model (F5). Genotyping results were obtained using primer pairs 3 and 6 to confirm Cre recombination and Hdac3 exon 3 deletion. In particular, when primer pair 3 was used, the Wt allele amplicon was 1118bp long, whilst the Hdac3 target locus allele recombined by Cre was only 326bp long (lane 9 in **Figure 7.4 D**). [Note here that there is still a band for the Post-FLP Hdac3 target allele amplicon at 1170bp, though it is not as intense as that in lane 8, indicating Cre recombination is not 100% efficient]. In addition, primer pair 6 could also be used to demonstrate the presence of the floxed allele, since it amplifies a region around exon 3, which is smaller by 82bp in comparison to the Wt allele (lanes 14-18, **Figure 7.4 F**). Real-time PCR was also used to quantify Col2α1-Cre expression of the F5 mice and normalised to type X collagen expression levels (see also **Figure 2.4**).

Sanger Sequencing was used to confirm the sequence of the amplicons produced from all the different breeding steps.

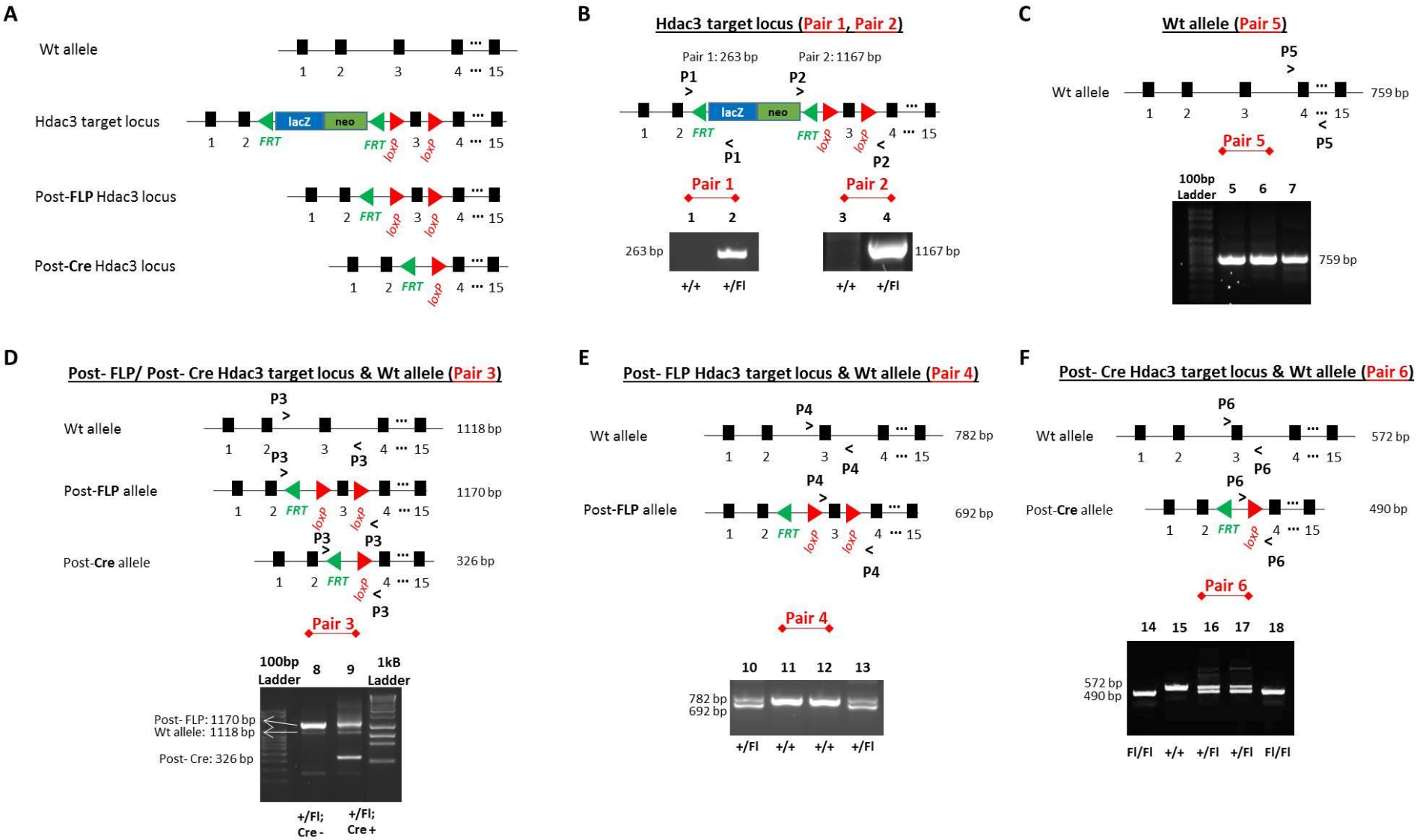
A
Wt allele
Hdac3 target locus
Post-FLP Hdac3 locus
Post-Cre Hdac3 locus
lacZ
neo
FRT
loxP
B
Hdac3 target locus (Pair 1, Pair 2)
Pair 1: 263 bp
Pair 2: 1167 bp
P1
P2
Pair 1
Pair 2
263 bp
1167 bp
+/+
+/Fl
C
Wt allele (Pair 5)
P5
759 bp
Pair 5
100bp Ladder
D
Post- FLP/ Post- Cre Hdac3 target locus & Wt allele (Pair 3)
P3
Wt allele
1118 bp
Post-FLP allele
1170 bp
Post-Cre allele
326 bp
Pair 3
100bp Ladder
1kB Ladder
Post- FLP: 1170 bp
Wt allele: 1118 bp
Post- Cre: 326 bp
+/Fl; Cre -
+/Fl; Cre +
E
Post- FLP Hdac3 target locus & Wt allele (Pair 4)
P4
Wt allele
782 bp
Post-FLP allele
692 bp
Pair 4
782 bp
692 bp
+/Fl
+/+
F
Post- Cre Hdac3 target locus & Wt allele (Pair 6)
P6
Wt allele
572 bp
Post-Cre allele
490 bp
Pair 6
572 bp
490 bp
Fl/Fl
+/+
+/Fl

Figure 7.4. Genotyping results from different primer pairs.

A. Wild type (Wt) allele, Hdac3 target locus, Post-FLP Hdac3 locus and Post Cre Hdac3 locus alleles. **B.** Primer pairs 1 and 2 were used to confirm Hdac3 target locus presence before any FLP or Cre recombination occurs. **C.** Primer pair 5 amplifies a region from Hdac3 exon 4 to exon 7 in the Wt gene. **D.** Primer pair 3 was used to distinguish between the presence of a Post-FLP and/ or a Post-Cre Hdac3 allele. **E & F.** Primer pairs 4 & 6 were used to confirm the presence of a Post-FLP floxed Hdac3 allele. Right Arrowheads indicate hybridization of the forward primer, while left arrowheads indicate where the reverse primer would hybridize. Black squares represent exons. The size of each PCR product is given in base pairs (bp).

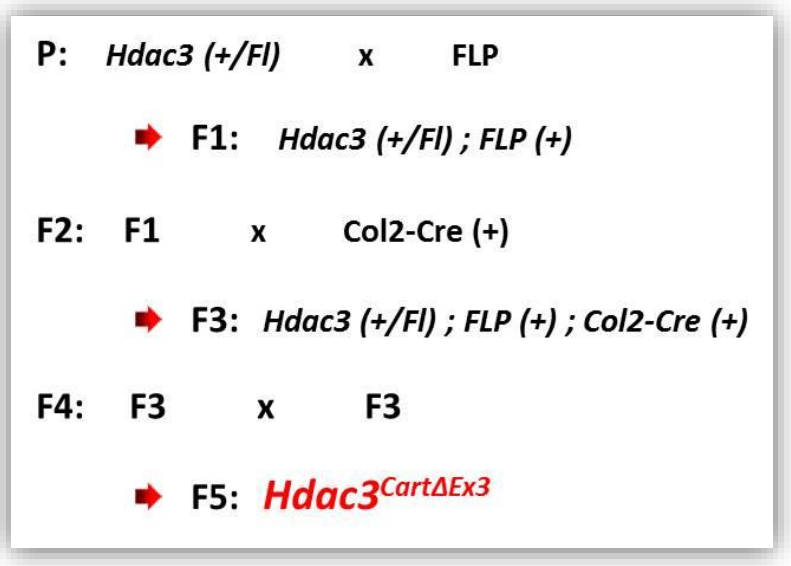

Figure 7.5. Selective breeding was performed in order to generate a cartilage-specific Hdac3 conditional knockout mouse model.

The steps performed in each generation are summarised above.

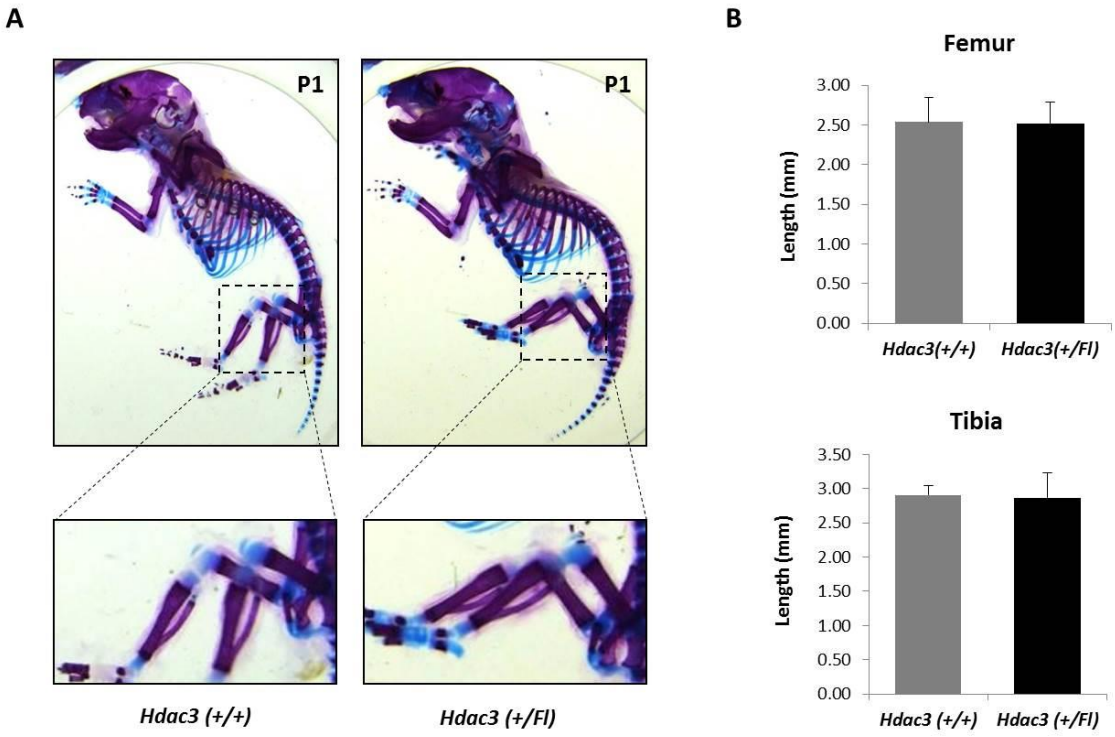

Figure 7.6. A. Whole mount Alizarin Red/ Alcian blue skeletal preparations from one day old *Hdac3(+/+)* (n=2) and *Hdac3(+/Fl)* (n=3) mice. **B.** Measurements of femoral and tibia length from one day old *Hdac3(+/+)* (n=2) and *Hdac3(+/Fl)* (n=3) *mice*.

Table 7.1 shows the expected genotypes at F5 after breeding *Hdac3(+/Fl); FLP(+); Col2-Cre(+)* animals and **Table 7.2** shows the expected and observed numbers of animals found from 8 independent litters at F5. Note here that FLP genotypes are not included, since all the animals used for the F4 breeding step were FLP (+) positive animals. For convenience, the heterozygous animals (*Hdac3(+/Fl); FLP(+); Col2-Cre(+)*) will thereafter be called *Hdac3(+/Fl);Col2-Cre(+)* or HET. Hdac3 conditional HET animals were born at higher rate (1/ 1.5) than the expected Mendelian ratio (1/2.7) as shown in **Table 7.2** and were a normal size (**Figure 7.7**). However, no conditional knockout (cKO) *Hdac3(Fl/Fl); Col2-Cre+* animals were born in 8 litters. [Wt and HET mice, but no cKO, were also present at E16.5 from 3 different litters, yet earlier developmental stages were not studied here due to limited time]. These findings indicate that Hdac3 may be necessary for pre-natal cartilage formation and bone growth before E16.5. Nonetheless, a detailed comparative analysis between the Wt and HET animals was performed at three weeks post-natal to determine cartilage development of the growth plate.

No size or weight difference was found at three weeks of age between the Wt and HET male or female mice (**Figure 7.7**). X-rays and bone measurements were performed as shown in **Figure 7.8 A** and have been previously described (Cameron et al., 2015). Femoral and tibial lengths were used to indicate endochondral bone growth and intercanthal distance (ICD) and skull length to measure intramembranous bone growth. Moreover, growth plates of three weeks old Wt and HET mice (**Figure 7.8 B**) were stained for haematoxylin and eosin (H&E), alcian blue and toluidine blue to compare cell morphology of the different zones and cartilage formation evidenced by the amount of glycosaminoglycans (GAG) and proteoglycans respectively.

At three weeks of age, endochondral bones in HET mice were a similar size to their Wt littermates (**Figure 7.9 A-B**), and no difference was found in the ICD or skull length between HET and Wt, indicating intramembranous bone formation also remained unaffected (**Figure 7.9 C-D**). H&E staining suggested growth plate zone lengths were of similar length in HET and Wt mice at three weeks of age (**Figure 7.10**, H&E staining). Cartilage formation was assessed by Alcian Blue staining which revealed similar content of GAGs in the Wt and HET growth plates at three weeks of age (**Figure 7.10**, Alcian Blue staining). Finally, no apparent difference in proteoglycan content was detected using Toluidine blue staining in Wt and HET mice (**Figure 7.10**, Toluidine Blue staining).

Gametes (F4)	***Hdac3 (+) ; Col2-Cre (+)***	***Hdac3 (+) ; Col2-Cre (-)***	***Hdac3 (Fl); Col2-Cre (+)***	***Hdac3 (Fl) ; Col2-Cre (-)***
Hdac3 (+) ; Col2-Cre (+)	Hdac3 (+/+) ; Col2-Cre (+/+)	Hdac3 (+/+) ; Col2-Cre (+/-)	Hdac3 (+/Fl) ; Col2-Cre (+/+)	Hdac3 (+/Fl) ; Col2-Cre (+/-)
Hdac3 (+) ; Col2-Cre (-)	Hdac3 (+/+) ; Col2-Cre (+/-)	Hdac3 (+/+) ; Col2-Cre (-/-)	Hdac3 (+/Fl) ; Col2-Cre (+/-)	Hdac3 (+/Fl) ; Col2-Cre (-/-)
Hdac3 (Fl); Col2-Cre (+)	Hdac3 (+/Fl) ; Col2-Cre (+/+)	Hdac3 (+/Fl) ; Col2-Cre (+/-)	Hdac3 (Fl/Fl) ; Col2-Cre (+/+)	Hdac3 (Fl/Fl) ; Col2-Cre (+/-)
Hdac3 (Fl) ; Col2-Cre (-)	Hdac3 (+/Fl) ; Col2-Cre (+/-)	Hdac3 (+/Fl) ; Col2-Cre (-/-)	Hdac3 (Fl/Fl) ; Col2-Cre (+/-)	Hdac3 (Fl/Fl) ; Col2-Cre (-/-)

Table 7.1. Punnett square of the expected genotypes at F5 generation after breeding *Hdac3(+/Fl); Col2-Cre(+/-)* heterozygous mice.

Genotypes	**Expected number of animals (50 animals in total from 8 Litters)**	**Observed number of animals (50 animals in total from 8 Litters)**
Hdac3 (+/+) ; Col2-Cre +	9	10
Hdac3 (+/Fl) ; Col2-Cre +	19	32
Hdac3 (Fl/Fl) ; Col2-Cre +	9	**0**

Table 7.2. Expected ratio and observed number of animals at F5 generation.

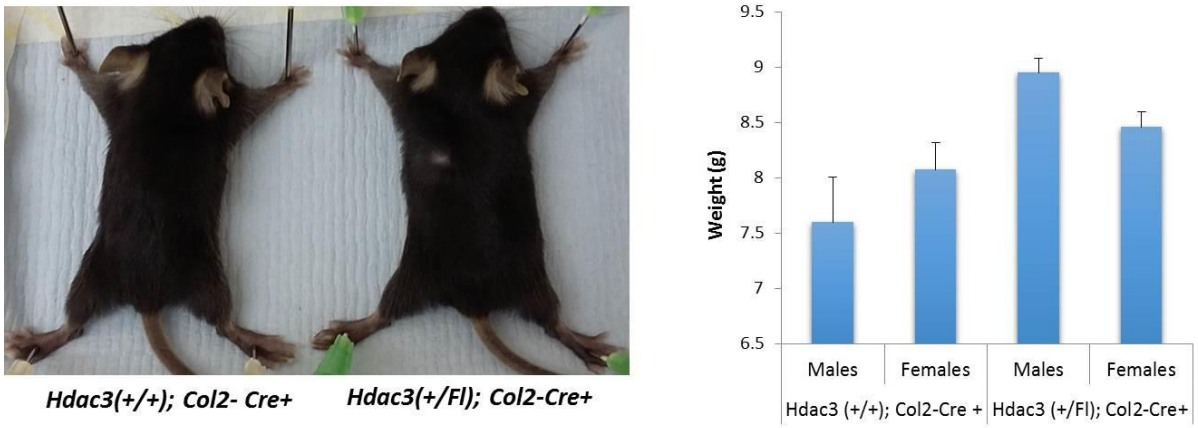

Figure 7.7. Conditional HET *Hdac3(+/Fl); Col2-Cre+* mice have similar size and weight to Wildtype *Hdac3(+/+); Col2-Cre+* littermates.

Representative image of 3-week old wildtype and HET male mice. Average weights of male (n=3) and female (n=7) wildtype mice and male (n=10) and female (n=10) HET mice at the time of weaning. Results are representative of the mean of n=10 Wt mice and n=20 HET mice +SD. For statistical analysis, an unpaired two-tailed student's t-test was performed.

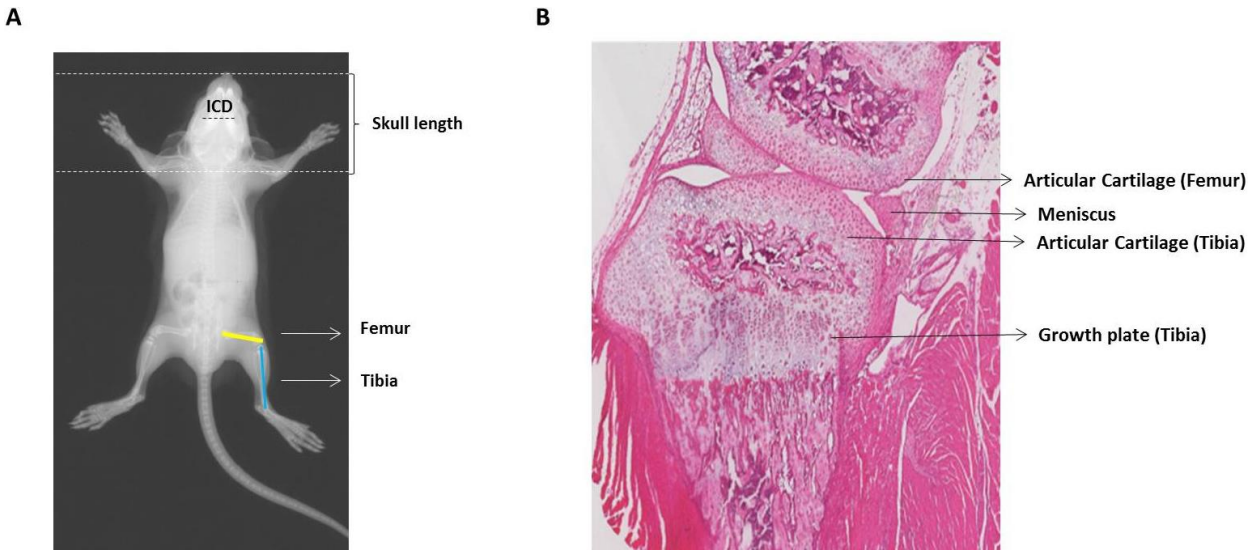

Figure 7.8. A. X-rays and bone measurements were conducted as indicated above (ICD= Intercanthal Distance, Skull length, Length of Femurs and Tibias were measured). **B.** Histological analysis of the growth plate was performed at three weeks of age to assess development of the cartilage between Wildtype *Hdac3(+/+);Col2-Cre/+* and HET *Hdac3(+/Fl); Col2-Cre/+* mice.

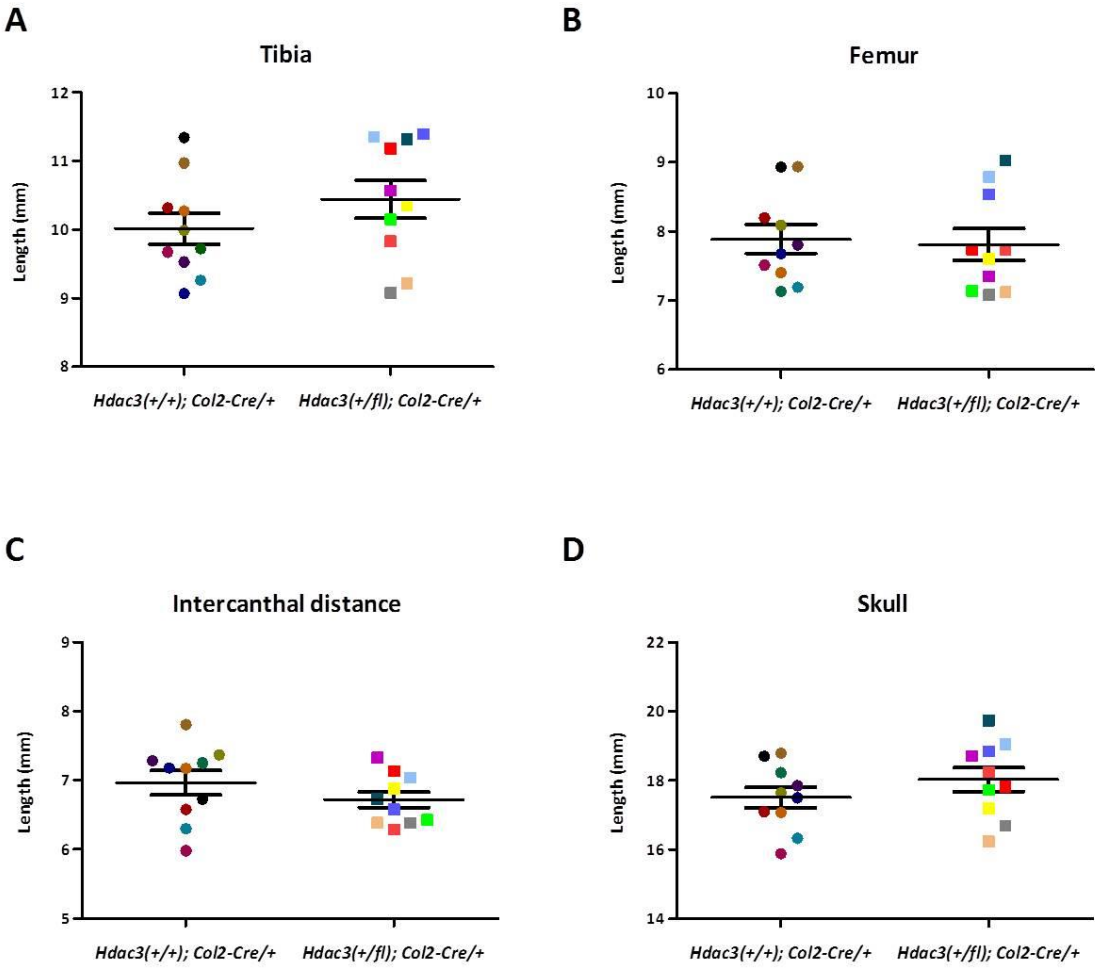

Figure 7.9. Morphometric characterization of HET *Hdac3(+/Fl); Col2-Cre/+* mice compared to Wildtype *Hdac3(+/+); Col2-Cre/+*.

A. Length of right and left tibias, **B.** right and left femurs, **C.** intercanthal distance and **D.** skull were measured at the time of weaning. Results are representative of the mean of n=10 Wt (male and female) mice and n=10 HET (male and female) mice. For statistical analysis, an unpaired two-tailed student's t-test was performed. Different colours represent different animals. The same animals were used for all measurements.

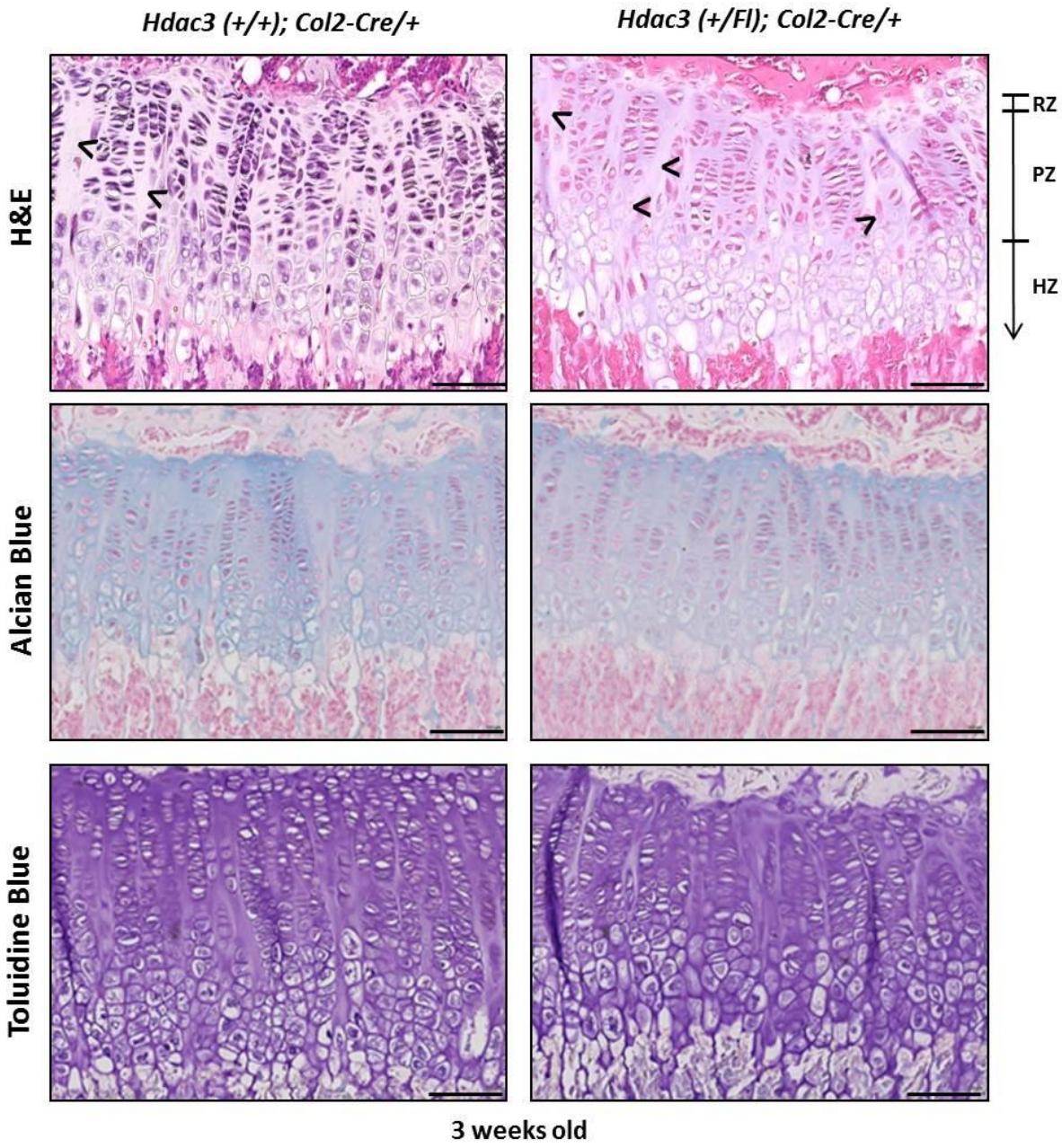

Figure 7.10. HET *Hdac3(+/Fl); Col2-Cre/+* growth plate structure and cartilage formation compared to Wildtype *Hdac3(+/+); Col2-Cre/+* littermates.

A. Representative images of Haematoxylin and Eosin (H&E) staining to assess chondrocyte column length in Wt *Hdac3(+/+); Col2-Cre/+* and HET *Hdac3(+/Fl);Col2-Cre/+* growth plates. Arrowheads indicate areas of hypo- cellularity. Ladder indicates the length of the Resting Zone (RZ), Proliferating Zone (PZ) and Hypertrophic Zone (HZ) in the growth plate of three-week old mice. **B.** Representative images of Alcian Blue staining to assess cartilage formation in Wt and HET growth plates and **C.** Representative images of Toluidine Blue staining to assess proteoglycan deposition in Wt and HET growth plates. Bar= 100μm

7.4 Discussion

The involvement of the epigenome in common complex human diseases is becoming increasingly clear and more feasible to study and understand due to new advances in genomic and computational technologies as well as the use of animal models. One of the most promising approaches towards drugs that can modify epigenetic traits has been seen in the development of Histone Deacetylase inhibitors (HDACi), some of which are already used for treatment of cancers and neurological conditions or are currently in clinical trials. (Richardson et al. 2016; Manal et al. 2016; Hull et al. 2016) Many additional uses have been proposed for these drugs, based on preclinical studies including in arthritis models. (Culley et al. 2013; Cai et al. 2015) Understanding the effects of these epigenetic-modifying drugs and the epigenome in general on the skeleton is of increasing interest because of its undoubtable importance in maintaining overall health and fitness. Therefore the main aim of this chapter was to understand how HDAC3 contributes to normal cartilage development *in vivo* and to assess its role in osteoarthritis (OA) using a selective HDAC3 inhibitor or the delivery of a siRNA, and eventually in DMM-induced OA in cKO Hdac3-null mice.

7.4.1 Hdac3 inhibition failed to rescue cartilage damage in the DMM model of osteoarthritis.

Previous data from our group support a chondroprotective effect of TSA *in vivo* in the DMM-induced OA mouse model (Culley et al. 2013). These findings were also confirmed by (Cai et al. 2015) in two different OA models, the DMM and a drug (monosodium iodoacetate, MIA) - induced OA mouse model after using the HDACi TSA. However, my study demonstrated that cartilage degeneration was not rescued after using TSA or the selective HDAC3i Apicidin in the DMM mouse model (**Figure 7.1**). There were no significant effects in the cartilage of the tibia or femur of either HDACi treated joints when compared to the control treated joints.

This opposing result could be due to the different administration method used in this study in comparison to the previous studies, and insufficient delivery of the drug to the cartilage chondrocytes of the knee joint. In particular, intra-articular injections were used in this study and performed twice in a four-week period, first at the day of the surgery and second two weeks post- surgery. In the two successful reports on the contrary, the compound was delivered subcutaneously either via daily (2.0mg/kg) injections (Cai et al. 2015) or via implanted osmotic pumps (1mg/kg/day) (Culley et al. 2013). Therefore these successful

delivery methods indicate that the drugs may need to be administered systemically and not locally. Furthermore, both HDACi were diluted in DMSO in this study to a final c=10mg/ml, while both successful studies have previously used PBS (Cai et al. 2015), ethanol or a mixture of 50% DMSO/ 50% polyethylene glycol 300 (Culley et al. 2013).
Moreover, although three groups of six mice were set up initially, the number of mice in the TSA-treated group was reduced to three; due to a joint infection the sections from three mice were not included in the final analysis. The small number of mice involved in this experiment may explain the non-significant results obtained. Another possible reason for not seeing any significant effect in the cartilage damage caused by DMM is that the drugs were not sterile or the injections were not sterile. This would explain why three of the TSA injected mice were inflamed and inflammation might have compromised cartilage damage in this group.

7.4.2 Intra-articular siRNA administration targeting Hdac3 in vivo in articular cartilage was inefficient.

Intra-articular injectable regimens might be a suitable way for developing, testing and finding a cure for OA and *in vivo* models currently available could be used to optimize these methods. Hence administration of intra-articular biomolecules targeting chondrocyte activity or synovial inflammation is a promising strategy for therapeutic intervention in OA. To understand what epigenetic alterations occur in chondrocytes following *Hdac3* depletion, a siRNA transfection was attempted to knockdown *Hdac3* specifically in articular cartilage chondrocytes of wildtype C57Bl/6 mice. Intra-articular injections for localized administration of siRNA/atelogene complexes were performed at final concentration 20µM and transfection efficiency assessed at day three and six post-injections. Atelogene is composed of atelocollagen, a highly purified type I collagen isolated from calf dermis by pepsin treatment. Immunohistochemistry (IHC) for Hdac3 revealed no significant difference between the siHdac3 + Atelocollagen (Atelogene) - treated and siHdac3 + PBS or siBuffer + PBS control joints following three (**Figure 7.2**) or six days (**Figure 7.3**) after the injections. However, intra-articular injections of miR-15a with Atelogene in the knee joint of an autoantibody induced- arthritis mouse model has previously been successfully delivered. (Nagata et al. 2009) In this paper, successful administration was examined one day and three days post-injections in the synovium of the joint capsule using qRT-PCR and IHC. The expression of miR-15a was also measured in other tissue-organs with no significant difference identified apart from the liver, where increased expression of miR-15a was found. The authors propose this could be the result of part of the double-stranded miRNA injectable dose to have moved

from the joint cavity to the systemic circulation and emphasize the importance of addressing this before any clinical studies can be performed. Therefore, it is possible that following three/six days after the injections were performed it is no longer possible to test for siRNA efficiency due to degradation or minimal retention in the joint capsule. Nevertheless, it is worth mentioning that other studies that have utilized the same transfection kit, used alternative administration routes including mainly intravenous and/or intraperitoneal systemic delivery of the siRNA or intratumor injections in the case of localized administration. (Mochizuki et al. 2012; Tanaka et al. 2013; Fujiwara-Okada et al. 2013; Shoji et al. 2013)

In this chapter the main goal was to firstly efficiently transfect an siRNA *in vivo* in normal wildtype mice and secondly to try the same regimens in the DMM-surgical OA mouse model. However, due to inefficient transfections in the wildtype mice, the second part was not studied. It has previously been reported that cartilage thickness increases with animal size and larger animal models more closely resemble human joints (Holyoak et al. 2016). Cartilage thickness is also critical for intra-articular retention of drugs, since diffusion binding kinetics depends on the square of cartilage thickness (Bajpayee et al. 2015). Therefore, smaller animal models, for example mice used in this study may not be suitable for evaluating or predicting intra-articular drug retention in humans. Inefficiency of the Atelogene kit is also possible and hence alternative delivery methods could be used for future studies.

Since OA pathology is restricted to the affected joint, intra-articular injections offer a number of benefits including low doses of local administration, high potency and minimal side effects compared to intravenous or orally administered drugs and supplements. In comparison intravenous administration of drugs usually results to poor localized delivery to the affected joints and often requires repetitive administration of large doses. Further, orally-administered drugs are often associated with complications to the gastrointestinal system. (Gupta & Eisen 2009) Nevertheless, one of the main disadvantages of intra-articular injections is the lack of retention which leads to decreased efficacy. This could be partly due to articular cartilage extracellular matrix properties, for example the dense type II collagen network, the avascularity and the negatively charged aggrecan molecules may prevent entrance of therapeutic agents into the cartilage matrix. (Rothenfluh et al. 2008) Therefore, a large research area has emerged in creating biomaterials to improve the delivery and retention times of drugs in the articular cartilage. (Holyoak et al. 2016)

The most common form of new biomaterials being tested for intra-articular delivery of drugs for OA treatment are nanoparticles (NP) onto which drugs can be loaded. A major benefit of nanoparticles is their ability to attach and bind to specific constituents of articular cartilage,

improve retention within the joint and hence slow the progression of the disease. To date, the primary categories of drugs delivered via nanoparticles are those that inhibit inflammation, those that can protect chondrocytes from apoptosis and promote chondrocyte differentiation and those that benefit from NP delivery to limit toxic systemic side effects. Hyaluronic acid is for example the primary candidate in the case of drug delivery via NP to inhibit inflammation, and it has been used in combination with salmon calcitonin. (Ryan et al. 2013) Salmon calcitonin has been shown to benefit cartilage metabolism and inhibits collagen breakdown by inhibiting MMPs. (Esenyel et al. 2013) IL-1 inhibitors are another category of drugs delivered by NPs to reduce inflammation. (Cunnane et al. 2001)

Preserving chondrocyte health and homeostasis is a major objective in OA, and so anti-apoptotic drugs may be useful in the treatment of OA. For example, brucine is an anti-apoptotic drug that has been loaded onto NPs and used to promote cartilage regeneration and inhibit apoptosis, though proven to be severely toxic to the central nervous system. (Chen et al. 2013) Kartogenin was also used in combination with NPs and shown to selectively differentiate MSCs into chondrocytes and thus may benefit from local delivery to the joint. (Kang et al. 2014) Intra-articular delivery of a peptidic NP complexed to NF-κB siRNA significantly reduced chondrocyte apoptosis and reactive synovitis in a murine model of controlled knee joint impact injury. (Yan et al. 2016) Lentiviral vector- mediated delivery of Toll-like receptor 7 gene short hairpin RNA (shRNA) on collagen-induced arthritis in rats showed promising results in terms of reducing ankle inflammation, articular indexes and radiographic and histologic scores. (Chen et al. 2012) Finally, intra-articular injections of biodegradable polymer microparticles which release controlled levels of anti-inflammatory siRNA have been successfully delivered in a rat model of painful temporomandibular joint inflammation, showing promising results in decreasing inflammation accompanied with reduced IL-6 expression levels. (Mountziaris et al. 2012)

7.4.3 Cartilage specific conditional knockout Hdac3 mice are embryonic lethal before E16.5.

Previous research (Bradley et al., 2013) demonstrated that Hdac3 is abundant in proliferating and hypertrophic growth plate chondrocytes of one-month old mice and can be detected as early as E14.5. To further determine the role of Hdac3 in chondrocytes during endochondral ossification, *Hdac3* gene was first conditionally deleted in cells expressing Cre recombinase under the control of *Col2α1* promoter (here is termed *Hdac3(Fl/Fl);Col2-Cre(+)* or

Hdac3$^{Cart\Delta Ex3}$). *Col2α1* has been shown to be expressed in embryonic cartilaginous tissues as early as E10.5 and in developing skeletal structures at E13.5. (Chen et al. 2007; Nakamura et al. 2006) Following selective breeding with FLP positive and Cre positive transgenic mice as shown in **Figure 7.5**, HDAC3 conditional HET animals were born at higher rate than the expected Mendelian ratio as shown in **Table 7.2** and were normal size (**Figure 7.7**). However, no conditional knockout (cKO) *Hdac3(Fl/Fl); Col2-Cre+* animals were born in 8 litters. Wt and HET mice, but no cKO, were also present at E16.5 from 3 different litters. These findings indicate that HDAC3 may be necessary for pre-natal cartilage formation and bone growth before E16.5. This could be due to defective DNA repair mechanism as it has previously shown for the global Hdac3 null mice. (Bhaskara et al., 2010) Deletion of Hdac3 from cartilage could also impair a number of cartilage-extrinsic phenotypes including for example angiogenesis which is necessary for normal endochondral ossification and bone mineral density as it was found for the Osterix-Cre Hdac3 cKO mice. (Razidlo et al., 2010)

Indeed, Carpio's et al. research also showed that *Col2α1* Hdac3 cKO mice are embryonic lethal between E10.5 and E16.5. (Carpio et al. 2016) While expected Mendelian ratios of heterozygous conditional mice were born, no Hdac3 cKO mice were born in their nine litters. However, Hdac3 cKO and conditional HET mice were detected at E10.5, but only HET were present at E16.5, indicating that *Hdac3* expression in chondrocytes is necessary during these early stages of skeletal formation between E10.5 and E16.5. (Carpio et al. 2016)

Since the Hdac3 cKO mice were embryonic lethal, the only alternative method that we could use to study the effect of Hdac3 loss in chondrocyte development/ proliferation would be to postnatally delete Hdac3 in order to overpass the embryonic lethality. This would be possible if using an inducible conditional transgenic line, which could induce Hdac3 knockout in specific developmental stages. For example, the tamoxifen-inducible Col2α1-Cre line (Col2α1ERT-Cre; The Jackson Laboratory- https://www.jax.org/strain/006774) (Nakamura et al. 2006) could have been used to generate Hdac3-cKO$_{Col2ERT}$, by injecting tamoxifen (if mice were to be used before weaning) or including it in the food (if the mice were to be used after weaning). Another example is the tamoxifen inducible Acan-CreER-Ires-Luc line (Lo Cascio et al. 2014) which uses an aggrecan gene enhancer to induce knockout specifically in cartilage, expresses firefly luciferase and has a tamoxifen-activatable Cre recombinase. The expression of the transgene is restricted to cartilage from embryonic to adult stages and one of the main advantages is the presence of luciferase which allows for visualisation of transgene expression in live animals. However, due to unavailability of such a transgenic line in Newcastle University it was time-wise impossible to perform these breedings. Furthermore, it

became aparrent during this thesis that the group of J.J. Westendorf had come to the same conclusions and were already performing these experiments (Carpio et al. 2016).

7.4.4 Hdac3(Fl/+);Col2-Cre/+ HET mice present normal intramembranous and endochondral ossification and growth plate morphology compared to wildtype Hdac3(+/+);Col2-Cre/+ mice.

My study demonstrated that cartilage- specific Hdac3 knockout was embryonic lethal. Nonetheless, a detailed comparative analysis between the Wildtype *Hdac3(+/+);Col2-Cre/+* and HET *Hdac3(Fl/+);Col2-Cre/+* animals was performed at three weeks post-natal to determine cartilage development of the growth plate.

No significant size or weight difference was observed at three weeks of age between the Wt and HET male or female mice (**Figure 7.7**), as evidenced by x-rays and bone measurements. Femoral and tibial lengths were used to indicate endochondral bone formation and intercanthal distance (ICD) and skull length to measure intramembranous bone growth. Endochondral bones of HET *Hdac3(Fl/+);Col2-Cre/+* mice were a similar size to the Wt *Hdac3(+/+);Col2-Cre/+* littermates at three weeks postnatally (**Figure 7.9 A-B**), and no difference was found in the ICD or skull length between HET and Wt, indicating intramembranous bone formation remained unaffected (**Figure 7.9 C-D**).

Furthermore, an analysis of the growth plates of three weeks old Wt and HET mice was performed to identify possible differences in the size or shape of the proliferative zone chondrocytes, or any difference in cartilage formation and proteoglycan synthesis of the growth plate cartilage. H&E staining suggested growth plate zone lengths were of similar length in HET and Wt mice at three weeks of age (**Figure 7.10**, **H&E staining**). Cartilage formation assessed by Alcian Blue staining which revealed similar content of GAGs in the Wt and HET growth plates at three weeks of age (**Figure 7.10**, **Alcian Blue staining**) and finally, no apparent difference in proteoglycan content was detected using Toluidine blue staining in Wt and HET mice (**Figure 7.10**, **Toluidine Blue staining**).

These data are in agreement with the KOMP-phenotyping results (https://www.mousephenotype.org/data/genes/MGI:1343091#order) comparing *Hdac3(+/Fl)* to *Hdac3(+/+)* mice. X-rays showed no difference in the size of tibias, shape of femur and femur- tibia angle, shape of pelvis, shape of ribs or the development of abnormal teeth. DEXA scans also revealed normal bone mineral density, bone content and bone size between heterozygous and wild type mice. However, some heterozygote *Hdac3(+/Fl)* showed

abnormal eye morphology and developed cataract and also some female heterozygote mice had significantly higher heart weight than the female Wild type mice. This observation has been previously linked to a high-fat diet in mice in which HDAC3 was postnatally deleted from the heart and skeletal muscle and induced lethality. (Sun et al. 2011)

Interestingly, postnatal ablation of Hdac3 in chondrocytes delays endochondral ossification. (Carpio et al. 2016) *Hdac3(Fl/Fl)* mice carrying a flanked exon 7 were bred with the tamoxifen-inducible Col2α1-Cre mice to generate Hdac3-cKO$_{Col2ERT.}$ These animals were given a single injection of tamoxifen at 5 days postnatally (P5) and HDAC3 expression and protein levels were significantly lower than normal at four and eight weeks of age. (Carpio et al. 2016) Although the inducible Hdac3 cKO weighed approximately 50% less than the control mice, these weight deficiencies were resolved by eight weeks of age. Severe delays in secondary ossification centre (SOC) formation were profound in tibiae of 9- and 14-day-old inducible Hdac3 cKO, but by four weeks of age this phenotype was also been resolved and SOC were fully formed in control and cKO animals. Though, growth plate defects in the inducible Hdac3 cKO mice were evident. In particular, the growth plates were thinner by 18% than those in the control animals in the interior side of the growth plate and 67% thicker on the medial side and 57% thicker on the lateral side. While tamoxifen did not have any effect on the growth plates of control animals, Hdac3 appear to be important for maintaining normal DNA integrity, indicated by increased phosphorylation of γH2A.X, a marker of DNA double-strand breaks, and also vasculogenesis, evidenced by reduced abundance of the angiogenic marker PECAM-1 (Platelet Endothelial Cell Adhesion Molecule-1). (Carpio et al. 2016)

It has also been proposed that Hdac3 regulates chondrocytes transcriptome and chromatin landscape (Carpio et al. 2016) and it is important for inflammatory gene expression programmes in rheumatoid arthritis (RA) fibroblast-like synoviocytes (FLS). (Angiolilli et al. 2017) It was shown that Hdac3 depleted chondrocytes had increased lysine acetylation of histones H3 and H4. Delays in chondrocyte maturation were confirmed by real-time PCR with reduced *Col2α1*, *Acan*, *Ihh* and *Col10α1* expression and decreased proteoglycan production observed. (Carpio et al. 2016) On the other hand, increased expression of genes encoding for cytokines, and are classically linked to inflammation such as *IL-6*, *Cxcl1* and *Saa3*, as well as catabolic factors including *MMP13* and *MMP3,* were found in Hdac3-depleted chondrocytes. (Carpio et al. 2016) Additionally, when HDAC3 was inhibited or depleted in rheumatoid arthritis-derived FLS, IL-1β inducible genes were significantly suppressed and IFN-dependent genes like *Cxcl11* and *Cxcl9* expression reduced. It is supported that HDAC3 is important for mediating type I IFN production and subsequent

STAT1 Tyr phosphorylation and activation in FLS, hence establishing a new potential therapeutic target in RA and type I IFN- driven auto-immune diseases. (Angiolilli et al. 2017)

The mechanism by which Hdac3 mediates catabolic gene expression in chondrocytes has also been studied and it is suggested that in Hdac3-depleted chondrocytes, Erk1/2, as well as its downstream target Runx2, are hyperphosphorylated, as a result of decreased expression and activity of the ERk1/2 specific phosphatase, Dusp6. Expression of Dusp6 and Erk1/2 kinase inhibitors reduced *MMP13* expression and restored matrix production in Hdac3-depleted chondrocytes. Furthermore, premature production of Erk1/2 and MMP13 was found in the growth plates of the inducible Hdac3 cKO. (Carpio et al. 2016) However, Dusp6 expression was not altered in my microarray experiment following HDAC3 inhibition by Apicidin or gene depletion.

It is therefore becoming apparent that HDAC3 plays an essential role in ensuring correct endochondral ossification during development and targeted delivery of HDAC3 selective inhibitors/ drugs or siRNAs should be further tested in order to fully understand its role in OA progression.

7.5 Conclusions

- HDAC pan inhibition using TSA, failed to recapitulate previous data regarding decreased cartilage degeneration in the OA-surgically induced DMM mouse model.
- HDAC3 selective inhibition by Apicidin did not show any significant difference in the cartilage damage observed in the DMM mouse model when compared to the vehicle-control injected mice.
- *In vivo* siHDAC3 intra-articular delivery did not efficiently decreased HDAC3 protein levels at three and six days post-injections.
- *Hdac3* deletion from Col2α1 expressing tissues causes embryonic lethality before E16.5 in mice.
- Postnatal comparison, at three weeks of age, between HET *Hdac3(Fl/+);Col2-Cre/+* and Wildtype *Hdac3(+/+);Col2-Cre/+* did not reveal any significant difference in neither endochondral nor intramembranous ossification and cartilage formation in the growth plates.
- Taken together my data indicate that haplo-insufficiency of Hdac3 has no effect on cartilage development, while early post-natal complete loss is embryonic lethal.

Chapter 8: General Discussion

8.1 Summary

Histone deacetylases regulate the acetylation pattern of chromatin to control gene expression and determine cell differentiation and mammalian development. Previous studies reported HDACs as potential regulators of the expression of major collagenases in articular cartilage and gene silencing studies identified class I HDACs and specifically HDAC3 as a key regulator of their expression. (Culley et al. 2013) Moreover, HDAC inhibitors including TSA have been assessed *in vivo* in surgically induced- and drug induced- osteoarthritis mouse models and showed a chondroprotective role. (Culley et al. 2013; Cai et al. 2015) The role of TSA HDAC-pan inhibitor has also been assessed *in vivo* in rats, whereby reduced gene expression and protein levels of MMP1, MMP3, MMP13 and increased expression of *TIMP1* were observed in the TSA-treated group and safranin-O staining indicated cartilage retention. (Qu et al. 2016) Very recently, Carpio et al. (2016) showed that cartilage Hdac3 is necessary for normal embryonic cartilage development and regulates transcriptome and chromatin landscape in chondrocytes (Carpio et al. 2016) . Previous studies also demonstrated the importance of HDACs in regulating the expression of many anabolic genes in chondrocytes such as *COL2α1*, *COL9α1*, and *ACAN*. (El-Serafi et al. 2011; Huh et al. 2007)

The aims of this project were to examine the effects of HDAC3 loss on gene expression using SW1353 chondrocytes and also on mesenchymal stem cells (MSC) – derived chondrogenesis. First, we sought to confirm previous studies which indicated HDAC3 as a critical mediator of IL-1 induced expression in chondrocytes (**Chapter 3**). To do this, HDAC pan- and selective inhibitiors were used and the expression of *MMP1*, *MMP13*, *IL-6* and *IL-8* were quantified with qRT-PCR. Then the effect of HDACi was determined in a BNC assay, where collagen release was significantly reduced following HDACi and IL-1 or IL-1+OSM stimulation, with no significant alteration in collagen breakdown at the basal level. Gene silencing of *HDAC3* confirmed the effect of the pan-HDACi and selective HDACi on collagenase and *IL-6* expression in chondrocytes and interestingly HDAC3 appears to have IL-1 specific functions in regulating *IL-8* expression. NF-κB signaling pathway components, in particular p65, are potentially good candidates here, as it has been suggested that HDAC3 is required to remove inhibitory acetyl-groups from p65 which then drives *IL-8* expression. Indeed, when a NF-κB luciferase reporter was assayed in the presence/absence of HDACi and IL-1 stimuli, the activation of the reporter was significantly decreased. Nevertheless, no downstream signaling

pathway component analysis was performed (see also section ***8.3 Limitations of the study and future work***). Immediate early gene expression was also analysed and *FRA-1* constitutes a good candidate gene in mediating the effect of HDAC3 in MMP gene expression regulation. However, more experiments required to define the role of FRA-1 on MMP expression in chondrocytes.

Next, we defined the global gene expression changes, transcription factor binding sites enrichments and pathways regulated by HDAC3 in chondrocytes by RNA microarray analysis, following RNAi for HDAC3 or HDAC3i using Apicidin (**Chapter 4**). Herein, a previous microarray analysis, performed by Dr Matt Barter, was taken into account and the data arised from the HDAC pan-inhibition using TSA were compared to my data from the selective HDAC3i Apicidin. This was the first time that collagen catabolism was identified in the GO predicted terms, as well as the first time that E2F binding sites were found in the IL-1 induced and repressed by both inhibitors gene lists. Interestingly, all the subsequent comparisons between the genes that are induced by IL-1 and repressed by either Apicidin, or siHDAC3 or both concluded in an enrichment for E2F-1 transcription factor. Most importantly and as indicated in the relevant tables, many of these genes were OA or cartilage related (see **Tables 4.2-4.6**).

The molecular mechanism of the HDAC3-mediated gene regulation and in particular the E2F-1/HDAC3 relationship was subsequently investigated in SW1353 chondrocytes and HEK293T cells (**Chapter 5**). Here, we showed that first of all HDAC3 and E2F-1 interact *in vitro* and we also predicted novel potential E2F-1 binding sites on the promoters of both MMP1 and MMP13. The effect of E2F-1 over-expression and gene knockdown on MMP expression was determined using MMP luciferase constructs and qRT-PCR. However, a direct association of either HDAC3 or E2F-1 on MMP promoters was now shown in this study and therefore should be confirmed. HDAC3 was also shown to be required for normal cell cycle progression and could be part of the E2F-1 pathway, positively regulating transition into the S phase of the cell cyle.

Finally, I sought to understand the role of HDAC3 in chondrocyte development by using a human MSC *in vitro* model lacking HDAC3 and by generating a cartilage-specific conditional knockout mouse model. Bone marrow derived MSCs were utilized and anabolic gene expression and proteoglycan synthesis determined following HDAC inhibition or *HDAC3* gene depletion during chondrogenesis (**Chapter 6**). HDACi prior to inducing chondrogenesis resulted in decreased anabolic gene expression and proteoglycan synthesis, although the time and duration of MSC treatment seems to play crucial role in altering specific epigenetic

programs. In contrast to the HDACi data, *HDAC3* gene silencing promoted anabolic gene expression and GAG synthesis, indicating siRNA-mediated gene depletion may be promising, as an alternative to drugs tissue engineering approach for the generation of healthy cartilage.

An Hdac3 cartilage specific conditional knockout mouse model was generated in addition to the DMM-OA mouse model, which were used to decide the effect of Hdac3 loss in murine development (**Chapter 7**). However, embryonic lethality of the cKO prevented phenotypic characterisation of the mutants and intra-articular injections of the HDACi in the DMM model did not ameliorate cartilage erosion.

8.2 Key results

The overall scope of my thesis was to determine the role of HDAC3 in the development and or/progression of osteoarthritis and in chondrogenesis.

In the context of the development and/or progression of osteoarthritis the key conclusions drawn from this study are:

- HDAC inhibition using TSA, MS-275 or Apicidin and RNAi for HDAC3 blocked IL-1-induced *MMP1*, *MMP13* and *FRA1* gene expression in SW1353 cells.
- HDACi decreased collagen release following cytokine stimulation in a BNC assay.
- NF-κB transactivation was decreased following HDAC inhibition both in the basal and IL-1 induced level.
- Microarray analysis showed all the genes repressed by siHDAC3 with/without IL-1 stimulation were enriched for E2F-1 transcription factor binding sites. And comparison of the IL-1 induced and siHDAC3 or Apicidin repressed genes are enriched for E2F-1 transcription factor binding sites in their promoters.
- HDAC3 can interact with E2F-1 transcription factor *in vitro* and E2F-1 binding sites have been predicted on both *MMP1* and *MMP13* promoters.
- Over-expressing E2F-1 reduced the transactivation of three MMP luciferase reporters, while HDAC3 inhibition or gene depletion further decreased luciferase activation.
- Gene silencing of E2F-1 up-regulates *MMP1* and *MMP13* expression.
- HDAC3 and E2F-1 are required for normal cell cycle progression and loss of either or both induced cell cycle arrest at the G1 phase.
- HDAC pan inhibition using TSA, failed to recapitulate previous data regarding decreased cartilage degeneration in the OA-surgically induced DMM mouse model. HDAC3 selective inhibition by Apicidin did not show any significant difference in the

cartilage damage observed in the DMM mouse model when compared to the vehicle-control mice.

In the context of chondrocyte differentiation/development the main conclusions are:

- HDAC inhibition using TSA, but not Apicidin, induces hyper-acetylation of α-tubulin and total lysines and decreases anabolic gene expression and proteoglycan deposition of MSC-differentiated chondrocytes.
- *HDAC3* gene depletion promotes anabolic gene expression of *SOX9, ACAN* and *COL2A1* and proteoglycan synthesis of MSC-differentiated chondrocytes.
- *Hdac3* deletion from Col2α1 expressing tissues causes embryonic lethality before E16.5 in mice. However, postnatally *Hdac3(Fl/+);Col2-Cre/+* heterozygous animals were phenotypically normal.

8.3 Limitations of the study and future work

By tailoring the experiments presented in this thesis, the existing data could be made more considerably robust. First, the experiments presented in **Chapter 3** demonstrated that HDACs and especially HDAC3 may positively regulate the induction of collagenase expression in chondrocytes, since inhibition or specific *HDAC3* depletion resulted in a significant repression of this induction. These experiments were conducted in SW1353 cells, it would therefore be worthwhile validating the effect of HDAC3 on *MMP* and *FRA1* gene expression regulation using human articular chondrocytes (HAC). However, previous studies have utilised HACs and partially confirmed the data presented in Chapter 3 (Culley et al. 2013) and SW1353 cells are a recognised model for studying IL-1 induced MMP gene expression regulation (Gebauer et al. 2005).

Another limitation of this study is that only the mRNA levels of MMPs were quantified and the protein levels/activity were not taken into account. The regulation of MMP activity is difficult to assess due to the multitude of mechanisms regulating the activity of these enzymes. The easiest way of analyzing total MMP levels is by analyzing mRNA transcript levels, rather than the protein levels or enzyme- activity due to complex protein regulation. In addition to the transcriptional regulation of MMPs, they are regulated at the translational level through trafficking and secretion by subcellular or extracellular localization, through zymogen activation, by binding to endogenous inhibitors, including TIMPs and α2-macroglobulin and finally through degradation by proteases. (Alameddine & Morgan 2016) However, Young et al. (2005) showed that the protein levels (by immunoblotting) of MMP1 and MMP13 as well

as the activity (by gelatin zymography) of MMP2 and MMP9 were reduced in the presence of TSA and IL-1+OSM. Alternatively, ELISA could have been used to measure MMP activity.

Since the induction of some genes such as *FRA1* requires dynamic changes in acetylation (Khan & Davie 2013), other post-translational modifications such as methylation or phosphorylation may be required for such a turnover and future studies should take this into account. Moreover, the effect of *FRA1* gene depletion on *MMP* or *E2F-1* expression remains unclear and needs to be determined. Additionally the effect of *E2F-1* on *FRA1* expression which in turn might impact upon MMPs was not studied, and these effects could be easily determined by siRNA mediated gene depletions.

A previous study comparing the expression of HDACs in normal and OA cartilage concluded that no significant difference in the expression of *HDAC1*, *HDAC2*, *HDAC3* or *HDAC8*, although a trend toward decreased expression of *HDAC1*, *HDAC3* and *HDAC8* in OA was found (Higashiyama et al. 2010). It would be worth validating some of the gene expression data presented in **Chapter 3**, using OA knee cartilage and comparing it to healthy control cartilage.

The role of HDAC inhibition on NF-κB transactivation was determined using luciferase assays (**Chapter 3**). However, whether siHDAC3 similarly affects NF-κB activity was not analysed and neither were downstream targets of NF-κB signalling pathway. It is known that NF-κB regulates over 200 genes involved in cell cycle and inflammation and is activated by cytokines (IL-1 or TNF-α) or bacterial products (lipopolysaccharide, LPS). (Pereira and Oakley, 2008) In order to analyse the potential action of HDACs and HDAC3 on the activation of signaling components of the NF-κB pathway, phosphorylated antibodies for some NF-κB subunits such as p65 or p50 could be used to test for activation and compared with total protein levels with/without HDACi or siHDAC3. Nuclear translocation of NF-κB could also be impaired following HDACi and this could be tested by immunofluorescence staining. DNA binding could be assessed by ChIP experiments or EMSA (Electro-mobility shift assays) and inhibitory κB α (IκB α) activity monitored by immunoblotting. HDAC3 protein association with any NF-κB transcription factors could be tested by co-immunoprecipitation experiments. Finally NF-κB component acetylation in the presence/ absence of HDACi or siHDAC3 could be monitored by immunoblotting.

Further to the results presented in **Chapter 5** (section **5.3.3**), yeast-two hybrid screening would confirm direct interaction of HDAC3 and E2F-1 transcription factor and Fluorescent Resonance Energy Transfer (FRET) could prove the involvement/requirement of DP1 transcription factor in this interaction. HDAC3 or E2F-1 potential DNA binding at or near

MMP promoters and the responsible for activation of transcription and binding domains could be identified using yeast-two hybrid screening. Whether HDAC3 is responsible for de-acetylating E2F-1 on K117, K120 and K125 should be determined, since this could be an alternative way of HDAC3-mediated regulation of E2F-1 transcription factor half-life and stability, (an antibody is available that recognizes the acetyl-K120 and K125 E2F-1).

EMSA could be used to show if HDAC3 can directly bind to two previously identified regulatory elements on *e2f-1* gene promoter (Panteleeva et al. 2004) or if E2F-1 transcription factor can associate with the chromatin upstream of *MMP1*/*13* promoters. Herein, sequential mutations of the E2F-1 predicted binding sites on the MMP promoters could be used for generating probes to validate direct E2F-1 binding. Alternatively, a luciferase reporter containing the two e2f-1 regulatory elements and similar experiments with the ones presented in **Chapter 5**, section **5.3.5.2**, could be performed and the effect of HDACi and/or siHDAC3 determined. Furthermore, the ChIP experiments performed in this study should be repeated since non-specific binding to the irrelevant IgG antibodies was detected, generating doubtful results. More than one positive and negative control genes should also be included in these experiments and a good candidate as a positive control gene for E2F-1 would be CDC6. Previous studies support an adverse effect of IL-1 stimulation on E2F-1 expression and downstream transcription (Ertosun et al. 2016) and E2F-1 was shown to be required for NF-κB- mediated IL-1β expression (Lim et al. 2007). However, the effect of IL-1 on E2F-1 and MMP expression in chondrocytes is not entirely clear and needs to be established.

With reference to the animal work presented in **Chapter 7**, the acetylation levels of proteins within the intra-articularly injected joints (HDACi- treated, section **7.3.1** ***The effect of Hdac3 inhibition on a DMM-induced osteoarthritis mouse model.***, and siRNA- treated, section **7.3.2** ***Intra-articular delivery of a siRNA targeting HDAC3 in C57Bl/6 mice joints*** were not examined in this thesis. Should, as expected, the HDACi (TSA or Apicidin) and siHDAC3 was successfully administered in the HDACi- treated joints; an increase in acetylation would confirm successful delivery. Sections of the TSA-, Apicidin- and siHDAC3- treated joints could have been stained for a total acetyl-Lysine and an acetyl-α-tubulin antibody and compared to the contralateral knee joints that had no treatment. Alternative delivery methods of the HDACi/ siHDAC3 such as minipumps (Culley et al. 2013) could be used to optimise successful administration.

Furthermore, cell proliferation and apoptosis assays were performed once using *Hdac3(Fl/+);Col2-Cre/+* heterozygous knee joint sections and compared to wildtype littermates. However, these experiments were not successful and staining quantification could

not be performed and neither the experiments could be repeated due to limited time. An IHC for Ki67, a proliferation marker, was also performed using siHDAC3-treated cartilage disc sections and compared to siCON sections from Chapter 6. These data are not presented here, since due to tissue folding of the sections, no staining quantification could be performed. However and based also on my results presented in **Chapter 5** indicating cell cycle arrest following *HDAC3* and *E2F1* depletion, it would be worth validating the effect of Hdac3 loss *in vivo* in cell proliferation/ apoptosis during cartilage development. Therefore different developmental stages of the HET mice could be used including for example one-, three-, six- and nine- week old animals and compared to wildtype mice.

One vital limitation of this project was the lethality of the Hdac3 cKO model that was generated. In order to overpass the embryonic lethality, the only alternative method would be to use an inducible conditional transgenic line, which could induce HDAC3 knockout in cartilage at specific developmental stages. Such examples were given in **Chapter 7**, section **7.4.3** and include the tamoxifen-inducible Col2α1-Cre line (Col2α1ERT-Cre; the Jackson Laboratory- https://www.jax.org/strain/006774) (Nakamura et al. 2006) and the tamoxifen inducible Acan-CreER-Ires-Luc line (Lo Cascio et al. 2014). However, due to unavailability of these transgenic lines in Newcastle University it was time-wise impossible to perform these breedings. So time-allowing it would be worthwhile performing the DMM surgery on the Hdac3 HET and/or establish an inducible cKO and perform the DMM on KO and wildtype animals to examine progression of cartilage degradation.

In summary, I have fulifilled the aims of my PhD, which were to dissect the role of HDAC3 in gene expression regulation in the development/progression of osteoarthritis and in chondrocyte differentiation. First, we confirmed the effect of HDAC3 on the IL-1 induced expression in chondrocytes and HDAC3 loss indicated decreased MMP expression. However, during MSC-chondrogenic differentiation HDAC3 knockdown resulted in an upregulation of *MMP13* in addition to increasing anabolic gene expression. Our results suggest a dual role for HDAC3, one in development and one in differentiated tissues. This dichotomic effect of HDAC3 in development and in inflammatory conditions could be mediated through E2F-1 transcription factor. For example, during an inflammatory response, HDAC3 by associating with E2F-1 and directly/indirectly binding to gene promoters could trigger MMP expression in chondrocytes. Disturbing this HDAC3/E2F-1 association alters IL-1 induced gene expression in chondrocytes. However, a role for HDAC3 and E2F-1 in cell cycle progression also became apparent in this thesis. It is therefore possible that during development, HDAC3/E2F-1 have a key role in the diferentiation/ maturation of the GP chondrocytes by controlling cell proliferation. Teasing these two roles of HDAC3 apart would be necessary for any future therapeutic approach involving HDAC3.

Appendix A

Genes in K-mean clusters shown in **Figure 4.3** are given in the Table below:

Figure 4.1 A-siHDAC3_Cluster 18	**Figure 4.1 B-siHDAC3_Cluster 24**	**Figure 4.1 C-siHDAC3_Cluster 23**	**Figure 4.1 D-Apicidin_Cluster 2**
ARL14	AJAP1	AARS	ACAT2
ATF3	AKR1C2	ABCB9	AHNAK
CSRNP1	BCL3	ABCC3	ALDH9A1
CCL2	BCOR	ABLIM1	AP2S1
CSF2	BIRC2	ACOT9	APCDD1L
DUSP1	BMF	ACSL3	ATP1A1
EFNA1	BPGM	ADK	ATP5I
EGR1	C1QTNF1	AFG3L2	ATP6AP2
EGR2	CCL20	AHSA1	ATP6V0E1
HBEGF	CCL7	AIFM1	AXL
IL8	CD83	AK2	AXL
IRF1	CD83	AKR1C3	B2M
JUNB	CXCL10	AKT1	BAMBI
MAFF	EGFR	ALCAM	BASP1
MAFF	EML1	ANX2P2	BSG
NFKBIZ	ETS2	APH1A	BUD31
SLC25A24	FAM167A	NAA10	C17orf45
TNFAIP3	FAM43B	ARHGEF18	C20orf24
ZFP36	FAT1	ARID5B	ROMO1
	GBP2	ARSD	CALD1
	GINS3	ASAP1	CALM3
	HLX	ASAP2	CALU
	AF176921	ASNSD1	CCT7
	IFIT2	ATP2B4	CDC37
	IFIT3	ATP6V0D1	CDH2
	IL11	ATP6V0E2	CDKN1A
	IL24	ATPIF1	CETN2
	IL32	AVPI1	CKAP4
	IRAK2	B4GALT5	CNN3

	KRT34	BAIAP2L1	COL1A1
	KRT75	BCL7C	COL1A2
	C11orf96	BMP4	COL5A1
	GATSL3	BSCL2	COL6A3
	FP15737	C11orf1	COX6B1
	LRIG1	C13orf15	CREB1
	LRIG1	INF2	CST3
	MSC	C16orf58	CSTB
	NAMPT	FOPNL	CTGF
	NEDD4L	C18orf10	CYB5B
	NFIL3	C19orf22	DAD1
	NKX3-1	C19orf50	DCBLD2
	NMI	C19orf60	DDB1
	NOC3L	C1GALT1C1	DDT
	NRG1	C20orf111	DRAP1
	OAS2	C21orf33	EDF1
	PARP12	C2CD2	EIF3B
	PARP9	C2orf29	EIF3D
	PGM3	RRP36	EIF4G2
	PPAP2B	C9orf119	EMP3
	PRIC285	C9orf78	EPN1
	RGMB	CALM1	ESD
	RIPK2	CANT1	FEZ2
	TYMP	CAPZB	FHL2
	SERPINA1	CAV2	FXYD5
	SERPINB2	CCND3	G6PD
	SERPINB2	CD97	GHITM
	SERPINB8	CD99L2	GNAI2
	SERPINB8	CDC16	GNS
	SLC25A28	CDKN3	GSPT1
	SLC2A6	CEBPD	GSTO1
	SLCO2B1	CEBPZ	H2AFY
	SOD2	CFDP1	HCFC1R1
	SPHK1	CGGBP1	HDAC1

	SPSB1	CHIC2	HIBADH
	TCEAL1	CHMP1A	HK1
	TJP2	CLINT1	HNRNPM
	TMEM132A	CMTM3	HNRNPA2B1
	TMPRSS3	CNIH	HNRNPM
	TNFAIP2	CNPY2	HPCAL1
	TNFRSF1B	CNRIP1	ILK
	TNIP1	COPE	ITM2B
	TRIM21	COPS4	JTB
	TRIM56	COPS6	KHDRBS1
	ZSWIM4	COPS8	LCP1
		COPZ1	LDOC1
		COQ2	C4orf48
		CORO1C	DKFZp686L07201
		CPNE1	NA
		CREB3L2	MAGED1
		CRK	URGCP
		CTNNA1	NCOA4
		CTSA	NDUFA1
		CTSB	NDUFAB1
		CTXN1	NDUFAF3
		CUEDC2	NDUFB2
		CXCR7	NDUFS8
		CYBRD1	NGFRAP1
		CYFIP1	NME1
		SPECC1L	NOP10
		DAG1	NPTN
		WDR68	NQO1
		DCTD	NUCB1
		DCTPP1	NUCKS1
		DDX17	ODC1
		DDX24	P4HB
		DEGS1	PAGE5
		DEK	PALLD

		DENND5A	PDLIM1
		DHCR24	PEA15
		DHX15	PFN2
		DIMT1L	POLR1D
		DLD	PPP2CA
		DNAJB6	PPP2R1A
		DUSP10	PRNP
		DUSP22	PRSS23
		DUSP23	PSAP
		EEF1A2	PSAP
		EFR3A	PSMA4
		EIF2A	PSMA5
		EIF4G1	PSMB6
		EMD	PTBP1
		ENG	PTTG1IP
		EPAS1	QARS
		EPDR1	RAB31
		EPRS	RARS
		ERAP2	REXO2
		ERCC1	RHOBTB3
		ERGIC3	RNF7
		EXOSC1	RRAGA
		EXOSC3	SAT1
		FADS1	SC4MOL
		FAM189B	SEMA3E
		FAM50A	Sep-09
		FAM98A	SERF2
		FBXL18	SERPINE1
		FBXO11	SH3BGRL3
		FBXO7	SH3KBP1
		FCAR	SHC1
		FERMT2	SLC16A3
		FGFRL1	SLC25A3
		FIBP	SNX3

		FIS1	SPCS1
		FKBP3	TCEAL4
		FLOT2	TIMM23
		FNDC3B	TIMP1
		FZD2	TIMP2
		GATAD2A	TM4SF1
		GLIPR2	TMBIM6
		GLT25D1	TMED3
		GNL2	TMED9
		GOT1	TMEM14C
		GPAA1	TMEM158
		GPS1	TMEM17
		GRINA	TMEM59
		GTF2E2	TMEM66
		GTF2F2	TNFRSF21
		H1F0	TRAM1
		HECTD1	TSPO
		HERC4	TXNRD1
		HIF1A	UBA1
		HIST1H2BD	UBA1
		HMGB2	UXT
		HMGCR	WBP2
		HNRNPA0	WDR1
		HNRNPA2B1	YWHAH
		HNRNPU	ZFAND5
		HNRNPUL1	
		HNRNPUL1	
		HOXA10	
		HOXC13	
		IARS	
		IDS	
		IFI27L2	
		IL7R	
		IMP4	

		IQGAP1	
		AEN	
		ITFG3	
		ITM2C	
		JMJD8	
		KDELR3	
		KIAA0196	
		KLHDC5	
		KLHL9	
		LAMP2	
		LANCL1	
		LANCL1	
		LAPTM4A	
		LARP6	
		LCMT1	
		FAM161A	
		METTL23	
		LOC151162	
		LOC375295	
		C12orf75	
		MXRA8	
		DTYMK	
		MXRA8	
		H2AFX	
		LOX	
		LPIN1	
		LSS	
		LUZP1	
		LYRM1	
		MAD2L2	
		MAN2B2	
		LAMTOR3	
		LAMTOR2	
		Mar-04	

		Mar-07	
		MATN2	
		MED20	
		MED6	
		MEG3	
		MFSD1	
		MGAT1	
		MGAT4B	
		MLEC	
		MMS19	
		MPP1	
		MRFAP1L1	
		MRPL17	
		MRPL18	
		MRPL22	
		MRPL27	
		MRPL40	
		MRPL41	
		MTPN	
		MTX2	
		MYL9	
		NAA20	
		NDRG1	
		NDUFB6	
		NDUFS7	
		NFATC2IP	
		NGDN	
		NGFRAP1	
		NIPA2	
		NPTN	
		NR2F2	
		NRGN	
		NSDHL	
		NUDT2	
		NUP37	
		OLFML3	
		OXSR1	
		PASD1	
		PDLIM7	

		PDPR	
		PDXDC1	
		PDXK	
		PELO	
		PFKFB3	
		PGLS	
		PHB2	
		PHLDA3	
		PICALM	
		PIGP	
		PLEKHB2	
		PMM1	
		PMPCB	
		PNMA5	
		POLR3GL	
		PPCS	
		PPIC	
		PPP2R4	
		PPP4R1	
		PPP6C	
		PQLC1	
		SGK223	
		PRC1	
		PRICKLE1	
		PRNP	
		PRPF31	
		PSMA3	
		PSME4	
		PSMG1	
		PTGFRN	
		PTPLAD1	
		PTPMT1	
		PTPRF	
		PUM1	
		PURB	
		PYGL	
		QDPR	
		RABEPK	
		RAD23A	
		RAI14	

		RALY	
		RDH11	
		NT5C1B	
		RHBDD2	
		RIN2	
		RNF149	
		RNF34	
		RPL34	
		RPS6KB2	
		RSPRY1	
		SAR1B	
		SCOC	
		SCYL1	
		SDF2L1	
		SDHAF2	
		SEC31A	
		SELM	
		Sep-11	
		SERINC3	
		SF3A2	
		TRA2B	
		SRSF4	
		SGK1	
		SH3GLB1	
		SIAH1	
		SIGMAR1	
		SIGMAR1	
		SIVA1	
		SLC11A2	
		SLC25A4	
		SLC35A2	
		SLC35B1	
		SLC39A1	
		SMAD3	
		SMAD5	
		SMC4	
		SNAI2	
		SPANXN3	
		SPNS1	
		SPOP	

		SRP68	
		SRRM2	
		SSR1	
		STARD7	
		STAT2	
		STAU1	
		STK4	
		STRA13	
		STUB1	
		STX3	
		SULF2	
		SYNC	
		SYNCRIP	
		TAF10	
		TARS	
		TBK1	
		TCEAL8	
		TEX11	
		TGFBI	
		TGFBR2	
		TIAF1	
		TIAL1	
		TIMM23	
		TK1	
		TLE4	
		TM2D1	
		TMCO3	
		TMED5	
		TMEM106C	
		TMEM126A	
		TMEM131	
		TMEM14A	
		TMEM179B	
		TMEM203	
		TMEM219	
		TMEM43	
		TMEM60	
		TMEM97	
		TMUB1	
		TNC	

		TNFAIP1	
		TNPO2	
		TOP2B	
		TPST1	
		TRAPPC1	
		TRAPPC4	
		TRIAP1	
		TRIB1	
		TRIM28	
		TRIM4	
		TRIP12	
		TRNP1	
		TROVE2	
		TSPAN3	
		TSR2	
		TUBB6	
		TWSG1	
		UBE2A	
		UBE2Z	
		UBP1	
		UBTD1	
		UGCG	
		UGP2	
		ULK1	
		USP9X	
		VAMP5	
		VPS41	
		WBSCR22	
		WDR13	
		WDR6	
		WDR61	
		WRNIP1	
		XPNPEP1	
		XYLT2	
		YIF1A	
		YIPF3	
		ZAK	
		ZC3HC1	
		ZDHHC7	
		ZDHHC9	

		ZMPSTE24	
		LOC100506144	
		RNF115	
		ZNF483	
		ZNF622	

Appendix B

Top 10 list of transcription factors (Tf) predicted by GATHER for siHDAC3 repressed genes.

TRANSFAC analysis for siHDAC3 repressed genes					
Basal- no IL-1		**IL-1 1 hour**		**IL-1 6 hours**	
Tf predicted	p-value	Tf predicted	p-value	Tf predicted	p-value
ELK1	< 0.0001	E2F	0.0002	E2F	< 0.0001
E2F	< 0.0001	E2F1	0.0002	E2F	< 0.0001
E2F-1	< 0.0001	NRF2: nuclear respiratory factor 2	0.0004	E2F	< 0.0001
E2F1	0.0002	E2F	0.0008	E2F1	< 0.0001
NRF2: nuclear respiratory factor 2	0.0002	E2F1	0.001	Nuclear Factor Y (Y box binding factor)	< 0.0001
E2F-1	0.0003	ELK1	0.002	E12	< 0.0001
E2F	0.0007	E2F-1	0.003	E2F1	< 0.0001
MYCMAX: c-Myc: Max binding sites	0.0008	E2F	0.004	E2F1	< 0.0001
E2F-1	0.002	E2F-1	0.004	Nuclear Factor Y (Y box binding factor)	< 0.0001
NFY: nuclear factor Y (Y-box binding factor)	0.002	E2F	0.005	E2F	< 0.0001

Appendix C

The FACs gating data from one experiment containing four replicates per treatment is shown below. Assays were performed twice and results are presented in **Figure 5.10**.

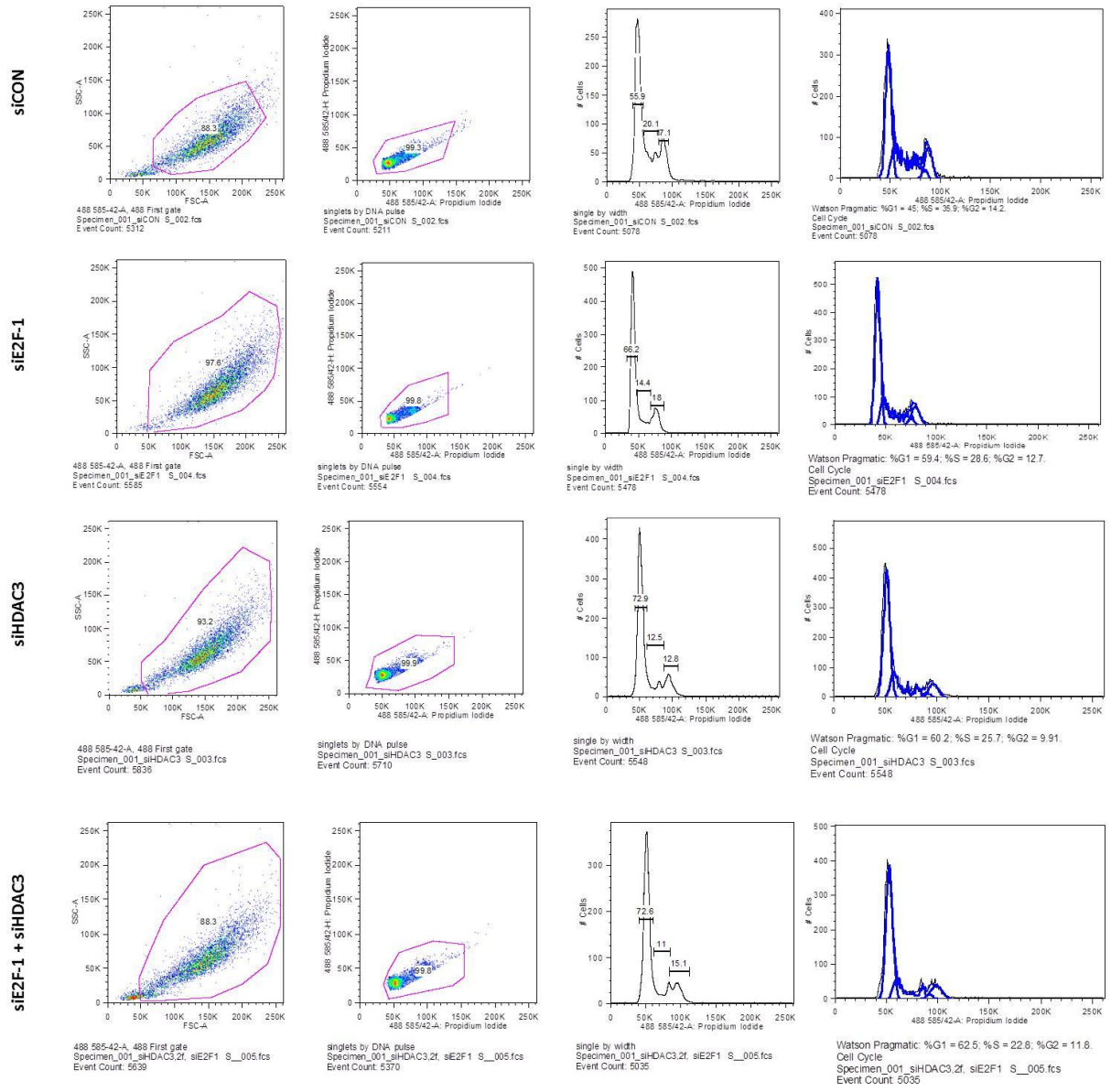

Presentations and Publications

Presentations

- **Tsompani D.**, Barter MJ., Young DA., (2016) The role of Histone Deacetylase 3 in chondrogenesis and Osteoarthritis. *UK-Pavia Connective Tissue Meeting, Newcastle, UK,* Best PhD presentation award.
- **Tsompani D.**, Barter MJ., Young DA., (2016) The role of Histone Deacetylase 3 in chondrogenesis and Osteoarthritis. *Proc. of CIMA/ CMAR epigenetics meeting, Newcastle, UK, October 14,* Oral presentation.
- **Tsompani D.**, Barter MJ., Rowan AD., Young DA., (2016) The role of Histone Deacetylase 3 in chondrogenesis and Osteoarthritis. *Proc. of Arthritis Research UK annual Fellows' meeting, Loughborough, UK, March 17-18,* Oral presentation.
- **Tsompani D.**, Barter MJ., Rowan AD., Young DA., (2015) The role of Histone Deacetylase 3 in chondrogenesis and Osteoarthritis. *Proc. of Arthritis Research UK annual Fellows' meeting, Loughborough, UK, March 19-20.* Poster presentation
- **Tsompani D.**, Barter MJ., Young DA., (2015) The role of Histone Deacetylase 3 in chondrogenesis and Osteoarthritis. *First ICM Poster evening, Newcastle, UK,* Best PhD poster prize

Publications

- **Tsompani D**., Barter MJ, Skelton A., Rowan AD., Clark I, Young DA, **(2017)** Histone deacetylase 3 depletion or specific inhibition reduces collagenase expression in chondrocytes through direct interaction with E2F-1 transcription factor. (*manuscript in preparation*)
- **Tsompani D.**, **Barter MJ**, Skelton A., Young DA, (**2017**) Circulating serum miRNAs as biomarkers for the progression of osteoarthritis in the destabilisation of the medial meniscus mouse model (*manuscript in preparation*).
- **Tsompani D.**, Barter MJ, Young DA, (**2016**) The role of histone deacetylase 3 in chondrogenesis and osteoarthritis. *Osteoarthritis and Cartilage*, **24**: S226
- **Tsompani D.**, Barter MJ, Rowan AD., Young DA, (**2015**) The role of histone deacetylase 3 in chondrogenesis and osteoarthritis. *International Journal of Experimental Pathology*, **96**: A14-A15

References

Afonina, I.S. et al., 2015. Proteolytic Processing of Interleukin-1 Family Cytokines: Variations on a Common Theme. *Immunity*, 42(6), pp.991–1004.

Ahmad, N.N. et al., 1991. Stop codon in the procollagen II gene (COL2A1) in a family with the Stickler syndrome (arthro-ophthalmopathy). *Proceedings of the National Academy of Sciences of the United States of America*, 88(15), pp.6624–7.

Akiyama, H., 2008. Control of chondrogenesis by the transcription factor Sox9. *Modern Rheumatology*, 18(3), pp.213–219.

Alameddine, H.S. & Morgan, J.E., 2016. Matrix Metalloproteinases and Tissue Inhibitor of Metalloproteinases in Inflammation and Fibrosis of Skeletal Muscles. *Journal of neuromuscular diseases*, 3(4), pp.455–473.

Allfrey, V.G., Faulkner, R. & Mirsky, A.E., 1964. Acetylation and Methylation of Histones and Their Possible Role in the Regulation of Rna Synthesis. *Proceedings of the National Academy of Sciences of the United States of America*, 51(1938), pp.786–94.

Andersen, T.L. et al., 2004. A scrutiny of matrix metalloproteinases in osteoclasts: Evidence for heterogeneity and for the presence of MMPs synthesized by other cells. *Bone*, 35(5), pp.1107–1119.

Baek, S.H. et al., 2002. Exchange of N-CoR corepressor and Tip60 coactivator complexes links gene expression by NF-κB and β-amyloid precursor protein. *Cell*, 110(1), pp.55–67.

Bajpayee, A.G. et al., 2015. A rabbit model demonstrates the influence of cartilage thickness on intra-articular drug delivery and retention within cartilage. *Journal of Orthopaedic Research*, 33(5), pp.660–667.

Bannister, A.J. & Kouzarides, T., 2011. Regulation of chromatin by histone modifications. *Cell research*, 21(3), pp.381–395.

Barksby, H.E. et al., 2006. Interleukin-1 in combination with oncostatin M up-regulates multiple genes in chondrocytes: Implications for cartilage destruction and repair. *Arthritis and Rheumatism*, 54(2), pp.540–550.

Barter, M.J. et al., 2015. Genome-wide microRNA and gene analysis of mesenchymal stem cell chondrogenesis identifies an essential role and multiple targets for miR-140-5p. *Stem Cells*, 33(11), pp.3266–3280.

Barter, M.J. et al., 2010. HDAC-mediated control of ERK- and PI3K-dependent TGF-β-induced extracellular matrix-regulating genes. *Matrix Biology*, 29(7), pp.602–612.

Barter, M.J., Bui, C. & Young, D.A., 2012. Epigenetic mechanisms in cartilage and osteoarthritis: DNA methylation, histone modifications and microRNAs. *Osteoarthritis and Cartilage*, 20(5), pp.339–349.

Bateman, J.F., 2001. The molecular genetics of inherited cartilage disease. *Osteoarthritis and cartilage*, 9 Suppl A, pp.S141-9.

Bauer, U. et al., 2000. Regulation of E2F1 activity by acetylation. , 19(4), pp.662–671.

Bhaskara, S. et al., 2011. HDAC3 is essential for the maintenance of chromatin structure and genome stability. *Cancer Cell*, 18(5), pp.436–447.

Bieda, M. et al., 2006. Unbiased location analysis of E2F1-binding sites suggests a widespread role for E2F1 in the human genome. *Genome Research*, pp.595–605.

Binné, U.K. et al., 2007. Retinoblastoma protein and anaphase-promoting complex physically interact and functionally cooperate during cell-cycle exit. *Nature cell biology*, 9(December), pp.225–232.

Böhme, K., Winterhalter, K.H. & Bruckner, P., 1995. Terminal differentiation of chondrocytes in culture is a spontaneous process and is arrested by transforming growth factor-beta 2 and basic fibroblast growth factor in synergy. *Experimental cell research*, 216(1), pp.191–8.

Boos, N. et al., 1999. Immunohistochemical analysis of type X-collagen expression in osteoarthritis of the hip joint. *Journal of Orthopaedic Research*, 17(4), pp.495–502.

Bose, P., Dai, Y. & Grant, S., 2014. Histone deacetylase inhibitor (HDACI) mechanisms of action: Emerging insights. *Pharmacology and Therapeutics*, 143(3), pp.323–336.

Botter, S.M. et al., 2009. ADAMTS5-/- mice have less subchondral bone changes after induction of osteoarthritis through surgical instability: implications for a link between cartilage and subchondral bone changes. *Osteoarthritis and Cartilage*, 17(5), pp.636–645.

Boutillier, A.L., Trinh, E. & Loeffler, J.P., 2003. Selective E2F-dependent gene transcription is controlled by histone deacetylase activity during neuronal apoptosis. *Journal of Neurochemistry*, 84(4), pp.814–828.

Bradley, E.W., Carpio, L.R. & Westendorf, J.J., 2013. Histone deacetylase 3 suppression increases PH domain and leucine-rich repeat phosphatase (Phlpp)1 expression in

chondrocytes to suppress Akt signaling and matrix secretion. *Journal of Biological Chemistry*, 288(14), pp.9572–9582.

Brehm, A. et al., 1998. Retinoblastoma protein recruits histone deacetylase to repress transcription. *Nature*, 391(6667), pp.597–601.

De Bruin, A. et al., 2003. Identification and Characterization of E2F7, a Novel Mammalian E2F Family Member Capable of Blocking Cellular Proliferation. *Journal of Biological Chemistry*, 278(43), pp.42041–42049.

Bui, C. et al., 2012. cAMP response element-binding (CREB) recruitment following a specific CpG demethylation leads to the elevated expression of the matrix metalloproteinase 13 in human articular chondrocytes and osteoarthritis. *FASEB journal : official publication of the Federation of American Societies for Experimental Biology*, 26(7), pp.3000–11.

Byers, P.H., 2001. Folding defects in fibrillar collagens. *Philosophical Transactions of the Royal Society of London. Series B, Biological Sciences*, 356(1406), pp.151–158.

Cai, D. et al., 2015. Histone deacetylase inhibition activates Nrf2 and protects against osteoarthritis. *Arthritis research & therapy*, 17, p.269.

Campanero, M.R. & Flemington, E.K., 1997. Regulation of E2F through ubiquitin-proteasome-dependent degradation: stabilization by the pRB tumor suppressor protein. *Proceedings of the National Academy of Sciences of the United States of America*, 94(6), pp.2221–2226.

Carpio, L.R. et al., 2016. Histone deacetylase 3 supports endochondral bone formation by controlling cytokine signaling and matrix remodeling. *Science Signaling*, 9(440), p.ra79-ra79.

Cavenee, W.K. et al., 1983. Expression of recessive alleles by chromosomal mechanisms in retinoblastoma. *Nature*, 305(5937), pp.779–784.

Cawston, T.E. et al., 2003. Cytokine synergy, collagenases and cartilage collagen breakdown. , 33, pp.125–134.

Cawston, T.E. & Wilson, A.J., 2006. Understanding the role of tissue degrading enzymes and their inhibitors in development and disease. *Best Practice & Research Clinical Rheumatology*, 20(5), pp.983–1002.

Chang, H.-M. et al., 2004. Induction of interferon-stimulated gene expression and antiviral responses require protein deacetylase activity. *PNAS*, 101(26), pp.9578–9583.

Chang, J.T. & Nevins, J.R., 2006. GATHER: A systems approach to interpreting genomic signatures. *Bioinformatics*, 22(23), pp.2926–2933.

Chang, S. et al., 2006. Histone Deacetylase 7 Maintains Vascular Integrity by Repressing Matrix Metalloproteinase 10. *Cell*, 126(2), pp.321–334.

Chavey, C. et al., 2008. Interleukin-8 Expression Is Regulated by Histone Deacetylases through the Nuclear Factor- B Pathway in Breast Cancer □.

Chen, H.-Z., Tsai, S.-Y. & Leone, G., 2009. Emerging roles of E2Fs in cancer: an exit from cell cycle control. *Nature reviews. Cancer*, 9(11), pp.785–97.

Chen, M. et al., 2007. Generation of a transgenic mouse model with chondrocyte-specific and tamoxifen-inducible expression of Cre recombinase. *Genesis*, 45(1), pp.44–50.

Chen, S.-Y. et al., 2012. Suppression of collagen-induced arthritis by intra-articular lentiviral vector-mediated delivery of Toll-like receptor 7 short hairpin RNA gene. *Gene therapy*, 19(7), pp.752–60.

Chen, Z. et al., 2013. Hyaluronic acid-coated bovine serum albumin nanoparticles loaded with brucine as selective nanovectors for intra-articular injection. *International Journal of Nanomedicine*, 8, pp.3843–3853.

Chiara, G. & Cancedda, R., 2009. Cartilage and Bone Extracellular Matrix. *Current Pharmaceutical Design*, 15(12), pp.1334–1348.

Chiba, T. et al., 2004. Identification of genes up-regulated by histone deacetylase inhibition with cDNA microarray and exploration of epigenetic alterations on hepatoma cells. *Journal of hepatology*, 41(3), pp.436–45.

Cho, Y. & Cavalli, V., 2012. HDAC5 is a novel injury-regulated tubulin deacetylase controlling axon regeneration. *The EMBO journal*, 31(14), pp.3063–78.

Choo, Q.Y. et al., 2010. Histone deacetylase inhibitors MS-275 and SAHA induced growth arrest and suppressed lipopolysaccharide-stimulated NF-κB p65 nuclear accumulation in human rheumatoid arthritis synovial fibroblastic E11 cells. *Rheumatology*, 49(8), pp.1447–1460.

Christensen, J. et al., 2005. Characterization of E2F8, a novel E2F-like cell-cycle regulated repressor of E2F-activated transcription. *Nucleic Acids Research*, 33(17), pp.5458–5470.

Claire Attwooll, E.L.D. and K.H., 2004. The E2F family: specific functions and overlapping interests. *The EMBO*, 23(10), pp.4709–4716.

Clark, I.M. et al., 2008. The regulation of matrix metalloproteinases and their inhibitors. *The*

International Journal of Biochemistry & Cell Biology, 40, pp.1362–1378.

Classon, M. & Harlow, E., 2002. The retinoblastoma tumour suppressor in development and cancer. *Nature reviews. Cancer*, 2(12), pp.910–7.

Clayton, A.L., Hazzalin, C.A. & Mahadevan, L.C., 2006. Enhanced Histone Acetylation and Transcription: A Dynamic Perspective. *Molecular Cell*, 23(3), pp.289–296.

Corr, M., 2008. Wnt-[beta]-catenin signaling in the pathogenesis of osteoarthritis. *Nat Clin Pract Rheum*, 4(10), pp.550–556.

Culley, K.L. et al., 2013. Class i histone deacetylase inhibition modulates metalloproteinase expression and blocks cytokine-induced cartilage degradation. *Arthritis and Rheumatism*, 65(7), pp.1822–1830.

Cunliffe, V.T., 2004. Histone deacetylase 1 is required to repress Notch target gene expression during zebrafish neurogenesis and to maintain the production of motoneurones in response to hedgehog signalling. *Development (Cambridge, England)*, 131(12), pp.2983–95.

Cunliffe, V.T. & Casaccia-Bonnefil, P., 2006. Histone deacetylase 1 is essential for oligodendrocyte specification in the zebrafish CNS. *Mechanisms of Development*, 123(1), pp.24–30.

Cunnane, G. et al., 2001. The effects of treatment with interleukin-1 receptor antagonist on the inflamed synovial membrane in rheumatoid arthritis. *Rheumatology (Oxford, England)*, 40(1), pp.62–69..

Dangond, F. et al., 1998. Differential display cloning of a novel human histone deacetylase (HDAC3) cDNA from PHA-activated immune cells. *Biochemical and biophysical research communications*, 242(3), pp.648–652.

Davidson, R.K. et al., 2006. Expression profiling of metalloproteinases and their inhibitors in synovium and cartilage. *Arthritis research & therapy*, 8(4), p.R124.

Day-Williams, A.G. et al., 2011. A variant in MCF2L is associated with osteoarthritis. *American Journal of Human Genetics*, 89(3), pp.446–450.

Drissi, H. et al., 2005. Transcriptional regulation of chondrocyte maturation: Potential involvement of transcription factors in OA pathogenesis. *Molecular Aspects of Medicine*, 26(3), pp.169–179.

Dudakovic, A. et al., 2015. Histone deacetylase inhibition destabilizes the multi-potent state of uncommitted adipose-derived mesenchymal stromal cells. *Journal of Cellular*

Physiology, 230(1), pp.52–62.

Dyson, N. et al., 1989. The human papilloma virus-16 E7 oncoprotein is able to bind to the retinoblastoma gene product. *Science*, 243(4893), p.934 LP-937.

Dyson, N., 1998. The regulation of E2F by pRB-family proteins. *Genes & Development*, 12(617), pp.2245–2262.

El-Serafi, A.T., Oreffo, R.O.C. & Roach, H.I., 2011. Epigenetic modifiers influence lineage commitment of human bone marrow stromal cells: Differential effects of 5-aza-deoxycytidine and trichostatin A. *Differentiation*, 81(1), pp.35–41.

Elaut, G. et al., 2007. A metabolic screening study of trichostatin A (TSA) and TSA-like histone deacetylase inhibitors in rat and human primary hepatocyte cultures. *The Journal of pharmacology and experimental therapeutics*, 321(1), pp.400–408.

Ertosun, M.G., Hapil, F.Z. & Osman Nidai, O., 2016. E2F1 transcription factor and its impact on growth factor and cytokine signaling. *Cytokine & growth factor reviews*, (2015), pp.1–9.

Esenyel, M., İçağasıoğlu, A. & Esenyel, C.Z., 2013. Effects of calcitonin on knee osteoarthritis and quality of life. *Rheumatology International*, 33(2), pp.423–427.

Evangelou, E. et al., 2009. Large-scale analysis of association between GDF5 and FRZB variants and osteoarthritis of the hip, knee, and hand. *Arthritis and Rheumatism*, 60(6), pp.1710–1721.

Eyre, D.R., Weis, M.A. & Wu, J.J., 2006. Articular cartilage collagen: An irreplaceable framework? *European Cells and Materials*, 12, pp.57–63.

Fajas, L. et al., 2002. The retinoblastoma-histone deacetylase 3 complex inhibits PPARγ and adipocyte differentiation. *Developmental Cell*, 3(6), pp.903–910.

Farre, D. et al., 2003. Identification of patterns in biological sequences at the ALGGEN server: PROMO and MALGEN. *Nucleic Acids Research*, 31(13), pp.3651–3653.

Ferrari, G. et al., 1998. Muscle Regeneration by Bone Marrow-Derived Myogenic Progenitors. *Science*, 279(5356), p.1528 LP-1530.

Ferreira, R. et al., 2001. Cell cyle-dependent recruitment of HDAC-1 correlates with deacetylation of histone H4 on an Rb-E2F target promoter. *EMBO Reports*, 2(9), pp.794–799.

Fox, S. et al., 2009. The basic science of articular cartilage: structure, composition, and function. *Sports health*, 1(6), pp.461–8.

Franceschini, A. et al., 2013. STRING v9.1: Protein-protein interaction networks, with increased coverage and integration. *Nucleic Acids Research*, 41(D1).

Friend, S.H. et al., 1986. A human DNA segment with properties of the gene that predisposes to retinoblastoma and osteosarcoma. *Nature*, 323(6089), pp.643–646.

Fujiwara-Okada, Y. et al., 2013. Y-box binding protein-1 regulates cell proliferation and is associated with clinical outcomes of osteosarcoma. *British journal of cancer*, 108(4), pp.836–47.

Fukui, N. et al., 2003. Stimulation of BMP-2 Expression by Pro-Inflammatory Cytokines IL-1 and TNF-α in Normal and Osteoarthritic Chondrocytes. *The Journal of Bone & Joint Surgery*, 85(suppl 3), p.59 LP-66.

Gao, Z. et al., 2006. Regulation of nuclear translocation of HDAC3 by IkappaBalpha is required for tumor necrosis factor inhibition of peroxisome proliferator-activated receptor gamma function. *The Journal of biological chemistry*, 281(7), pp.4540–7.

Garlanda, C., Dinarello, C.A. & Mantovani, A., 2013. THE INTERLEUKIN-1 FAMILY: BACK TO THE FUTURE. *Immunity*, 39(6), pp.1003–1018.

Gebauer, M. et al., 2005. Comparison of the chondrosarcoma cell line SW1353 with primary human adult articular chondrocytes with regard to their gene expression profile and reactivity to IL-1β. *Osteoarthritis and Cartilage*, 13(8), pp.697–708.

Genin, P., Morin, P. & Civas, A., 2003. Impairment of Interferon-Induced IRF-7 Gene Expression due to Inhibition of ISGF3 Formation by Trichostatin A. *Journal of Virology*, 77, pp.7113–7119.

Giacinti, C. & Giordano, a, 2006. RB and cell cycle progression. *Oncogene*, 25(38), pp.5220–7.

Glasson, S.S. et al., 2005. Deletion of active ADAMTS5 prevents cartilage degradation in a murine model of osteoarthritis. *Nature*, 434(7033), pp.644–648.

Goldring, M.B. et al., 1988. Interleukin 1 suppresses expression of cartilage-specific types II and IX collagens and increases types I and III collagens in human chondrocytes. *Journal of Clinical Investigation*, 82(6), pp.2026–2037.

Goldring, M.B. & Marcu, K.B., 2009. Cartilage homeostasis in health and rheumatic diseases. *Arthritis research & therapy*, 11(3), p.224.

Grant, P.A. et al., 1997. Yeast Gcn5 functions in two multisubunit complexes to acetylate nucleosomal histones: Characterization of an ada complex and the saga (spt/ada)

complex. *Genes and Development*, 11(13), pp.1640–1650.

Gupta, M. & Eisen, G.M., 2009. NSAIDs and the gastrointestinal tract. *Current Gastroenterology Reports*, 11(5), pp.345–353.

Haberland, M., Mokalled, M.H., et al., 2009. Epigenetic control of skull morphogenesis by histone deacetylase 8 service Epigenetic control of skull morphogenesis by histone deacetylase 8. , pp.1625–1630.

Haberland, M., Montgomery, R.L. & Olson, E.N., 2009. The many roles of histone deacetylases in development and physiology: implications for disease and therapy. *Nature reviews. Genetics*, 10(1), pp.32–42.

Hamilton, J.A., 2008. Colony-stimulating factors in inflammation and autoimmunity. *Nat Rev Immunol*, 8(7), pp.533–544.

Han, B. et al., 2013. Trichostatin a stabilizes the expression of pluripotent genes in human mesenchymal stem cells during ex vivo expansion. *PLoS ONE*, 8(11).

Han, J.W. et al., 2000. Apicidin, a histone deacetylase inhibitor, inhibits proliferation of tumor cells via induction of p21WAF1/Cip1 and gelsolin. *Cancer research*, 60(21), pp.6068–74.

Hargreaves, D.C., Horng, T. & Medzhitov, R., 2009. Control of Inducible Gene Expression by Signal-Dependent Transcriptional Elongation. *Cell*, 138(1), pp.129–145.

Harper, J.W. & Elledge, S.J., 1999. Skipping into the E2F1-destruction pathway. *Nature cell biology*, 1(May), pp.5–7.

Higashiyama, R. et al., 2010. Correlation between MMP-13 and HDAC7 expression in human knee osteoarthritis. *Modern Rheumatology*, 20(1), pp.11–17.

Hoffmann, E. et al., 2002. Multiple control of interleukin-8 gene expression. *Journal of Leukocyte Biology* , 72(5), pp.847–855.

Holyoak, D.T. et al., 2016. Osteoarthritis: Pathology, Mouse Models, and Nanoparticle Injectable Systems for Targeted Treatment. *Annals of Biomedical Engineering*, 44(6), pp.1–14.

Honda, K. & Taniguchi, T., 2006. IRFs: master regulators of signalling by Toll-like receptors and cytosolic pattern-recognition receptors. *Nature reviews. Immunology*, 6(9), pp.644–658.

Hoorens, A. et al., 2001. Distinction Between Interleukin-1 – Induced Necrosis and Apoptosis of Islet Cells. *Diabetes*, 50(Il), pp.551–557.

Hubbert, C. et al., 2002. HDAC6 is a microtubule-associated deacetylase. *Nature*, 417(6887), pp.455–458.

Huh, Y.H., Ryu, J. & Chun, J., 2007. Regulation of type II collagen expression by histone deacetylase in articular chondrocytes. *The Journal of biological chemistry*, 282(23), pp.17123–17131.

Hull, E.E., Montgomery, M.R. & Leyva, K.J., 2016. HDAC Inhibitors as Epigenetic Regulators of the Immune System : Impacts on Cancer Therapy and Inflammatory Diseases. , 2016.

Hunter, D.J. & Felson, D.T., 2006. Osteoarthritis. *BMJ (Clinical research ed.)*, 332(7542), pp.639–42.

Hye Joung, K. et al., 2016. Enhancement of human mesenchymal stem cell differentiation by combination treatment with 5-azacytidine and trichostatin A. *Biotechnology Letters*, 38, pp.167–174.

Iglesias, M. et al., 1998. Human papillomavirus type 16 E7 protein sensitizes cervical keratinocytes to apoptosis and release of interleukin-1alpha. *Oncogene*, 17(10), pp.1195–205.

Ingram, L. et al., 2011. E2F-1 regulation by an unusual DNA damage-responsive DP partner subunit. *Cell death and differentiation*, 18(1), pp.122–32.

Jenuwein, T. & Allis, C.D., 2001. Translating the Histone Code. *Science*, 293(5532), p.1074 LP-1080.

Ji, P. et al., 2004. An Rb-Skp2-p27 pathway mediates acute cell cycle inhibition by Rb and is retained in a partial-penetrance Rb mutant. *Molecular Cell*, 16(1), pp.47–58.

Jiang, Y. et al., 2002. Pluripotency of mesenchymal stem cells derived from adult marrow. *Nature*, 418(6893), pp.41–49.

Johansen, F.-E. & Prywes, R., 1994. Two Pathways for Serum Regulation of the c-fos Serum Response Element Require Specific Sequence Elements and a Minimal Domain of Serum Response Factor. *MOLECULAR AND CELLULAR BIOLOGY*, 14(9), pp.5920–5928.

Johnson, C.A. et al., 2002. Human class I histone deacetylase complexes show enhanced catalytic activity in the presence of ATP and co-immunoprecipitate with the ATP-dependent chaperone protein Hsp70. *Journal of Biological Chemistry*, 277(11), pp.9590–9597.

Johnson, J.L. et al., 2012. Regulation of matrix metalloproteinase genes by E2F transcription factors: Rb-Raf-1 interaction as a novel target for metastatic disease. *Cancer Research*, 72(2), pp.516–526.

Kallsen, K., Andresen, E. & Heine, H., 2012. Histone deacetylase (HDAC) 1 controls the expression of beta defensin 1 in human lung epithelial cells. *PloS one*, 7(11), p.e50000.

Kang, M.L. et al., 2014. Intra-articular delivery of kartogenin-conjugated chitosan nano/microparticles for cartilage regeneration. *Biomaterials*, 35(37), pp.9984–9994.

Karagianni, P. & Wong, J., 2007. HDAC3: taking the SMRT-N-CoRrect road to repression. *Oncogene*, 26(37), pp.5439–5449.

Kawasaki, T. & Kawai, T., 2014. Toll-like receptor signaling pathways. *Frontiers in Immunology*, 5(SEP).

Kevorkian, L. et al., 2004. Expression Profiling of Metalloproteinases and Their Inhibitors in Cartilage. *Arthritis and Rheumatism*, 50(1), pp.131–141.

Khan, D.H. & Davie, J.R., 2013. HDAC inhibitors prevent the induction of the immediate-early gene FOSL1, but do not alter the nucleosome response. *FEBS Letters*, 587(10), pp.1510–1517.

Kim, H.J. & Bae, S.C., 2011. Histone deacetylase inhibitors: molecular mechanisms of action and clinical trials as anti-cancer drugs. *Am J Transl Res*, 3(2), pp.166–179.

Kim, J.H. et al., 2014. Regulation of the catabolic cascade in osteoarthritis by the zinc-ZIP8-MTF1 axis. *Cell*, 156(4), pp.730–743.

Kim, S. & Kaang, B.-K., 2017. Epigenetic regulation and chromatin remodeling in learning and memory. *Experimental & Molecular Medicine*, 49(1), p.e281.

Kimura, H. et al., 2003. Transcription of mouse DNA methyltransferase 1 (Dnmt1) is regulated by both E2F-Rb-HDAC-dependent and -independent pathways. *Nucleic Acids Research*, 31(12), pp.3101–3113.

Klampfer, L. et al., 2004. Requirement of histone deacetylase activity for signaling by STAT1. *Journal of Biological Chemistry*, 279(29), pp.30358–30368.

Knutson, S.K. et al., 2008. Liver-specific deletion of histone deacetylase 3 disrupts metabolic transcriptional networks. *The EMBO Journal*, 2751, pp.1017–1028.

Kobayashi, M. et al., 2005. Role of interleukin-1 and tumor necrosis factor alpha in matrix degradation of human osteoarthritic cartilage. *Arthritis and rheumatism*, 52(1), pp.128–135.

Kouzarides, T., 2007. Chromatin Modifications and Their Function. *Cell*, 128(4), pp.693–705.

Kozaci, L.D. et al., 1998. Stromelysin 1, neutrophil collagenase, and collagenase 3 do not play major roles in a model of chondrocyte mediated cartilage breakdown. *Mol Pathol*, 51(5), pp.282–286.

Kraus, V.B. et al., 2010. The OARSI histopathology initiative - recommendations for histological assessments of osteoarthritis in the guinea pig. *Osteoarthritis and Cartilage*, 18(SUPPL. 3), pp.S17–S23.

Kretsovali, A., Hadjimichael, C. & Charmpilas, N., 2012. Histone deacetylase inhibitors in cell pluripotency, differentiation, and reprogramming. *Stem Cells International*, 2012.

Kuhn, K., Hashimoto, S. & Lotz, M., 2000. IL-1β Protects Human Chondrocytes from CD95-Induced Apoptosis. *J Immunol*, 164(4), pp.2233–2239.

Lagger, G. et al., 2002. Essential function of histone deacetylase 1 in proliferation control and CDK inhibitor repression. *EMBO Journal*, 21(11), pp.2672–2681.

Lavrrar, J. & Farnham, P., 2004. The Use of Transient Chromatin Immunoprecipitation Assays to Test Models for E2F1-specific Transcriptional Activation. *The journal of Biological Chemistry*, 279(44), pp.46343–46349.

Lee, J.-S. et al., 2006. HES1 Cooperates With pRb to Activate RUNX2-Dependent Transcription. *J Bone Miner Res*, 21(6), pp.921–933.

Lee, J.W. et al., 2004. Chondrogenic differentiation of mesenchymal stem cells and its clinical applications. *Yonsei medical journal*, 45 Suppl, pp.41–47.

Li, Z. et al., 2014. Differential regulation of MMPs by E2F1, Sp1 and NF-kappa B controls the small cell lung cancer invasive phenotype. *BMC cancer*, 14(1), p.276.

Li, Z. et al., 2011. Epigenetic dysregulation in mesenchymal stem cell aging and spontaneous differentiation. *PLoS ONE*, 6(6).

Lim, C.A. et al., 2007. Genome-wide Mapping of RELA(p65) Binding Identifies E2F1 as a Transcriptional Activator Recruited by NF-κB upon TLR4 Activation. *Molecular Cell*, 27(4), pp.622–635.

Lin, Z. et al., 2016. A quinazoline-based HDAC inhibitor affects gene expression pathways involved in cholesterol biosynthesis and mevalonate in prostate cancer cells. *Molecular bioSystems*, 12(3), pp.839–849.

Lindner, C. et al., 2015. Investigation of association between hip osteoarthritis susceptibility

loci and radiographic proximal femur shape. *Arthritis and Rheumatology*, 67(8), pp.2076–2084.

Liu, B. et al., 2013. Interaction of E2F7 transcription factor with E2F1 and c-terminal-binding protein (CtBP) provides a mechanism for E2F7-dependent transcription repression. *Journal of Biological Chemistry*, 288(34), pp.24581–24589.

Liu, C.L. et al., 2005. Single-Nucleosome Mapping of Histone Modifications in S. cerevisiae. *PLOS Biology*, 3(10), p.e328.

Longworth, M.S. & Laimins, L.A., 2006. Histone deacetylase 3 localizes to the plasma membrane and is a substrate of Src. *Oncogene*, 25(32), pp.4495–4500.

Losson, H. et al., 2016. Natural Compound Histone Deacetylase Inhibitors (HDACi): Synergy with Inflammatory Signaling Pathway Modulators and Clinical Applications in Cancer. *Molecules*, 21(11), p.1608.

Lu, X. et al., 2016. Development of chidamide for peripheral T-cell lymphoma, the first orphan drug approved in China. *Intractable & rare diseases research*, 5(3), pp.185–91.

Ludlow, J.W. et al., 1989. SV40 large T antigen binds preferentially to an underphosphorylated member of the retinoblastoma susceptibility gene product family. *Cell*, 56(1), pp.57–65.

Luyten, F.P., Tylzanowski, P. & Lories, R.J., 2009. Wnt signaling and osteoarthritis. *Bone*, 44(4), pp.522–527.

Ma, Y. et al., 2002. Identification of novel E2F1-regulated genes by microarray. *Archives of biochemistry and biophysics*, 399(2), pp.212–24.

Macdonald, N. et al., 2005. Molecular basis for the recognition of phosphorylated and phosphoacetylated histone H3 by 14-3-3. *Molecular Cell*, 20(2), pp.199–211.

Magnaghi-Jaulin, L. et al., 1998. Retinoblastoma protein represses transcription by recruiting a histone deacetylase. *Nature*, 391(6667), pp.601–605.

Majumdar, M.K. et al., 2007. Double-knockout of ADAMTS-4 and ADAMTS-5 in mice results in physiologically normal animals and prevents the progression of osteoarthritis. *Arthritis and Rheumatism*, 56(11), pp.3670–3674.

Malfait, A.M. et al., 2010. ADAMTS-5 deficient mice do not develop mechanical allodynia associated with osteoarthritis following medial meniscal destabilization. *Osteoarthritis and Cartilage*, 18(4), pp.572–580.

Manal, M. et al., 2016. Inhibitors of histone deacetylase as antitumor agents: A critical

review. *Bioorganic Chemistry*, 67, pp.18–42.

Martel-Pelletier, J. et al., 2008. Cartilage in normal and osteoarthritis conditions. *Best Practice and Research: Clinical Rheumatology*, 22(2), pp.351–384.

McQuown, S.C. & Wood, M.A., 2011. NIH Public AccesHDAC3 and the Molecular Brake Pad Hypothesis. *Neurobiol Learn Mem.*, 96(1), pp.27–34.

Mengshol, J.A., Mix, K.S. & Brinckerhoff, C.E., 2002. Matrix metalloproteinases as therapeutic targets in arthritic diseases: Bull's-eye or missing the mark? *Arthritis and Rheumatism*, 46(1), pp.13–20.

Messeguer, X. et al., 2002. PROMO: detection of known transcription regulatory elements using species-tailored searches. *Bioinformatics (Oxford, England)*, 18(2), pp.333–334.

Van Meurs, J.B.J., 2017. Osteoarthritis year in review 2016: genetics, genomics and epigenetics. *Osteoarthritis and Cartilage*, 25, pp.181–189.

Millard, C.J. et al., 2017. Targeting Class I Histone Deacetylases in a "Complex" Environment. *Trends in Pharmacological Sciences*, xx, pp.1–15.

Mitchell, T.J. & John, S., 2005. Signal transducer and activator of transcription (STAT) signalling and T-cell lymphomas. *Immunology*, 114(3), pp.301–312.

Mitsiades, C.S. et al., 2004. Transcriptional signature of histone deacetylase inhibition in multiple myeloma: biological and clinical implications. *Proceedings of the National Academy of Sciences of the United States of America*, 101(2), pp.540–5.

Miyamoto, Y. et al., 2007. A functional polymorphism in the 5[prime] UTR of GDF5 is associated with susceptibility to osteoarthritis. *Nat Genet*, 39(4), pp.529–533.

Mochizuki, S. et al., 2012. Effect of ADAM28 on carcinoma cell metastasis by cleavage of von willebrand factor. *Journal of the National Cancer Institute*, 104(12), pp.906–922.

Montgomery, R.L. et al., 2007. Histone deacetylases 1 and 2 redundantly regulate cardiac morphogenesis, growth, and contractility. *Genes and Development*, 21(14), pp.1790–1802.

Montgomery, R.L. et al., 2008. Maintenance of cardiac energy metabolism by histone deacetylase 3 in mice. *Journal of Clinical Investigation*, 118(11), pp.3588–3597.

Moore, P.S. et al., 2004. Gene expression profiling after treatment with the histone deacetylase inhibitor trichostatin A reveals altered expression of both pro- and anti-apoptotic genes in pancreatic adenocarcinoma cells. *Biochimica et Biophysica Acta - Molecular Cell Research*, 1693(3), pp.167–176.

Mountziaris, P.M. et al., 2012. Intra-articular controlled release of anti-inflammatory siRNA with biodegradable polymer microparticles ameliorates temporomandibular joint inflammation. *Acta Biomaterialia*, 8(10), pp.3552–3560.

Mueller, M.B. & Tuan, R.S., 2011. Anabolic/Catabolic balance in pathogenesis of osteoarthritis: identifying molecular targets. *PM & R : the journal of injury, function, and rehabilitation*, 3(6), pp.S3–S11.

Murdoch, A.D. et al., 2007. Chondrogenic differentiation of human bone marrow stem cells in transwell cultures: generation of scaffold-free cartilage. *Stem cells (Dayton, Ohio)*, 25(11), pp.2786–96.

Murphy, G. et al., 2002. Matrix metalloproteinases in arthritic disease. *Arthritis Research*, 4(S3), pp.39–49.

Murphy, G. & Nagase, H., 2009. Progress in matrix metalloproteinase research. *Molecular Aspects of Medicine*, 29(5), pp.290–308.

Murphy, G. & Nagase, H., 2008. Reappraising metalloproteinases in rheumatoid arthritis and osteoarthritis: destruction or repair? *Nat Clin Pract Rheum*, 4(3), pp.128–135.

Muthukkumar, S. et al., 1996. Interleukin-1 Induces Growth Arrest by Hypophosphorylation of the Retinoblastoma Susceptibility Gene Product RB. *The Journal of Biological Chemistry*, 271(10), pp.5733–5740.

Nakajima, H. et al., 2001. Functional interaction of STAT5 and nuclear receptor co-repressor SMRT: Implications in negative regulation of STAT5-dependent transcription. *EMBO Journal*, 20(23), pp.6836–6844.

Nakamura, E., Nguyen, M. & Mackem, S., 2006. Kinetics of tamoxifen-regulated Cre activity in mice using a cartilage-specific CreERT to assay temporal activity windows along the proximodistal limb skeleton. *Developmental Dynamics*, 235(9), pp.2603–2612.

Natalie Dror, Michal Alter-Koltunoff, Aviva Azriel, Ninette Amariglio, Jasmine Jacob-Hirsch, Sharon Zeligson, Avigail Morgenstern, T.T. & Hansjorg Hauser, Gideon Rechavi, Keiko Ozato, B.-Z.L., 2007. Identification of IRF-8 and IRF-1 target genes in activated macrophages. *Mollecular Immunology*, 44, pp.338–346.

New, M., Olzscha, H. & La Thangue, N.B., 2012. HDAC inhibitor-based therapies: Can we interpret the code? *Molecular Oncology*, 6(6), pp.637–656.

Nicolas, E., Ait-Si-Ali, S. & Trouche, D., 2001. The histone deacetylase HDAC3 targets RbAp48 to the retinoblastoma protein. *Nucleic acids research*, 29(15), pp.3131–6.

Nishibuchi, G. & Déjardin, J., 2017. The molecular basis of the organization of repetitive DNA-containing constitutive heterochromatin in mammals. *Chromosome Research*, 10.

Noé, V. et al., 1998. Retinoblastoma protein associates with SP1 and activates the hamster dihydrofolate reductase promoter. *Oncogene*, 16(15), pp.1931–1938.

Nusinzon, I. & Horvath, C.M., 2003. Interferon-stimulated transcription and innate antiviral immunity require deacetylase activity and histone deacetylase 1. *Proceedings of the National Academy of Sciences of the United States of America*, 100, pp.14742–14747.

O'Neill, L. a & Greene, C., 1998. Signal transduction pathways activated by the IL-1 receptor family: ancient signaling machinery in mammals, insects, and plants. *Journal of leukocyte biology*, 63(6), pp.650–657.

Oeckinghaus, A. & Ghosh, S., 2009. The NF-kappaB family of transcription factors and its regulation. *Cold Spring Harbor perspectives in biology*, 1(4), p.a000034.

Ohne, Y. et al., 2016. IL-1 is a critical regulator of group 2 innate lymphoid cell function and plasticity. *Nat Immunol*, 17(6), pp.646–655.

Onyekwelu, I., Goldring, M.B. & Hidaka, C., 2009. Chondrogenesis, joint formation, and articular cartilage regeneration. *Journal of Cellular Biochemistry*, 107(3), pp.383–392.

Panteleeva, I. et al., 2004. HDAC-3 participates in the repression of e2f-dependent gene transcription in primary differentiated neurons. *Annals of the New York Academy of Sciences*, 1030, pp.656–660.

Paradis, F.H. & Hales, B.F., 2015. The effects of class-specific histone deacetylase inhibitors on the development of limbs during organogenesis. *Toxicological Sciences*, 148(1), pp.220–228.

Peach, C.A., Carr, A.J. & Loughlin, J., 2005. Recent advances in the genetic investigation of osteoarthritis. *Trends in Molecular Medicine*, 11(4), pp.186–191.

Pediconi, N. et al., 2003. Differential regulation of E2F1 apoptotic target genes in response to DNA damage. *Nature cell biology*, 5(6), pp.552–558.

Pittenger, M.F. et al., 1999. Multilineage Potential of Adult Human Mesenchymal Stem Cells. *Science*, 284(5411), p.143 LP-147.

Poole, R.M., 2014. Belinostat: first global approval. *Drugs*, 74(13), pp.1543–54.

Prasadam, I. et al., 2010. ERK-1/2 and p38 in the Regulation of hypertrophic changes of normal articular cartilage chondrocytes induced by osteoarthritic subchondral osteoblasts. *Arthritis and Rheumatism*, 62(5), pp.1349–1360.

Prasadam, I. et al., 2013. Impact of extracellular matrix derived from osteoarthritis subchondral bone osteoblasts on osteocytes: role of integrinβ1 and focal adhesion kinase signaling cues. *Arthritis research & therapy*, 15(5), p.R150.

Pun, Y.L. et al., 1994. Clinical Correlations of Osteoarthritis Associated with a Single???Base Mutation (Arginine519 to Cysteine) in Type II Procollagen Gene. *Arthritis & Rheumatism*, 37(2), pp.264–269.

Qu, H. et al., 2016. Trichostatin A increases the TIMP-1/MMP ratio to protect against osteoarthritis in an animal model of the disease. *Molecular medicine reports*, pp.2423–2430.

Rabinovich, A. et al., 2008. E2F in vivo binding specificity : Comparison of consensus versus nonconsensus binding sites. *Genome Research*, 18, pp.1763–1777.

Rascle, A., Johnston, J.A. & Amati, B., 2003. Deacetylase activity is required for recruitment of the basal transcription machinery and transactivation by STAT5. *Molecular and cellular biology*, 23(12), pp.4162–4173.

Razidlo, D.F. et al., 2010. Histone deacetylase 3 depletion in osteo/chondroprogenitor cells decreases bone density and increases marrow fat. *PLoS ONE*, 5(7).

Rengel, Y., Ospelt, C. & Gay, S., 2007. Proteinases in the joint: clinical relevance of proteinases in joint destruction. *Arthritis research & therapy*, 9, pp.1–10.

Richardson, P.G. et al., 2016. Deacetylase Inhibitors as a Novel Modality in the Treatment of Multiple Myeloma. *Pharmacological research*.

Rider, P., Carmi, Y. & Cohen, I., 2016. Biologics for Targeting Inflammatory Cytokines, Clinical Uses, and Limitations. *International Journal of Cell Biology*, 2016, pp.1–11.

Roach, H.I. et al., 2005. Association between the abnormal expression of matrix-degrading enzymes by human osteoarthritic chondrocytes and demethylation of specific CpG sites in the promoter regions. *Arthritis and Rheumatism*, 52(10), pp.3110–3124.

Roelofs, A.J., Rocke, J.P.J. & De Bari, C., 2013. Cell-based approaches to joint surface repair: A research perspective. *Osteoarthritis and Cartilage*, 21(7), pp.892–900.

Rosato, R.R. et al., 2010. Histone deacetylase inhibitors activate NF-kappaB in human leukemia cells through an ATM/NEMO-related pathway. *The Journal of biological chemistry*, 285(13), pp.10064–77.

Rosner, M., Schipany, K. & Hengstschläger, M., 2013. Merging high-quality biochemical fractionation with a refined flow cytometry approach to monitor nucleocytoplasmic

protein expression throughout the unperturbed mammalian cell cycle. *Nat. Protocols*, 8(3), pp.602–626.

Rothenfluh, D.A. et al., 2008. Biofunctional polymer nanoparticles for intra-articular targeting and retention in cartilage. *Nature materials*, 7(3), pp.248–254.

Rowan, A.D. & Young, D.A., 2007. *Frontiers in Bioscience*, 12, pp.536–550.

Ryan, S.M. et al., 2013. An intra-articular salmon calcitonin-based nanocomplex reduces experimental inflammatory arthritis. *Journal of Controlled Release*, 167(2), pp.120–129.

Sakamoto, S., Potla, R. & Larner, A., 2004. Histone Deacetylase Activity Is Required to Recruit RNA Polymerase II to the Promoters of Selected Interferon-stimulated Early Response Genes. *The Journal of Biological Chemistry*, 279(39), pp.40362–40367.

Saklatvala, J., 1986. Tumour necrosis factor alpha stimulates resorption and inhibits synthesis of proteoglycan in cartilage. *Nature*, 322, pp.547–549.

Sandy, J.D., 2006. A contentious issue finds some clarity: On the independent and complementary roles of aggrecanase activity and MMP activity in human joint aggrecanolysis. *Osteoarthritis and Cartilage*, 14(2), pp.95–100.

Shahrara, S. et al., 2007. Differential expression of the FAK family kinases in rheumatoid arthritis and osteoarthritis synovial tissues. *Arthritis Research and Therapy*, 9(5), p.R112.

Shin, B.S. et al., 2014. Quantitative determination of absorption and first-pass metabolism of apicidin, a potent histone deacetylase inhibitor. *Drug Metabolism and Disposition*, 42(6), pp.974–982.

Shoji, M. et al., 2013. Anti-Influenza Activity of C60 Fullerene Derivatives. *PLoS ONE*, 8(6).

Simkin, P. a, 2008. A biography of the chondrocyte. *Annals of the rheumatic diseases*, 67(8), pp.1064–8.

Singh, S., Johnson, J. & Chellappan, S., 2010. Small molecule regulators of Rb-E2F pathway as modulators of transcription. *Biochimica et Biophysica Acta - Gene Regulatory Mechanisms*, 1799(10–12), pp.788–794.

Smith, A.G., 2001. Embryo-Derived Stem Cells: Of Mice and Men. *Annual Review of Cell and Developmental Biology*, 17(1), pp.435–462..

Söder, S. et al., 2002. Ultrastructural localization of type VI collagen in normal adult and osteoarthritic human articular cartilage. *Osteoarthritis and Cartilage*, 10(6), pp.464–470.

Stanelle, J. et al., 2002. Gene expression changes in response to E2F1 activation. *Nucleic Acids Res*, 30(8), pp.1859–1867.

Di Stefano, L., Jensen, M.R. & Helin, K., 2003. E2F7, a novel E2F featuring DP-independent repression of a subset of E2F-regulated genes. *EMBO Journal*, 22(23), pp.6289–6298.

Sun, Z. et al., 2013. Deacetylase-Independent function of HDAC3 in transcription and metabolism requires nuclear receptor corepressor. *Molecular Cell*, 52(6), pp.769–782.

Sun, Z. et al., 2011. Diet-induced lethality due to deletion of the Hdac3 gene in heart and skeletal muscle. *Journal of Biological Chemistry*, 286(38), pp.33301–33309.

Tanaka, H. et al., 2013. Targeting Aurora kinase A suppresses the growth of human oral squamous cell carcinoma cells in vitro and in vivo. *Oral oncology*, 49(6), pp.551–9.

Trivedi, C.M. et al., 2007. Hdac2 regulates the cardiac hypertrophic response by modulating Gsk3 beta activity. *Nature medicine*, 13(3), pp.324–31.

Tullai, J.W. et al., 2007. Immediate-early and delayed primary response genes are distinct in function and genomic architecture. *Journal of Biological Chemistry*, 282(33), pp.23981–23995.

Valdes, A.M. et al., 2011. The GDF5 rs143383 polymorphism is associated with osteoarthritis of the knee with genome-wide statistical significance. *Ann*, 70(5), pp.873–875.

VanderMolen, K.M. et al., 2011. Romidepsin (Istodax, NSC 630176, FR901228, FK228, depsipeptide): a natural product recently approved for cutaneous T-cell lymphoma. *The Journal of antibiotics*, 64(8), pp.525–31.

Vega, R.B. et al., 2004. Histone deacetylase 4 controls chondrocyte hypertrophy during skeletogenesis. *Cell*, 119(4), pp.555–566.

Vincenti, M.P. & Brinckerhoff, C.E., 2002. Transcriptional regulation of collagenase (MMP-1, MMP-13) genes in arthritis: integration of complex signaling pathways for the recruitment of gene-specific transcription factors. *Arthritis research*, 4(3), pp.157–164.

Wallace, D.M. & Cotter, T.G., 2009. Histone deacetylase activity in conjunction with E2F-1 and p53 regulates Apaf-1 expression in 661W cells and the retina. *Journal of Neuroscience Research*, 87(4), pp.887–905.

Wang, H. et al., 2006. Histone H3 and H4 ubiquitylation by the CUL4-DDB-ROC1 ubiquitin ligase facilitates cellular response to DNA damage. *Molecular cell*, 22(3), pp.383–94.

Wang, J.P. et al., 2011. Trichostatin A inhibits TGF-β1 induced in vitro chondrogenesis of hMSCs through Sp1 suppression. *Differentiation*, 81(2), pp.119–126.

Weber, A., Wasiliew, P. & Kracht, M., 2010. Interleukin-1 (IL-1) Pathway. *Science Signaling*, 3(105), p.cm1 LP-cm1.

Weinmann, a S. et al., 2001. Use of chromatin immunoprecipitation to clone novel E2F target promoters. *Molecular and cellular biology*, 21(20), pp.6820–6832.

Weiss, C. et al., 2003. JNK phosphorylation relieves HDAC3-dependent suppression of the transcriptional activity of c-Jun. *EMBO Journal*, 22(14), pp.3686–3695.

Wells, J. et al., 2002. The identification of E2F1-specific target genes. *Proceedings of the National Academy of Sciences of the United States of America*, 99(6), pp.3890–3895.

White, R. et al., 1983. Perspectives on Genes and the Molecular Biology of Cancer.

Wolter, S. et al., 2008. c-Jun controls histone modifications, NF-kappaB recruitment, and RNA polymerase II function to activate the ccl2 gene. *Molecular and cellular biology*, 28(13), pp.4407–23.

Xiong, G. & Xu, R., 2014. ROR Binds to E2F1 To Inhibit Cell Proliferation and Regulate Mammary Gland Branching Morphogenesis. *Molecular and Cellular Biology*, 34(16), pp.3066–3075.

Xu, S. et al., 2013. Effect of the HDAC inhibitor vorinostat on the osteogenic differentiation of mesenchymal stem cells in vitro and bone formation in vivo. *Nature Publishing Group*, 34(10), pp.699–709.

Xu, X. et al., 2007. A comprehensive ChIP – chip analysis of E2F1 , E2F4 , and E2F6 in normal and tumor cells reveals interchangeable roles of E2F family members. *Genome Research*, 17, pp.1550–1561.

Yamaguchi, K. et al., 2005. Histone deacetylase inhibitors suppress the induction of c-jun and its target genes including COX-2. *Journal of Biological Chemistry*, 280(38), pp.32569–32577.

Yamaguchi, M. et al., 2005. Histone deacetylase 1 regulates retinal neurogenesis in zebrafish by suppressing Wnt and Notch signaling pathways. *Development (Cambridge, England)*, 132(13), pp.3027–43.

Yan, H. et al., 2016. Suppression of NF-κB activity via nanoparticle-based siRNA delivery alters early cartilage responses to injury. *Proceedings of the National Academy of Sciences* , 113(41), pp.E6199–E6208.

Yang, W.-M. et al., 1997. Isolation and characterization of cDNAs corresonding to an additional member of the human histone deacetylase gene family. *J. Biol. Chem.*, 272,

pp.28001–28007.

Yang, W.M. et al., 2002. Functional domains of histone deacetylase-3. *Journal of Biological Chemistry*, 277(11), pp.9447–9454.

Yoshida, M. et al., 1990. Potent and specific inhibition of mammalian histone deacetylase both in vivo and in vitro by trichostatin A. *Journal of Biological Chemistry*, 265(28), pp.17174–17179.

Young, D. a et al., 2005. Histone deacetylase inhibitors modulate metalloproteinase gene expression in chondrocytes and block cartilage resorption. *Arthritis research & therapy*, 7(3), pp.R503–R512.

Zhang, Q. et al., 2008. Differential Toll-like receptor-dependent collagenase expression in chondrocytes. *Annals of the rheumatic diseases*, 67(11), pp.1633–1641.

Zhang, X. et al., 2005. HDAC3 is regulated by interaction with Protein Serine / Threonine Phosphatase 4. *Genes and Development*, 3, pp.827–839.

Zhang, Y. et al., 2008. Mice Lacking Histone Deacetylase 6 Have Hyperacetylated Tubulin but Are Viable and Develop Normally. *MOLECULAR AND CELLULAR BIOLOGY*, 28(5), pp.1688–1701.

Zhang, Y. et al., 2003. Repression of E2F1-mediated transcription by the ErbB3 binding protein Ebp1 involves histone deacetylases. *Nucleic Acids Research*, 31(8), pp.2168–2177.

Zhao, Y. et al., 2005. Inhibitors of histone deacetylases target the Rb-E2F1 pathway for apoptosis induction through activation of proapoptotic protein Bim. *Proceedings of the National Academy of Sciences of the United States of America*, 102(44), pp.16090–5.

Zhou, R. et al., 2013. Histone Deacetylases and NF-kB Signaling Coordinate Expression of CX3CL1 in Epithelial Cells in Response to Microbial Challenge by Suppressing miR-424 and miR-503 D. Zilberstein, ed. *PLoS ONE*, 8(5), p.e65153.

Ziesché, E. et al., 2013. The coactivator role of histone deacetylase 3 in IL-1-signaling involves deacetylation of p65 NF-κB. *Nucleic Acids Research*, 41(1), pp.90–109.

Zych, J. et al., 2013. The epigenetic modifiers 5-aza-2'-deoxycytidine and trichostatin A influence adipocyte differentiation in human mesenchymal stem cells. *Brazilian journal of medical and biological research*, 46(5), pp.405–16.